THE STUDY OF AN

ADAPTIVE BIT RATE MODEM

FOR

METEOR SCATTER COMMUNICATIONS

GRAHAM JOHN MEYEROWITZ

A thesis submitted to the faculty of Engineering, University of Cape Town, in partial fulfilment of the requirements for the degree of Master of Science in Engineering.

CAPE TOWN 1990

DECLARATION

I declare that this thesis is my own, unaided work. It is being submitted for the Degree of Master of Science in Engineering in the University of Cape Town. It has not been submitted before for any degree or examination in any other University.

signature removed

(Signature of candidate)

13th day of September 1990

To my parents, Lollie and Jackie Meyerowitz.

ACKNOWLEDGEMENTS

I would like to express my appreciation to:

Dr. R. Braun, my supervisor for his invaluable advice and assistance throughout the course of my work.

Mr. P. Handley, for his support, and original motivation, without whom this project could not have been undertaken.

Mr. S. Schrire, for his excellent technical advice.

Mrs. J. Fold, for her administrative help.

Financial assistance from SALBU, PTY, LTD.

Table of Contents

C H A P T E R 1

INTRODUCTION

The use of Meteor Scatter Communication Systems for transmitting telemetric and other data across the country is proving to be very popular in South Africa. Current systems operate at constant bit rates of 4 k bit/sec and are limited to average throughputs of 50 bit/sec. A modem is required that will maximise this average throughput of data by offering a selection of higher bit rates. The study of an adaptive variable bit rate modem to perform this task is presented here. The final aim of this thesis is to document the design, implementation and testing of an adaptive bit rate modem.

1.1 BACKGROUND

The orbital path that Earth follows around the sun is filled with meteoric debris from space. These meteors enter the atmosphere and burn up, forming long columns of ionised particles approximately 80-120 kilometres above the Earths' surface. Although they diffuse within a few seconds, the scattered ionised particles reflect radio signals and are of sufficient duration to support radio communication over distances up to 2000 Km, hence the name Meteor Scatter Communication (MSC). These columns, or trails, of ionised particles can be up to 200 km in length [1.1]. The particles dissipate under their own velocities and by upper atmospheric winds. The largest trails can only support communications for up to 3 seconds giving rise to another common name, Meteor Burst Communication (MBC).

The frequency range of meteor-burst radio propagation is 30-100 Mhz, the lower limit being determined by the desire to avoid reflections via the ionospheric scatter mechanism. The upper limit is determined by receiver sensitivity limitations, since reflections at higher frequencies are weaker than those at lower frequencies.

A communication link is set up between two stations when a meteor is oriented in the ionosphere at the critical angle that provides a reflection of waves between the two stations in both directions. The proper orientation is such that the angles of incidence and reflection in the transmitter-meteor-receiver path are equal. An illustration of a link is shown in Fig. 1.1.

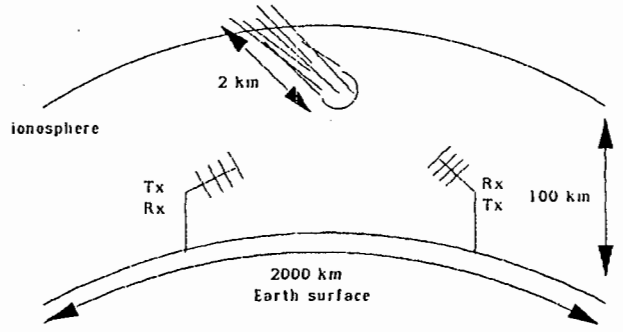

FIGURE 1.1 : *Meteor Scatter Communication.*

1.2 HISTORY

The possibility of radio wave reflections from meteor trails was first mentioned by Nagaoka in 1927 [1.2] as an explanation for sudden sharp increases in shortwave broadcast reception. In 1931 Pickard [1.3] noticed that these propagation anomalies increased during meteor showers. It was thus established that radio propagation could occur via scattering from inhomogeneities in the upper atmosphere and in particular from meteor scatter. The three modes of propagation become known as Ionoscatter (irregularities in lower ionosphere), Meteorscatter (re-radiation from ionised trails caused by burn up of meteors), Troposcatter (irregularities in troposphere).

In 1935, Skellet [1.4] postulated that the mechanism of reflection was free electrons in the meteor trail. The onset of the second world war put an end to most civilian meteor scatter research.

During 1957 much literature appeared in the Proceedings of the IRE covering meteor scatter theory and techniques. One such article [1.9] discusses the potential of a variable bandwidth system which lays the groundwork for the adaptive, bit rate modem. Progress of these systems was hindered by the magnetic storage equipment that could not operate at the high speeds required.

Also in 1957 experimental evidence proved the use of meteor scatter for facsimile communication. Frequency modulation was used at a bandwidth of 27 kHz [1.10]. In the seventies, interest in meteor scatter was renewed because of the development of microprocessors, enabling inexpensive implementation of sophisticated system control and inexpensive solid-state memories and components.

In 1977 the STC communications system, COMET [1.5], showed the usefulness of a constant bit rate system, which used Automatic Request for Repetition (ARQ) and diversity reception to provide several telegraph channels on a 1000 km path. In the concluding paragraph it was stated that "it is possible to establish several 50-baud communication channels with very high reliability. The only drawback is that time delays of one minute or so can occur due to the intermittent nature of the propagation." The text goes further to predict that "a tenfold increase in signalling rate of 20 000 baud can readily be used," but on the average, " the most practical increases in transmission rate would be one which resulted in a minimum average rate of 2000 baud. This would require burst rates of between 20 to 80 kbit/sec, depending on the other circuit parameters."

Improvements in throughput using an adaptive rate modem became a reality in the eighties, with the ever more reliable and fast solid state devices. In 1987 Weitzen [1.6] concluded that bit rates up to 1 Mbit/sec can be accommodated over meteor trails for a short periods during any one day, only if an adaptive scheme is used.

The interest in Meteor Scatter Communications has been sustained because it is a cheap alternative to satellite communications for beyond-line-of-sight links. The use is however limited to intermittent data communication.

Also in 1987 bit rates of 64 kbit/sec and message lengths of 8000 characters had been achieved using a technique called *dynarate* [1.7]. This implies the ability to dynamically vary the data rate as a function of received signal strength. In this way, maximum bit rates of 500 kbit/sec have been predicted. Another technique to control the operating bit rate that is very microprocessor intensive has been reported [1.8].

The progress from constant bit rate modems to variable bit rate systems has thus been described. It is with these developments in mind that further work is required to achieve maximum throughput of data over the channel in the short link time available by exploiting the concept of an adaptive variable bit rate modem.

1.3 SPECIFICATIONS

The modem is the interface between the computer and the transmitter/receiver unit as shown in Fig. 1.2.

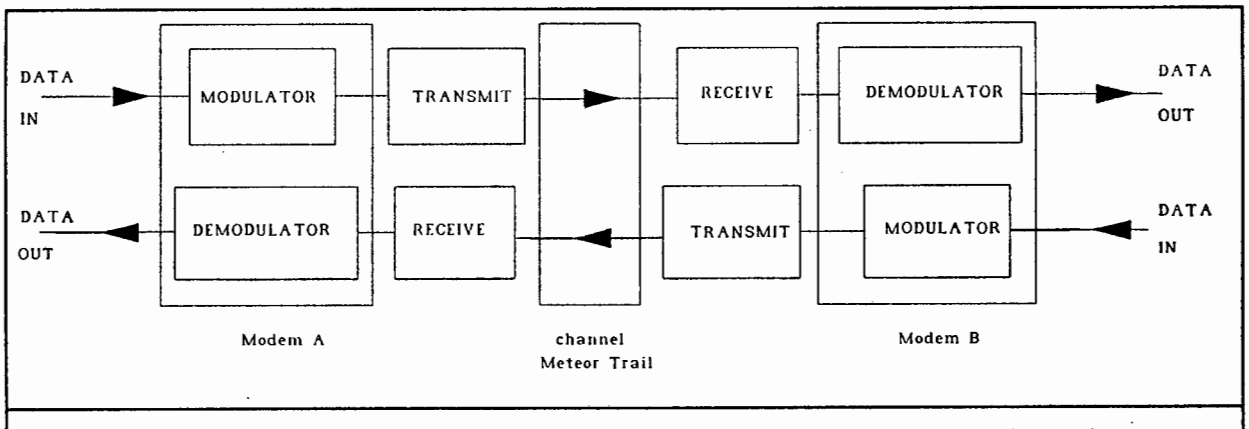

Figure 1.2 : *A block diagram of the complete communication system.*

The hierarchy of a complete Meteor Burst system consists of many layers of hardware from the controlling computers to the

antennas. The modem is part of the physical layer which also includes, the RF transmitter and the RF receiver. The data link layer consists of a host computer which communicates directly with the modem via an RS-232 link. The figure shows the position of the modem in the complete system. The system is full duplex. Such systems are presently being used at a constant bit rate of 4 kb/sec in South Africa. An adaptive bit rate modem will replace the constant bit rate modem in such a system. The design of an adaptive variable bit rate modem begins with specifications as set out in table 1.1.

The contents of this thesis are outlined as follows. Chapter two is a discussion of the properties of a meteor channel and how the channel affects radio waves. The results of this chapter lay the ground work for the choice of modulation technique. Chapter three presents the various digital modulation techniques that are feasible on a meteor scatter link. The chosen modulation technique, and methods of adaptively varying bit rate. The result of this chapter is the system that will be designed and implemented. Chapter four documents the design and implementation of the modem.

Chapter five includes the tests performed on the actual system and the results obtained by measurement. The conclusion of the thesis is given in chapter six. A short conclusion has been included at the end of each chapter.

Data rate	4 Kbit/sec to more than 100 Kbit/sec
Maximum bit rate step	2:1
Modulation format	Any
Input data	NRZ, synchronous, RS-232
Input Carrier Frequency	700 KHz (Input from power amplifier)
Input data clock	Generated by modem (Input from computer)
Output	Shaped baseband data or 21.4 Mhz modulated carrier (Output to power amplifier).
Carrier synchronisation time	6 m sec maximum.
Bit clock sync. time	6 msec maximum.
Modem synchronisation time	10 msec maximum.
Data rate switching	Seamless, preserving phase continuity.
Output S/N measurement	Not required.
Forward error correction	Not required.
Expected Bit Error Rate (BER)	10^{-2} to 10^{-8}.

TABLE 1.1 : *Specifications of the adaptive bit rate modem.*

NOTE :

1. The modulator is to accept commands from a host computer as to which bit rate should be current and exactly when to change bit rate.

2. The demodulator is to change to a new bit rate by way of a signal which is sent by the transmit station just before the bit rate takes place. The bit rate change is to be made without error (seamlessly).

1.4 REFERENCES

[1.1] Oetting, J. D., **An Analysis of Meteor Burst Communications for Military Applications**, IEEE Trans. on Comms. Vol. COM-28 No. 9 SEPT. 1980.

[1.2] Nagaoka, H., **Possibility of disturbance of radio transmissions by meteor showers**, Proceedings Imperial Academy of Tokyo, No. 5 , 1929.

[1.3] Pickard, G. W., **A Note on the Relation of Meteor Showers and Radio reception,** Proceedings of the IRE, vol. 19, No. 7, July 1931.

[1.4] Skellet, A. M., **The Ionisation Effects of Meteors,** Proceedings IRE, Vol. 23, No. 6, June 1935.

[1.5] Brown, D. W., **The potential of Meteor-Burst Communications with particular reference to the Comet System,** Communications Division , SHAPE Technical Center, The Hague, Netherlands.

[1.6] Weitzen, J. A., **The Feasibility of High Speed Digital Communications on the Meteor Scatter Channel**, phD thesis, University of Wisconsin-Madison, 1983.

[1.7] Smith, D. K., Donitch, T.J., **Variable Rate Applications In Meteor Burst Communications**, Meteor Communications Corporation, Kent, WA.

[1.8] Chang, S. S. L., **A Feedback Adaptive Variable Rate Meteor Burst Communication System**, IEEE International Conference On Communications, Philadelphia, P.A., 12-15 June 1988, Digital Technology - Spanning The Universe, Vol. 1 pp 423-429, IEEE , New York, 1988.

[1.9] Montgomery, G. F., **Intermittent Communication with a Fluctuating Signal**, Proceedings of the IRE Dec. 1957,pp.1678-1684.

[1.10] Bliss , W. H., Wagner, Jr , R. J. Wickizer, G. S., **Experimental Facsimile Communication Utilising Intermittent Meteor Ionisation** , Proc. IRE , Correspondence pp. 1734 - 1735, Dec.1957.

C H A P T E R 2

THE CHANNEL

This chapter deals with the natural channel of the communication system. The natural channel is defined by the environmental limits imposed on a transmitted radio wave between two communicating antennas. This includes the characteristics of the meteor trail pertaining to radio propagation. The discussion of the *non-natural* channel or the *synthetic* channel is done in the following chapter. That includes any filtering done by the modulator and the demodulator.

For the purpose of the discussion of the modem it will be assumed that the transmitter and the receiver, as described by Fig. 1.2, do not modify or interfere with the signal in any way between the output of a modulator and the input to a demodulator over a link. These sub-systems appear transparent to a modulator and a demodulator in one link.

As shown in Fig. 2.1, the natural channel is modelled by a transmittance, $H_c(\omega)$ and Added White Gaussian Noise (AWGN). The synthetic channel is modelled by two transmittances, $H_t(\omega)$ and $H_r(\omega)$ at the transmitter and at the receiver, respectively. The complete channel consists of all three transmittances in cascade.

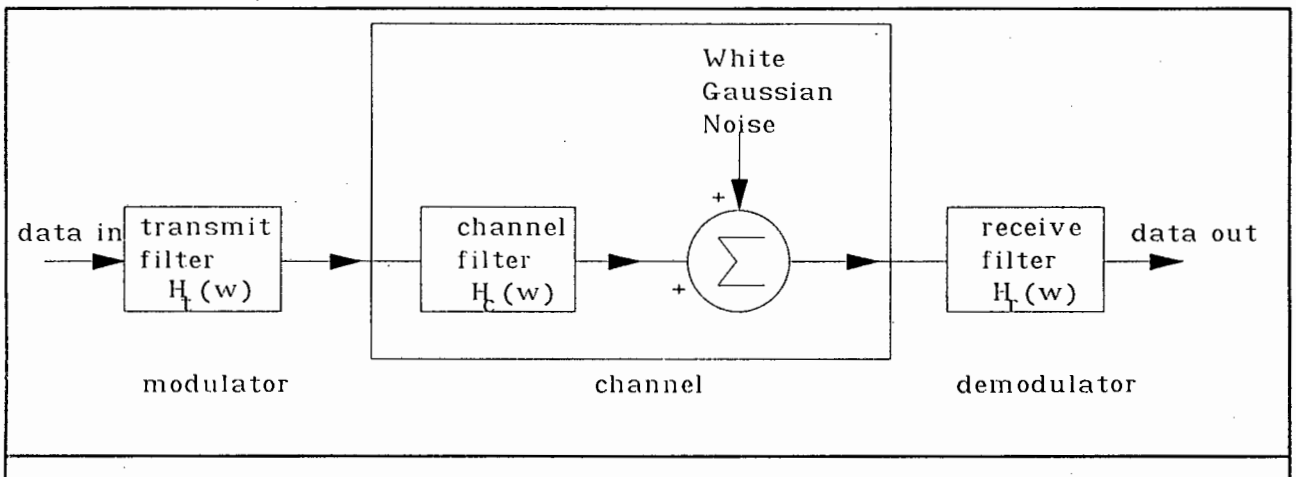

FIGURE 2.1 : *Communication channel.*

2.1 CHANNEL CHARACTERISTICS

The meteor scatter channel has been analysed by other authors and the channel can be completely specified in terms of four parameters: channel gain, Doppler spread, channel availability, and multipath spread [1.6]. This chapter describes these four parameters and shows how they affect radio propagation. A fifth effect on radio propagation is that of noise added to the radio signal, including the modem itself as a contributor.

Meteor trails are broadly characterised as either underdense or overdense, depending on the line density of free electrons in the trail [2.1]. Overdense meteor trails have a high density of free electrons with line densities of 2×10^{14} electrons per meter. This is regarded as a conducting surface. Lower densities are studied as secondary fields where individual electrons perform the reflection. These are under-dense trails which cause scattering by tenuous distributions.

In general, underdense trails are shorter lived but much more numerous than overdense trails. Further classification of trails has been done [2.1] and numerous different classes have been recorded according to the received signal envelope shape. Some examples : Sine Overdense, Classic Underdense and Sinusoidal Overdense. Examples of two such trails are illustrated in Fig. 2.2.

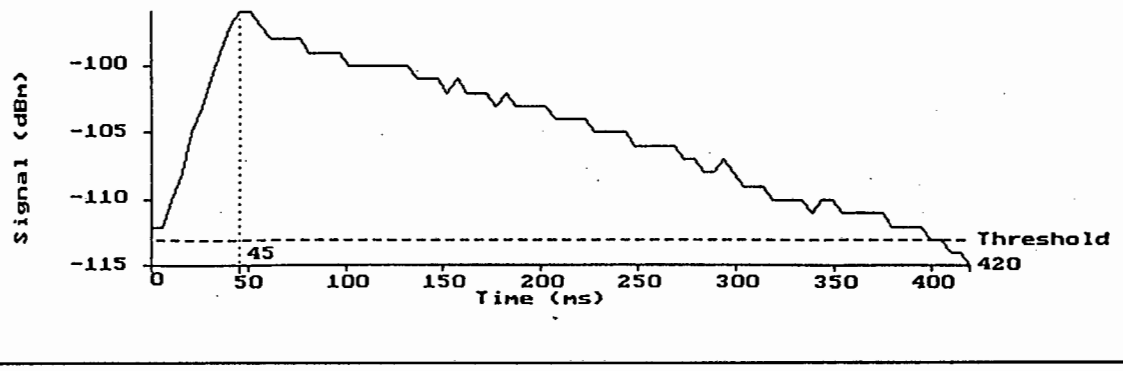

(a)

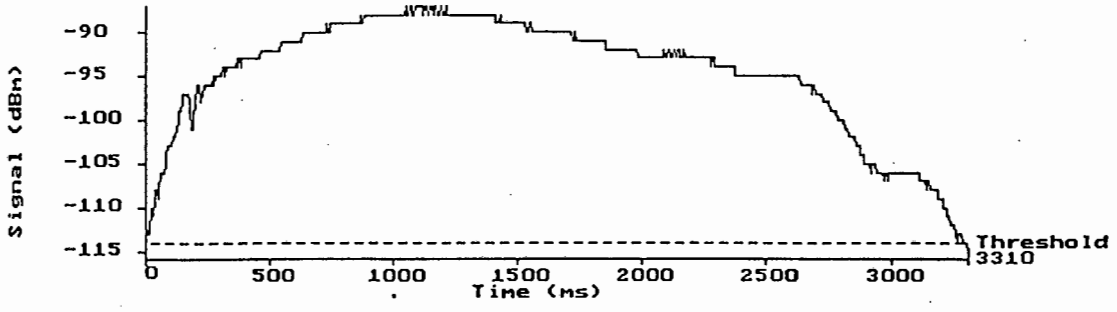

(b)

Figure 2.2 : *Actual reflected signals from a (a) Classic Underdense trail and a (b) Non-Sine Overdense trail [2.1].*

2.1.1 CHANNEL GAIN

The gain of the channel has been described mathematically for both underdense and overdense trails [1.6]. These equations are of no use to the design of the modem since it is preferable to use measurements taken from actual trails. Experimental evidence of the gain can be observed from the received signals from actual trails, with reference to Fig. 2.2. From these two trails and others that have been recorded in the reference [2.1], the following summary has been compiled:

1. Maximum received signal strengths are about -90 dBm.

2. The noise floor of the system defines the lowest signal

strength that can be received, typically -112 dBm. The maximum operating signal-to-noise (S/N) environment is therefore 22 dB.

3. The received gain fluctuates randomly during the existence of a trail, eventually fading to zero dB.

4. The received gain fluctuates from trail to trail with very few trails reflecting signals in the same way.

This confirms the variation in the medium and shows the low signal-to-noise environment that must be expected.

2.1.2 DOPPLER SPREAD

Doppler spread is the frequency spread of the carrier caused by reflections off a moving trail. Since trails are constantly moving the received carrier frequency can shift away from its expected value.

On a meteor scatter link two types of Doppler occur, namely; Body Doppler and Early-fast Doppler. The former type is predominant. The latter is a transient phenomenon observed during the formation of a trail.

Body Doppler has been measured [1.6] for 2200 trails. This data showed that the vast majority of trails have a body Doppler in the range $-2\ \text{Hz} < F_D < 2\ \text{Hz}$. Other work led to the estimate $-1\ \text{Hz} < F_D < 1\ \text{Hz}$ [2.5].

Information about the Doppler Spread therefore indicates that the channel should be able to sustain coherent communications since the magnitude of the shift is well within the limits of typical carrier recovery system lock up times.

2.1.3 MULTIPATH SPREAD

Multipath spread is the time spread of a modulated carrier which defines the phase response of the *natural* channel. The

multipath profile of the channel is generally determined by two distinct phenomena. The first is caused by reflections from the original trail, from a second trail, or from ionospheric effects. The second, less important phenomenon is due to the non-zero radius of a trail [1.6].

In the past, the lack of interest in high speed digital communications on meteor links made detailed studies of the channel multipath profile unnecessary. However, in order to implement high speed modems, it is necessary to establish what the multipath effect is. To do this signals from commercial television stations were received [2.3]. Such signals provide a readily available source of wideband probing signals. Visual multipath measurements were made from TV pictures from Tashkent, USSR received in Pakistan. These experiments showed that 4 Mhz signals were received, for long enough to be visually captured. Wait times for reception of such signals were typically 15 min. The longest burst recorded, lasted 15 sec.

Subsequent experiments done in the USA used an improved method of determining the multipath [1.6]. That is, the vertical equalisation pulses which are transmitted with television programmes have a rigorous specification by the Federal Communications Commission (2.03 μs wide spaced every 29 μs). This provided unambiguous multipath information with a resolution of 0.5 μs.

In these experiments, signals were received over a five month period, showing that for most of the trails, spreading was less than 0.6 μs. From these results, it was concluded [1.6] that the coherent bandwidth of the channel and thus the maximum data rate which can be transmitted without Intersymbol Interference is 4 M bit/sec. That is, for short term underdense trails in which the limit is imposed by the non-zero diameter of the trail. The limit reduces to about 2 Mbit/sec for long duration trails in which the maximum rate is imposed by high altitude wind warping.

2.1.4 CHANNEL AVAILABILITY

The availability of the channel is the time available for communications over a twenty four hour period. The occurrence of trails is not continuous and the channel is intermittent, limiting data throughput. Availability depends on:

1. The *number of meteors* that occur with a high enough electron line density to support communications and the correct orientation with respect to two communicating stations.

2. The *length of time* that they can sustain communications.

If channel availability is high then the throughput of data will increase. The occurrence of meteors varies daily and seasonally. Meteor shows sometimes occur which increase availability. A statistical analysis of the occurrence of meteor trails is given in sub section 2.3.1. For the sake of a definition, the inherent channel availability during a twenty four hour period is simply calculated as being

$$Availability = \frac{1}{24\,hours}\sum_{i=1}^{N}\left(\Delta T_u\right)_i \times 100\,\% \qquad for\ 0 < t < 24\,hours \qquad (2.1)$$

Where : $(\Delta T_u)_i$ = the useable duration of the i^{th} trail.

Availability is the opposite of *wait time* over any period. Wait time is the average time spent waiting for trails over a twenty four hour period.

Example: to calculate the availability of the link.

When transmitting at a constant bit rate of 4 kbit/sec, a usable trail occurs every one minute, on average, and lasts for one second, on average. This implies an average availability of:

$\mathbf{A}_{ave} = 1/60 = 0.01666 = 1.67\ \%$

The following is a table representing the number of meteors entering the atmosphere over a twenty four hour period, that have potential for communication [1.6].

Mass (gram)	Radius (cm)	Number of this mass or > per day	Electron line density e/m
10^3	4.0	10^2	10^{20}
10^2	2.0	10^3	10^{19}
10	0.8	10^4	10^{18}
1	0.4	10^5	10^{17}
10^{-1}	0.2	10^6	10^{16}
10^{-2}	0.08	10^7	10^{15}
10^{-3}	0.04	10^8	10^{14}
10^{-4}	0.02	10^9	10^{13}
10^{-5}	0.0008	10^{10}	10^{12}

TABLE 2.1 : *Relative Distribution of meteors as a function of mass [1.6].*

The table is for interest only and will not be used quantitatively. In this discussion it is not necessary to predict the channel availability but it is necessary to define the qualifying terms highlighted above, namely;

1. Which meteors are useable.

2. How long a meteor remains useable after it has come into existence.

It is these limits that will aid the final user in rating the useability of each trail with respect to the modem. With respect to the modem, this time available for transmission must be utilised as efficiently as possible. Synchronisation time at the beginning of a trail must be kept to a minimum. Therefore, the actual time available for data communication

is less than the time of the trail existence because of the practical time limits imposed by circuitry. The utilisation of a trail is considered in section 2.2.2.

2.1.5 NOISE

The noise level at the receiver which defines the minimum signal power that can be received, can consist of any combination of the many noise sources within the frequency range of interest i.e. 30 - 100 Mhz. The two main groups of noise contributors are man-made interference and natural interference [2.2]. A comprehensive list of all noise sources has been given in the reference. One omnipresent and strictly unavoidable form of man-made interference is thermal noise in the receiver components. However, the most prominent noise source is Galactic noise introduced by spurious high-frequency radio waves that penetrate the atmosphere from space.

At the carrier frequency of interest, 50 Mhz, galactic noise does fall off with bandwidth [3.6 chap. 4], however galactic noise is still typically 7 to 16 dB above the thermal noise of receiver. This has been measured from existing systems operating in South Africa. The total noise power at the receiver is assumed to be white and proportional to the bandwidth of the receiver. The total noise power is modelled by a resistor that has a temperature which represents the combination of environmental and receiver noise power:

$$N = kTB \quad Watts \quad (2.2)$$

Where:

k = 1.38 x 10^{-23}, Boltzmann's constant, J/^{o}K.
T = noise-source temperature of receiver and the incident galactic noise, ^{o}K.
B = bandwidth of received signal, Hz.

The noise threshold at the receiver is set by this power, **N**. An important explanation of the variables used to indicate signal to noise ratios will now be explained.

Carrier-to-noise ratio will be referred to as **S/N** or **C/N** in this text. This is a power ratio of signal power to noise power (Watts / Watts) and is dimensionless. These quantities are measurable in practice using power and root-mean-square (RMS) voltage meters.

The theory of modulation techniques usually refers to $\mathbf{E_b/N_o}$ as the signal-to-noise ratio. Where $\mathbf{E_b}$ is the received signal energy, having units Watt/Hz, and $\mathbf{N_o}$ is noise spectral density, having units Watt/Hz. However, these quantities are difficult to measure in practice. A conversion between **S/N** and $\mathbf{E_b/N_o}$ is given by [3.1, chap. 4] as :

$$\frac{E_b}{N_o} = \frac{C}{N}\left(\frac{B_w}{f_b}\right) \quad dB \qquad (2.3)$$

Where: $\mathbf{1/f_b = T}$ is the bit period in seconds, $\mathbf{B_W}$ is the equivalent noise bandwidth of the receiver, in Hz. For example, the case of the second order Butterworth filter, the values $\sqrt{S}$ and $\sqrt{N}$ are measured by an rms volt-meter at the receiver output, each quantity in the absence of the other. The noise equivalent bandwidth of this filter is , $\mathbf{B_W = 1.1/T}$ [appendix A]. Therefore :

$$\frac{E_b}{N_o} = 1.1\left(\frac{S}{N}\right) \quad dB$$

2.1.6 SUMMARY OF CHANNEL CHARACTERISTICS

Received signal levels rise and fade during the existence of a trail. Each trail has a different maximum and minimum received signal strength and hence the maximum received signal power-to-noise power ratio (S/N) of each trail varies from trail to trail.

The total noise power at the receiver is proportional to the receiver bandwidth and is predominantly caused by the environment. Therefore the S/N received can be increased by decreasing the receiver bandwidth.

Each trail has a different duration. The usable duration of each trail varies from 200 msec. to 3 sec., occasional longer bursts of up to 15 sec. have been recorded. The trails occur intermittently and arrive at any moment.

The Doppler spread has no significant effect on communications.

The multipath effects sets an upper limit on the maximum bit rate. However, the usability of each trail is determined by the received S/N level and not the phase coherence.

The error rate varies up or down proportionally with S/N. In a variable rate system, an attempt is made at maintaining a constant error rate and a constant received S/N level. This is done by adjusting the system bandwidth (bit rate) up or down when the received signal level rises or falls, respectively. This can explained as follows:

In section [2.1.5] the amount of noise in the system is shown to be proportional to bandwidth. As the received signal power fades it is necessary to reduce the noise power level as well, thereby maintaining a constant S/N. To decrease the noise power at the receiver the bandwidth of the receiver must be reduced. This implies decreasing the bit rate. It can therefore be said that:

1. The maximum bit rate that each trail supports varies from trail to trail.

2. The bit rate that each trail supports varies during its existence. The capacity reaches a peak at some point during the trail and then decays. Some trails have several peaks.

3. High bit rates can only be sustained for short intervals, while the S/N is high.

2.2 METEOR SCATTER CHANNEL CAPACITY

The capacity of the link is therefore determined by the signal-to-noise level received. Useful communication is said to commence once the received signal strength is sufficiently greater than the noise threshold ,such that the error rate, $P_e < 10^{-2}$ and the receive bit rate, $B = B_{min}$ (bit/sec). Where B_{min} is the lowest (or only) operating bit rate of the modem. Communications ends when the error rate drops below the minimum. For the following discussion of the capacity two definitions are given :

2.2.1 CHANNEL THROUGHPUT

Channel throughput is defined as the total number of bits that can be sent during a trail existence. For a constant bit rate system this can be stated as a bit count

$$TH_{trail} = T_m \cdot f_b \quad bits \qquad (2.4)$$

However a more rigorous prediction of the throughput of the channel is done in sub section 2.3.1.

2.2.2 CHANNEL UTILISATION

Channel utilisation is a measure of how well each trail is used. A well utilised channel is one in which the maximum data rate has been transmitted and the throughput has been maximised. The channel utilisation is the actual throughput achieved over a channel divided by the total throughput theoretically achievable over the channel, below a particular error rate, P_e.

$$U = \frac{actual\ \ throughput}{theoretical\ \ throughput\ \ limit} \times 100\,\%$$

The theoretical throughput limit is given in Fig.2.5 of

2.3 THEORETICAL ADAPTIVE MODEM OPERATION

The theoretical operation of an adaptive bit rate modem is now explained. With the aid of an example, the expected results obtained are compared with those of a constant bit rate system.

EXAMPLE

One communicating station, A, probes another station, B. As soon as B receives a signal of relative strength, B transmits back to A acknowledging the link. Let the received signal at B be that of Fig. 2.2 (a). The received signal is at a maximum at -95 dBm and drops off as shown.

Consider the received S/N of the trail shown in 2.2 (a). In this case both the signal and the noise were measured in a 2 Khz bandwidth at the output of the receiver. From the figure, the received S/N level can be determined as

$$\left(\frac{S}{N}\right)_r = P_r dBm - N_t dBm \quad dB \qquad (2.5)$$

Where P_r is the received signal power and N_r is the noise threshold power. Measurements taken from the figure given in table 2.2. show that the S/N measured in a fixed bandwidth drops with the received signal.

Time (m sec)	50	100	150	200	250	300	350
S (dBm)	-95	-100	-102	-103	-105	-108	-110
N (dBm)	-121	-121	-121	-121	-121	-121	-121
(S/N) dB	26	20	19	18	16	13	11

TABLE 2.2 : *Measured received signal-to-noise ratio.*

(i) Constant bit rate modem

In a constant bit rate system, the modems do not switch bit rate at all, but maintain the link at one rate until the signals fade and the link terminates. In such a case, it is necessary to select the optimum bit rate for a particular trail. Since trail behaviour is difficult to predict, it becomes impossible to select the best constant bit rate for each trail, that will maximise throughput. There exists a trade off between bit rate and wait time (duty cycle). The use of high bit rates will only be possible with high wait times, the use of low bit rates is possible at shorter wait times.

Consider using the trail at a constant bit rate of 2 kbit/sec, since this trail has been measured in 2 Khz bandwidth. If a Differential Encoded Binary Phase Shift Keyed (DEBPSK) modulation system is used, table 2.2 results in the following probability of error (P_e) for corresponding S/N ratios. A relationship between P_e and S/N for DE-BPSK is available from Fig. 3.1. The origin of this relationship will be explained in the following chapter.

S/N (dB)	P_e
26	$< 10^{-9}$
20	$< 10^{-9}$
19	$< 10^{-9}$
18	$< 10^{-9}$
16	$< 10^{-9}$
13	$5x10^{-9}$
11	$6x10^{-7}$

TABLE 2.3 : *Probability of error and received signal-to-noise of a Classic Underdense trail operating at f_b = 2 kbit/sec.*

When using a constant bit rate of 2 kbps, this channel has been under utilised since the minimum allowable bit error rate for the modem is Pe < 10^{-2}. Thus any received bit error rate below this value is taken to be unnecessarily small. An increase in bit rate can be allowed with a resulting drop in S/N and increase in error rate, as long as the error rate is kept at 10^{-2}.

(ii) Adaptive Variable bit rate modem

In the case of the adaptive bit rate modem, the modems will initially communicate at the slowest bit rate. The receive strength is measured and transmitted back to the respective transmitting station, which then switches to the highest possible rate. This rate is sustained until the received strength drops below, say, -100 dBm and a slower bit rate is required to maintain the P_e. The receiver sends a message to the transmitter to switch down in rate. This changing of bit rates occurs in steps until the receive strength fades below the noise threshold value.

Consider an adaptive bit rate modem operating as explained above. The modem is required to operate from 4 kbit/sec to at least 128 kbit/sec, in multiples of two. Table 2.4 shows the switching rule of the system. The transmitter will switch bit rate according to the absolute S/N measurements in column one. An absolute measurement is one which is taken in a fixed bandwidth (here 2 kHz), irrespective of the current bandwidth of operation. The second column shows the corresponding bit rates. The third column shows the corresponding system bandwidth employing a matched receive filter (see next chapter). This particular S/N vs bit rate relationship has been established for the sake of the example. Notice that the receiver bandwidth decreases as the **absolute** received S/N ratio drops. However, the relative S/N measured at each bandwidth, will be constrained to a small range of values around a chosen set point. An appropriate set point is Pe = 10^{-3} and a S/N = 8 dB.

E_b/N_o^* (dB) (2 kHz bandwidth)	BIT RATE (k bit/sec)	BANDWIDTH (Khz)
> 18	128	128
16 - 18	64	64
13 - 15	32	32
10 - 12	16	16
8 - 10	8	8
< 8	4	4

TABLE 2.4 : *Adaptive bit rates versus signal-to-noise ratio.*

The two cases are shown in Fig 2.3 (a) and (b) respectively. The constant bit rate operates at one bit rate of 2 kbps only, while the adaptive bit rate modem changes bit rate at the moments in time according to the rule of table 2.4.

* assumming that E_b/N_o = S/N (the case of Nyquist, matched filters) [3.1]

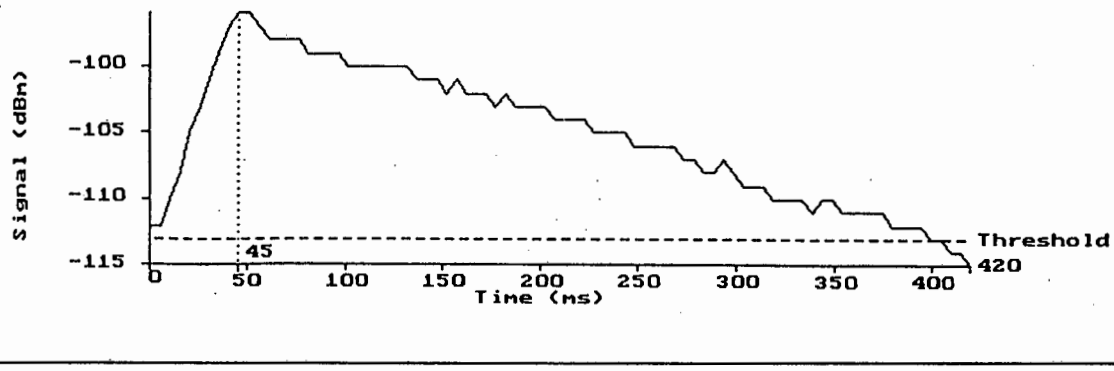

(a)

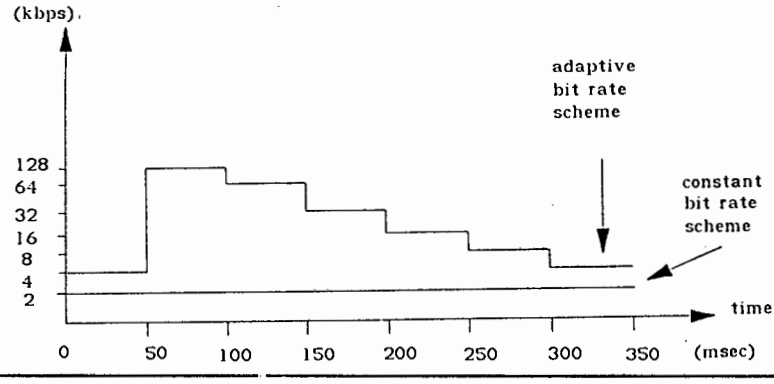

(b)

FIGURE 2.3 : *(a) Constant bit rate vs (b) adaptive bit rate operation.*

The increase in throughput can be calculated as follows:

Constant bit rate of 2 kbit/sec

Throughput = 350 msec x 2000 bits = **700 bits.**

Variable bit rate of 4 kbit/sec up to 128 kbit/sec

Throughput = (50E-3 x 128E3) + (50E-3 x 64E3) + (50E-3 x 32E3) + (50E-3 x 16E3) + (50E-3 x 8E3) + (100E-3 x 4E3) = **12800 bits**

An increase in throughput of eighteen times.

{ Example ends }

A similar result has been proved [1.7] by way of an implementation of an adaptive bit rate modem, shown in Fig. 2.4. The detected RF signal shows the trail strength to be about -96 dBm, enough to support a 256 kbps data rate. This system has a maximum data rate of 64 kbps, so it jumps to that rate at the start of the data exchange. After about 400 msec, the S\N ratio has dropped to about 10 dB at 64 kbps, so the link is slowed to 32 kbps. As the signal continues to fade, the data rate is halved until, at 2 kbps, the signal is lost.

In this case, two thirds of the throughput (2394/3402) characters) occurred at the first (maximum) data rate. It is reported [1.7] that the typical trail supports 1/2 of the throughput at the highest bit rate, 1/4 at the second bit rate, 1/8 at the third rate, etc. If the system would have remained at the probe rate of 8 kb/s, the throughput would only have been 560 characters. The increase in throughput is therefore six times. The limits to this implementation of an adaptive bit rate modem are discussed in the following chapter.

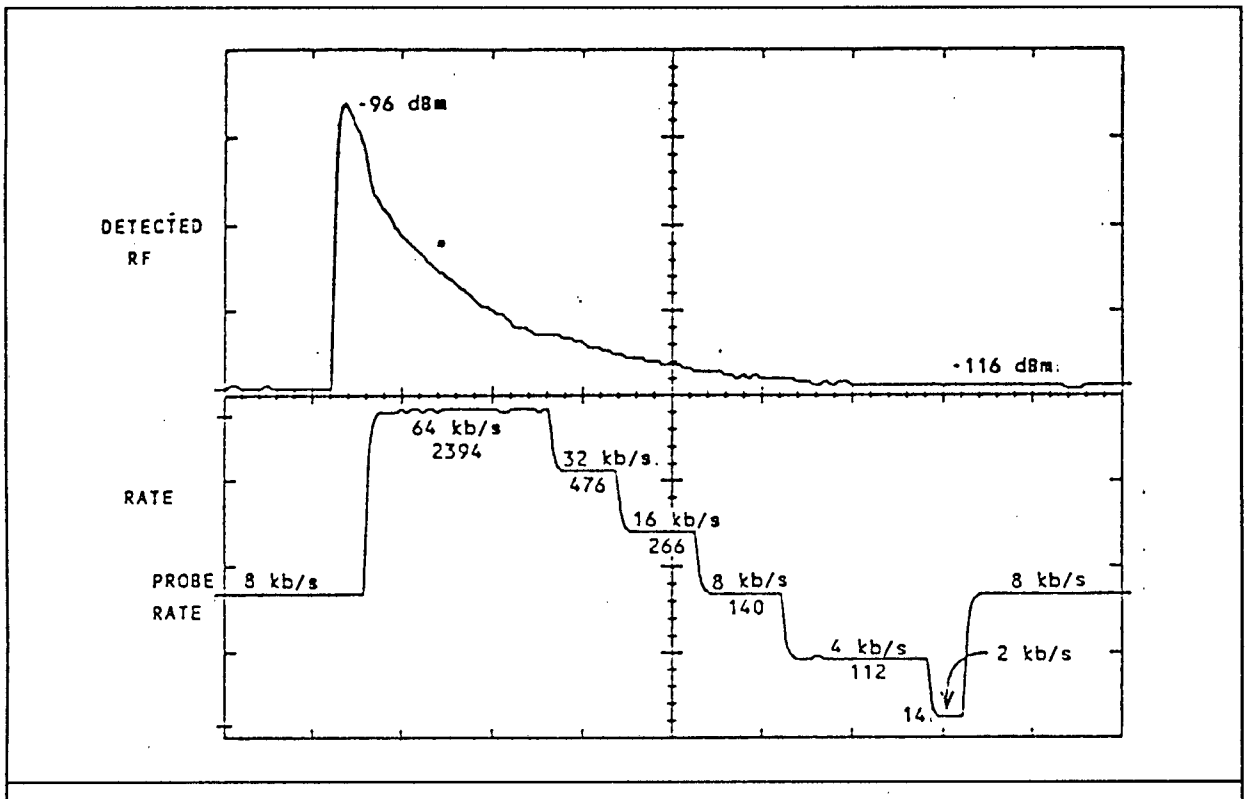

FIGURE 2.4 : *Variable Rate on Large meteor[1.7].*

2.4 ANALYTICAL COMPARISON OF THREE TYPES OF SYSTEMS [1.8]

The previous discussion of the optimum utilisation of a meteor trail, only considers one trail. The question still remains, whether the adaptive bit rate modem will show an increase in throughput over a constant bit rate system over many meteor trails? Since all trails are different in strength, duration and occurrence.

An analytical discussion of the improvement in this case has been done [1.8]. In this reference, three schemes are compared, namely; a variable adaptive bit rate scheme, a constant bit rate system and a constant bit rate system employing automatic message repeat request (ARQ). The discussion that follows briefly discusses the result of[1.8].The ARQ system is omitted from the explanation. To make the comparison meaningful, the same channel model is used for all three systems.

CHANNEL MODEL[1.8]

1. The received signal power during one meteor burst can be represented as

$$P = P_m e^{-t/B} \quad W \qquad (2.6)$$

where P_m is the peak power, and B is a time constant.

2. P_m and B are random variables for the ensemble of meteor bursts. For each individual burst, P_m and B are constants. the distributions of P_m and B are independent:

f(a) = average number of meteor bursts per second with $P_m \geq a$.

$P_B(b)$ = probability of B >= b.

3. The occurrences of meteor bursts are Poisson.

4. The frequency function f(a) can be expressed as:

$$f(a) = K_1\left(a^{-n} - P_1^{-n}\right) \quad , \left(0 < a \le P_1\right) \qquad (2.7)$$

where P_1 is the maximum value of the peak power, and f(a) = 0 for a > P_1. Equation (2.7) gives a probability density function

$$p(a) = c a^{-(n+1)} \quad for\ a \le P_1$$
$$= 0 \qquad for\ a > P_1$$

which has been well documented in the literature for low density bursts [2.7]. The frequency function f(a), is directly measurable and the variable *n* has been established empirically [2.8] to range between 0.57 and 0.96. The relationship between F and P_1 is approximated well by this equation, although the variation in *n* indicates the inconsistency in predicting meteor masses and meteor arrival. A value of 0.6 is used in this analysis.

Let E denote the received signal energy per bit for a prescribed signal to noise ratio (e.g. 10 dB). Let μ denote the bit rate, and P_o denote a lowest designated pulse power. then

$$P_o = \mu E \quad W \qquad (2.8)$$

for a constant bit rate system. For a variable bit rate system (2.8) is replaced by

$$P_o = \mu_o E \quad W$$

where μ_o is the lowest bit rate of the system. for both types of systems transmission ceases when P < P_o.

Once the channel model has been set up the the three mentioned cases are then analysed, namely the adaptive bit rate scheme, the constant rate scheme and the ARQ scheme. The procedure is as follows:

The number of bits in a burst is calculated, N(a,b). For the constant bit rate case this equals the product of the bit rate and the trail duration. For the variable bit rate case, this depends on the bit rate which is assumed to vary in proportion with the received power. The number of bits in a burst is the result of an integration of the received power above a threshold, for the duration of the trail. The throughput rate equation (average bits/sec) is given as

$$N(a,b) = \mu t_1 = \mu b \ln \frac{a}{P_o} \qquad (2.11)$$

for the constant bit rate case, and

$$N(a,b) = \frac{1}{E}\int_0^{t_0} P\,dt \qquad (2.12)$$

$$\Rightarrow \quad = \frac{b}{E}(a - P_o)$$

for the variable bit rate case. Once the throughput has been calculated for any trail, as a function of *a*, the received power and *b*, the duration of the burst, the average throughput rate per burst, N, is calculated,

$$N = \int_0^{\infty}\int_{P_o}^{P_1} N(a,b)\,df(a)\,dP_B(b) \qquad (2.13)$$

The result of the integration is an equation of throughput rate, N, in terms of the specific throughput f(n,x) where $x = P_O/P_1$.

$$f(n,x) = \frac{x}{n}\left(x^{-n} - 1 + n\ln x\right)$$

for the constant rate modem and

$$f(n,x) = \frac{n}{1-n} - \frac{x^{1-n}}{1-n} + x$$

for the variable bit rate modem. A plot of f(n,x) for the three cases is shown in Fig. 2.5 (an explanation for the third case has been omitted), which indicates the improvement in throughput obtained with an adaptive bit rate scheme over the other two schemes.

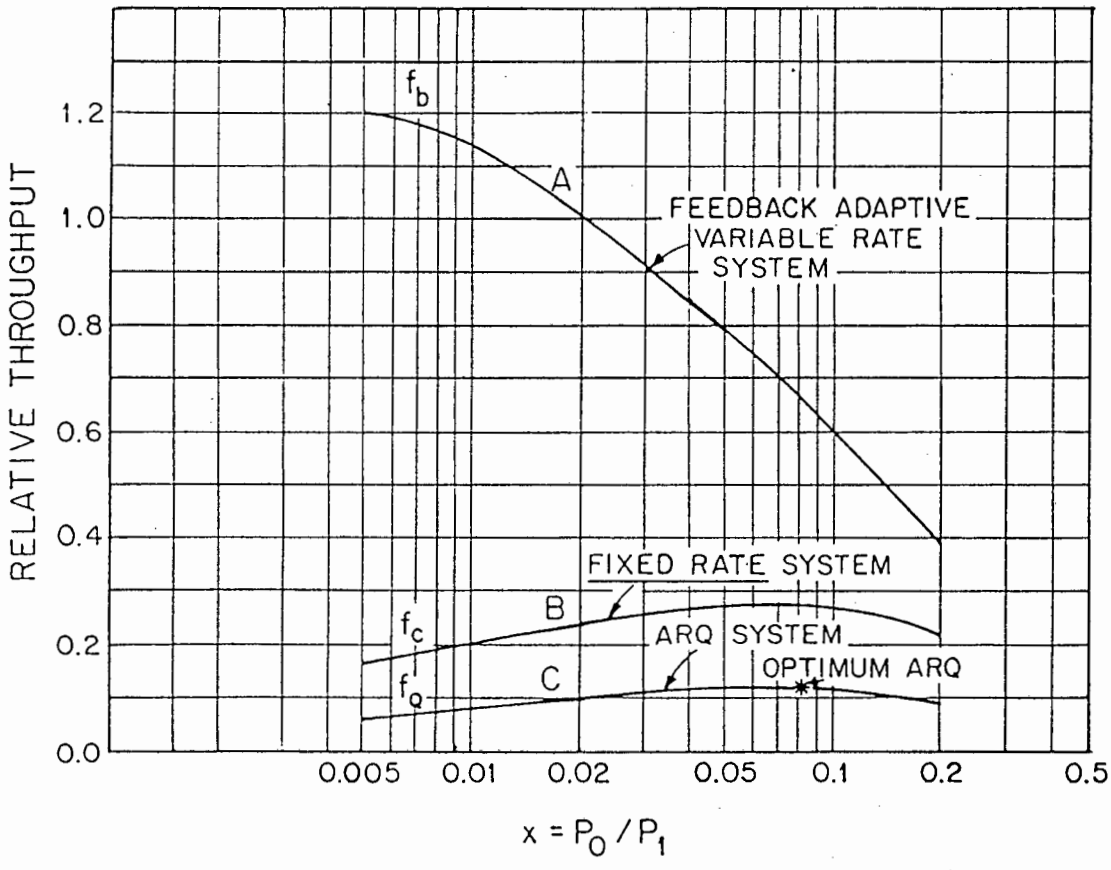

FIGURE 2.5 : *Throughput of three types of communication systems [1.8].*

2.5 PRACTICAL OPERATIONAL LIMITS

The two shortcomings of the theory of the adaptive bit rate modem of sub-section 2.4 are :

1. The received trail shape is limited to a decaying exponential, which is not the case for many recorded trails [2.1].

2. It is assumed that the adaptive bit rate modem varies continuously with the received signal-to-noise ratio. However, it is impractical to have a continuously varying bit rate. Such a system would forever be changing bit rate and would have no time to synchronise or demodulate data. Therefore equation (2.12), used to calculate the throughput per burst, when applied to a practical adaptive bit rate modem, should not be a continuous integral, but rather a discrete summation. The adaptive bit rate modem then switches between discrete bit rates at certain absolute received power levels. This is shown as follows:

$$N(a,b) = \frac{1}{E}\sum_{t=0}^{t_0} P_t \Delta t \qquad (2.14)$$

the graph of variable bit rate of Fig. 2.5 will not show the same large improvement over a constant bit rate system. The improvement may still exist, but will depend on the discrete steps chosen in the summation.

Other practical considerations are that channel utilisation can also be degraded by the practical modem limits. For example, lock up times of synchronised loops and rate change circuits. The increase in throughput is much less than would seem from the above theoretical predictions. The practical limits of the adaptive bit rate modem are described as follows:

The time taken from the moment the receiver receives sends a command for a new bit rate, until the receiver locks onto a new rate is called the rate change delay time, RCD, calculated as :

$$RCD = t_{rd} + t_{cd} + t_{td} + t_{cd} + t_{rld} \quad sec.$$

Where :

t_{rd} = time taken from the moment the receiver measures a fade until the transmitter in the same unit transmits this information back to the first transmitter.

t_{cd} = time taken for message to reach destination over meteor scatter path (this delay occurs twice as the message is relayed in a feedback type loop).

t_{td} = time taken from the instant the message to change rate is received until the transmitter actually changes rate.

t_{rld} = time taken for receiver to lock onto the new rate from the arrival of the command for the new rate. This is the lock up time of the control circuitry.

This sets a minimum delay between bit rate changes, RCD_{min}. Therefore the modems will operate at each bit rate for a minimum time even if the signal fade is much faster than this minimum time.

Beyond the control of the modem is the transmission of measurements regarding bit rate in the feedback path provided by the full duplex arrangement, t_{rd} and t_{td}. This must be done with minimum delays allowing fast response of the modem to changes in the received channel fade on both sides of a link. Also, the time taken to transmit this message, t_{cd}, is roughly calculated as being the time taken for electromagnetic radiation to traverse a distance of 1500 Km ,

$$t_{cd} = \frac{1.5 \times 10^6}{3 \times 10^8 \times 0.9} \text{sec} = 5.5 msec$$

The speed of propagation is less than the speed of light by a velocity factor taken as 0.9 here. This time is not accurate but gives an indication as to the time that is lost from sending a message to receiving a message. Also, the distance between two stations is a variable.

The speed of the modem to switch to the new bit rate, at the receiver, is given by t_{rld}. For example, if a trail only lasts for 1 sec, and three rate changes are required during this period, 333 msec are available for communicating at each bit

rate. The RCD must not exceed, say 40 msec. The practical limitations can be reduced to some extent by the modem design. Hence the specifications given in chapter one on carrier lock up times and modem synchronisation.

2.6 CONCLUSION

It has been predicted that high speed communications can be accommodated over a meteor scatter link [1.6]. It has been predicted that an adaptive bit rate modem will offer higher throughput over constant bit rate modems [1.8] and indeed proved to be the case [1.7].

The effect of the amplitude fade dominates over the effect of the phase incoherence. The channel bit rate capacity is therefore determined by the received signal-to-noise ratio. A consequence of this is, that the upper bit rate limit of 1 Mbit/sec, that is set by phase incoherence on large meteors can only be achieved if the received S/N during the trail at 1 Mbit/sec is sufficiently large.

The meteor scatter channel can therefore be described as a power limited environment.

The *natural* channel can be modelled as having a time varying characteristic. Both the amplitude response and phase response changes during the existence of a link. However, the channel will be assumed to have a flat amplitude spectrum and a linear phase response over the finite bandwidth of interest during the useful existence of the trail. The following chapter will explain the modulation techniques that are available and how a selection to use one technique has been made.

2.7 REFERENCES

[2.1] Melville, S. W. ; Larson, J. D. ; Letschert, R. Y. ; Goddard, W. D. **The Classification of Meteor Trail Reflections By a Rule Based System**, The Transactions of the South African Institute of Electrical Engineers, Sept. 1989, pp. 104-116.

[2.2] Mackenzie, R. A. **BMS Meteor Observer's Handbook, Vol. V : Radio Scatter Meteor Work,** British Meteor Society, Dover, England, 1986.

[2.3] Ahmad, K. H. ; Javed, A. and Grossi, M. D. **Adaptive Communications via Meteor Forward Scattering**, Pakistan International Symposium on Elec. Eng. Nov. 1972.

[2.4] Weitzen, J. A., Michael, J. S., Scofidio, R. A., Quinn, J. , **Characterising the Multipath and Doppler Spreads of the High-Latitude Meteor Burst Channel,** IEEE Transactions on Communications, VOL. COM-35, No.10 . Oct. 1987.

[2.5] Grossi, M. D. , Southworth, R. B. and Rosenthal, S. K., **Observation of Meteor Winds above Illinois**, Progress in Astronautics and Aeronautics, Vol. 17, Thermospheric Circulation, MIT Press. Cambridge, Ma. 1972.

[2.6] Ziemer R. E. , Peterson R. L. , **Digital Communications and Spread Spectrum Systems**, Macmillan Publishing Company, New York, Collier Macmillan Publishers, London.

[2.7] Campbell L. L. Hines C. O. **Bandwidth Considerations in a JANET System** , Proc. of the IRE, Vol. 45 No. 12 , Dec 1957 pp.1658 - 1660.

[2.8] Eshleman V. R. Manning L. A. **Radio Communications by Scattering from Meteoric Ionisation** , Proc. of the IRE, Vol. 42, pp. 530-536, March 1954.

C H A P T E R 3

MODULATION TECHNIQUE

3.1 INTRODUCTION

The choice of modulation technique links four system parameters, namely ; *bit rate* (f_b), *bandwidth* (**W**), *signal-to-noise* (**S/N** or E_b/N_o) environment and the acceptable *probability of error* (P_e). From the conclusion of chapter two it can be stated that the meteor scatter channel is a power limited environment. That is, a modulation technique is required that can transmit the highest possible bit rate in a relatively low signal to noise environment (8 dB) with a probability of error of 10^{-2} or less, at the expense of bandwidth. To achieve optimum communications with the above parameters, a power efficient modulation technique is required, which satisfies the more general, normalised objectives of table 3.1 :

P_e	E_b/N_o (theoretical)	E_b/N_o (practical)
10^{-4}	**8.4 dB**	**10.8 dB**
10^{-8}	**12 dB**	**15 dB**

Table 3.1 : *Performance objectives for a power efficient modem [3.1].*

A power efficient modulation technique contrasts with a bandwidth efficient modulation technique. The latter offers high data rates using relatively small bandwidths at the expense of a high signal-to-noise ratio. The former, allows communications at comparable or higher bit rates than that of the previous scheme in a low signal-to-noise environment at the expense of a relatively wider bandwidth. Since no bandwidth limitations have been imposed in the specifications, the power efficient systems are preferred.

Figure 3.1 shows a comparison of the most power efficient digital modulation schemes. Without any explanation as to the origins of Fig. 3.1, it is shown here. The origin of the curves will be explained in section 3.4.3.1 . Numerous other methods of digital modulation exist, which result in a greater P_e for a given **S/N** environment. For example Frequency Shift Keying (FSK) and Amplitude Shift Keying (ASK) [3.6]. Other digital schemes which offer a comparable performance to the figure are Correlative phase shift keying (COR-PSK) [3.6] and Gaussian Minimum Phase Shift Keying (GMSK) [3.7]. These schemes offer bandwidth efficiency as well as power efficiency and are most widely used where bandwidth limits as well as power limits are imposed.

The diagram shows that Binary phase shift key (BPSK); Gray coded Quadrature phase shift key (QPSK), Offset Quadrature phase shift key (OQPSK) and Minimum shift key (MSK) modulation, all have the equivalent P_e vs E_b/N_o relationship. Only these four schemes will be further investigated as possible solutions on the meteor scatter channel.

An adaptive bit rate modem must also include a system for indicating bit rate changes. Solutions to this problem will also be discussed in this chapter. Before further discussion, a brief history of modulation techniques for Meteor Burst Communication is given. These techniques provide insight into solving the problem for an adaptive bit rate modem.

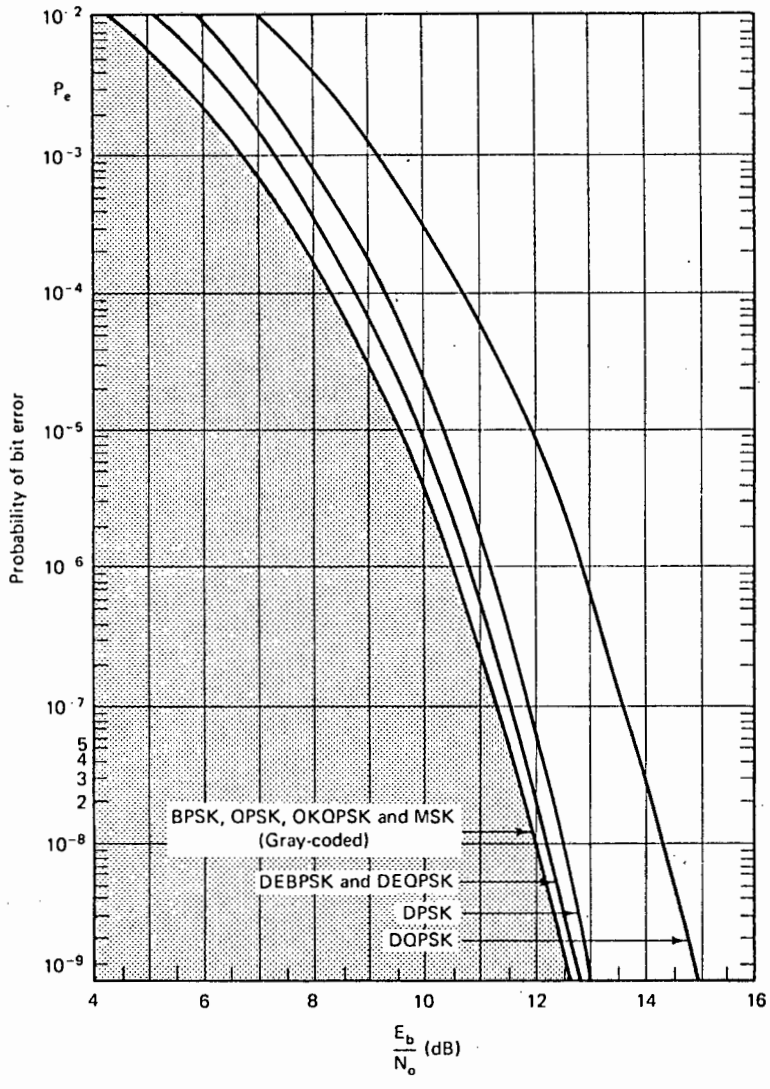

Figure 3.1: *Theoretical Pe = f(Eb/No) performance of coherent BPSK, DEBPSK, coherent QPSK, and DQPSK modems (gray encoded). Additive white gaussian noise and intersymbol-interference-free model [3.1].*

3.2 HISTORY

The STC COMET system used Frequency Shift Keying (FSK) with a total deviation of 5 Khz and a signalling rate of 2000 baud [1.5]. A typical system reported in [1.6] operates with coherent BPSK modulation at 4 kbit/sec is used. The received level is -114 dBm to obtain a BER of 10^{-3}. Coherent Bi-phase keying (BPSK) has also been recommended by other authors [3.3].

Non-coherent systems are more robust in the presence of multipath induced intersymbol interference. It has been determined that coherent tracking of a signal propagating via meteors through the atmosphere, leads to better performance [3.3].

BPSK provides a good basis for a discussion of other power efficient modulation techniques and will be further investigated in the following sections. Although coherent ASK and FSK schemes have been used in the past the predicted performance of such schemes is not as good as BPSK and will not be investigated further. Before any discussion on the modulation technique, the data source that will be used, is discussed.

3.3 BASEBAND NRZ DATA

The data that the modem accepts from the host computer is in the Non-Return-to-Zero format (NRZ). More generally, this format is termed unipolar. A unipolar waveform transmits a pulse for a code **1** and no pulse for a code **0**. For a symbol interval of duration T_b sec, the unipolar waveform is illustrated in Fig. 3.2 (a), and is the format of data to be accepted from a host computer. The pulse illustrated is said to be an NRZ type because it occupies the full symbol intervals' duration, T_b sec.

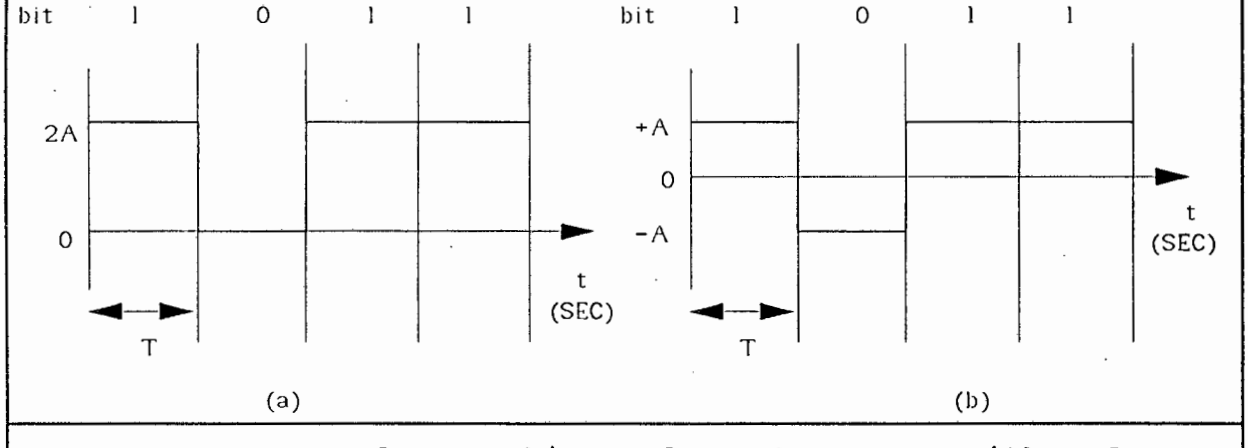

FIGURE 3.2 : *A random NRZ binary data stream (a) with a dc level (unipolar), (b) without a dc level (polar).*

A Polar waveform is required if Phase Shift Keying is to be used as a modulation technique. This is because a polar waveform multiplied directly to a carrier generates a carrier with 180° phase shifts at the instants of the data edges. This is achieved by eliminating the dc offset of the unipolar waveform.

3.3.1 SPECTRAL DENSITY OF NRZ DATA

The spectral density of NRZ baseband data is given here. Consider the two possible data signals of Fig. 3.2 (b):

$$g_1(t) = \begin{cases} +A \text{ volts} & -\frac{T_s}{2} < t \leq \frac{T_s}{2} \\ 0 \text{ volts} & \text{elsewhere} \end{cases}$$

and

$$g_2(t) = \begin{cases} -A \text{ volts} & -\frac{T_s}{2} < t \leq \frac{T_s}{2} \\ 0 \text{ volts} & \text{elsewhere} \end{cases} \qquad (3.1)$$

The Fourier transform of $g_1(t)$ is given as:

$$G_1(f) = \int_{-\infty}^{\infty} g(t) e^{-j2\pi ft} dt = \int_{-T_s/2}^{T_s/2} A e^{-j2\pi ft} dt$$

$$= \frac{A}{-j2\pi f} \int_{-T_s/2}^{T_s/2} e^{-j2\pi ft} d(-j2\pi ft)$$

$$G_1(f) = \frac{A}{\pi f} \sin(\pi f T_s) \qquad (3.2)$$

Similarly,

$$G_2(f) = -\frac{A}{\pi f} \sin(\pi f T_s) \qquad (3.3)$$

As $G_1(f) = -G_2(f)$, it is evident that $G_1(0) = -G_2(0)$ which is non-zero. At integer multiples of the signalling frequency ($f = m f_s$), we have

$$G_1(f = mf_s) = \frac{A}{\pi m f_s}\sin(\pi m f_s T_s)$$

$$= \frac{A}{\pi m f_s}\sin(\pi m) = 0$$

Similarly,

$$G_2(f = mf_s) = \frac{A}{\pi m f_s}\sin(\pi m) = 0$$

From the Fourier Transform the spectral density can be obtained as

$$w_s(f) = 2f_s p(1-p)|G_1(f) - G_2(f)|^2$$

Assuming that the binary 'ones' and 'zeros' are equiprobable, i.e. P(-A) = P(+A) = 0.5.

$$w_s(f) = 2f_s \cdot 0.5 \cdot 0.5 \cdot \left(2\frac{A}{\pi f_s}\sin(\pi f T_s)\right)^2$$

$$\omega_s(f) = 2A^2 T_s\left(\frac{\sin(\pi f T_s)}{\pi f T_s}\right)^2 \qquad (3.4)$$

This is the complete spectral density of equiprobable, balanced NRZ data. The dc component is zero and there are no other discrete components. The first spectral zero occurs for $f = 1/T_S = f_S$, that is, at the signalling frequency. Even though the dc component is zero, spectral density has its maximum value $2A^2T_S$ at $f = 0$. Note the difference in terminology between the dc component and the spectral density at zero frequency. A typical NRZ spectrum is shown in figure

3.3. Notice the spectral nulls that occur at multiples of the bit rate, or at $f = n.f_s$ (n = 1,2,3,4,...). f_s = 4 kbps in this case.

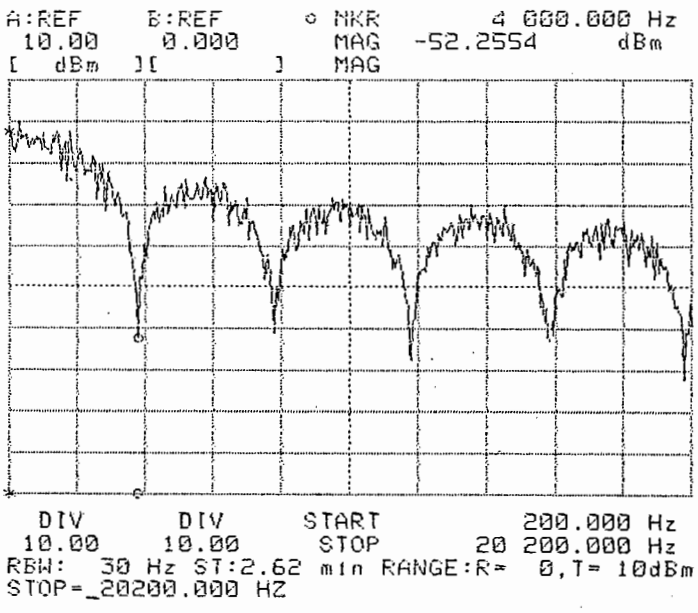

FIGURE 3.3 : *Spectrum of NRZ data at 4 kbit/sec.*

3.4 BINARY PHASE SHIFT KEYING

Bi-phase or binary PSK systems (BPSK) are considered to be the simplest form of phase-shift keying (M = 2). With reference to Fig. 3.4 (a), consider one data bearing signal, m(t), which is to modulate a sinusoidal carrier given by $\cos(w_c t)$. Using BPSK the data signal can only consist of binary ones or zeros. Using a non-return to zero format of the binary data, and multiplying this by the carrier directly, results in the following waveform:

$$s(t) = A \cdot m(t) \cdot C \cdot \cos(\omega_c t + \theta) \qquad (3.5)$$

Where :

C is the peak carrier amplitude.
A is the peak data amplitude.
ω_c is the carrier.
θ is the initial phase.

Since $m(t) = \pm 1$ (binary bit stream), the modulated signal has two states $s_1(t)$ and $s_2(t)$ given by:

$$s_1(t) = +A \cdot C \cdot \cos(\omega_c t + \theta)$$
$$s_2(t) = -A \cdot C \cdot \cos(\omega_c t + \theta) \qquad 0 \le t \le T_b \quad (3.6)$$

Where T_b sec. is the period of one binary state. Binary Phase Shift Keying is therefore a single carrier system.

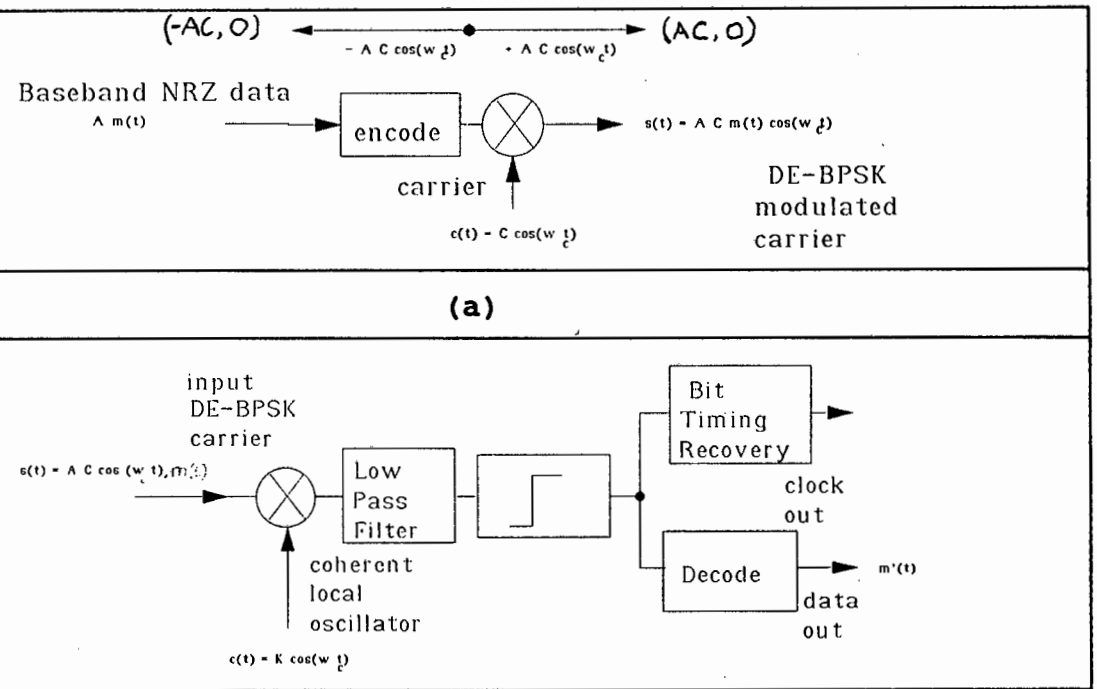

FIGURE 3.4 : *BPSK (a) modulator and (b) demodulator.*

The modulated signal is given by (3.5) above and can be rewritten:

$$s(t) = AC\cos(\omega_c t + \phi(t) + \theta) \quad (3.7)$$

Where $\phi(t)$ is the phase angle of 180^o or 0^o introduced by modulating the carrier by the NRZ data.

The signals that generate a BPSK waveform are shown in figures 3.5 (a) through (d). The digital data from the computer viewed in (a) unipolar or (b) polar format, is multiplied by a carrier,

having no phase relationship with the data. The result is the un-filtered, BPSK waveform of (d). The two phase states of Fig. 3.5 (d) are shown in Fig. 3.4 (a) by a line vector having magnitude and direction. This is termed the constellation diagram, because it illustrates the possible states of the carrier as a constellation of coordinate points. For the carrier having frequency, ω_c, amplitude $A \cdot C$ and phase 0^o and 180^o, the coordinates are shown as (AC,0) and (-AC,0) respectively.

For equiprobable NRZ baseband signals (+1 and -1 volt normalised input data) time-domain multiplication is equivalent to double-sideband suppressed carrier amplitude modulation (DSB-SC-AM) which can be seen from equation (3.5). The equivalent representation in equation (3.7) implies that a phase shift-keyed (PSK) signal is obtained.

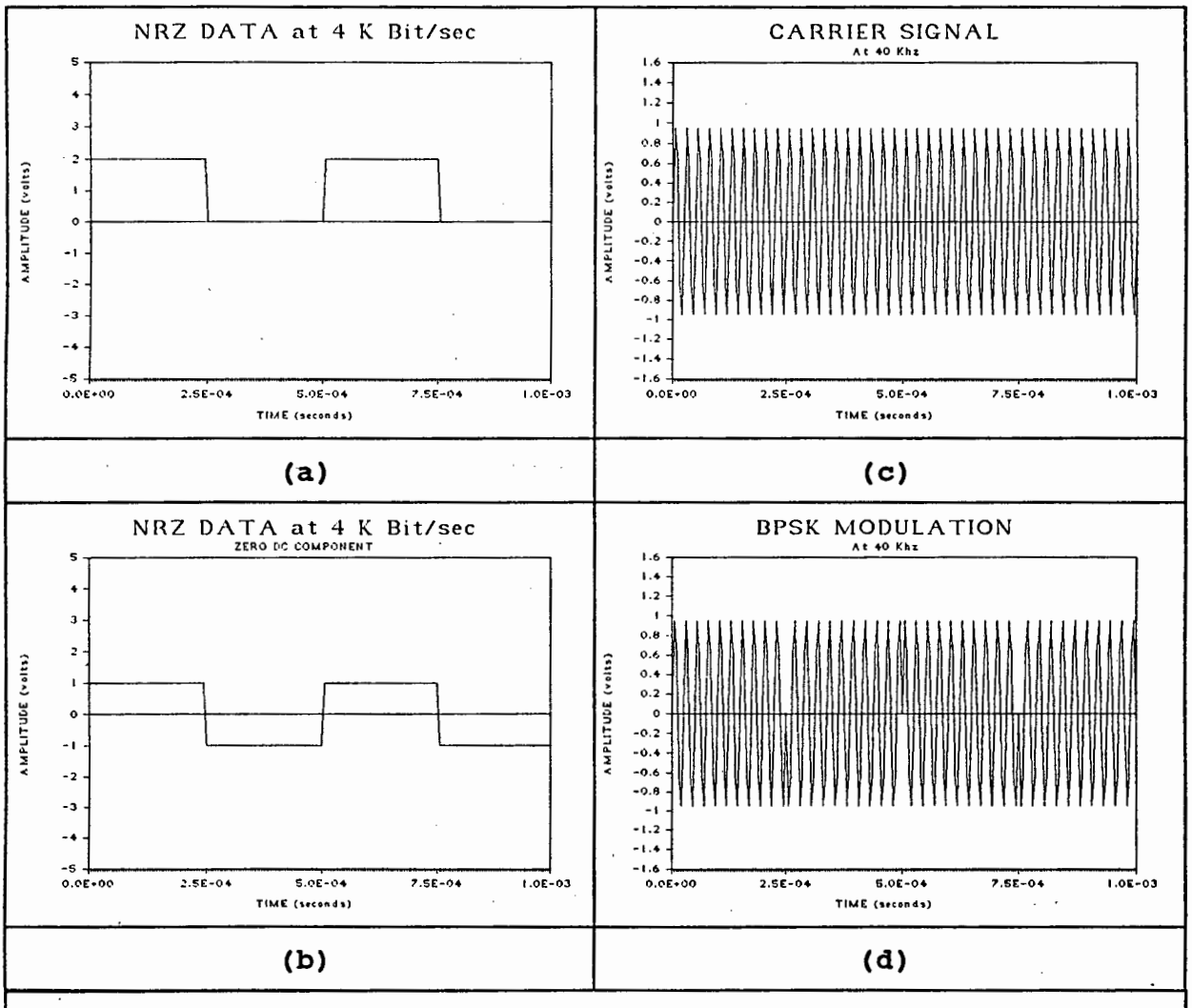

Figure 3.5: *(a) NRZ data at 4 K bit/sec. (b) NRZ data at 4 K bit/sec, no dc component. (c) Carrier signal at 25 KHz. (d) BPSK modulated carrier with 180° phase changes.*

For coherent demodulation a carrier frequency that is synchronised with the received modulated wave is required as shown in Fig 3.4 (b). A carrier recovery system is required to provide the receiver-multiplier with a sinusoidal frequency that has exactly the same phase and frequency as the transmitted unmodulated carrier wave. The received modulated carrier s(t) is multiplied by the coherent oscillator, $c(t) = K\cos(\omega_o t + \theta_o)$, followed by a low pass filter. In PSK systems the information is contained in the phase of the carrier signal. The output of the multiplier is given by

$$\begin{aligned} p(t) &= s(t)\cdot K\cos(\omega_o t + \theta_o) \\ &= ACKm(t)\cos(\omega_c t + \theta)\cdot\cos(\omega_o t + \theta_o) \end{aligned} \quad (3.8)$$

θ is the initial phase. Using a trigonometric identity:

$$p(t) = \frac{1}{2}\overline{K}m(t)\left[\cos\left((\omega_c - \omega_o)t + \theta - \theta_o\right) + \frac{1}{2}\cos\left((\omega_c + \omega_o)t + \theta + \theta_o\right)\right] \quad (3.9)$$

The receive low-pass filter removes the double frequency spectral component at $\omega_c + \omega_o$ $rad/\sec$. At the threshold comparator input, we have:

$$q(t) = \frac{1}{2}\hat{m}(t)\overline{K}K_f\cos(\Phi(t)) = K\cdot\hat{m}(t) \quad (3.10)$$

if $\Phi(t) = (\omega_c - \omega_o)t + \theta - \theta_o = 0$, also $K = \overline{K}K_f/2$, represents a constant gain, while $\hat{m}(t)$ is the time-variable bandlimited baseband signal.

A threshold comparator makes a decision as to whether the recovered bit is a 'one' or a 'zero' ($+K$; $-K$ volts respectively) and provides a digital output. The bit timing recovery circuit recovers the bit clock from this recovered data.

3.5 DIFFERENTIALLY ENCODED BINARY PHASE SHIFT KEYING

Most practical carrier-recovery circuits introduce a *phase ambiguity* into the recovered carrier. In binary PSK demodulators the recovered carrier is not necessarily the required $\cos(w_c t)$ signal; it might equal $\cos(w_c t)$ or $\cos(w_c t + 180^o)$. Thus a steady 180^o phase error in the recovered carrier is possible. The error inverts the demodulated data stream and causes a 100% error rate. Fortunately, the insertion of a simple differential encoder into the transmitter and a differential decoder into the receiver avoids errors that could be introduced by this phase ambiguity.

This modification to BPSK is called Differential Binary PSK (DBPSK) or Differentially Encoded - Binary PSK (DE-BPSK). This process effectively transfers the bit level information into the bit edges, so that if a 180^o phase **transition** occurs at the receiver it is decoded as a binary *one* and if no phase transition occurs (0^o phase shift) then a binary *zero* is decoded. A differentially encoded bit stream is shown below in Fig. 3.6. In generation of a differentially encoded bit, d_k, of an encoded sequence $\{d_k\}$, the present bit, b_k, of the original message sequence $\{b_k\}$ and the previous bit, d_{k-1}, are compared. If there is no difference between b_k and d_{k-1}, then $d_k = 0$; otherwise, $d_k = 1$. This can be expressed as:

$$d_k = b_k \oplus d_{k-1} = \overline{b_k} \cdot d_{k-1} + b_k \cdot \overline{d_{k-1}} \qquad (3.11)$$

Follow the arrows in Fig.3.6 using equation 3.11 and the code can be generated. Using the same process again on the encoded stream yields the original bit stream. From now on, the terms BPSK, QPSK and MSK, are generic and it is assumed that differential coding is used in all cases.

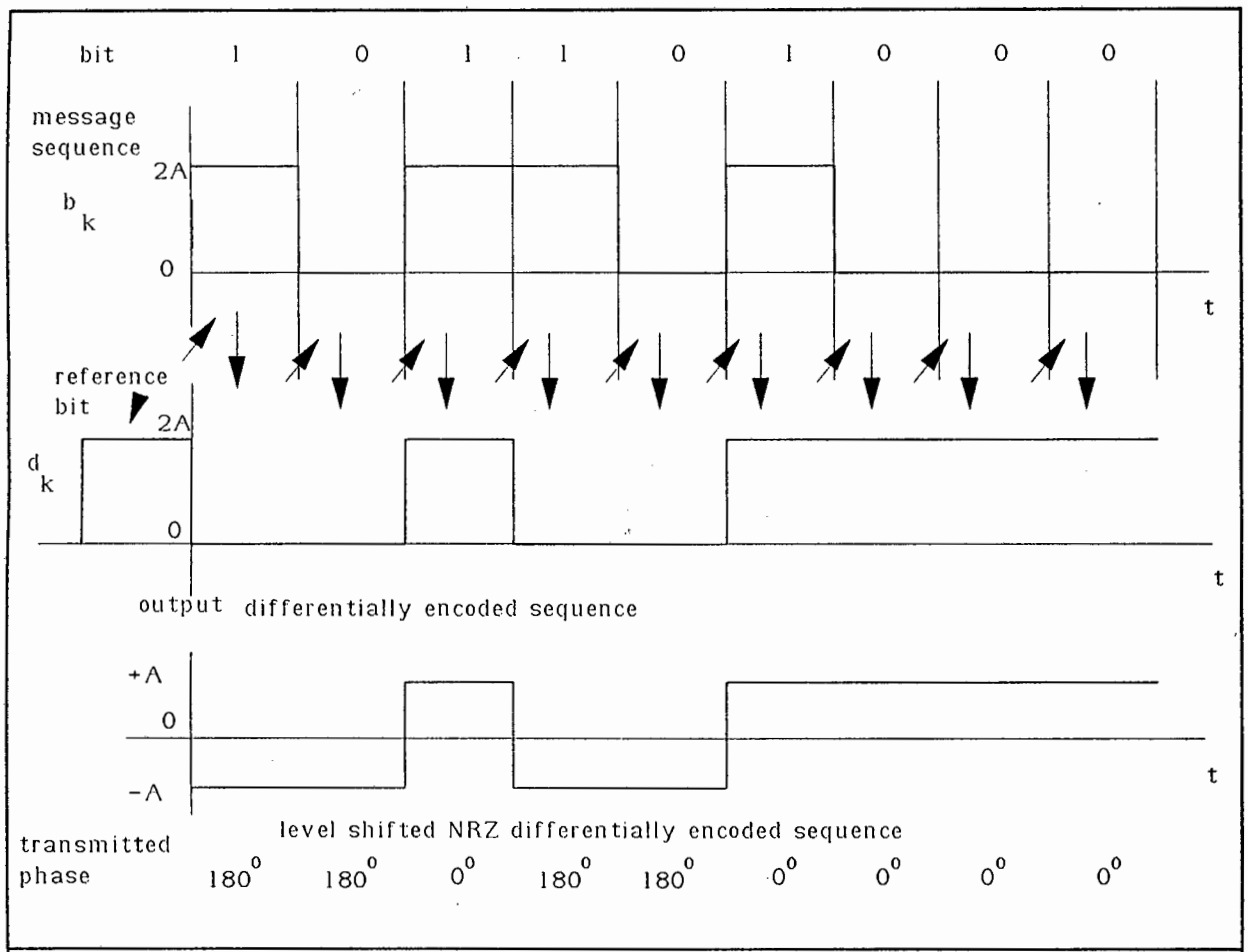

FIGURE 3.6 : *An explanation of Differential Encoding*

3.6 SPECTRUM OF BPSK SYSTEMS

The spectral density $w_S(f)$ of equiprobable non-return-to-zero (NRZ) signals was derived in section 3.3.1 (see equation 3.4). In binary systems the bit duration equals the symbol duration ($T_b = T_S$). From section 3.4 polar NRZ modulating a carrier gives a BPSK signal which is equivalent to a DSB-SC modulator. Thus the baseband spectrum is translated so as to be centered around the carrier frequency, f_c. It is given by:

$$\omega_s(f) = 2KA^2T_b\left[\frac{\sin(\pi(f-f_c)T_s)}{\pi(f-f_c)T_s}\right]^2 \qquad (3.12)$$

Where K is the proportionality constant of the multiplier. The unfiltered (infinite bandwidth) modulated spectra is shown in

Fig. 3.7. Notice that BPSK is a suppressed carrier modulation scheme and no discrete component exists at the carrier frequency. Also notice the spectral nulls at the integer multiples of the bit rate frequency. For a bit rate of $f_b = f_s =$ 4 Kbit/sec, these nulls occur at frequencies of $\mathbf{f_n = f_c +/- n.4}$ **Khz**, where n = 1,2,3,4,etc. Differential encoding has no effect on the frequency spectrum.

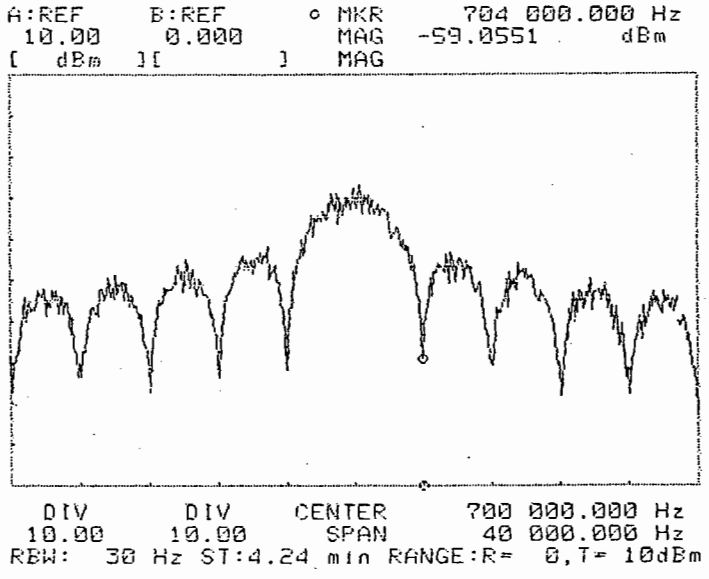

Figure 3.7 : *Spectrum of BPSK modulation at 700 KHz.*

3.7 OPTIMUM RECEIVER FOR BINARY DIGITAL MODULATION SYSTEMS

In this section, the optimum receiver for general binary digital transmission systems is stated. A receiver is said to be optimum if it yields the minimum probability of error, $\mathbf{P_e}$, for a given **S/N**. It is assumed that additive white Gaussian noise (AWGN) is the only system perturbance, and that the bandwidth is not constrained; that is, an infinite bandwidth intersymbol-interference-free channel is available. The system model used as well as the derivation for the optimum receiver is given in appendix G and has been taken from [3.1].

The optimum receiver is found by first expressing the probability of error in terms of the signal-to-noise ratio, and

then minimising the probability of error, by maximising the signal-to-noise ratio at the receiver output. The probability of error at the output of the receiver as derived in appendix G, as equation G-4 is re-stated here:

$$P_e = 0.5\,erfc\left[\frac{s_{o2}(T_b) - s_{o1}(T_b)}{2\sqrt{2}\sigma_o}\right] \qquad (3.13)$$

Where erfc(y) is defined by

$$erfc(y) = \frac{2}{\sqrt{\pi}}\int_y^\infty e^{-z^2}dz \qquad y > 0$$

and

$$N_T = \sigma_o^2 = \int_{-\infty}^{\infty} |H(f)|^2 G_n(f)df$$

is the total noise power (noise variance) at the receiver filter output.

$s_{o2}(T_b) - s_{o1}(T_b)$ is the output signal at the output of the receiver at the sampling instant, t = T_b.

From equation (3.13) it is concluded that the probability of error is a function of the difference (distance) between the two output signals in the sampling instant, **t = T_b** sec, and of the rms noise voltage σ_o. The error function erfc (y) decreases monotonically with y; thus the probability of error decreases with the increasing difference between the received sampled signals. Based on Schwartz's inequality and the additive white Gaussian noise assumption, **$G_n(f) = N_o/2$**, it is concluded in appendix G, that the signal-to noise ratio is maximised if

$$H(f) = mS_{od}^*(f)e^{-j2\pi T_b f}df$$

where **m** is a constant that represents the receiver filter gain. The gain constant of linear filters has evidently no influence

on the output signal-to-noise ratio and without loss of generality, set **m = 1**. The optimum receiver transfer function $\mathbf{H_o(f)}$ is thus given by

$$H_o(f) = S_{od}^*(f)e^{-j2\pi T_b f} \qquad (3.14)$$

By means of the inverse Fourier transform, the receiver impulse response corresponding to $\mathbf{H_o(f)}$ is

$$h_o(t) = \int_{-\infty}^{\infty} S_{od}(f)e^{j2\pi f(T_b - t)}df$$

$$= s_2(T_b - t) - s_1(T_b - t)$$

$$\Rightarrow h_o(t) = s(T_b - t) \qquad (3.15)$$

where

$$s(T_b - t) = s_2(T_b - t) - s_1(T_b - t)$$

Observe that $\mathbf{s_1(t)}$ and $\mathbf{s_2(t)}$ represent the transmitted signals at the modulator output. The result of equation (3.13) states that the impulse response of the optimal receiver equals the difference of the $\mathbf{T_b}$-second shifted time reverse of $\mathbf{s_1(t)}$ and $\mathbf{s_2(t)}$. In other words, the receiver is matched to the difference of the transmitted waveforms and therefore is known as a *matched filter* receiver. This difference is sampled and compared to the optimal threshold l_{opt}. An alternative optimal receiver structure is illustrated in Fig. 3.8. this is the *correlation receiver*. It is now shown that the correlation receiver and the matched filter are identical.

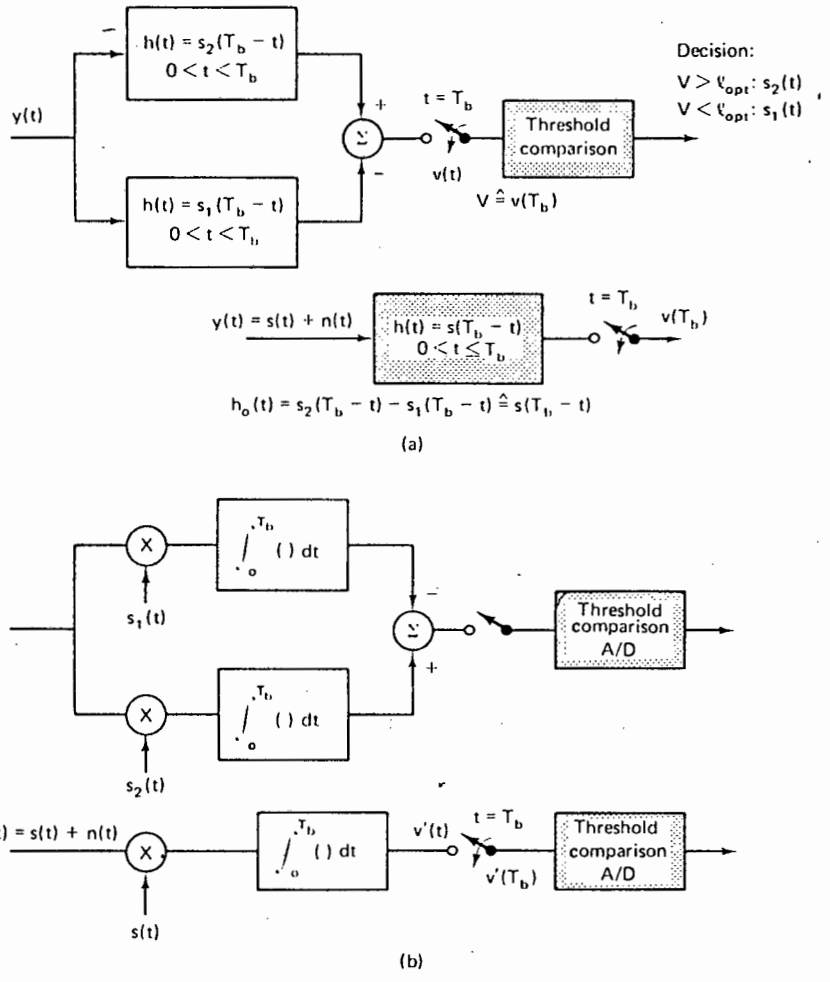

FIGURE 3.8 : *(a) matched filter receiver. (b) Its equivalent correlation receiver for binary signalling in white Gaussian noise. Note that s(t) is an infinite bandwidth modulated carrier [3.1].*

The output of the matched filter receiver is

$$v(t) = h(t) * y(t) = \int_0^{\infty} s(T_b - \tau) y(t - \tau) d\tau$$

$$= \int_0^{T_b} s(T_b - \tau) y(t - \tau) d\tau$$

since

$$h(t) = \begin{matrix} s\ (T_b - t) & 0 \le t \le T_b \\ 0 & elsewhere \end{matrix}$$

Let **t = T_b** and change variables to $\alpha = T_b - \tau$, which gives

$$v(T_b) = \int_0^{T_b} s(\alpha) y(\alpha) d\alpha$$

The output of the correlator at the sampling instant, t = T_b, is obtained by inspection of Fig.3.8 , it is

$$v'(T_b) = \int_0^{T_b} s(t) y(t) dt$$

Observe that $v(T_b) = v'(T_b)$, the output of the matched filter and correlator receiver are identical at the sampling instant, t = T_b sec. The value of the sampled output is compared to the threshold level; thus for the equivalence condition it is sufficient to have equal output values at the sampling instant.

When non bandlimited sinusoidal carriers are transmitted, i.e. 100% of the signal energy, the correlation receiver (matched filter) can be implemented by an integrator and a sampler, after demodulation by multiplication. The impulse response of an ideal integrator is a rectangular pulse of duration **T** sec, where **T** can be set by an output dump at **T_b** sec.

This integrate and dump receiver is only an optimal receiver if an infinite bandwidth sinusoidal carrier reaches the receiver input. If any bandlimiting occurs either by the transmitter or by the channel, then this receiver is no longer optimal and the receive filter must be re-matched to the transmitted signal shape. If 100 % of the energy is transmitted and a non-matched filter is used, the recovered data will be impaired by either ISI or by noise or both. A discussion of non-ideal filtering of BPSK is given in the following sub-sections.

3.7.1 PERFORMANCE OF THE OPTIMAL RECEIVER

Recall that the probability of error performance, P_e, of a coherently demodulated DEBPSK signal was illustrated in Fig.(3.1) as a function of E_b/N_o. The curve represents the performance of the optimal system using a matched filter receiver and is derived in appendix G. It does not take into account practical imperfections associated with receivers, such as phase jitter. These problems are dealt with in chapter five. The ideal probability of error of a BPSK waveform (no differential encoding) for a receiver, in the presence of white Gaussian noise, as given by G-4 in appendix G is stated here as

$$P_e = \frac{1}{2} erfc(\gamma)$$

Where

$$\gamma = \frac{s_{o2}(T_b) - s_{o1}(T_b)}{2\sqrt{2}\sigma_o}$$

and in the case of the matched filter, the maximum value given by

$$\gamma = \sqrt{\frac{2}{N_o}\int_{-\infty}^{\infty} |S_{od}(f)|^2 df}$$

Recall $s_{od}(t) = s_2(t) - s_1(t)$ and using Parsevals' theorem

$$\gamma^2 = \frac{2}{N_o}\int_{-\infty}^{\infty} [s_2(t) - s_1(t)]^2 dt$$

$$= \frac{2}{N_o}\left(2E_b - 2\sqrt{E_{1b}E_{2b}}\rho_{12}\right)$$

Assuming that the signals are equiprobable, the average

received signal energy, measured in a T_b-second interval is

$$E_b = E_{av} = \frac{1}{2}\left(E_{1b} + E_{2b}\right)$$

and $E_{1b} = E_{2b}$. Eb and E_{av} are the average signal energy of the received signal, stated in appendix G.

$$\rho_{12} = \frac{1}{\sqrt{E_1 E_2}} \int_{-\infty}^{\infty} s_1(t) s_2(t) dt \qquad -1 \le \rho_{12} \le 1$$

is the normalised finite time correlation coefficient of the two waveforms. E_1 and E_2 represent the energy of the transmitted signals, $s_1(t)$ and $s_2(t)$ measured in a T_b duration interval. The correlation coefficient ρ_{12} represents a measure of similarity between the two signals $s_1(t)$ and $s_2(t)$. For antipodal signalling (BPSK) the two signals are exactly dissimilar and $\rho = -1$. The probability of error for straight BPSK is,

$$P_e = \frac{1}{2} erfc \sqrt{\frac{E_{avb}}{N_o}} \qquad (3.16)$$

3.7.2 PERFORMANCE OF A SUB OPTIMAL RECEIVER

In this example a second order Butterworth filter has been studied. The reasons will become clear in chapter 4. Equation G-4 of appendix G gives the general statement of the probability of error of a system with added white Gaussian noise. Restated as

$$P_e = 0.5 erfc\left[\frac{s_{o2}(T_b) - s_{o1}(T_b)}{2\sqrt{2}\sigma_o}\right] \qquad (3.17)$$

This can be applied to a Butterworth filter. The corresponding signal output, $s_o(t)$ and noise output, σ_o of the filter must be determined.

When using a second order Butterworth filter after a multiplier in a synchronous detector, as shown in Fig. (3.9), the performance of the correlator receiver is degraded from that of the optimum receiver for two reasons:

Firstly, the ratio of peak signal to root-mean-square (rms) noise at the output of a non-optimum detection filter will not be the theoretically maximum value, which is $\mathbf{2E/N_o}$ for a filter matched to the signal, **E** being the signal energy and $\mathbf{N_o/2}$ the noise power spectral density.

Secondly, a sub-optimum filter will introduce intersymbol interference from one symbol period to succeeding symbol periods because of its transient response. The step response of the second order Butterworth filter is found using the following technique:

The transfer function of the second order, Butterworth filter is given as:

$$T(s) = \frac{1}{s^2 + \sqrt{2}s + 1} \qquad (3.18)$$

This is a normalised transfer function, to de-normalize to a - 3dB frequency of $\mathbf{f_{-3dB}}$ = 4 kHz, substitute for **s**:

$$s = \frac{s}{2 \cdot \pi \cdot 4000}$$

The result is

$$T(s) = \frac{V_{out}(s)}{V_i(s)} = \frac{(8000\pi)^2}{s^2 + \sqrt{2}(8000\pi)s + 8000\pi^2} \qquad (3.19)$$

$V_{out}(s)$ is calculated for a step response, $v_{in}(t) = A.u(t)$, or $V_{in}(s) = \frac{A}{s}$

. Assuming all initial conditions to be zero, $V_o(s)$ is then determined using a partial fraction expansion of $V_o(s)$ and then finally performing an inverse Laplace Transform to give:

$$v_{out}(t) = A\left[1 - \sqrt{2}e^{-\frac{t}{\sqrt{2}\tau}}\cos\left(\frac{t}{\sqrt{2}\tau} - \pi/4\right)\right]u(t) \qquad (3.20)$$

where $\tau = 1/(2\pi f_3)$. The step response is illustrated in figure 3.9. In this example, **T** is the bit period and **1/T** = f_C = 4 Khz is the -3dB frequency of the low pass filter. The sampling instant is at t = 0.25 m sec.

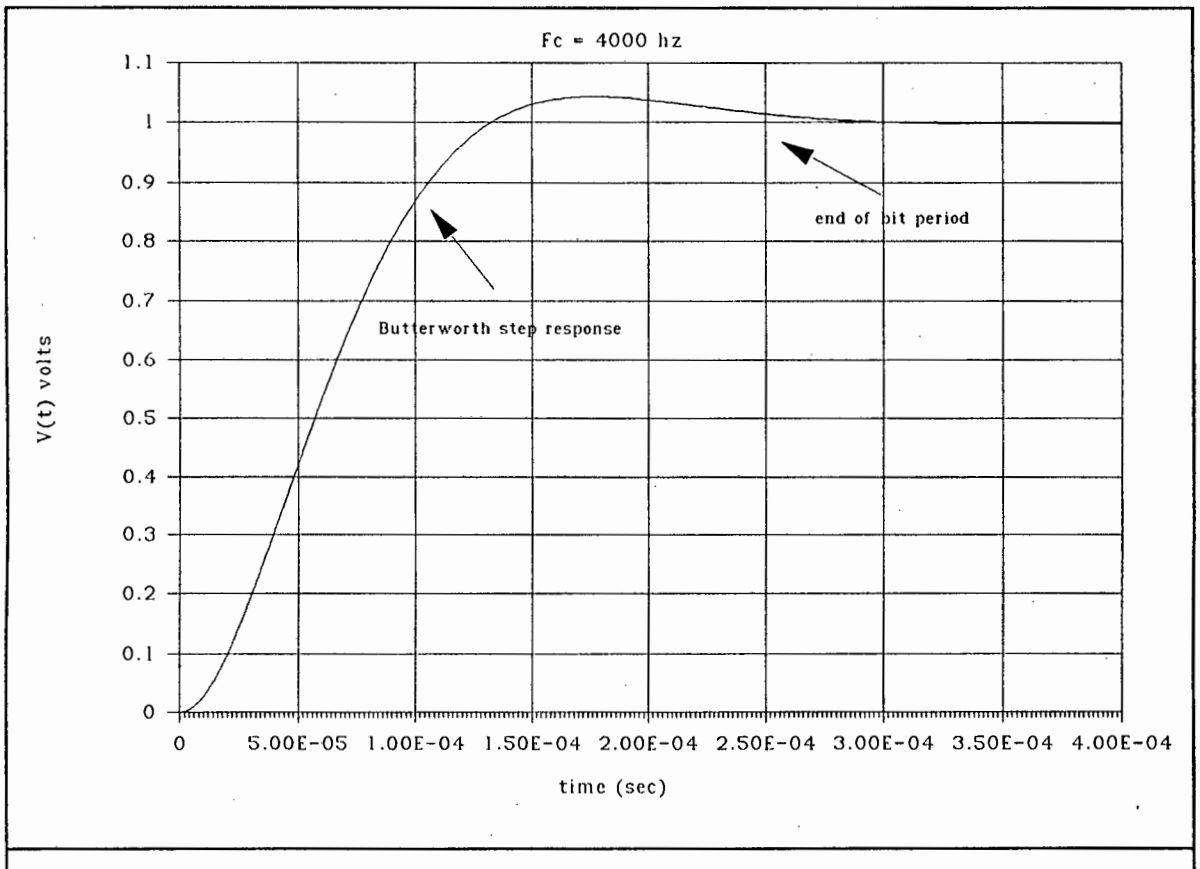

FIGURE 3.9 : *Step response of a second order Butterworth filter.*

From Fig. 3.9 the Butterworth response has settled to 98 % of its steady state value after **T** sec and after **2T** seconds to 100 %. Therefore, the effect of intersymbol interference only

between two successive bits will be analysed. It is assumed that the intersymbol interference on successive bits after two bits is negligible.

Consider the response of the filter to four possible 2-bit sequences (1) one-one, (2) one-zero, (3) zero-one, and (4) zero-zero, being $v_a(t)$, $v_b(t)$, $v_c(t)$ and $v_d(t)$, respectively. The signal component at the output of the detection filter at the end of the second bit interval, t = 2T sec, for the first input sequence is:

$$v_a(2T) = A\left[1 - \sqrt{2}Ae^{-2\frac{T}{\sqrt{2}\tau}}\cos\left(\left(2\frac{T}{\sqrt{2}\tau}\right) - \pi/4\right)\right] \qquad (3.21)$$

Similarly expressions are obtained for $v_b(2T)$, $v_c(2T)$ and $v_d(2T)$. Note that

$$v_c(2T) = -v_b(2T)$$
$$v_d(2T) = -v_a(2T)$$

The probability of error given any data sequence, is [2.6]

$$P(\epsilon \backslash a) = Q\left[\sqrt{\frac{|v(2T)|^2}{\sigma_N^2}}\right] \qquad (3.22)$$

Where Q[.] is defined by $erfc(x) = 2Q(\sqrt{2}x)$ as given in appendix G and σ_N is the variance of the noise component at the detection filter output. Equation (3.22) can be derived by integrating the probability density function of the low pass filter output at time t = 2T from $-\infty$ to 0.

The variance of the noise at the filter output is given by

$$\sigma_N^2 = B_N N_o$$

$$= \left(\sqrt{2}\frac{\pi}{4}\right) f_3 N_o$$

$$= \frac{\sqrt{2}N_o}{8}\frac{}{\tau} \qquad (3.23)$$

Where:

$$B_N = \frac{\pi/4}{\sin(\pi/4)} = \frac{\sqrt{2}\pi}{4}$$

is the noise equivalent bandwidth of the second order Butterworth filter explained in appendix A.

For the first data sequence the probability of error is found by substituting equations 3.21 and 3.23 into 3.22 which gives

$$P(e\backslash a) = Q\left[\sqrt{\left(\frac{8}{\sqrt{2}}\frac{\tau}{N_o}\right)\left[A\left(1-\sqrt{2}e^{-\sqrt{2}\frac{T}{\tau}}\cos\left(\left(\sqrt{2}\frac{T}{\tau}\right)-\pi/4\right)\right)\right]^2}\right] \qquad (3.22)$$

P_e can be written in terms of τ/T and $\mathbf{E_b/N_o} = \mathbf{(A^2T / N_o)}$, writing $\mathbf{E_b/N_o}$ in terms of the matched filter.

$$P(e\backslash a) = Q\left[4\sqrt{\frac{2}{1}}\sqrt{\frac{\tau}{T}}\sqrt{\frac{E_b}{N_o}}\left[1-\sqrt{2}e^{-\sqrt{2}\frac{T}{\tau}}\cos\left(\left(\sqrt{2}\frac{T}{\tau}\right)-\pi/4\right)\right]\right] \qquad (3.23)$$

With an identical result for $P(e\backslash d)$. Similarly, $P(e\backslash b)$ and $P(e\backslash c)$ can be derived and $P(e\backslash b) = P(e\backslash c)$.

Assuming the sequence (1),(2),(3) and (4) to be equally probable, the average probability of error is

$$P(e) = \frac{1}{4}[P(e\backslash a) + P(e\backslash b) + P(e\backslash c) + P(e\backslash a)P(e\backslash d)]$$

$$= \frac{1}{2}[P(e\backslash a) + P(e\backslash b)]$$

The complete probability of error has been calculated [3.8], the results of which are illustrated by the curves of Fig. 3.10.

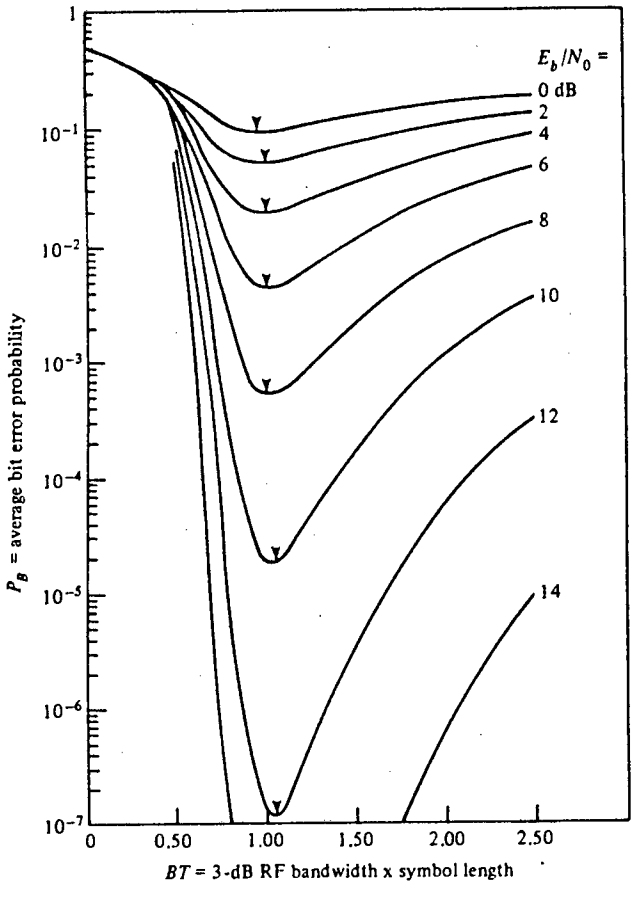

FIGURE 3.10 : *Two pole Butterworth data filter detection of coherent BPSK [3.8].*

Figure 3.10 shows the average probability of error versus BT product, where B is the two sided or RF equivalent detection filter bandwidth, with E_b/N_o as a parameter for a double pole Butterworth filter. For the one-sided baseband filter f_{-3dB} = 1/2 B. The optimum BT is $BT \approx 1.1$, where T is the symbol duration, or $f_{-3dB}T \approx 0.6$.. Since BT is weakly dependent on Eb/No, this is taken as being the best value for BT. From reference [2.6 chap. 3], the amount of out of band energy of an NRZ signal is 10 % where $f_{-3dB}T = 1$ and 1 % where $f_{-3dB}T = 5$.

3.7.3 THE EFFECT OF DIFFERENTIAL ENCODING [3.1]

When using a differentially encoded baseband data stream, two bits (symbol intervals) are involved in a differential

decoder, the decoding function degrades overall error probability, because, a decision made on a current bit depends on the decision made on the previous bit, so that if the previous bit was an error, then the current bit will be wrong.

Consider the decoder. First, suppose the currently arriving bit is correct; an error is made only if the adjacent earlier bit was in error. The probability of this joint event occurring is $P_e(1-P_e)$. Next, suppose the current bit is in error; the output is in error only if the adjacent earlier bit is correct (both bits in error will result in a correct output). Again this joint event has probability $P_e(1-P_e)$. The overall probability of a decoded bit being in error, as the sum of these two probabilities, denoted by $P_{e(diff)}$, is

$$P_{e(diff)} = 2\ P_e(1-P_e)$$

If P_e is small,

$$P_{e(diff)} \approx 2\ P_e$$

The approximate effect of differentially encoding data in a DEBPSK system is therefore, a doubling of the probability of bit errors. This increase in error probability is considered small in this application and the advantages of differentially encoded data more than justify its use. The P_e for DEBPSK as illustrated in Fig. 3.1 is given here as:

$$P_e \approx erfc\sqrt{\frac{E_{avb}}{N_o}}$$

3.8 ALTERNATIVE MODULATION SCHEMES

The alternative power efficient modulation schemes that are available for use on the Meteor Scatter channel are Quadrature Phase Shift Keying (QPSK), Offset QPSK and Minimum Shift Keying (MSK). All three schemes, namely; QPSK, OQPSK and MSK are digital phase modulation schemes. They each modulate the phase in a different way. The general carrier waveform that fits all schemes is written:

$$s(t) = A\cos\left[2\pi f_o t + \phi(t) + \theta\right] \qquad (3.24)$$

Where $\phi(t)$ is the modulation and θ is the initial phase of the system.

The baseband equivalent power spectra of the four schemes are compared in Fig. 3.11 . It can be observed that the advantage of using MSK and QPSK over BPSK is a doubling in the spectral efficiency, which enables the transmission of double the bit rate in the same bandwidth. Also the main sidelobe has more of the total energy, which gives a more compact spectrum.

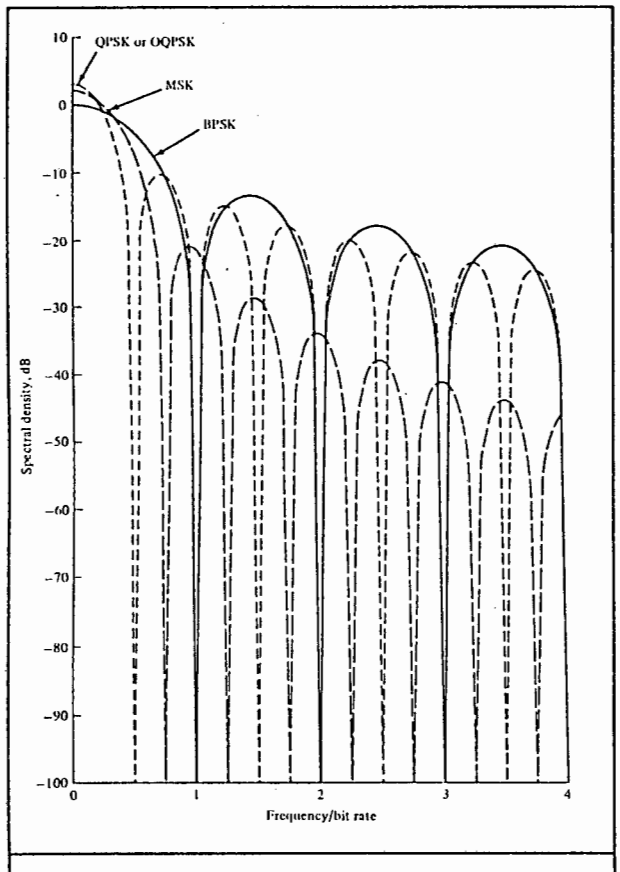

FIGURE 3.11 : *Baseband equivalent power spectra for BPSK, QPSK or O-QPSK and MSK [2.6].*

3.8.1 QPSK, OQPSK

Consider two data-bearing signals, $m_1(t)$ and $m_2(t)$ which are to be modulated. These data signals can be independent of

each other or can be derived from a single data stream. Using two carriers, with a quadrature phase relationship, the transmitted signal is:

$$s(t) = A_1 m_1(t)\cos(2\pi f_o t + \theta) + A_2 m_2(t)\sin(2\pi f_o t + \theta)$$

In a binary system $m_1(t) = m_2(t) = +/- 1$. The block diagram of the modulator and demodulator for such a scheme is shown in Fig. 3.12 (a). The input data is shown having a bit period T_b sec. which is split into two parallel symbol streams each of period $T_s = 2.T_b$ sec. Shown in Fig. 3.12 (b).

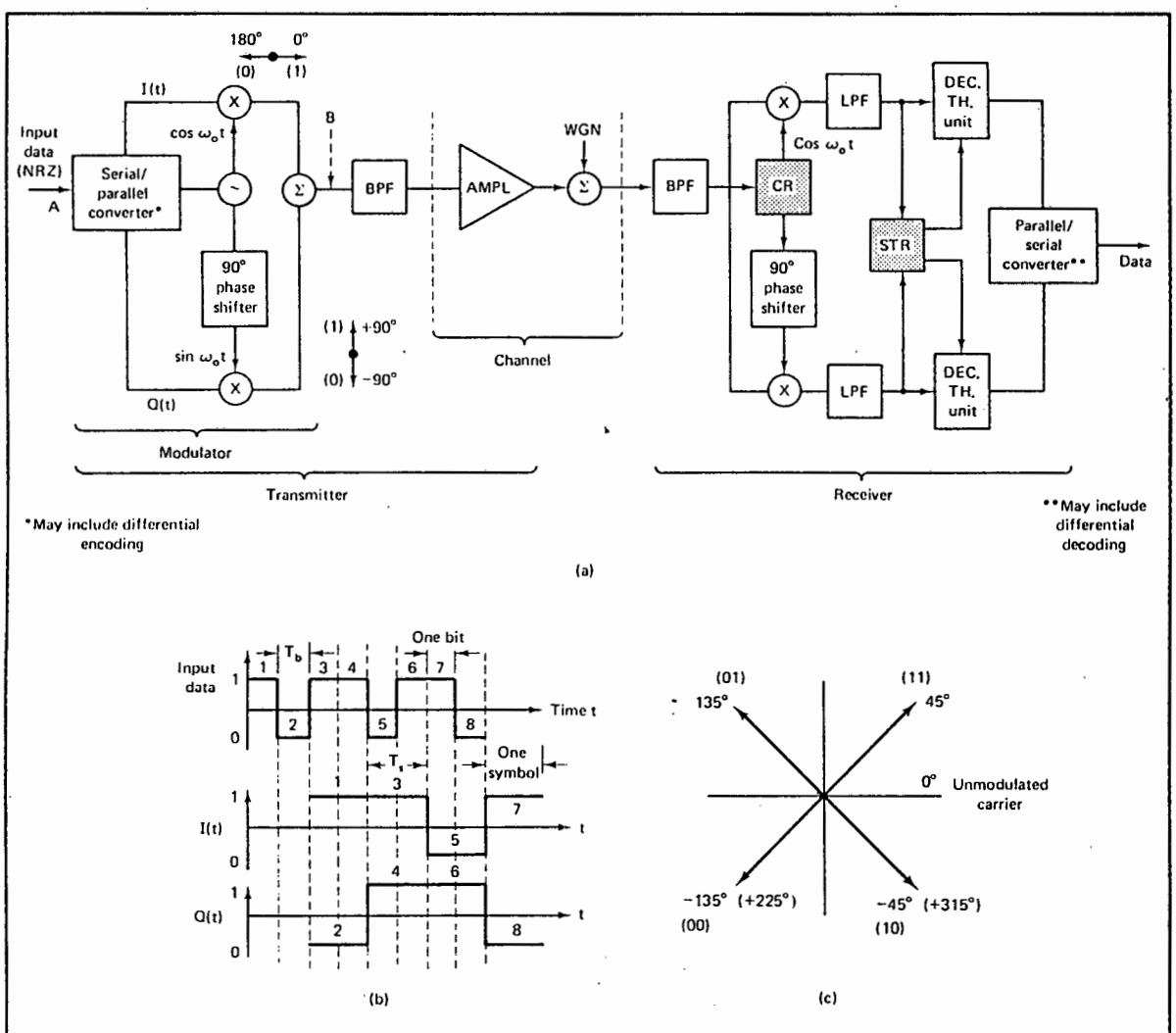

FIGURE 3.12 : *QPSK system representation. (a) Block diagram of modulator and demodulator. (b) Modulator data streams.* **(c)** Constellation diagram [3.1].

The carrier can be written as

$$s(t) = A\cos(2\pi f t + \phi(t) + \theta)$$

Where :

$$\phi(t) = arctan\left(\frac{-A_2 m_2(t)}{A_1 m_1(t)}\right)$$

$$A = \sqrt{A_1^2 + A_2^2}$$

s(t) is in effect a constant amplitude digitally phase-modulated signal like BPSK. The corresponding constellation diagram of signal vectors is shown in figure 3.12 (c) for m_1 and m_2 binary values. The phase deviations take place on the values:

$$\phi(t) = +atan(A_2/A_1) \qquad +atan(A_2/A_1) + \pi$$
$$-atan(A_2/A_1) \qquad -atan(A_2/A_1) + \pi$$

If one of the data stream $m_1(t)$ or $m_2(t)$ is delayed by T/2 sec. before multiplication then no 180^o phase changes can occur in the final modulated carrier, and only 90^o phase changes between states are possible. This is offset QPSK (OQPSK) having the identical power spectra to that of QPSK. However, experiments have shown that the envelope of OQPSK tends to remain more constant when the waveform is bandpass filtered. Thus it is preferable to use OQPSK in applications where significant bandlimiting is required. A OQPSK waveform is less susceptible to the nonlinear effects of a power amplifier operating in saturation, including spectrum re-spreading.[2.6]

3.8.2 ERROR PERFORMANCE OF QPSK (OPTIMAL RECEIVER) [3.1]

This analysis is done to compare the usefulness of QPSK over BPSK, by comparing the error performance of BPSK from section 3.7.1 to the error performance of QPSK which will be described here. The performance derived here is based on the theoretical coherent demodulator model of Fig. 3.12 (a). Two performance derivations are presented. In the first, somewhat

heuristic derivation, we use the result obtained for BPSK modems, presented in section 3.7.1. Here a relationship between the probability of bit error and the probability of symbol error, is also derived.

1. Heuristic Derivation for Coherent QPSK Systems.

From an examination of the block diagram of the coherent QPSK demodulator, Fig. 3.11, we can conclude that the P_e performance of the in-phase, I, and quadrature-phase, Q, channels is independent and that in a symmetrical bandpass channel the performance of these orthogonal channels is identical.

We designate the probability of error of the in-phase BPSK demodulator (upper path) as $\mathbf{P}_{eI}$ and of the quadrature-phase (lower path) as $\mathbf{P}_{eQ}$. The average probability of correct symbol reception, $\mathbf{P}_C$, at the QPSK receiver output equals the product of $\mathbf{P}_{CI}$,$\mathbf{P}_{CQ}$, where $\mathbf{P}_{CI}$ and $\mathbf{P}_{CQ}$ represent the independent correct decision probabilities of the I and Q binary PSK demodulators, respectively. Thus we have

$$P_C = (1 - P_{eI})(1 - P_{eQ})$$

The corresponding QPSK symbol error rate is

$$P_e = 1 - P_C = P_{eI} + P_{eQ} - P_{eI} P_{eQ}$$

Since PeI = PeQ and PeI and PeQ are typically small quantities ($< 10^{-2}$), we obtain a good approximation for the overall probability of symbol error of the QPSK demodulator. It is given by

$$P_E \approx P_{eI} + P_{eQ} = 2P_{eI} = 2P_{eQ}$$

The probability of error of the individual BPSK demodulators is

$$P_{eI} = P_{eQ} = \frac{1}{2} erfc\left(\sqrt{\frac{E_b}{N_o}}\right) = P_{eBPSK}$$

Finally, the probability of symbol error, $P_{E,QPSK}$ of the coherent QPSK receiver is

$$P_{EQPSK} = 2P_{eI} = erfc\left(\sqrt{\frac{E_b}{N_o}}\right)$$

where

$$erfc(y) = \frac{2}{\sqrt{\pi}} \int_y^{\infty} e^{-z^2} dz \qquad for\, y > 0$$

Assuming that the system parameter $\mathbf{E_b/N_O}$ is specified, the probability of symbol error of the QPSK system is twice that of the BPSK system. This corresponds to an increased $\mathbf{E_b/N_O}$ requirement of approximately 0.3 dB if the same symbol error rate as in BPSK systems is required.

The symbol error rate shown above is the combined symbol error rate of both channels. The *bit error rate* will be derived, which is the probability of an error on the recovered bits after having been combined in the parallel to serial convertor.

2. Relation of the Bit Error Rate ,P_{eQPSK}, to the Symbol Error Rate P_{EQPSK}

The Gray-coded and non-Gray-coded cases are illustrated in Fig. 3.13. In the Gray-coded "constellation," adjacent phase states or symbols differ by only one bit, whereas in the non-Gray-coded case the adjacent states differ by one or by two bits.

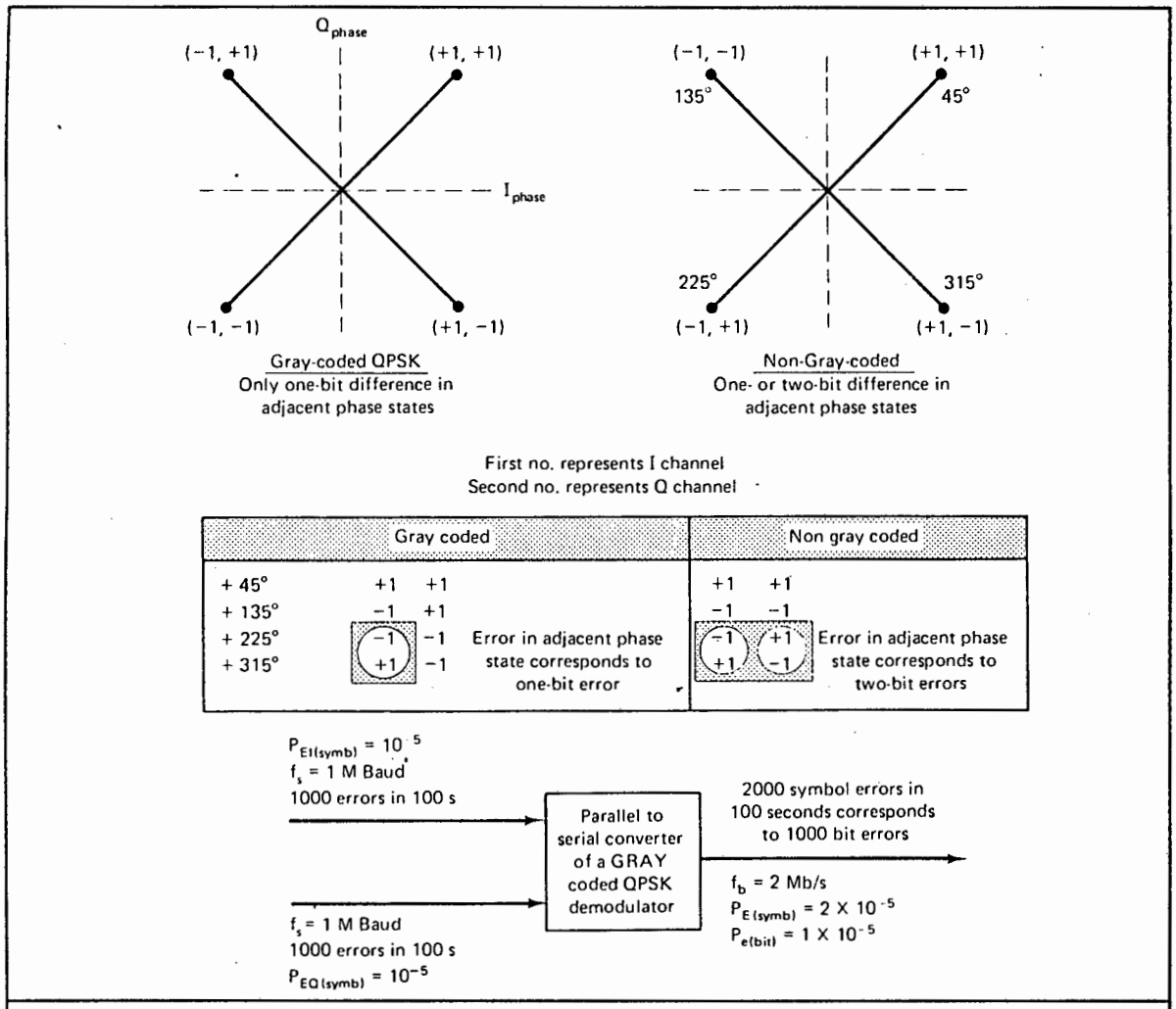

FIGURE 3.13 : *Bit error rate, P_e, and symbol error rate, P_E, relation in QPSK systems [3.1].*

Thus, in the Gray-coded signal constellation case, *one symbol error* corresponds to *one bit error*. In the non-Gray-coded case illustrated, an interchange of adjacent phase states corresponds, 50% of the time, to two bit errors. The **bit** error rate of the Gray-coded QPSK modem is therefore written,

$$P_{aQPSK} = \frac{1}{2} P_{EQPSK} = \frac{1}{2} erfc\left(\sqrt{\frac{E_b}{N_o}}\right)$$

The theoretical bit performance of coherent QPSK systems is illustrated in Fig. 3.1. Note that the bit error rate

performance of the Gray-coded QPSK and of the Gray-coded offset-keyed four phase OK-QPSK modems is identical with that of coherent BPSK modems.

3.9 SUMMARY OF MODULATION TECHNIQUES

To summarise the four power efficient modulation techniques discussed, DEBPSK is the simplest to implement. It requires half of the transmitter power that the other three schemes require because only a single carrier is used.

Gray-coded QPSK offers the most to a meteor scatter system, because it offers double the spectral efficiency to BPSK in the same noise environment.
The costs of a QPSK system over a BPSK system are:

1) Double the power is required to transmit another quadrature carrier over BPSK which uses only one carrier. However the time required to transmit a message is halved, therefore the power-per-bit required is the same.

2) Added system complexity means that the theoretical system performance will be more difficult to attain in practice compared with implementing a BPSK system.

The doubling of the bit rate allowed by a Gray-coded QPSK system means better utilisation of the meteor channel and double the throughput. However, for reasons of low system complexity, as well as keeping in line with previous trends of Meteor Scatter Systems, it has been decided to design an adaptive bit rate BPSK system. A QPSK system is an extension of a BPSK system and if the results of the modem are promising, then an extension to a QPSK system can be made.

MSK has been avoided because the spectral efficiency offered does not increase the allowable bit rate in the same noise environment compared with QPSK, but merely compacts the spectrum. This is only useful in a bandwidth restricted environment.

In the following discussion on incorporating an adaptive bit rate change technique into the modulation technique, QPSK is mentioned for the sake of comparison and discussion.

3.10 RATE CHANGE SIGNALLING

Besides the need for a power efficient modulation scheme the modem is required to adapt automatically to a rate change. In this regard, the transmitter must be able to change bit rate at any moment and the receiver must be able to *sense* the change in bit rate and adapt to it without loss of data. Two different concepts are discussed as solutions to this problem, namely :

1. Explicit rate detect - BPSK or QPSK using data channel (Time division multiplexed technique).

2. Explicit rate detect - BPSK or QSPK using auxiliary channel (Frequency division multiplexed technique).

An adaptive bit rate technique is required that will fit in with the modulation technique.

3.10.1 EXPLICIT SIGNALLING USING the DATA CHANNEL

An explicit system signals a warning of an impending rate change prior to the actual occurrence of the rate change. The demodulator can then switch filter bandwidth exactly as the bit rate changes, so that no bits are lost in the transition. This has been done by transmitting a frame in the data stream which tells the demodulator that a new bit rate will commence immediately after the frame ends [1.7]. The receiver is thus given warning of the rate change, and can switch receive filter bandwidth and clocking circuitry as soon as the rate change has occurred, shown in Fig. 3.14.

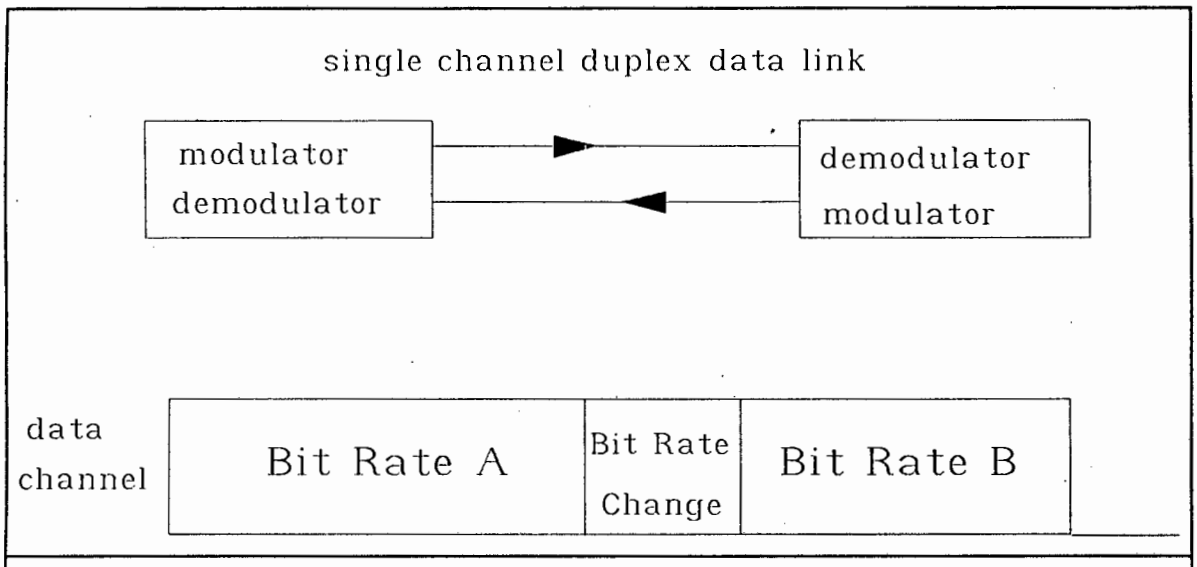

FIGURE 3.14 : *Explicit data rate change technique.*

This is a time-division multiplexed scheme, in which the data rate change signal is time division multiplexed with the data. The disadvantage of this system is that it requires the use of the data stream. This is undesired for two reasons; firstly, the amount of data that can be transmitted is limited on a meteor scatter channel by the short time given to transmit, and this frame could be used by data; secondly, microprocessor control is required to interpret this frame and control the modem and therefore the speed of response is determined by the speed and capabilities of the microprocessor.

One way of overcoming the wasted frames in such a TDM scheme is to increase bit rate to compensate for extra information. This may be done using Gray-coded QPSK where the spectral efficiency is double that of BPSK, thus transmitting at twice the bit rate, in the same bandwidth for the same P_e vs E_b/N_o environment. The cost is that an extra carrier added at the transmitter requires double the power to transmit.

3.10.2 EXPLICIT SIGNALLING USING an AUXILIARY CHANNEL

This is the system that has been pursued in this research. An auxiliary channel implies using a channel other than the data

channel to transmit information regarding an impending rate change prior to the occurrence of the rate change. The auxiliary channel is operated in parallel with the data so that the rate change command can be synchronised with the rate change, as indicated in Fig 3.15.

The demodulator can then switch to the new rate by switching data receive filter bandwidth as well as bit timing recovery circuitry to the new bit rate. This is to be done synchronously to eliminate the possible loss of data. The advantages of such a scheme over the previously mentioned idea is that:

1) The actual data-channel is not used for the transmission of this data-rate-control information, allowing the data-channel to be used for data only.

3) Synchronising the rate change can be done at the physical layer by switching filter bandwidths and timing circuitry without intervention by the data layer (host computer). This saves processor time.

This is a frequency multiplexed scheme. The auxiliary channel is either a carrier channel other than the main carrier or a baseband channel other than the data. Further discussion of this technique follows by considering QPSK and BPSK and frequency division multiplexing (FDM).

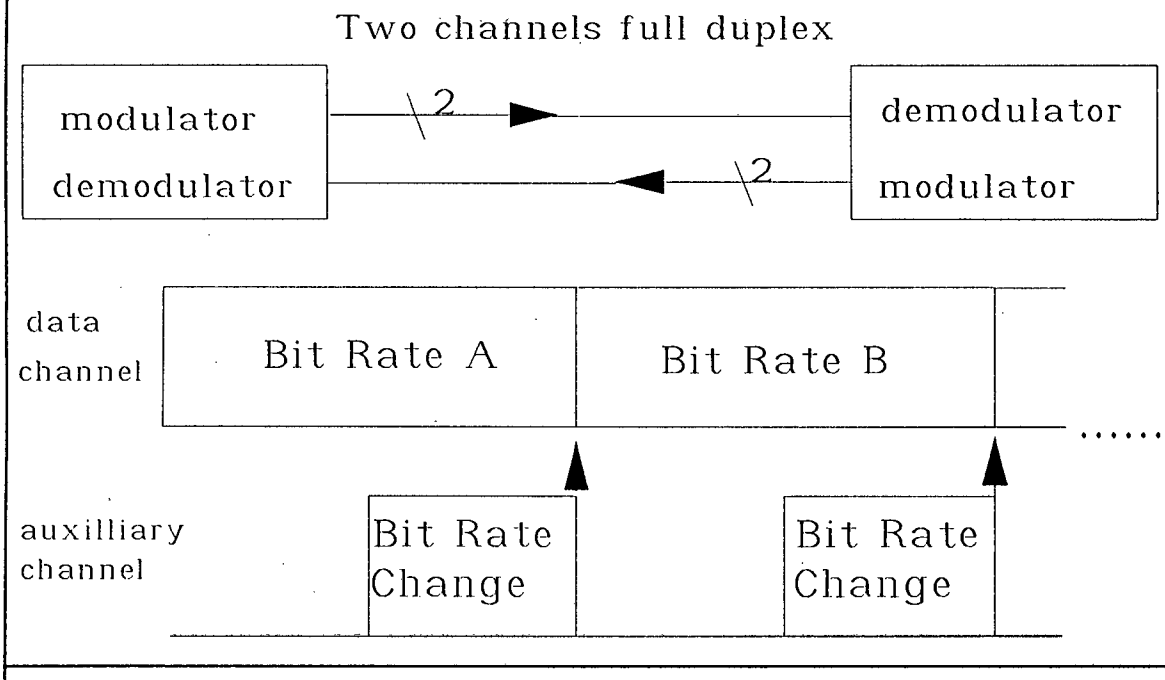

FIGURE 3.15 : *Explicit rate signalling using an auxiliary channel.*

3.10.2.1 QPSK WITH TWO INDEPENDENT CHANNELS

Quadrature Phase Shift Keying has been described before as the sum of two BPSK carriers modulated having a quadrature-phase relationship. When the two carriers are used to send one data stream the advantage is that the spectral efficiency is double that of using a single BPSK carrier or the same Pe vs E_b/N_o. This is obtained at the expense of added carrier power required.

Consider the case of using the one carrier for data and the other carrier for rate change data. The second data channel is only used to supervise the control of changing bit rates. The current bit rate can be continuously transmitted until there is a change of bit rate, in which case the supervisory information will warn the receiving modem before the change takes place.

This implies using the two channels as independent BPSK channels, in which case the spectral efficiency of each channel is identical to that of BPSK and extra power is only required when the quadrature channel is needed.

The probability of error of each channel as shown in section 3.8.2 is identical to the probability of error of a single BPSK channel. So that the two quadrature channels can be used as two separate BPSK channels operating in parallel.

This technique offers the best compromise of communicating both the data and the supervisory information on independent BPSK channels, simultaneously. The price is added complexity and increased transmit power required for transmission of a quadrature carrier. This technique has been avoided because the supervisory information is only needed for 10% of transmission time which does not justify the doubling in circuitry that is required.

3.10.2.2 BPSK OR QPSK WITH AN ADDED TONE

This is the technique that has been implemented using BPSK but would be suitable for a QPSK system as well. A modified Binary Phase Shift Keying modulator can be used to transmit the rate change information as well as the bit stream as follows.

Consider the spectrum of baseband NRZ (Fig. 3.3) and that of the BPSK modulated carrier (Fig. 3.8). It was shown that the baseband spectrum contains nulls at the frequency of the bit rate, $f = n.f_b$ ($n = 1,2,3,..$) or in the case of the modulated carrier, at frequencies of $f = f_c +/- n.f_b$. It is proposed that a tone be added at the first null of the baseband spectrum. This tone will convey the information regarding a bit rate change which is transmitted prior to the bit rate change. This is an FDM technique. The resulting spectrum of the baseband and the modulated carrier is shown in Fig. 3.16.

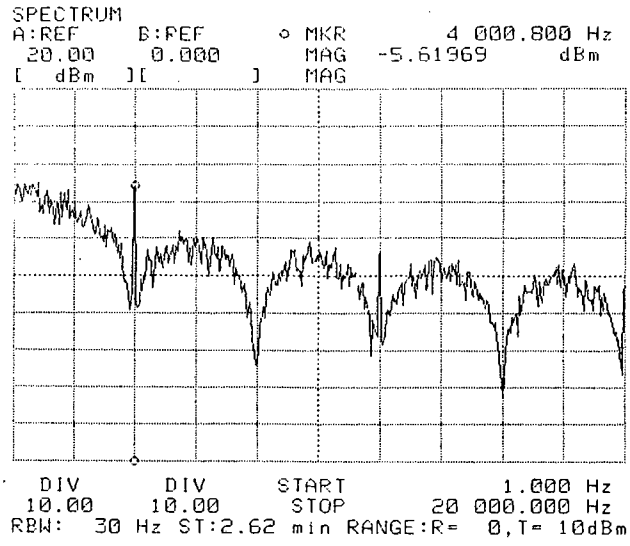

(a)

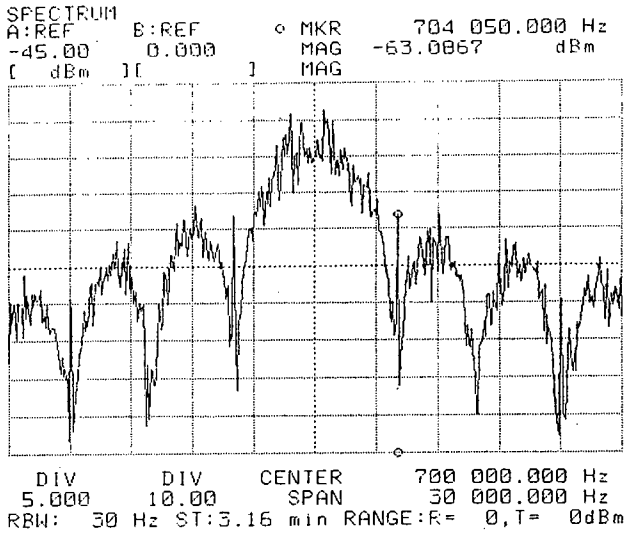

(b)

Figure 3.16 : *Spectrum of (a) baseband NRZ and (a) BPSK modulation with added clock.*

To derive an expression for the new modulated carrier. Let the clock be denoted by:

$$f_{CLK}(t) = \sin(\omega_m t)$$

The spectrum of this clock is a discrete component occurring at the frequency, $\omega = \pm\omega_m$ rad/sec. Adding this clock to the baseband spectrum and then modulating the result can be written in the time domain as:

$$V_o(t) = (\sin(\omega_m t) + m(t))\cos(\omega_c t) \qquad (3.25)$$

Alternatively;

$$V_o(t) = \sin(\omega_m t)\cos(\omega_c t) + m(t)\cos(\omega_o t) \qquad (3.26)$$

$$\Rightarrow V_o(t) = \left(\frac{1}{2}\right)(\sin((\omega_m + \omega_o)t) + \sin((\omega_m - \omega_o)t)) + m(t)\cos(\omega_o t) \quad (3.27)$$

$$\Rightarrow V_o(t) = \frac{1}{2}[\sin(\omega_m + \omega_o)t + \sin(\omega_m - \omega_c)t] + \cos(\omega_o t + \phi(t))$$

Where $\phi(t)$ is the phase angle of 0^o or 180^o introduced by the binary modulation. The baseband waveform is shown in Fig. 3.17 (a). The time domain representation of $V_o(t)$ is given in Fig. 3.17 (b). The carrier envelope is no longer constant but is the fluctuating shape of the added clock. Data information is now carried in the phase of the carrier while the bit rate information is in the phase of the envelope.

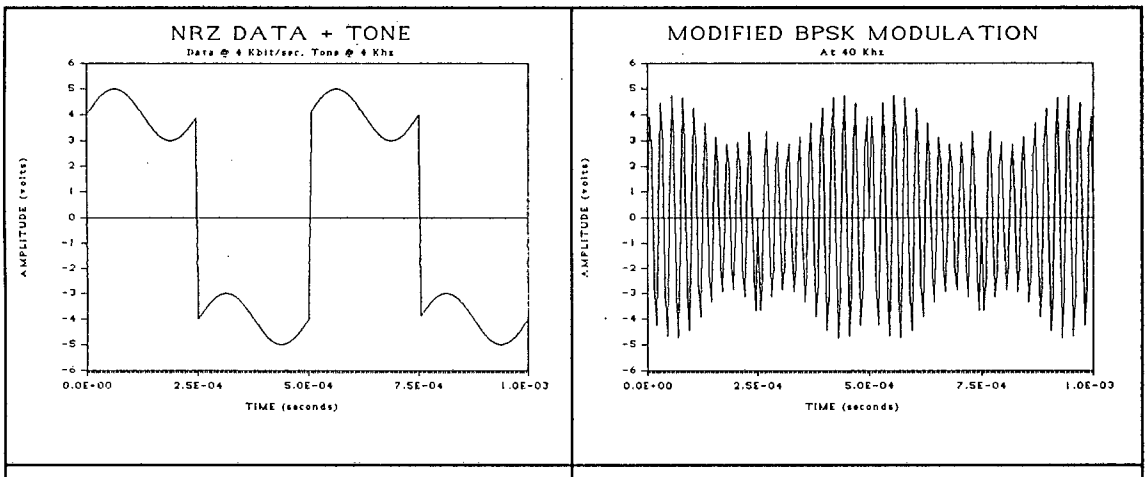

(a) **(b)**

Figure 3.17 : *(a) NRZ data added to the tone at baseband. (b) Modified BPSK waveform with non-constant envelope.*

The tone is added in phase with the data as shown so that at the matched filter sampling instant $V_{tone}(T) = 0$ V. An ideal matched filter at the demodulator will be able to recover the bits without any interference from the tone. This is further explained in Fig. 3.20.

The modified BPSK modulator required, is shown in Fig. 3.18 (a). Note the changes from Fig. 3.4 (a). To extract the tone a modification to the conventional DEBPSK demodulator of Fig. 3.4 (b), is required. The circuit that has been designed is given in Fig. 3.18.(b) Comparison of these two diagrams shows the necessary modification. After carrier demodulation, a multiple bandpass filter (tuned to the six different frequencies), filters out the tone from the demodulated data+tone combination.

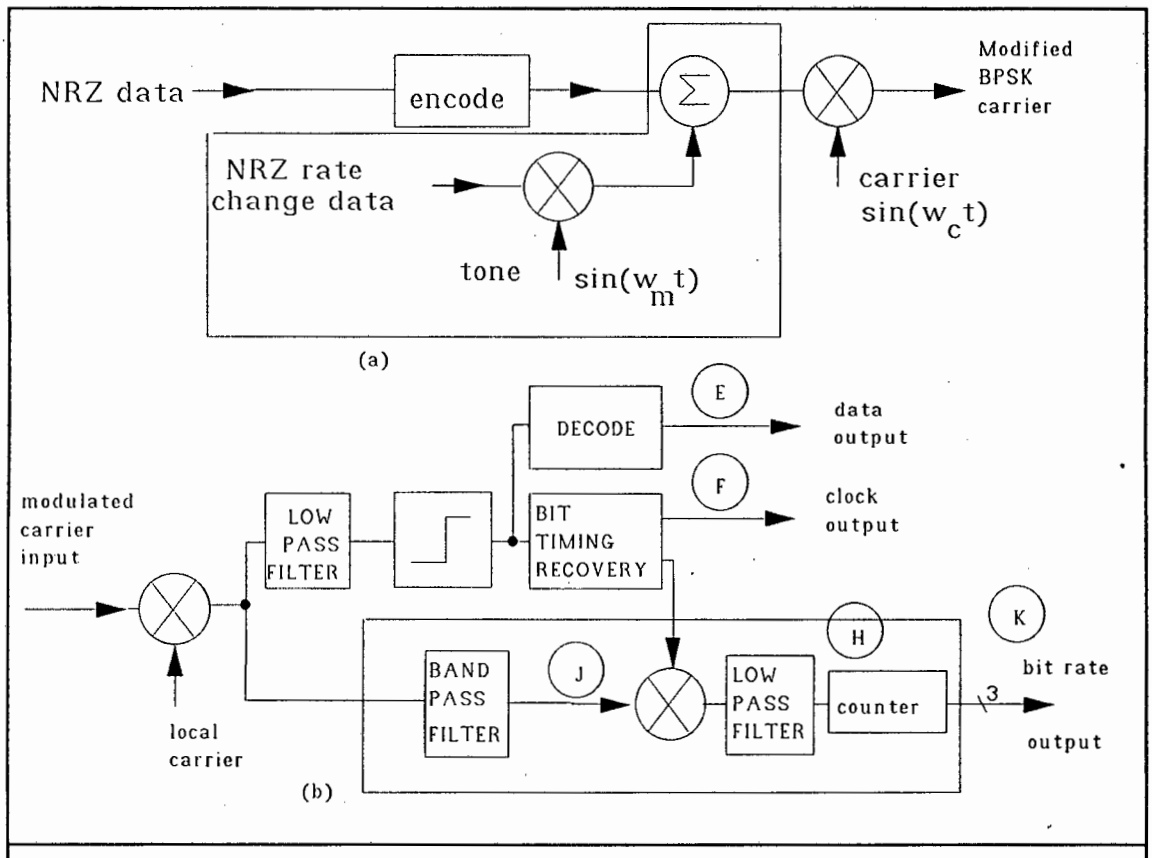

FIGURE 3.18 : *Modified BPSK modulator and demodulator.*

Actually transmitting information regarding the new bit rate can be done in numerous ways, sub-sections 3.10.2.2.1 and 3.10.2.2.2 discuss two ideas. The interference of the tone with the data recovery process is analysed as follows. With reference to sub-sections 1.3.3.1 and 1.3.3.2, the regular data is recovered by a correlator receiver having either an ideal matched filter after the multiplier or a non-optimum low-pass filter.

If matched filtering is used at the demodulator, then the tone will be integrated out to zero over one period at the demodulator. The data is sampled after the bit period T sec, at which point, the contribution from the tone is zero. The results of a simulation of this process is shown in Fig.3.19. This has been done using a hand calculation of

the output of a time convolution of data+tone signal with an integrate-and-dump filter. The output of the convolution is given by :

$$y(t) = t + \frac{aT}{2\pi}(1 - \cos(\omega t)) \quad for \quad 0 \le t \le T$$

$$y(t) = T\left\{2 - \frac{a}{2\pi}[1 - \cos(\omega(t-T))]\right\} - t \quad for \quad T \le t \le 2T$$

Where T sec. is the bit period, $\omega\, rad/\sec = 2\pi/T$ is the tone frequency, **a** is the peak tone amplitude (**a** <= 1) and the amplitude of the input step is unity. Selecting different values of **a**, gives three different tone-data ratios, which is the amplitude of the tone divided by the amplitude of the bit. As shown in Fig 3.19 (a) to (c) is tone/data = 10%, 50% and 100 %, respectively. The figures show that the output of the filter at t = T sec is V = T volts = 0.25 mV, which is not altered by the tone even under a high tone-to-data ratio.

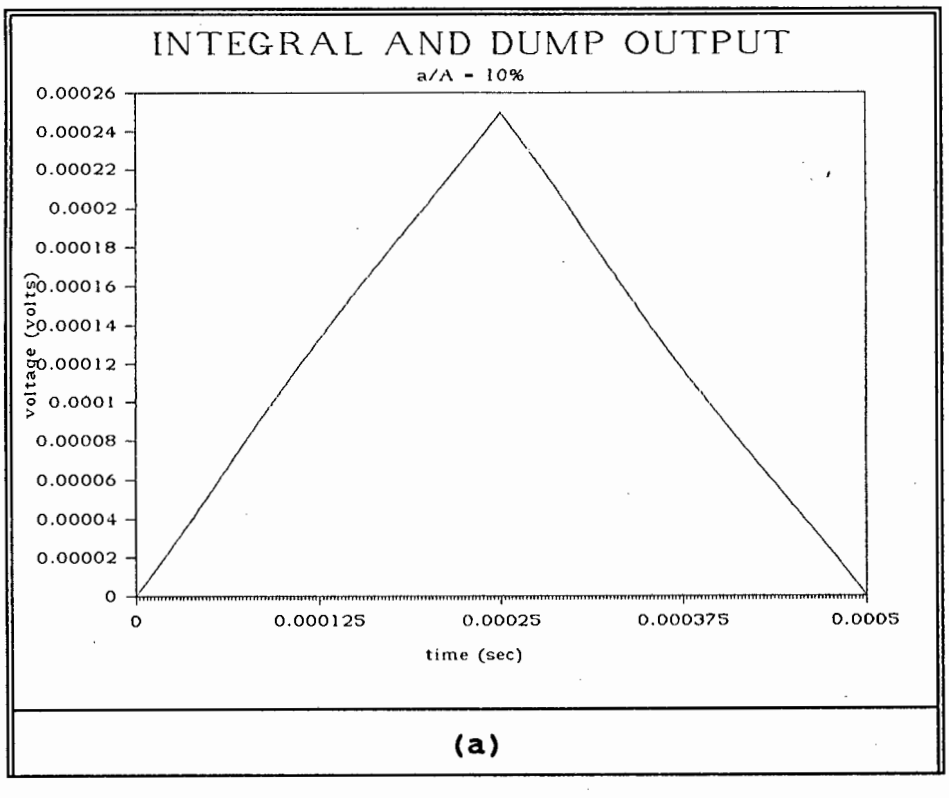

(a)

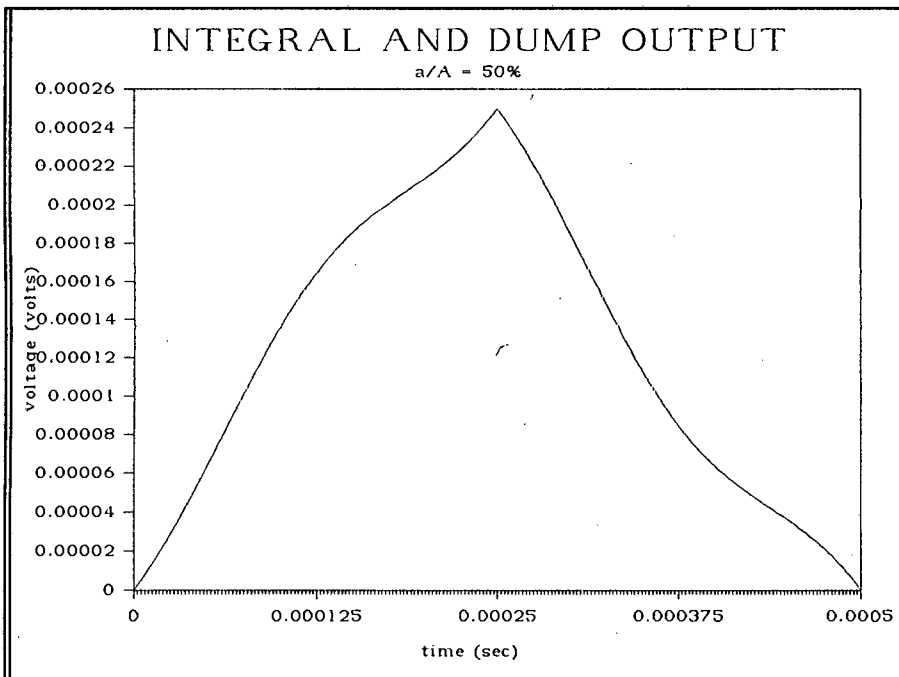

(b)

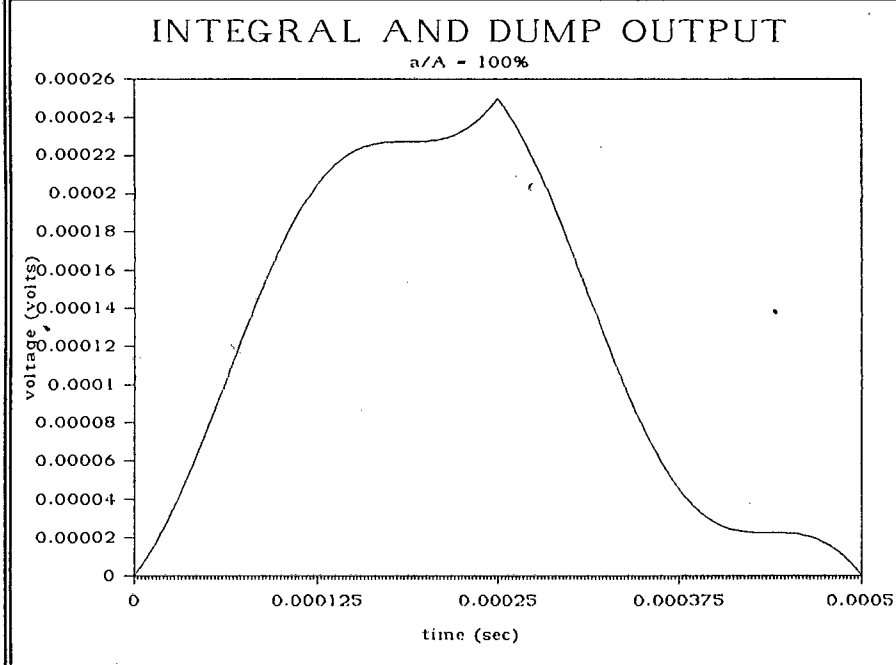

(c)

FIGURE 3.19 : *Matched filter output to various inputs.*

If non-matched filtering is used, the output of the correlator receiver will be a low-pass filtered version of the data + tone. A simulation of the process of filtering

the data + tone combination through a second order Butterworth filter has been done, using the transfer function of equation 3.19 with an input

$$v_i(t) = \left[A + a\sin(\omega_m t)\right]u(t)$$

Applying a Laplace transform:

$$V_i = \frac{A}{s} + a\frac{\omega_m^2}{s^2 + \omega_m^2}$$

The output time waveform is given by

$$y(t) = A\left[1 - \sqrt{2}\ e^{-\frac{\omega_c}{\sqrt{2}}t}\cos\left(\frac{\omega_c}{\sqrt{2}}t - \frac{\pi}{4}\right)\right] + a\left(e^{-\frac{\omega_o}{\sqrt{2}}t}\cos\left(\frac{\omega_o}{\sqrt{2}}t - \frac{\pi}{4}\right) - \frac{a}{\sqrt{2}}\cos(\omega_o t)\right) \quad t \geq 0$$

Where **A** is the peak step amplitude, **a** is the peak tone amplitude, ω_c is the filter cut off in rad/sec, ω_o is the tone frequency in rad/sec, **T** is the bit period. In this example $\omega_o = \omega_c = \frac{3\pi}{T}$.

This is plotted in Fig. 3.20 (a) to (c), showing the increasing tone interference as the tone to data ratio (**a/A**) is increased from 10 %, 60 % to 100% , respectively. The voltage at time t = T sec is always a maximum, but the actual value is a function of the input tone level. Relative to the step response, three different voltage levels, occur namely ; 110 % , 140 % and 170 % , according to the three mentioned inputs.

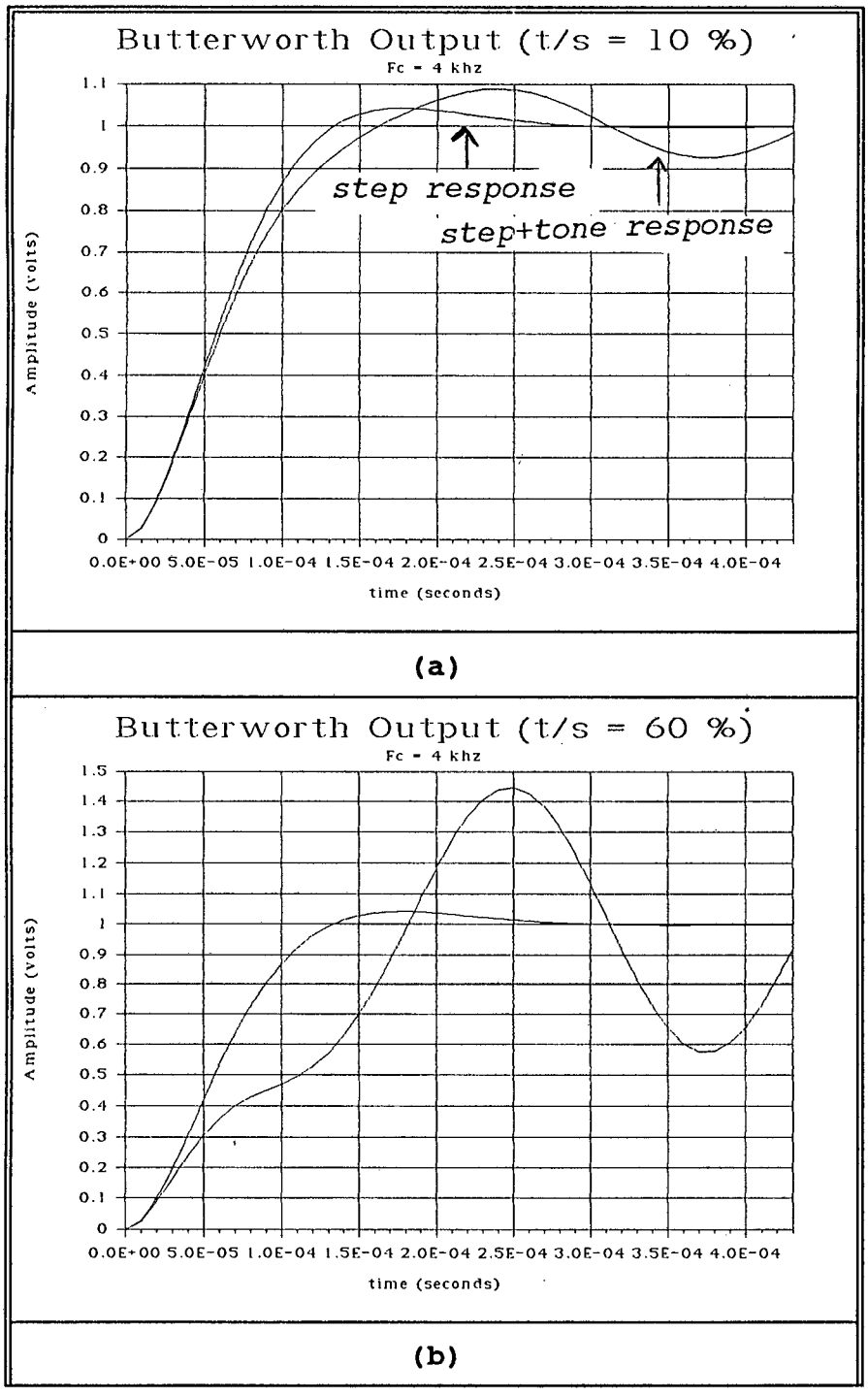
Butterworth Output (t/s = 10 %)
Fc = 4 khz
step response
step+tone response
Amplitude (volts)
time (seconds)
0.0E+00 5.0E-05 1.0E-04 1.5E-04 2.0E-04 2.5E-04 3.0E-04 3.5E-04 4.0E-04
(a)
Butterworth Output (t/s = 60 %)
Fc = 4 khz
Amplitude (volts)
time (seconds)
0.0E+00 5.0E-05 1.0E-04 1.5E-04 2.0E-04 2.5E-04 3.0E-04 3.5E-04 4.0E-04
(b)

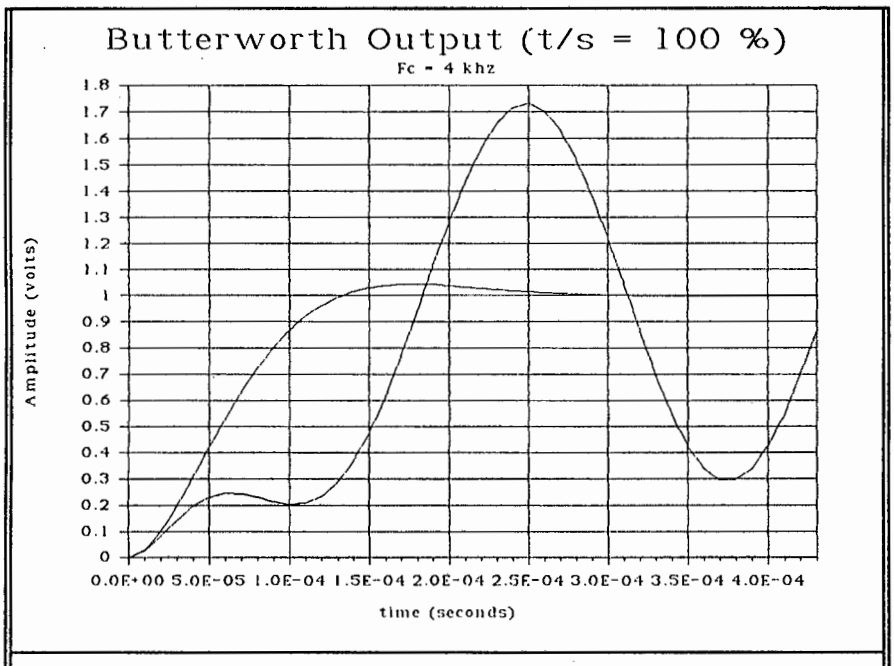

(c)

FIGURE 3.20 *:2nd order Butterworth filter output to various inputs.*

The output at time t = T sec for non-matched filters, like the second order Butterworth is proportional to the amplitude of the tone. Thus in the case of the second order Butterworth detection, the effect of the tone has not been eliminated. However, the data can still be recovered. The addition of white Gaussian noise will effect the non-optimum filter output more severely than that of the ideal.

Also, the graphs do not show ISI, as only one input pulse has been considered. With reference to Fig. 3.20 (c), the output at 100% tone-to-data ratio shows a distorted shape, which is susceptible to ISI that can cause errors when a decision is made at a comparator input.

3.10.2.2.1 Phase Shift Key Modulate (PSK)

The method of transmitting a message via the tone is explained with the aid of Fig.3.21. The waveforms are lettered according to Fig. 3.18 (b). The tone is always

transmitted with the data and is filtered out at the demodulator as shown by (J). As soon as a command to change bit rate arrives at the transmitter, the transmitter applies two 180° phase shifts to the tone. The two phase shifts represent a one-bit word consisting of a start edge, and a stop edge. The start edge is decoded as being the beginning of the message, and the stop edge, the end. The delay in-between the two represents a certain time T_B sec. which indicates the new bit rate.

The tone is received with the two phase shifts (J). The correlator receiver demodulates this bit to baseband (H). The start edge starts a counter which counts at the rate of the current data clock (F). The stop edge stops the counter. As the counter stops, the new bit rate is immediately read off the counter outputs (K). This selects the new receive filter required for the new bit rate. The data at the two bit rates is shown by (E).

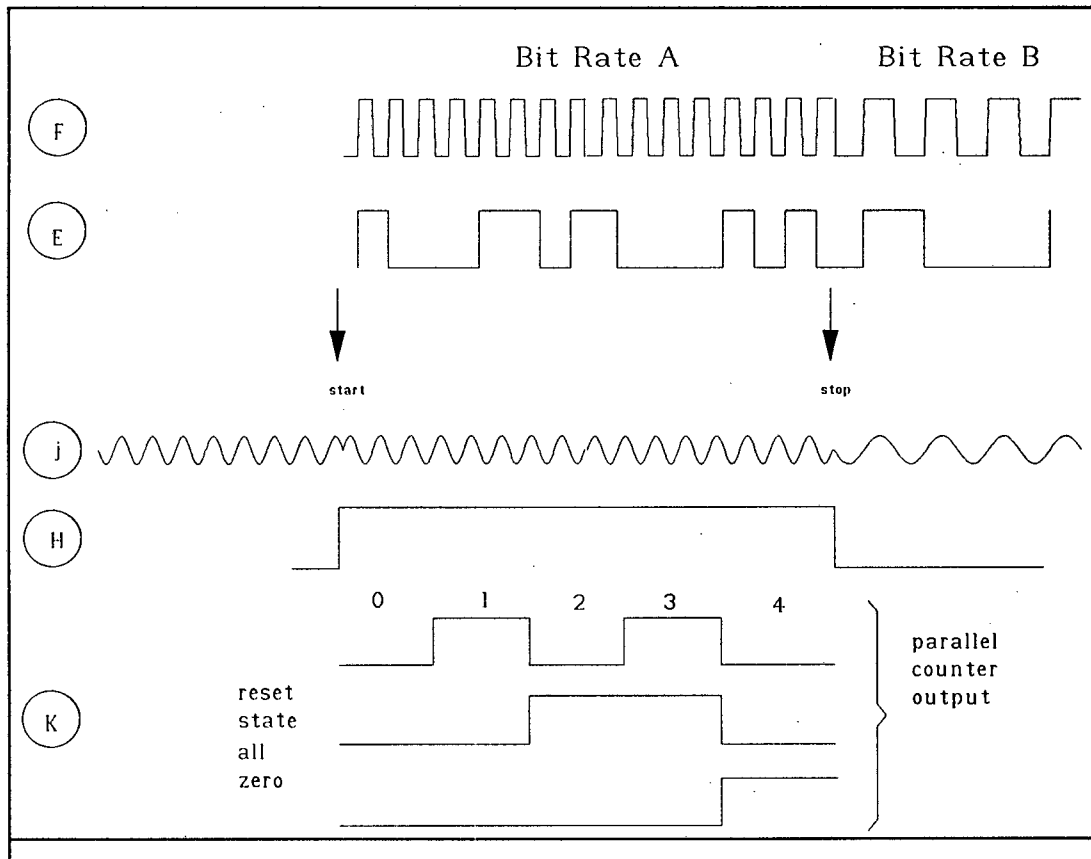

FIGURE 3.21 : *Tone signalling rate change.*

The time T_B for the different bit rates is calculated as given in table 3.2. To signal a change from 4 kbit/sec, to 128 kbit/sec, a 5 msec bit, which corresponds to 100 Hz, is the minimum time it will take to modulate the tone. The data rate clock will have counted to 0.005 * 4000 = 20 in this time, indicating a change to 128 kbit/sec. If a rate change to 64 kbit/sec is required, a 6 msec bit is modulated. In this case the receive counter counts to 24, indicating a change to 64 kbit/s. This continues for all bit rates in such a way that at any bit rate, when the receiver counter counts up to 20, it always implies a change to 128 kbit/sec, a count to 24 implies a change to 64 kbit/sec and so on down to a count of 40 which implies 4 kbit/sec. Signalling bit rate changes in this way minimises the time taken at the slowest bit rate to signal a rate change (max. of 9 msec).

	Next bit rate (kbps)					
	4	8	16	32	64	128
count :	40	36	32	28	24	20
current bit rate k bit/s	Bit period (msec)					
4		9	8	7	6	5
8	5		4	3.5	3	2.5
16	2.5	2.25		1.75	1.5	1.25
32	1.25	1.125	1		0.75	0.625
64	0.625	0.5625	0.5	0.4375		0.3125
128	0.3125	0.28125	0.25	0.21875	0.1875	

TABLE 3.2 : *Control words required for bit rate selecting.*

3.10.2.2.2 Amplitude Shift Key modulate (ASK)

An alternative method of transmitting the information in the tones is to send a tone only when necessary. That is, the modem will operate as a regular BPSK system until such time that a bit rate needs changing. At such a time, a burst of tone could be sent of a particular duration. The duration of the pulse indicates the next bit rate. The ASK system appears as shown in Fig 3.22. The appearance of the tone signifies a new bit rate. The absence of the tone signals that no bit rate change is required.

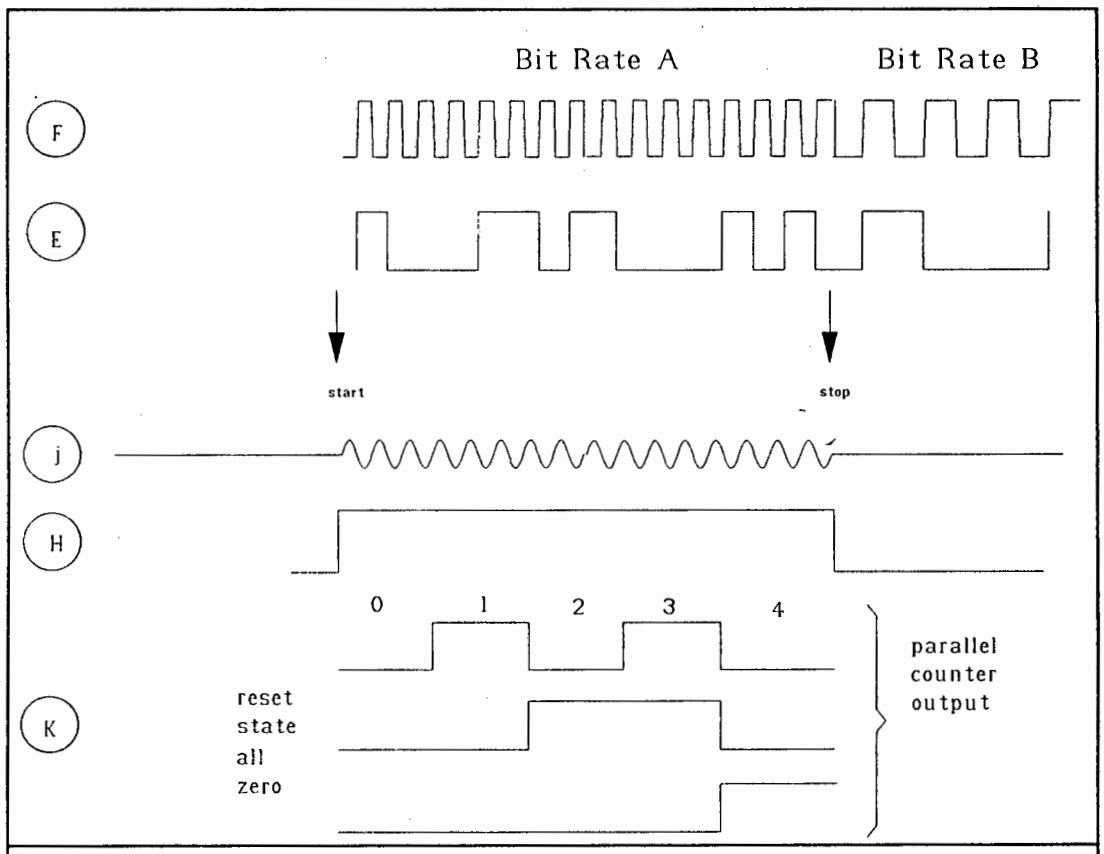

FIGURE 3.22 : *ASK rate change mechanism explained.*

The tone can be used to indicate which rate to select, by using a scheme as shown in table 3.2. The tone can be turned ON for a period indicating the next bit rate. A graphical illustration of the proposed system is shown in Fig. 3.23 for the case of ASK (ON-OFF keying)

modulation on the tone. A coherent demodulator multiplies the recovered clock (from the bit timing recovery circuit) with the filtered tone (from the data-plus-tone combination).

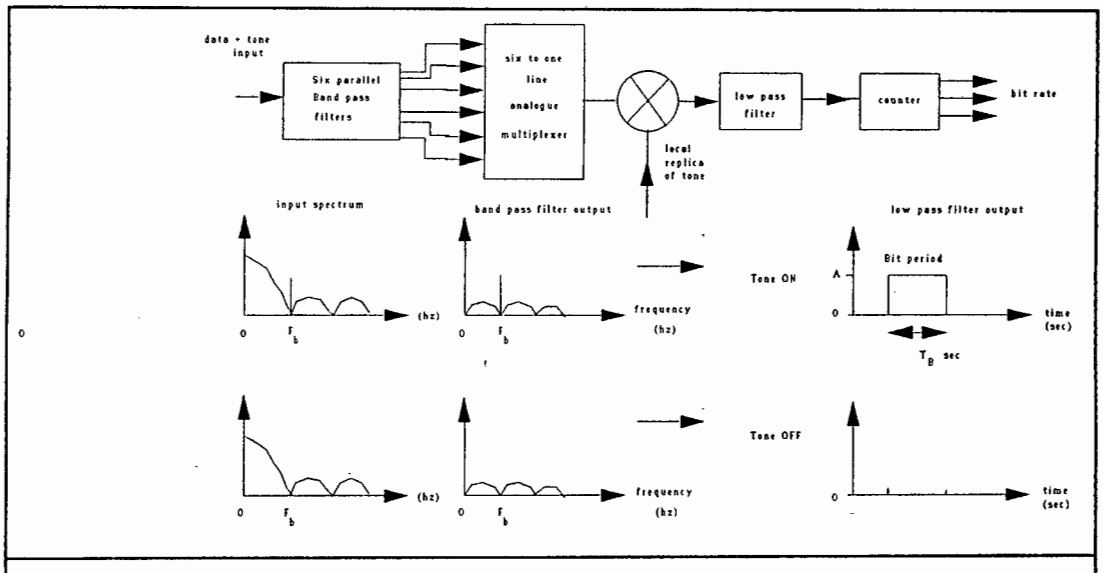

FIGURE 3.23 : *Tone recovery system.*

3.11 CONCLUSION

A power efficient modulation technique is required for meteor scatter communication. The use of DEBPSK as the modulation technique is justified because it is the simplest scheme to implement and the cheapest scheme in terms of power required.

The usefulness of DEBPSK has been proved many times in practice. Limiting the spectrum of DEBPSK before transmission is not required because no bandwidth restrictions have been placed on the system. It is an extra and unnecessary process.

To optimise the received S/N of a DEBPSK, matched filtering must be used at the receiver. For the case of baseband square waves being transmitted, an integrate and dump filter is the optimum implementation. A second order Butterworth filter can be used as a non-optimum data recovery baseband filter.

The addition of an auxiliary channel to a DEBPSK waveform, is possible, and allows the transfer of rate change information simultaneously with data. The data can be demodulated without any interference from the tone using optimal filtering. Use of a sub-optimal filter, however will cause amounts of ISI and possible S/N degradation. This can be limited if the tone-data-ratio < 100 %.

The tone can be recovered with a band pass filter after demodulation. The ability to demodulate the tone and the effect that the data has on this process will be investigated in chapter five. The implementation is discussed next.

3.12 REFERENCES

[3.1] Feher, K., **Digital Communications, Satellite/Earth Station Engineering**, Prentice-Hall Inc., Englewood Cliffs, N.J. U.S.A.

[3.2] Peebles, P. Z. Jr., **Digital Communication Systems**, Prentice-Hall International Editions.

[3.3] Richmond, R. L., **Getting the Most out of Meteor Burst Communications**, Military Electronics / Countermeasures, 1982.

[3.4] Schonhoff, T. A., **Symbol Error Probabilities for M-ary CPFSK Coherent and Noncoherent Detection**, IEEE Transactions on Communications, pp. 644 - 652 , June 1976.

[3.5] Lindsay, W. and Simon, M., **Telecommunications Systems Engineering**, Prentice-Hall, Englewood Cliffs, N.J., 1973.

[3.6] Stremler, F. G., **Introduction to Communication Systems**, Addison-Wesley Publishing Company, second edition.

[3.7] Hirade, Dr. K . **Mobile Radio Communications** in, Feher, K., **Digital Advanced Communications Systems and Signal Processing Techniques**, chapter 10, Prentice-Hall, Inc. Englewood Cliffs, New Jersey.

[3.8] Jones, J. J., **Filter Distortion and Intersymbol Interference Effects on PSK Signals**, IEEE Transactions on Communication Technology, Vol. COM-29, No. 2 , April 1971.

C H A P T E R 4

SYSTEM DESIGN AND IMPLEMENTATION

4.1 INTRODUCTION

The system of Fig. 3.18, in section 3.10.2.2., of chapter three is the modified DE-BPSK modulator and demodulator that has been implemented and is described in this chapter. The modem has been assembled from standard solid state devices. Attention has been given to low power consumption with the use of CMOS devices. The power supply throughout the modem has been standardised to +6 V, -6 V, and GND. Digital devices are powered by + 12 V.

Detailed circuit diagrams are given with component and signal values, with the complete circuit given in appendix H. Both the modulator and demodulator have been assembled in a modular style with different circuits placed on veroboard, pc-board and breadboard (Fig. 4.31). Breadboard layout has been used for the more experimental parts of the circuit that required component changes for testing. All of the modules have been connected to a common Earth which is provided by an aluminium ground plane. High frequency coupling is provided from the modules to this ground plane. Separate power supplies, isolated with voltage regulators have been used for the carrier recovery circuit.

4.2 MODULATOR

A more detailed block diagram of the modulator appears as shown in Fig. 4.1. The individual blocks, lettered from (A) to (E) will be explained as well as the waveforms.

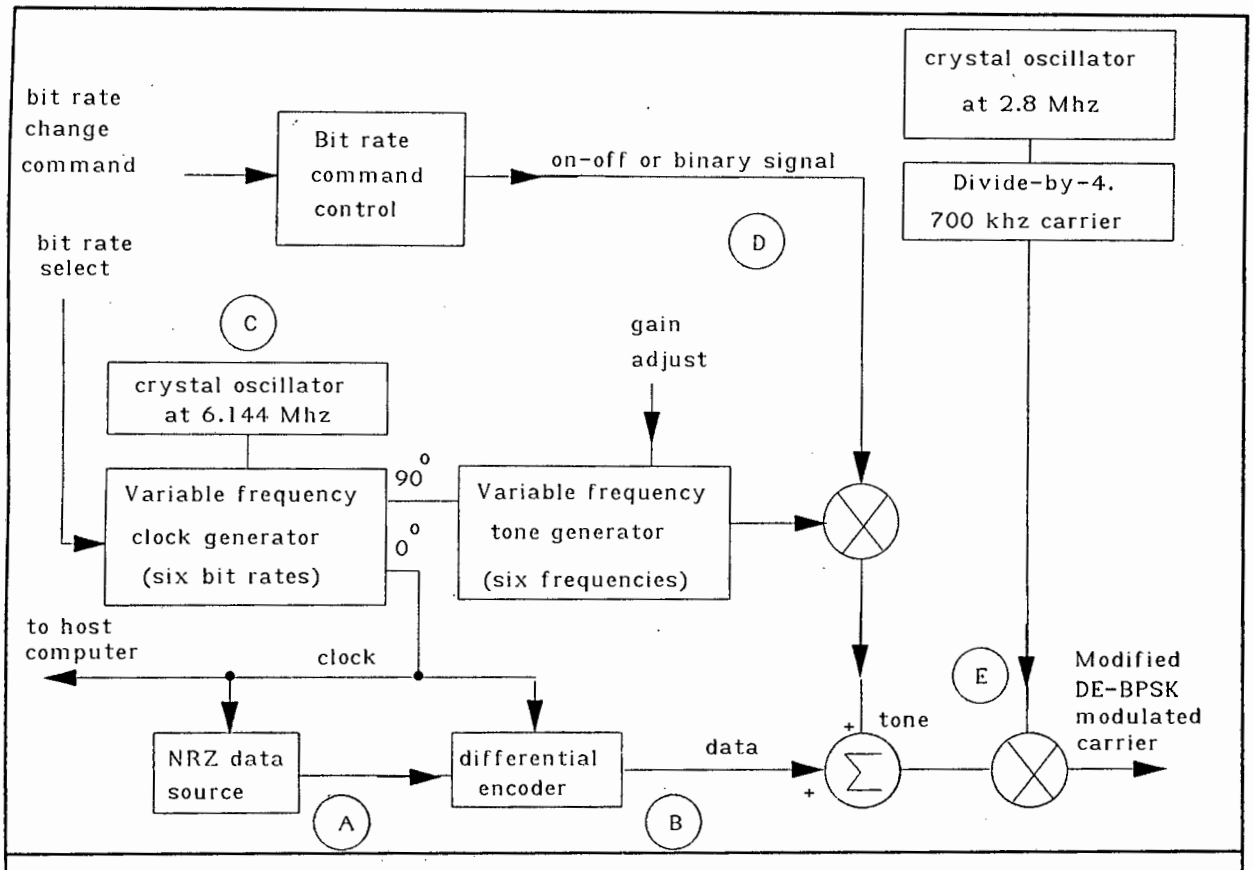

FIGURE 4.1 : *Complete block diagram of modulator.*

Note :

1. No band pass filtering or pulse shaping is performing by the modulator and 100% of the baseband energy is transmitted.

2. The bit rate will be controlled by the host computer via three parallel control lines and one tone modulating line. For test purposes, no computer has been used and the four control lines are connected to the output of a ring counter. An external clock increments the ring counter which has six different states each one corresponding to a different bit rate.

4.2.1 CRYSTAL OSCILLATORS

Crystal oscillators are used to source all clocks and data signals on the modulator. The crystal provides the most solid

oscillator available. Crystals are available and are inexpensive. The oscillator circuit used for both the carrier generation and the bit rate clock generation is the CMOS oscillator shown in Fig. 4.2 . The frequency limit placed on the oscillator is set by the maximum frequency operation of CMOS when powered by +/- 12 V. This is approximately 8 Mhz. CMOS CD4069 inverters have been used.

The two crystals used are a 6.144 Mhz crystal for the bit rate clocks and a 2.8 Mhz crystal for the 700 Khz carrier. The final modulator design must operate at 21.4 Mhz, however the demodulator operates at 700 Khz and for the purpose of testing the system, the carrier frequency output from the modulator must equal the demodulator input and 700 Khz has been chosen as the test frequency.

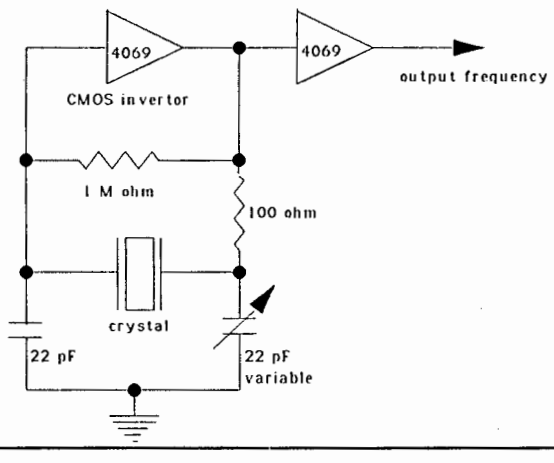

FIGURE 4.2 : *Crystal oscillator circuit used for generation of a 6.144 Mhz as well as a 2.8 Mhz oscillation.*

4.2.2 (A) DATA SOURCE

A data source is required while building and testing the modem in the laboratory. A Pseudo-random data sequence known as Pseudo-random (PR) noise is used. it is assumed that the data that will be transmitted in practice will be equiprobable and random. Sufficiently long PR sequences approximate equiprobable, random data streams. Such data streams are necessary because, the bit timing synchronisation

system that is discussed in sub-section 4.3.2, might have a degraded performance or even lose lock and thereby cause a burst of data errors if a long series of **1**'s or a long series of **0**'s is transmitted.

When data is random, the energy of the baseband signal and of the corresponding modulated RF carrier is sufficiently dispersed to reduce the peaks of the power flux-density (power spectral density). If, however, the baseband pulse train includes a periodic pattern, discrete line components appear in the modulated RF spectrum. With an appropriate choice of taps, an N-bit shift register is capable of generating a scrambled output sequence whose maximum periodic length is $L = 2^N - 1$ binary digits, at a bit rate $f_b = 1/T_b$. The power spectral density of a PRBS, $w_{PR}(f)$, consists of discrete spectral lines separated by $1/LT_b$ Hz. It is given by [3.1]

$$w_{PR}(f) = \frac{L+1}{L^2}\left(\frac{\sin \pi f T_b}{\pi f T_b}\right)^2 \sum_{n=-\infty, n\neq 0}^{\infty} \delta\left(f - \frac{n}{LT_b}\right) + \frac{1}{L^2}\delta(f) \qquad (4.1)$$

The density of the spectral lines thus depends on the bit rate and the code length used. For example, comparing the spectral content of the highest bit rate, 128 kbps, using two different code lengths (i) 15 bit (ii) 65536 bit.

(i) The spectral content of the code length of 15 bits consists of spectral lines at intervals of 128000/15 = 8.544 Khz.

(ii) The spectral content of the code length of 65536 bits contains spectral lines at intervals of 128000/65536 = 1.953 Hz which is close enough to approximate a continuous spectrum.

The design of the feedback maximal length shift register used, has been obtained from [4.5]. A typical modulo-2 shift register implementation of a PN generating code is given in

Fig. 4.3 .

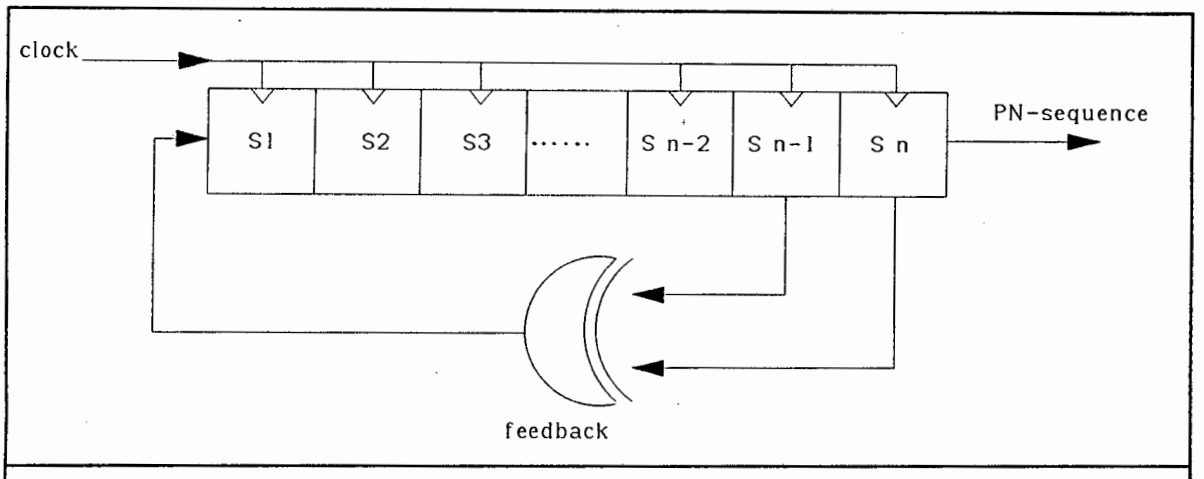

FIGURE 4.3 : *Maximal length PN sequence generator.*

Three different code lengths have been used, a 15 bit length, a 31 bit length and a 65535 bit length code. These can be implemented using sixteen single-bit shift registers as shown in the circuit of Fig. 4.4 . Switch SW3 selects the bit length sequence. The clock input determines the rate at which the data is to be transmitted.

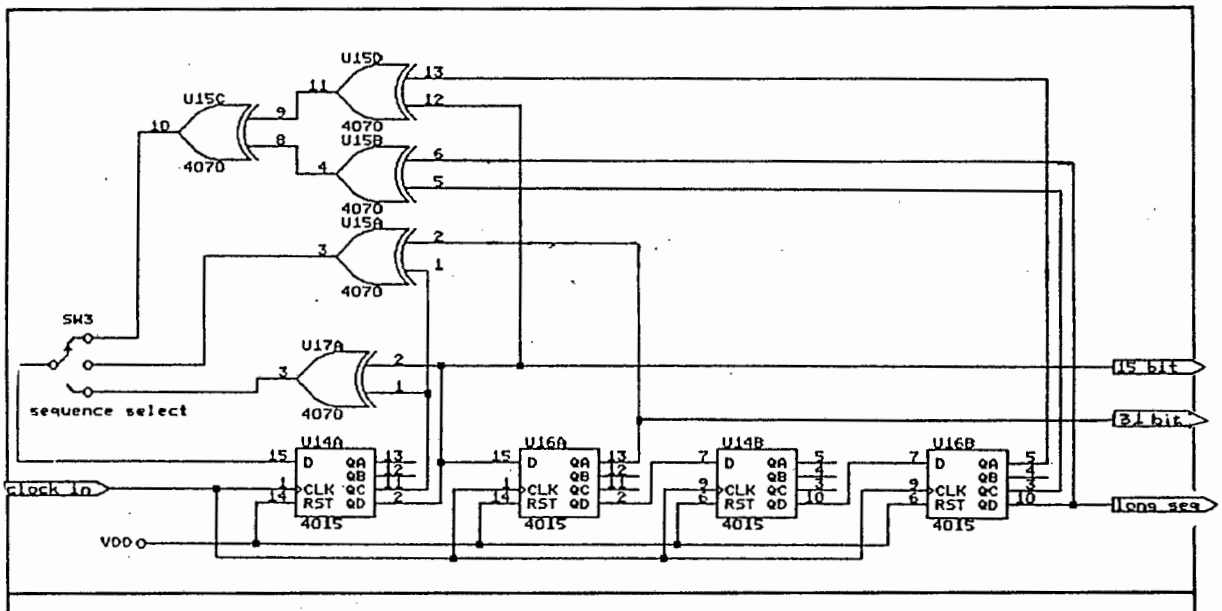

FIGURE 4.4 : *PN generator circuit diagram.*

4.2.3 (B) DIFFERENTIAL ENCODER

The differential encoder, encodes a binary NRZ stream into another NRZ stream as described in section 3.4.1 and can be implemented using a T-Flip Flop. The state equation for a T-flip flop matches that of the differential code. The T-flip flop state equation is given by:

$$Q(t+1) = Q(t) \cdot \overline{T} + \overline{Q(t+1)} \cdot T \qquad (4.2)$$

The differential code state equation is given by

$$d_k = \overline{b_k} \cdot d_{k-1} + b_k \cdot \overline{d_{k-1}} \qquad (4.3)$$

The equations are equal to one another, if we put:

$Q(t) = d_{k-1}$
and,
$T = b_k$

Fig. 4.5 (a) shows the required encoder and 4.5 (b) is an implementation of the encoder. The input data stream is thus fed into the T input (J connectd to K) and the output is taken from Q. A clock at the bit rate must be applied to the clock input of the T-flip flop. The T-flop flop is assembled using a CMOS 4027 device.

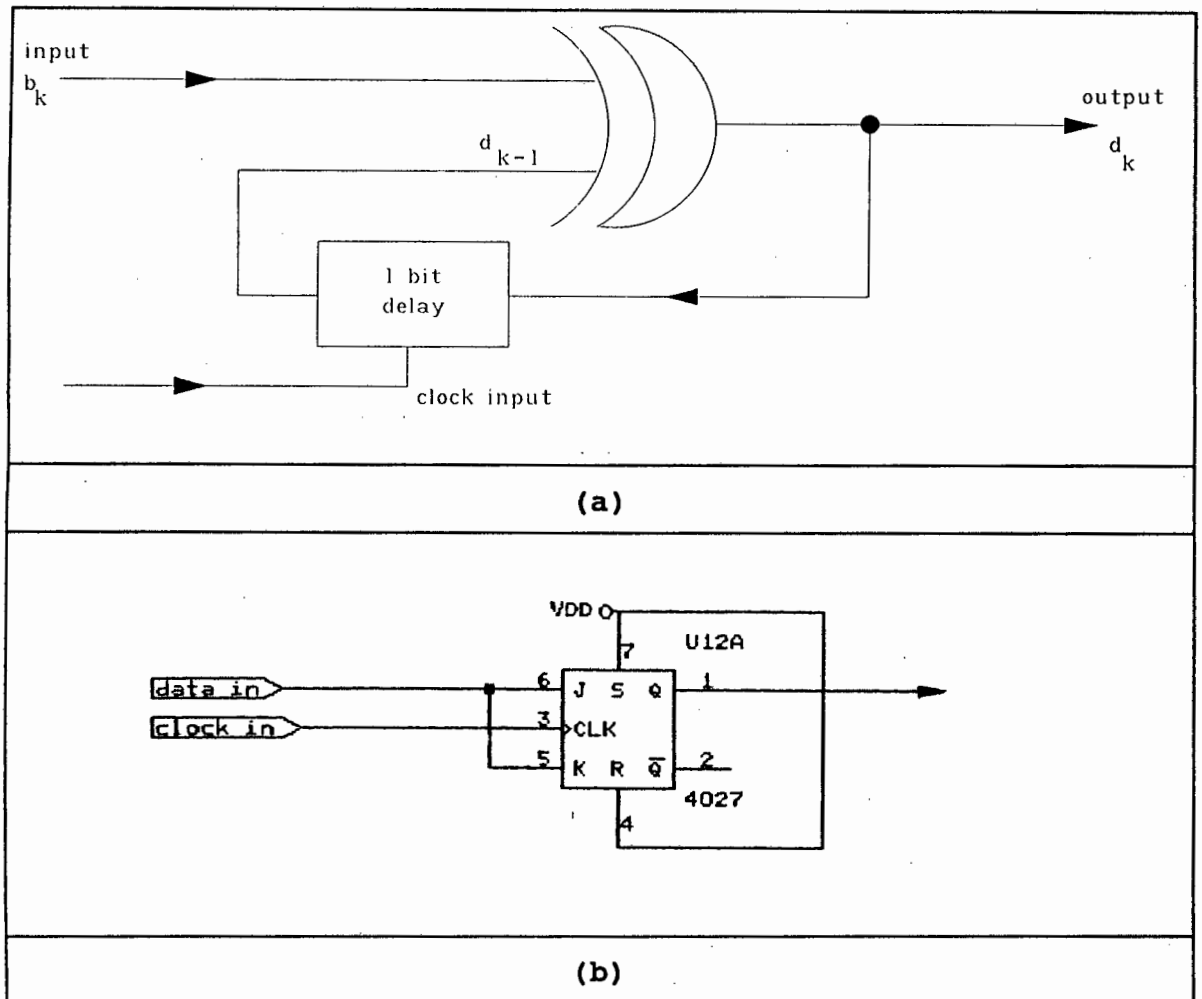

FIGURE 4.5 : *Diagram of differential encoder showing (a) the required process and (b) an implementation of the process.*

4.2.4 (C) VARIABLE FREQUENCY CLOCK GENERATOR

The variable frequency clock generator provides two signals: One is the modulator baseband clock which is used to synchronise any data that is to be transmitted. The other is a quadrature version of this clock which is further synthesised and is used as a tone, described in the next sub-section. The clock generator can be selected to provide any one of six clock rates.

The generator consists of a crystal oscillator set at 6.144 Mhz. The bit rate clock is first divided by three, using two J-K flip flops. The 2048 Khz clock is then applied to the CD4040BC device. This is a 12 stage ripple counter that

divides the clock down further to **double** the six different clock frequencies required, namely ,f_{CLK} = 256 Khz, 128 Khz, 64 Khz, 32 Khz, 16 Khz, and 8 Khz. These are fed into a CD4512C 8-channel data selector, which selects a clock signal to be current. The double frequency is used to generate a 90° (quadrature-phase) clock. The original clock is then further divided-by-two to give the required clock rate. The in-phase clock signal is used to clock the differential encoder and the data source, so that bits can be read into the modulator. The quadrature-phase clock is further integrated to provide six, in-phase tones.

The current bit rate is selected via the the multiplexer which accepts a three bit word indicating the bit rate. The bits 000 to 101, counting in binary, select one of the six bit rates respectively. The circuit is shown in Fig. 4.6.

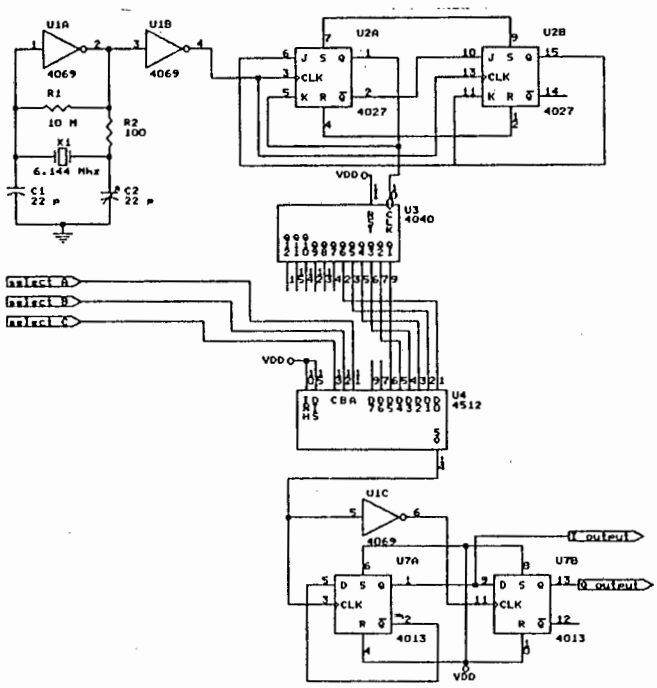

FIGURE 4.6 : *Multi-bit rate clock generator.*

4.2.5 (D) VARIABLE FREQUENCY TONE GENERATOR

The six different tone frequencies that must be added to the data are generated from the clock signal that has been selected by the multiplexer as explained above. Each clock that is generated by the variable frequency clock circuit has been shifted by 90^{o} to pre-compensate for the shift introduced by the integration process. The square wave is then integrated to give a triangular waveform which is used as the tone. The resulting tone must be in phase with the clock that generated it (sub-section 3.10.2.2).

A sinusoid is not strictly required for this purpose. A triangular waveform is used because of the convenience of generating such a waveform from a square wave at six different frequencies. Initially other ideas were tested. For example a sine wave generator can be implemented by third order low pass filter, which filters out the second and higher harmonics of the square wave. The circuit that was considered was discarded because of the complication of a high order filter duplicated six times.

With reference to Fig. 4.7 six lines passing from the frequency dividers are passed into a resistor bank, which is controlled by analogue switches. The analogue switches used are DG308 devices. These switches were chosen because of their fast switching time of 130 nsec. A decoder is required to decode the three bit line select into a six line select.

Each tone is integrated with the same time constant determined by **C4 = 910 pF**, and $R19 = 10M\Omega$. The following is the step response equation, used to select the input resistors, R_i, labelled R24 to R29, so that the tones are all of the same amplitude,

$$V_o(t) = -\frac{R_{19}}{R_i}\left(1 - e^{-\frac{t}{R_{19}C_4}}\right)$$

The component values are as shown in Fig.4.7.

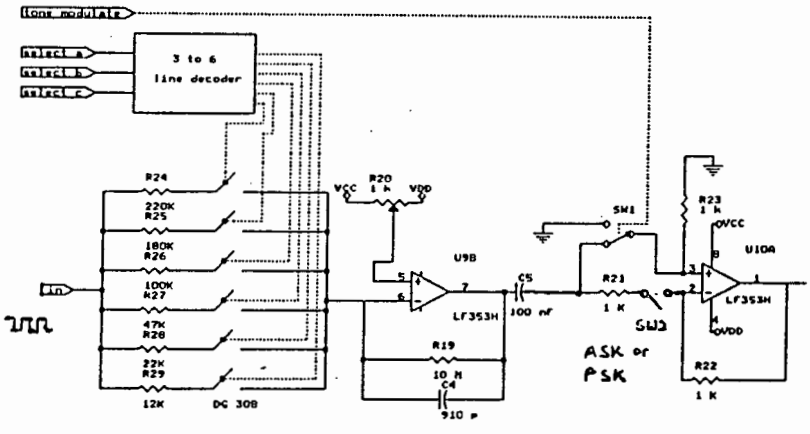

FIGURE 4.7 : *Multi-frequency tone generator and modulator.*

Variable resistor R20 sets the dc bias for all of the tones. Switch SW2 selects the type of modulation, either PSK or ASK. In PSK mode, the op.amp. U10A, is switched by SW1 between the two configurations of *inverter* and *follower* ,thus phase shifting the input tone by a 180^{o}. In the ASK mode, the operational amplifier (op. amp.) U10A, is switched (again by SW1) between the two configurations of *OFF* (GND) and *ON* (*follower* mode). The output of op. amp. U10A is connected to one of the summer inputs. The amplitude of all the tones can be adjusted by variable resistor R31 = 10 k. This is used so that the effect of different tone amplitudes can be analysed (Fig. 4.9 (a)). Switch SW1 has been implemented using two single-pole-single-throw analogue switches from the DG308 device.

4.2.6 BIT RATE CONTROL

The bit rate control has been done by either hard wiring the modulator and the demodulator to a particular bit rate for testing, or by using the two control circuits of Fig. 4.8. At the modulator, a clock applied to the counter at a low frequency of say 1 Hz, moves the output states of the 4029 counter (U30) through a count sequence from zero to five. Each state switches the modulator to a new bit rate in

increasing order. Once the counter reaches six it resets itself to zero and the process repeats. A similar such circuit is used at the demodulator.

The clock can either be hard-wired, thus controlling both modulator (mod.) and demodulator (demod.) together or, the tone can be modulated by the slow clock at the mod. and recovered at the demod. This is a simplified control technique compared with the method of section 3.10.2.2.1 .

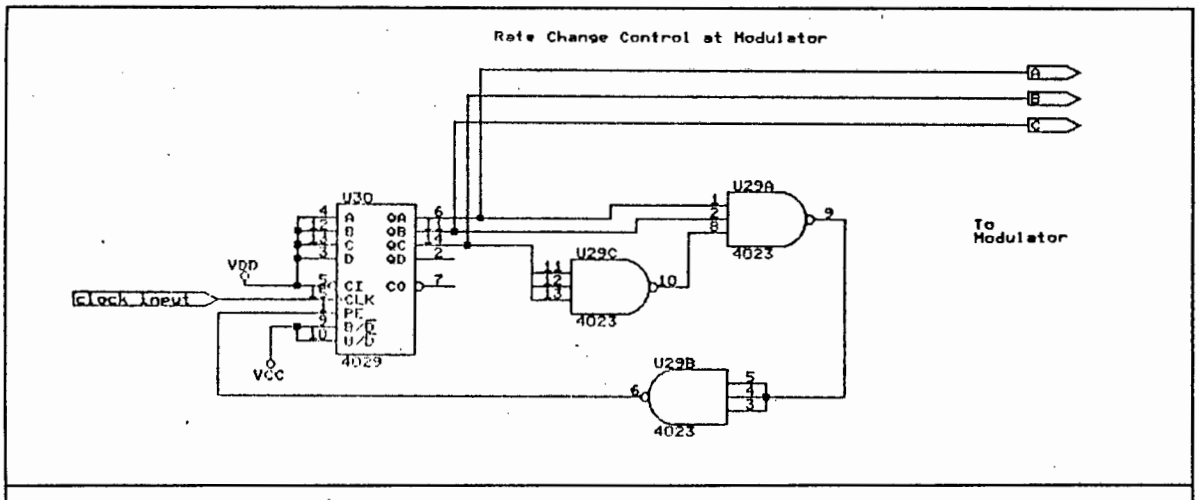

(a)

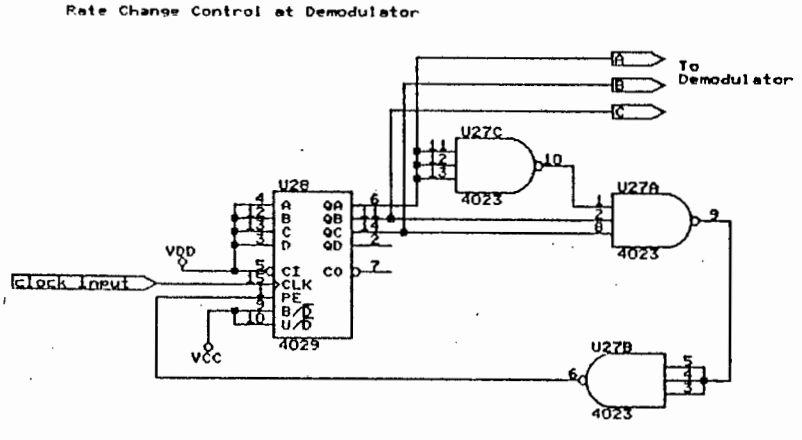

(b)

FIGURE 4.8 : *Bit rate change control (a) at modulator and (b) at demodulator.*

4.2.7 (E) SUMMER, CARRIER GENERATOR AND ANALOGUE MULTIPLIER

The summation of the two baseband signals namely; the data and the tone is done through the an LM6361 op. amp, shown in fig.4.9. This device has a Gain-bandwidth product of 50 MHz. The closed loop gain has been set to less then unity and results in an output data signal of 1.5 V_{p-p}. The output of the summation is passed to the analogue multiplier for modulation with the carrier. The square wave carrier is generated by a crystal oscillator and a divide-by-four frequency divider.

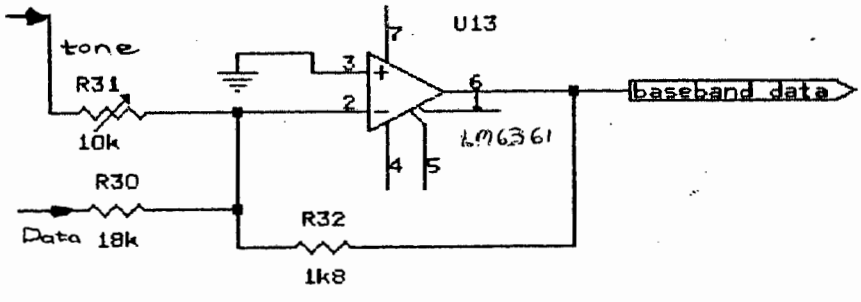

(a)

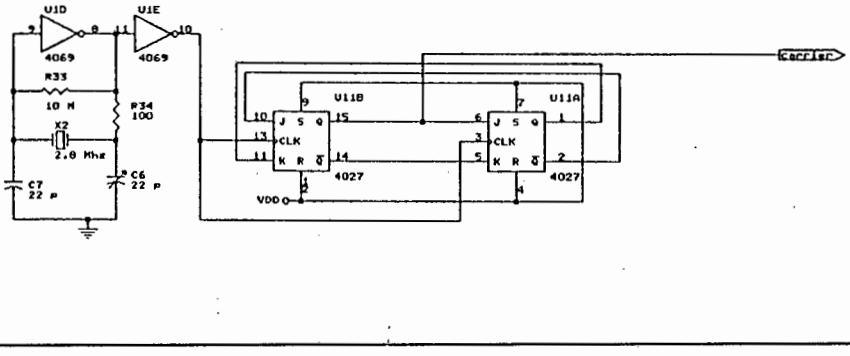

(b)

FIGURE 4.9 : *(a) Data+tone baseband summer and (b) carrier generator.*

The analogue multiplier used to perform the modulation is the XR2208 device shown in Fig. 4.10. Other devices that were tried for this purpose were the passive multiplier SRA-1 and a chopper multiplier. The XR2208 multiplier has been used

because of its versatility in providing gain adjustment. It also provides a double-balanced output and 40 dB carrier suppression.

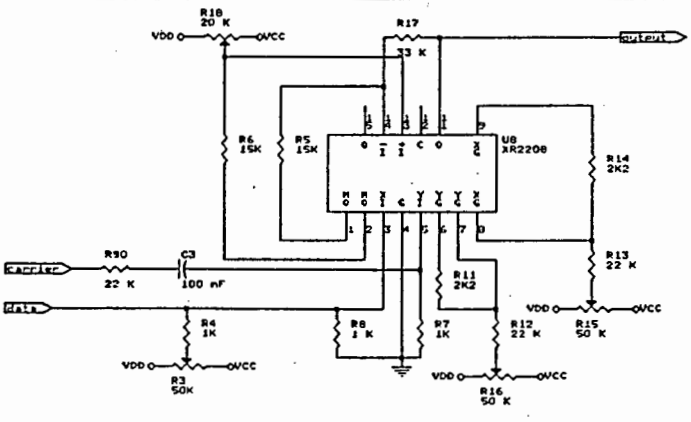

FIGURE 4.10 : *Circuit diagram of multiplier.*

Using the multiplier with a finite gain, it is necessary to balance the X and Y channel gains using resistors R15 and R16. The procedure is given in the data book. The XR2208 has been configured as a multiplier feeding an amplifier. The gain of the system is set by the following formulae provided in the data-book

$$K_M \cdot K_A = \left(\frac{25}{R_x R_y}\right)\left(\frac{R_f}{R_i + 6}\right) \qquad (4.4)$$

where all resistors are given in $k\Omega$, K_m is the multiplier gain set by the x-gain (R_X = R14) and the y-gain (R_Y = R11) and K_a is the amplification. The carrier suppression is set by resistor R4. This is adjusted for maximum carrier suppression of about 40 dB. With a supply voltage of 12 V, the input voltages must be : - 4 V < V_{in} < + 2 V, in order to maintain linear operation of the multipliers. The multiplier output has a -3dB bandwidth of about 2 Mhz which is sufficient for the carrier of 700 Khz.

4.2.8 MODULATOR SUMMARY

The modulator has been assembled on a pc-board. A photograph of the modulator is given in Fig. 4.31 (a). The picture is not to scale and the real dimensions are give in 4.31 (b). The modulator is denoted by, **A** and the pn-data generator by, **K**. The complete circuit diagram is given in appendix H, page H-1. The board has a few adjustable points, namely:

1) The PN sequence length can must be chosen.

2) The bit rate can be set manually using dip-switches or controlled with the adaptive rate change circuit.

3) The amplitude of the added tone can be adjusted.

4) The tone modulation technique is chosen as either PSK or ASK.

5) The amplitude of the output modulated carrier can be changed.

4.3 DEMODULATOR

Demodulation of the modified DE-BPSK suppressed carrier waveform is done identically to conventional DE-BPSK. The demodulator regenerates the carrier and demodulates the baseband information. Bit timing is then regenerated and differential decoding reveals the original bit stream. The circuit modification appears after demodulation since the baseband signal contains the added tone which is filtered out indicating the rate changes (Fig. 3.19).

A discussion of the various methods available to demodulate DE-BPSK is done as well as an explanation of the circuits used. The choice of demodulator is explained with the use of table 4.1. The various decisions are arranged in a tree format. The head of the tree is the Differentially encoded modulated carrier. The second level shows the two methods of demodulation, Differential BPSK (DBPSK), and Differentially Encoded BPSK (DEBPSK). DBPSK is the method of implementing a demodulator without having to regenerate a coherent carrier. The advantage is that differential decoding is performed simultaneously with the demodulation process.

DEBPSK is the method of implementing a demodulator by regenerating a local carrier. This has the advantage of better tracking performance to varying input carrier frequencies. The disadvantage is that data recovery and clock extraction is necessary to perform the differential decoding. The implementation of the both demodulators is shown in Fig. 4.12.

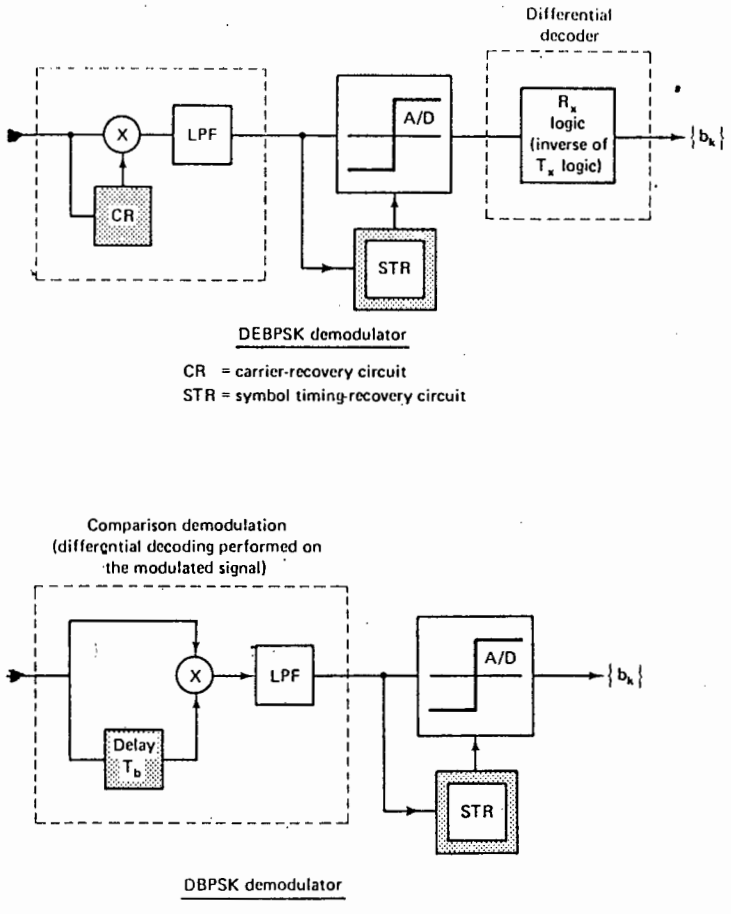

FIGURE 4.12 : *Comparison of demodulation of differential BPSK [3.1].*

BPSK and DE-BPSK have been named according to the implementation of the demodulator. The two different schemes are illustrated in Fig. 4.12. DEBPSK is the preferred technique to implement for two reasons; firstly, an accurate analogue delay required for carrier recovery in a DBPSK system is difficult to obtain; secondly DE-BPSK has an improved P_e vs S/N achieved by regenerating a local carrier.

Once DEBPSK has been chosen, the type of carrier recovery system is selected. It has been shown that the optimum device for tracking suppressed carrier signals at low SNR's is either the Costas loop or a squaring loop, since they exhibit equivalent performance in the presence of AWGN noise [4.3], either option can be implemented. A Costas loop carrier recovery system has been chosen for two reasons: (i) because of the advantage of

simultaneous data recovery with carrier recovery; (ii) the Costas loop requires only low pass filters, whereas the squaring loop requires band pass filtering of the received carrier which has been avoided.

With reference to Fig. 4.13, the operation of the demodulator is described as follows:

At the input to the demodulator is the carrier recovery circuit which extracts a coherent carrier from the signal. The baseband data is demodulated simultaneously, with the carrier recovery process. In cascade with this circuit is a bit timing recovery circuit which extracts the timing in the bits. Also in cascade with the carrier recovery is the tone extraction circuit and tone processing circuit. The output of this circuit controls the current bit rate of the demodulator. A differential decoder, clocked with the recovered clock yields the final demodulated data.

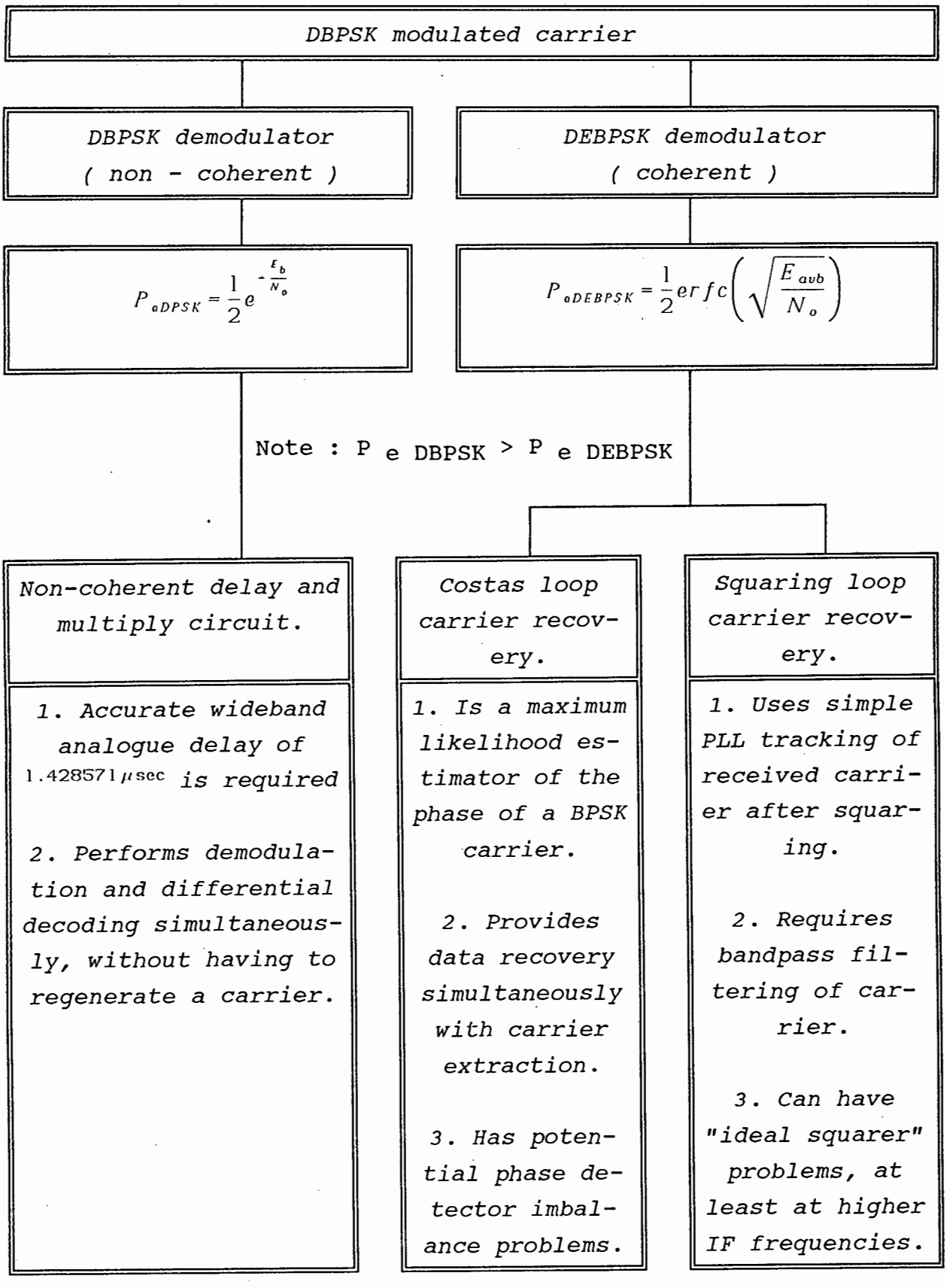

TABLE 4.1 : *Discussion of choice of demodulator implementation.*

The rest of the chapter explains the constituent blocks of Fig. 4.13, namely;

A : Costas loop carrier recovery.
B : Bit timing recovery.
C : Tone demodulation and bit rate control.
D : Data recovery and decoding.

The spectrum of the demodulated baseband appears in Fig 3.16 (a). The discrete clock component is not used for bit timing recovery, but only for rate change signalling because it is only transmitted intermittently. Bit timing must be recovered from the continuous baseband spectrum which is discussed in 4.3.2. Tone demodulation and bit rate signalling is discussed in 4.3.3. Data recovery is discussed in 4.3.4.

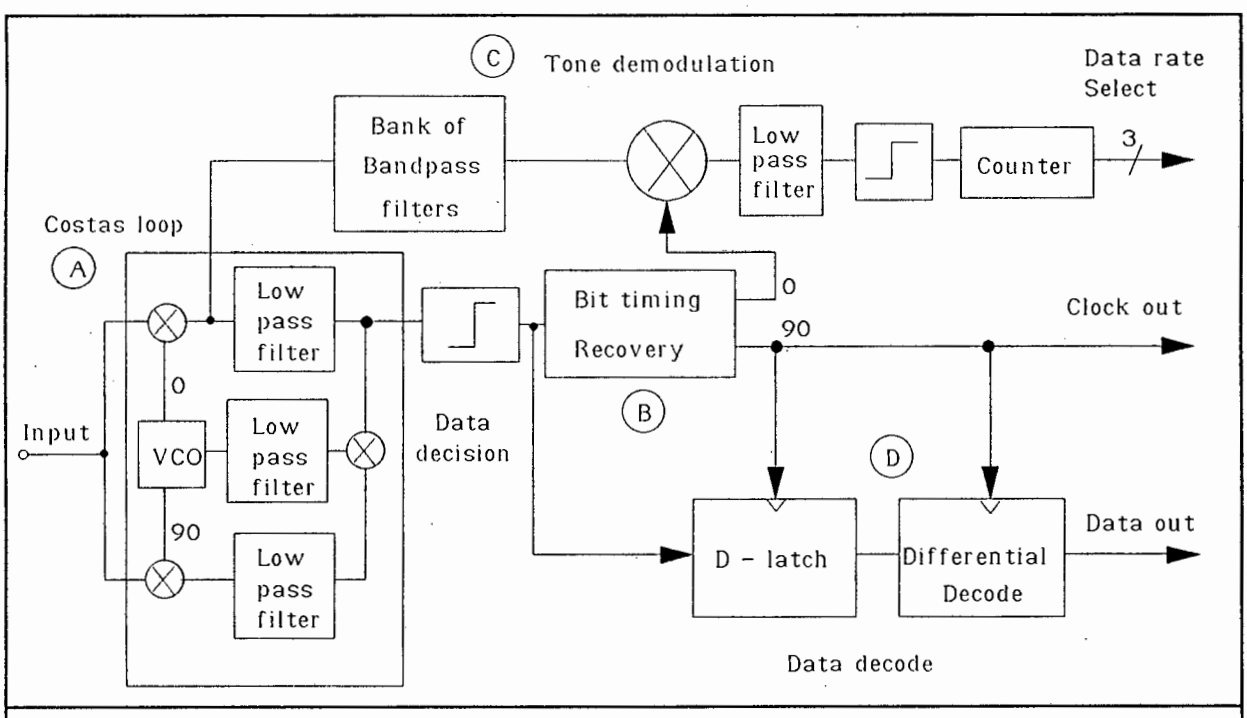

FIGURE 4.13 : *Demodulator block diagram.*

4.3.1 (A) COSTAS LOOP CARRIER RECOVERY

The carrier recovery circuit is a synchronous tracking loop that tracks a suppressed carrier waveform. A simple phase lock loop can not be used to track such a signal, because the phase lock loop requires a large carrier waveform to lock onto.

The suppressed carrier loop *reconstructs* the carrier by multiplying the baseband streams together, removing the modulation and providing a dc voltage proportional to phase error which drives a VCO into lock. The following is an analysis of a two-phase tracking loop.

The original Costas loop [4.1] is a two phase synchronous receiver that was used for suppressed carrier amplitude demodulation. This demonstrated that suppressed carrier tracking loops were possible. With reference to the basic Costas Loop of Fig. 4.14, a simple explanation is given.

The incoming signal is a suppressed carrier binary phase shift key signal written here as :

$$y(t) = A\,m(t)\cdot\cos\left(\omega_c t + \theta\right)$$

Where **A** is the input amplitude, **m(t)** is the baseband data , ω is the carrier frequency , θ is the initial phase. This input signal is mixed or multiplied with an **in-phase** and a **quadrature-phase,** coherent local oscillator signal. This pair of multiplier and low-pass filter combination, can be described as a correlator receiver and a phase detector, respectively.

When the loop is in-lock, the **in-phase arm** (I-channel) produces the demodulated data, $\hat{m}(t)$, and the **quadrature-phase arm** (Q-channel) produces zero volts. The product of the two arm voltages at the output of **loop multiplier** will be zero.

The narrow, **loop filter** output is a dc voltage which drives the **voltage controlled oscillator** (VCO), holding the loop in lock.

The local oscillator must be maintained at proper phase to the input carrier so that the data demodulation occurs without error. If the local oscillator phase drifts from its proper value by a few degrees the I-channel will remain essentially unaffected but there will now appear some data output from the Q-channel. This Q-channel data will have the same polarity as the I-channel data for one direction of local oscillator phase drift and opposite polarity for the opposite direction of local oscillator phase drift. The Q data level is proportional to the magnitude of the local oscillator phase angle error for small errors. Thus by simply combining the I and Q data signals in the loop multiplier, the data is squared, $m^2(t) = 1$, which cancels the data out. A dc control signal is obtained which automatically corrects for local oscillator phase errors.

It should be noted that the phase control information is derived entirely from the side-band components of the BPSK signal at baseband and that a large carrier component is not required. Since both synchronisation and demodulation are accomplished in complete independence of a large carrier, suppressed carrier transmissions may be employed.

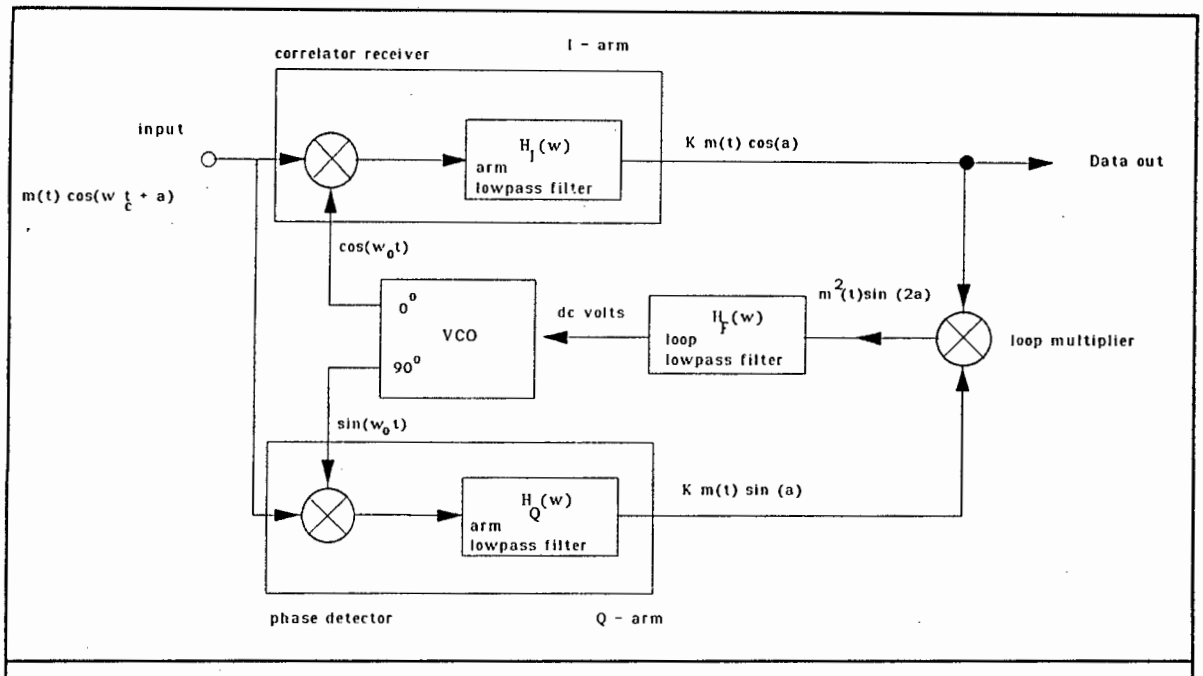

FIGURE 4.14: *Costas Loop.*

The addition of the I-channel distinguishes this loop from the simple phase-lock-loop (PLL), however the Q-channel and indeed the closed loop control operates identically to that of a simple PLL. The bandwidth of the two low pass filters, $H_Q(w)$ and $H_I(w)$ must be large enough to pass the data and filter out the unwanted double frequency component resulting from the multipliers and high frequency noise. The double frequency term occurs at $2f_c$ = 1.4 MHz, and the highest bit rate is f_b = 128 Kbps. The bandwidth of the loop filter, $H_F(w)$, is typically narrow since the output must be a dc voltage to drive the VCO. Therefore this filter determines the dynamic response of the loop.

In order to design a loop, two factors are considered; (i) minimising the phase variance in the presence of added white Gaussian noise; (ii) designing for a specific closed loop dynamic response and transient response. First a discussion of the phase variance of the Costas loop is given, and then the design procedure of the loop parameters that define the loop response. It is found that the former is a function of the arm filters while the latter a function of the loop filter.

4.3.1.1 PHASE VARIANCE

The derivation of phase variance in the loop caused by AWGN has been analysed in appendix C. First the derivation for the Stochastic differential equation (SDE) of the Costas loop is obtained. Then, from the (SDE), the phase error variance is obtained, which is given by C-10, of appendix C and restated here. The linearised phase error variance has been obtained which is stationery [4.3]. The actual phase error variance is unbounded, so that it is not a useful measure of tracking performance. All variables are defined in appendix C. Phase variance is

$$\sigma^2_{\phi_e} = \frac{4N_oB_L}{\alpha P}\frac{\left(\frac{\dot{\alpha}}{\alpha}+\frac{N_oB_{LP}}{\alpha P}\right)}{1-\left(\frac{8TB_L}{(\alpha P)^2}\sum_{l=1}^{\infty}R_d^2(lT)\right)} \quad rad^2 \qquad (C-10)$$

The phase variance can then be calculated for different arm filters. It is shown that matched filters in the arms, minimise phase variance and are therefore the best choice. However, when considering the operation of the loop in acquisition mode, there exists no data clocking signal to operate the integrate and dump filter. Therefore, second order Butterworth filters have been used in the Costas loop arm filters. Integrate and dump filters can be added outside the loop to provide optimum data recovery once the loop has acquired lock and is in tracking mode.

The phase variance for these two cases has been studied, and given by equations 4.12 and 4.13 [4.3]. The phase error variance employing a matched filter is :

$$\sigma^2_{\phi} = \frac{N_oB_L}{P}\left(1+\frac{N_o}{2PT}\right) \quad rad^2 \qquad (4.12)$$

The phase error variance for the nth order Butterworth filter :

$$\sigma_\phi^2 = \frac{N_o B_L}{\alpha P}\left[\frac{\alpha'}{\alpha} + \frac{N_o B_{LP}}{\alpha P}\left(1 - \frac{1}{2n}\right)\right] \qquad rad^2 \qquad (4.13)$$

The output bit energy, $Eb = Es = P \cdot \alpha \cdot T = P \cdot \alpha \cdot / B_{LP}$. Both the above equations are inversely proportional to the signal-to-noise ratio, $2E_S/N_O$. The matched filter version is superior in the sense of smaller phase error variance. The graphs of Fig. 4.15. show the minimum phase variance as a function of E_b/N_O and filter bandwidth, for four different arm filters. The second order Butterworth is denoted by (2). A relatively higher bandwidth is required at high S/N ratios.

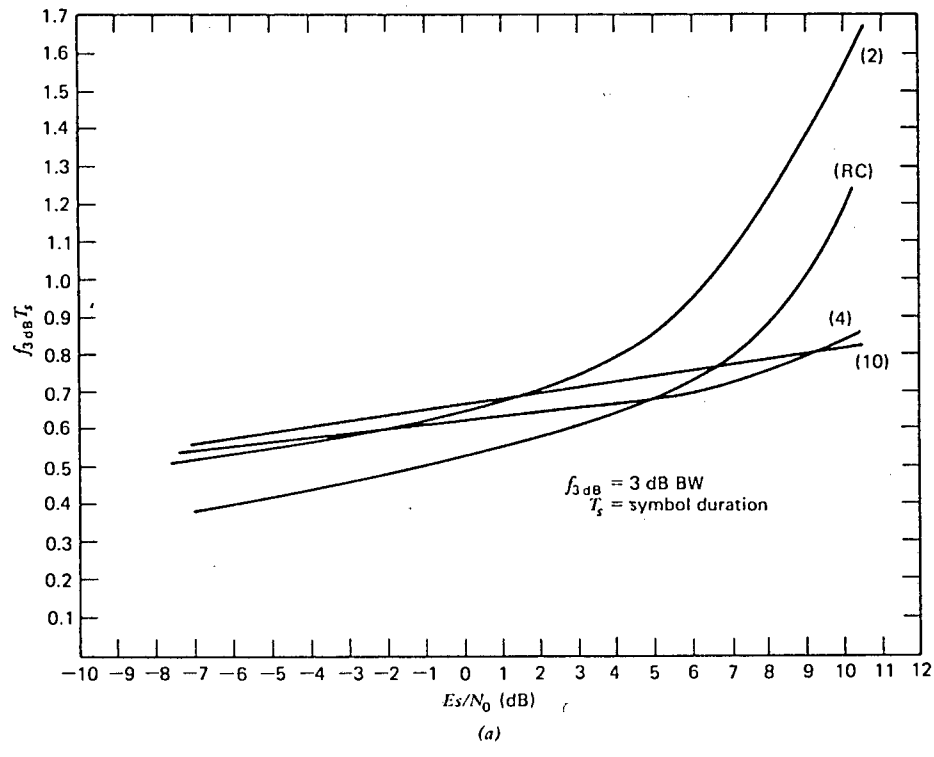

FIGURE 4.15 : *Optimum 3-dB data filter bandwidth for NRZ data [4.3].*

For the second order Butterworth the optimum value is about $f_{-3dB} \approx 0.65/T$. The actual value of $\mathbf{f_{-3dB}}$ is not very critical in terms of minimising σ_ϕ^2 since the optimum is spread over a range of $\mathbf{E_b/N_S}$ values. In fact, 20% - 30% changes in $\mathbf{f_{-3dB}}$ cause only a few percent increase in tracking error variance.

4.3.1.2 DYNAMIC RESPONSE

The Costas loop is a closed loop feedback control system and the dynamic response can be found as shown in sub-section 1.2 of appendix C. The analysis shows how the Costas loop is controlled by the quadrature-phase arm and the feedback control transfer function obtained is identical to a simple phase locked loop. The result is a simplified, single feedback loop repeated in Fig. 4.16.

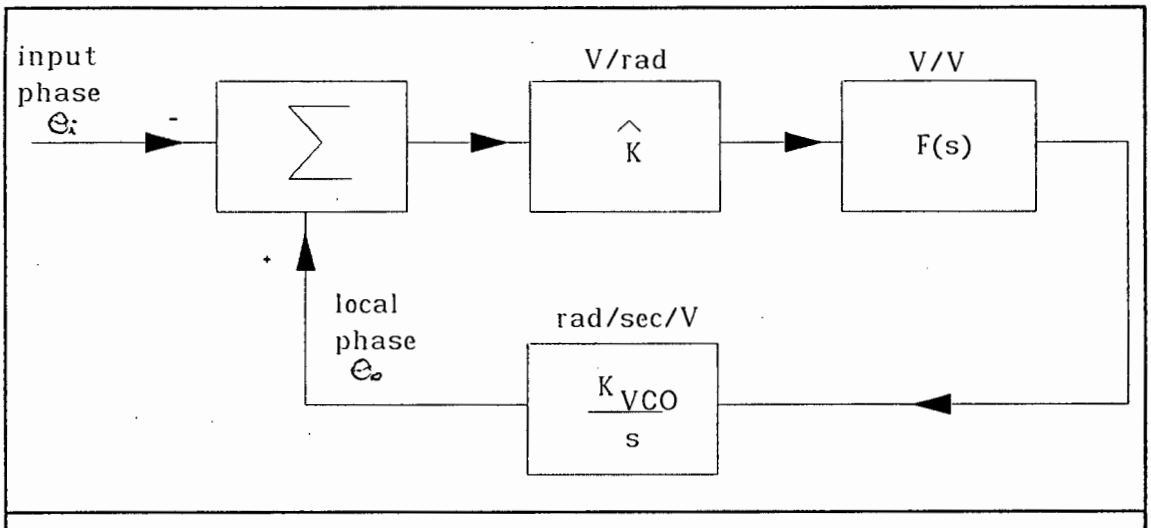

FIGURE 4.16 : *Linearised loop.*

The input is phase θ_i and the output is phase θ_o. Conventional phase-locked loop theory is applied and the loop parameters such as natural frequency (ω_n), damping ratio (ζ), open loop gain ($\mathbf{K_{ol}}$) can be determined and designed. A root locus analysis is used to describe loop stability. The following sub-section explains the steps to designing the Costas loop. Results from appendix B and C are used.

4.3.1.2.1 LOOP DESIGN

The Costas loop is designed by choosing the parameters of the closed loop transfer function, such that the loop is stable, and the dynamic response is adequate. The

closed loop transfer function is given as equation B-11 and has been re-written here with for active, lead-lag, loop filter.

$$T(s)=\left(\frac{AK_{ol}(\tau_2 s+1)}{s((\tau_2+\tau_1)s+1)+AK_{ol}(\tau_2 s+1)}\right) \qquad (4.14)$$

Where $\tau_1 = R_3C$ and $\tau_2 = R_2C$. Equation 4.14 can be written:

$$T(s)=\frac{s\omega_n\left(2\zeta-\frac{\omega_n}{K_{ol}}\right)+\omega_n^2}{s^2+2\zeta\omega_n s+\omega_n^2} \qquad (4.15)$$

Where:

$$\omega_n=\sqrt{\frac{K_{ol}}{\tau_1+\tau_2}} \quad rad/\sec \qquad (4.16)$$

$$\zeta=\frac{1}{2}\sqrt{\left(\frac{K_{ol}}{\tau_1+\tau_2}\right)\left(\tau_2+\frac{1}{K_{ol}}\right)} \qquad (4.17)$$

The major design constraint when selecting the bandwidth of the closed loop transfer function is the received signal-to-noise ratio. For small received signal-to-noise ratio, the loop bandwidth will be designed to be small, to eliminate as much as noise as possible. However this is at the expense of lock-in range. A trade-off exists between designing a wide loop bandwidth, which gives fast acquisition and a wide acquisition range, or a narrow loop bandwidth which eliminates noise resulting in better tracking. From Fig. B-4 and equation B-18, the natural frequency determines the acquisition range of the loop. The choice of components follows five steps :

1. Select natural frequency , $\omega_n = 750(2\pi) = 4712 \quad rad/\sec$

2. Choose a damping ratio of $\zeta = 0.707$.

3. The open loop gain is determined from the required tracking range of the loop. In reality a very small Doppler shift is expected (< 10 Hz) and the tracking range should be small, but a narrow tracking range requires a very accurate crystal based voltage controlled oscillator (VCXO), that has a gain of a few volts/Hz. An R-C VCO has been used which is less sensitive (see 4.3.1.2.5) and a wider tracking range is selected. Set

$$\Delta\omega_H = \pm 43982 \quad rad/\sec = K_{ol}$$

4. Calculate the time constants for the loop filter components:

$$\tau_1 + \tau_2 = \frac{K_{ol}}{\omega_n^2} \quad \sec$$

$$\tau_1 + \tau_2 = \frac{14000\pi}{(4712)^2}$$

$$= 2\times 10^{-3} \quad \sec$$

$$\tau_2 = \left(\frac{2\zeta}{\omega_n} - \frac{1}{K_{ol}}\right) \quad \sec$$

$$\tau_2 = 277\times 10^{-6} \quad \sec$$

$$\Rightarrow \quad \tau_1 = 1.7\times 10^{-3} \quad \sec$$

5. Select C = 10 nF, R2 and R3 are then calculated. The -3dB frequency of the loop filter is given by :

$$f_{-3dB} = \frac{1}{2\pi C\sqrt{R_3^2 - R_2^2 + 2R_2R_3}}$$

The equivalent noise bandwidth of the closed loop given by equation B-16 ofappendix B is, B_N = **3.2 kHz.** The component values used had an insignificant variation as listed in table 4.2.

ω_n (rad/sec)	ζ	K_{ol}	R_2 (Ω)	R_3 (Ω)	C (Farad)	f_{-3dB} (Hz)
4560	0.208	43000	6k8	200k	10n	77

TABLE 4.2 : *Costas loop design summary.*

The loop filter turns out to be very narrow at 77 Hz. This results in a good dc signal to drive the VCO, however, this limits the maximum frequency error through the loop filter to 77 Hz. The problem is that when the demodulator is turned on and a 700 Khz carrier appears at the input to the loop, if the VCO output is at a value such that the error frequency is greater than 77 Hz, the loop will never acquire lock. The solution is to ensure that the VCO output can never swing to such a value, but this implies a very sensitive VCO gain of a few Hz per volt. For this thesis a sensitive VCO has not been used and the VCO gain is set at K_{VCO} = 6 kHz/V. The power supply is +/- 6 V, which implies a maximum VCO output swing of 1 Khz about 700 Khz. On start up, it may be necessary to sweep the VCO to acquire lock, due to the wide VCO sweep.

The next step is to set the rest of the constituent gain transmittances of the open loop gain K_{ol}, as given by equation C-27 of appendix C, namely; K_{m3}, K_{PD1}, F(0) and K_{m2}. K_{PD1} and K_{r} are functions of the multiplier gain, input voltage amplitude, local oscillator amplitude, and arm-filter gain. Both arm-filter are set to unity gain in the passband. Both the phase detector multiplier and the correlator receiver multiplier are set identically. The gains are K_{m2} = 8 V^{-1} and K_{PD1} = 0.64 V/rad respectively.

K_{m3} = 1.13 V^{-1} , the loop multiplier gain.

F(0) is the dc gain of the loop filter = R_3/R_1. These resistors are used to make up the complete open loop gain as follows:

$$F(0) = 43000 \cdot \sqrt{2}/(K_{PD1} \cdot K_{m3} \cdot K_{VCO} \cdot K_{mi} \cdot \overline{V}) = 3$$

Therefore $R_1 = R_3/3 = 66 \quad k\Omega$

The acquisition range can be calculated to be , $\Delta\omega_a = 2\zeta\omega_n = 1897 \ rad/sec$, which is small, making acquisition difficult.

4.3.1.2.2 MULTIPLIERS

Four analogue multipliers are used in the demodulator, three in the Costas loop and one for the tone detector. All have been implemented using XR2208 four-quadrant, active, analog multipliers. The devices offer flexibility in designing gain and bandwidths required and interface easily with digital logic and other analogue, monolithic circuits.

Within the Costas loop there are *two arm* multipliers (in-phase and quadrature-phase) and *one loop* multiplier. The design equations are the same for all three cases. The gain of the multipliers with the *on-chip* differential op. amp. placed ahead as an amplifier, is given by equation 4.4. The *loop filter* uses the *on-chip* op. amp. of the *loop* multiplier. The input to the two arm multipliers can be ac coupled, however the loop multiplier is a dc multiplier and can not be ac coupled. Appendix H gives the complete circuit diagram showing all three multipliers.

In order for the the multipliers to operate linearly the input voltages must be kept within a range specified in the data sheets. For a power supply of +/- 6 V, the range is - 4 V < V_{in} < 2 V. All the multipliers used in the Costas loop have been biased to operate linearly.

4.3.1.2.2.1 ARM MULTIPLIERS

The arm multipliers are set up using equations 4.4. When analysed in the loop, the quadrature-phase arm multiplier is included with the low pass filter. The combination is analysed as a phase detector with units of V/rad. This gain is dependent on the input voltage. By fixing the input voltage, the voltage/rad gain is constant and is measured as follows:

View the output of the arm filter on an oscilloscope. Apply an unmodulated carrier to the Costas loop input from a variable frequency generator. Sweep the input frequency until the beat frequency is < 100 Hz. Just before the loop locks onto the input, the beat frequency passes through a maximum amplitude. The peak to peak voltage at this maximum is measured and occurs at the maximum phase difference between the local oscillator and the input, i.e. at $\Delta\theta = \pi \ rad$. The gain is calculated as $K_{PD1} = V_{p-p}/\pi \ V/rad$. The phase detector is configured as shown in Fig. 4.17. The in-phase arm multiplier also is configured as shown in Fig. 4.17.

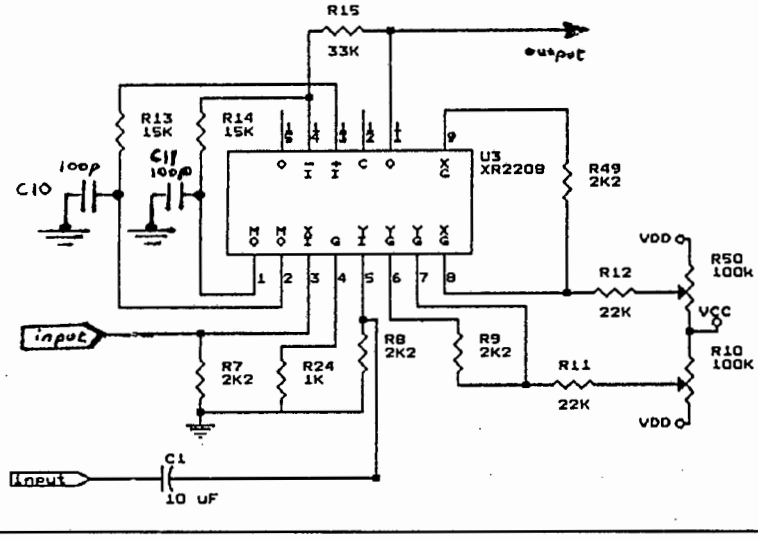

FIGURE 4.17 : *Multipliers used in Costas loop as phase detectors.*

4.3.1.2.2.2 LOOP MULTIPLIER

The configuration used for this multiplier is shown in Fig 4.18. The two inputs and the output are dc coupled with the circuit because the input is a dc control signal and the output is a dc control signal. The *on-chip* op. amp. has been configured as a lead-lag low pass filter, described next.

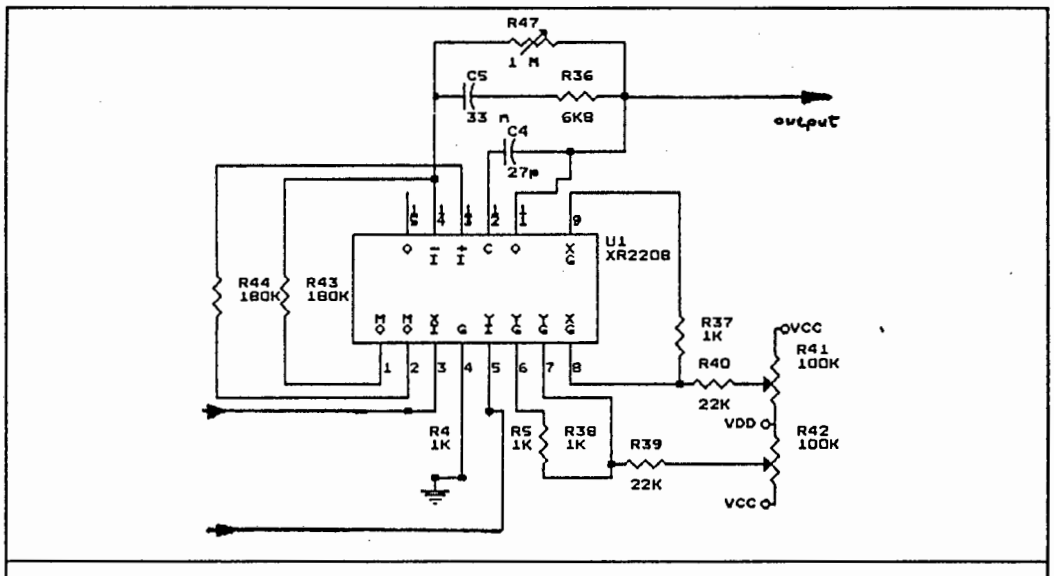

FIGURE 4.18 : *DC multiplier used in Costas loop.*

4.3.1.2.3 LOOP FILTER

The loop filter is a first order active lead-lag filter, implemented with the op. amp. supplied on the XR2208 multiplier. The external components shown in Fig.4.18, correspond to the components given in Fig. B2 as follows,

R1 = R43 = R44
R2 = R36
R3 = R47
C = C5
The explanation of the loop filter operation is given in appendix B.

4.3.1.2.4 ARM FILTERS

These filters play a dual role, when the loop is out-of-lock, the output of the phase detector is an error voltage, required to steer the loop back into lock; when the loop is in-lock the in-phase arm filter is a data filter that provides the demodulated data. In chapter three section [3.4.3.2] it was shown that optimum data filters employing second order Butterworth filters must be set at a -3 dB bandwidth approximately equal to the inverse of the bit period, $\mathbf{f_{-3dB} = 0.6/T\ Hz}$. In section 4.3.1.1.1 the optimum -3 dB bandwidth to minimise the variance in the Costas loop is $\mathbf{f_{-3dB} = 0.65/T\ Hz}$. These values are almost identical and are both loosely dependent on signal-to-noise environment. The chosen value has been set at $\mathbf{f_{-3dB} = 1/T\ Hz}$.

The Costas loop must demodulate six different bit rates. Thus the arm filters must be able to pass these six different bit rates. To implement a variable bandwidth low pass filter, various options are available. Using a conventional filter circuit, different bandwidths can be obtained by switching in suitable component values when required. This is cumbersome when second order filters are required.

A most suitable choice to implement such a variable bandwidth filter is the Switched Capacitor filter. These data sampling filters have recently become popular circuit devices where precise control of filter cut off is required. Filter bandwidth is controlled by an applied clock which can be fine tuned. Two second order filters are available on one integrated circuit package. Flexibility is allowed in the design of different filter configurations. In this use, second order, Butterworth filters have been designed.

These filters are limited in gain-bandwidth product, but newer products are becoming available all the time. The device that has been chosen is a very recent National model LMF100, which has a gain-bandwidth (G-BW) product of 100 Khz. There are however filters made by Maxim which offer a 130 Khz G-BW product.

A switched capacitor filter is a sampled data filter, and as such, differs in many ways from conventional continuous-time filters. The clock frequency applied to the device is the sampling frequency which must be twice the highest frequency component of the input spectrum, to avoid aliasing. Anti-alias filters have been used to reduce energy at high frequencies. R-C low pass filters are used as shown in Fig. 4.17. $R = 6k\Omega$ the internal resistance of the multiplier and C10 = C11 = 100 pF , combined gives f_{-3dB} = 265KHz.

On start up at the demodulator, the filter bandwidth will be defined at a preset position. The applied clock that selects the filter bandwidth, is derived from a separate oscillator as shown in Fig 4.19. A CMOS oscillator has been used, in an RC network. The oscillator is set at 3.5 Mhz which is the maximum clock frequency that can be applied to the LMF100. Using a 4040 device (U43) this frequency is divided by two, five times, to give six different clock frequencies, each selects one of the six different bandwidths. Each bandwidth is thus half of the previous.

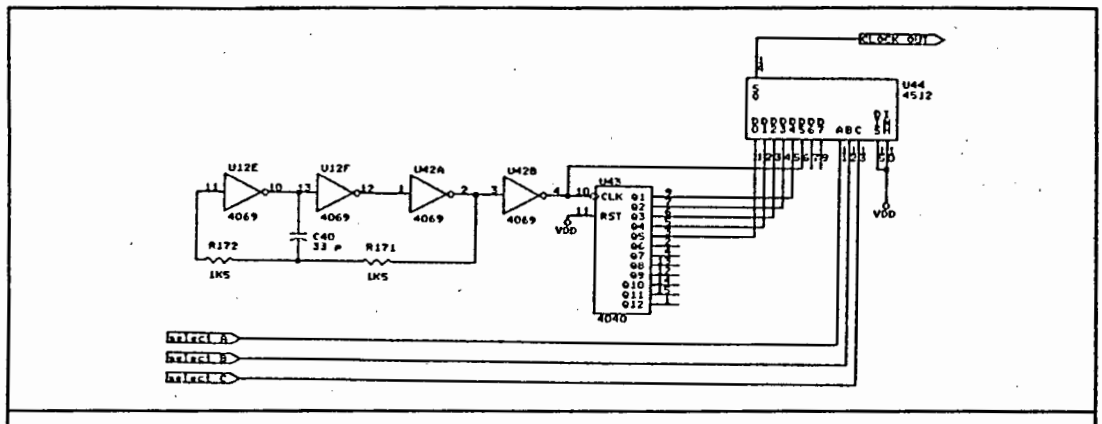

FIGURE 4.19 : *Switched capacitor clock generator.*

The switched capacitor design equations are described in the appendix D along with the chosen resistor values. By selecting four external resistors the device is set to give the six different cut off frequencies by selecting one of the derived clocks.

Amplitude and phase response plots have been measured for all six cut off frequencies, which are also given in appendix D. The two arm filters are on the same monolithic i.c. and have been assembled using the identical components. Therefore, only one filter has been analysed with results which apply for the other arm filters. The Phase characteristic of each filter is almost linear in the passband. The amplitude characteristic has a second order roll-off of -40dB/decade. The -3dB amplitude is shown and measured at 1.1 f_b Hz.

4.3.1.2.5 VOLTAGE CONTROLLED OSCILLATOR

Voltage Controlled Oscillator (VCO) is an XR2207 device that provides a square wave at the frequency set by the input voltage, V_C. A quadrature-phase output is obtained from this square wave by integrating the output. The op. amp. placed after the VCO is shown in Fig 4.20. The VCO is set up with the following equations: The center frequency is given by

$$f = \frac{1}{R_3 C} \quad Hz$$

and varies with the input voltage according to the following equation

$$f = \frac{1}{R_3 C}\left[1 - \frac{V_C R_3}{R_C V_-}\right] \quad Hz$$

The voltage to frequency conversion gain is given by

$$K = \frac{\Delta f}{\Delta V_C} = -\frac{1}{R_C C V_-} \quad Hz/Volt$$

The gain is negative which implies that a positively increasing voltage applied to the input, decreases the output frequency. $\mathbf{R_3}$ and **C** are chosen for a centre frequency of 700 Khz at zero volts input. $\mathbf{R_C}$ is then set for the required volts-to-frequency gain. The VCO output frequency is then linearly dependent on the input voltage $\mathbf{V_C}$.

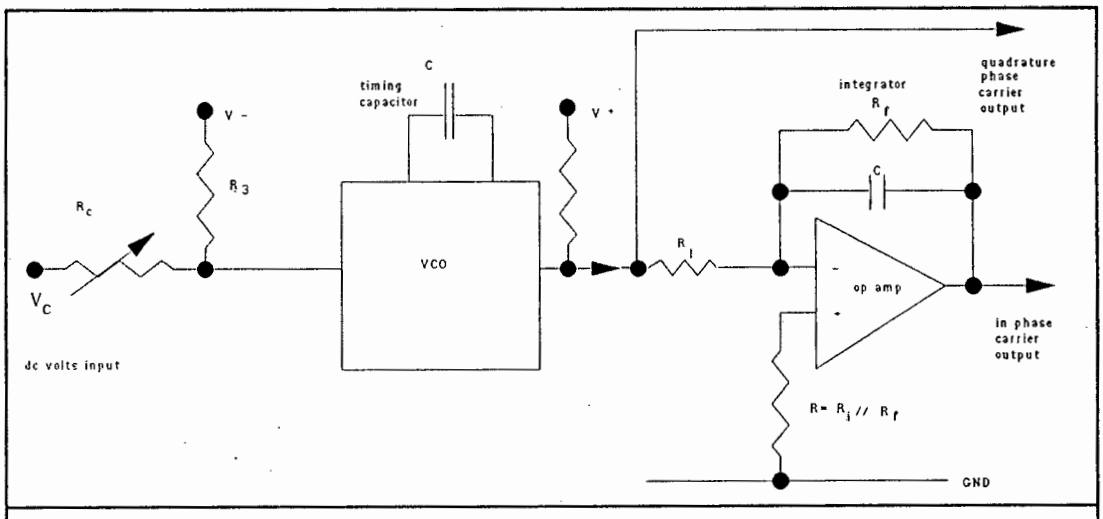

FIGURE 4.20 : *VCO used in Costas loop.*

The 90° phase shift is generated by integrating the square wave output of the XR2207. The integrator is

implemented with an LF351 op. amp. The integration time constant is 5μsec. A 4 V_{p-p}, 700 kHz input square wave results in a 3.5 V_{p-p} triangular wave.

The op. amp. configuration is an inverter which implies that the output waveform has a -90^{o} phase shift. The negative gain of the VCO is thus cancelled out in the complete open loop gain expression, which is the product of all the dc gain transmittances around both arms of the loop (equation C-27, appendix C).

If the phase difference between the input and local oscillator is positive, i.e. the input frequency is greater than the local oscillator, then the positive error voltage will cause an increase in VCO frequency, thus pulling the loop into lock.

The output waveforms of the XR2207 and the inverter are shown in Fig. 4.21. The peak-peak voltage in both cases is 1.5 V. The voltage has been reduced by the potential divider network at the input to the loop multipliers. The markers could not be accurately placed on the display, and the frequency **is** exactly 700 Khz.

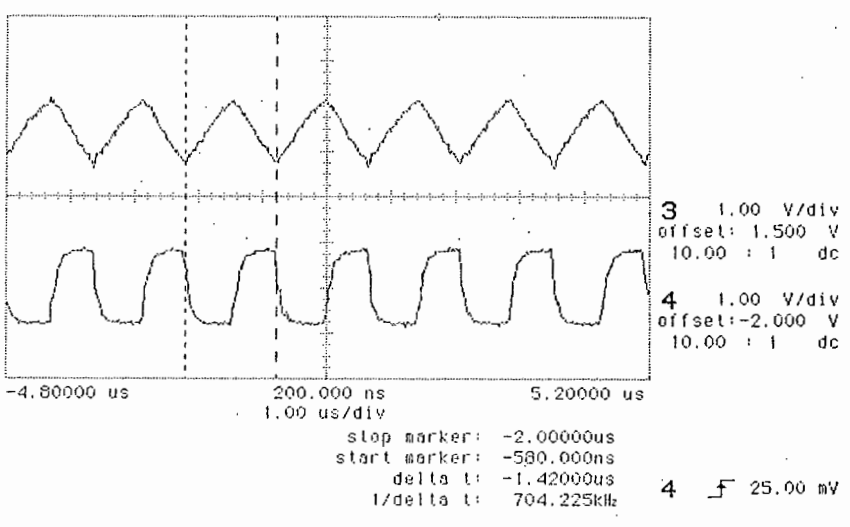

FIGURE 4.21 : *Local oscillator signals.*

4.3.2 (B) BIT SYNCHRONISATION

Bit timing recovery or bit synchronisation is the process of recovering a clock from the demodulated data, at the frequency of the current data rate. This clock is then used to clock the received data through the differential decoder and then into a digital recording device, memory, a screen, or printer.

The recovered NRZ data contains no timing information. The spectrum of Fig. 3.17 (a), is a continuum, possessing no discrete spectral line. In order to extract timing, the data is delayed and multiplied, which generates a train of timing spikes at the bit edges. This is a nonlinear process which is commonly used [2.6, chap. 6] as shown in Fig. 4.22. This process transforms the spectral nulls at all integer multiplies of the bit rate into harmonics at these frequencies. A bandpass filter selects the first harmonic for the input to a phase locked loop which finally provides a synchronous clock for the data.

The actual circuit has an inherent propagation delay caused by the finite delay of the components. To eliminate this small difference between the data and the recovered clock, a data latch has been used to ensure synchronism between the clock and the data.

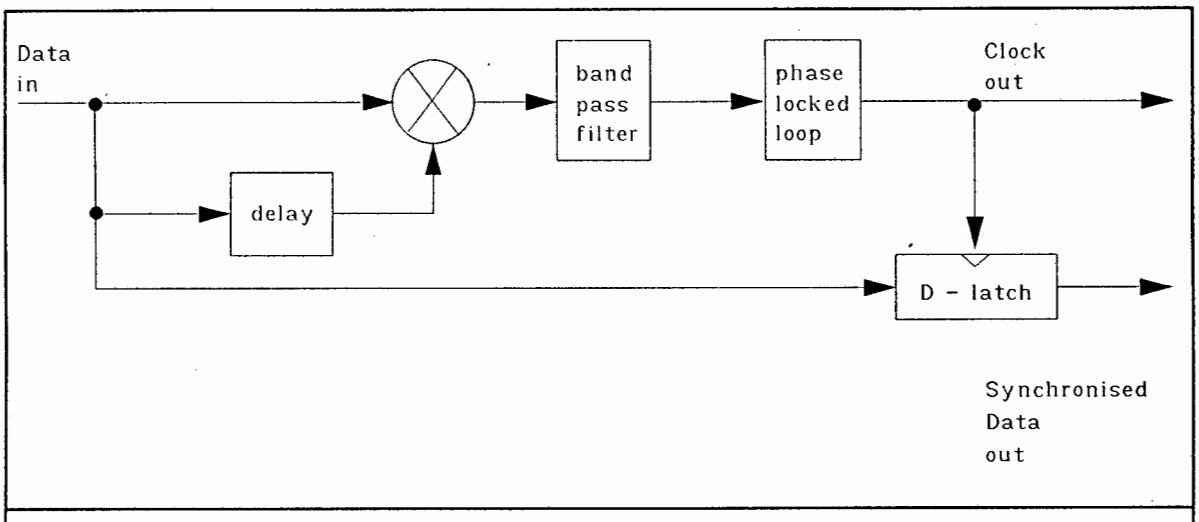

FIGURE 4.22 : *Bit timing recovery technique.*

The input is digital data and a simple RC-delay is used which gives a pulses of period $\tau = 3\mu$sec., every time a bit edge occurs. In such circuits an optimum pulse width can be found which gives maximum energy in the first harmonic [2.6 chap. 6]. The analysis given in the reference shows that the optimum delay is half the bit period, $\tau = T/2$ sec. A monostable (4047) is used to provide an exact pulse width.

Since six bit rates are used, different pulse widths are required for each bit rate. The monostable is set by a fixed capacitor and a variable bank of resistors. The required resistor is selected each time for a particular delay, using an analogue multiplexer (4051). The circuit is shown in Fig. 4.23 (a). The optimum delay at each bit rate was initially set at $\tau = T/2$sec and then improved by experimentation. For the highest bit rate of f_b = 128 kbps, the output pulses are shown in Fig. 4.23 (b), along with the spectrum. The optimum pulse width is found to be $\tau = 4.4\mu$sec. Notice the null in the spectrum occurring at f = 1/4.4 KHz = 227 Khz. The peak occurs at the bit period, f = 128 KHz.

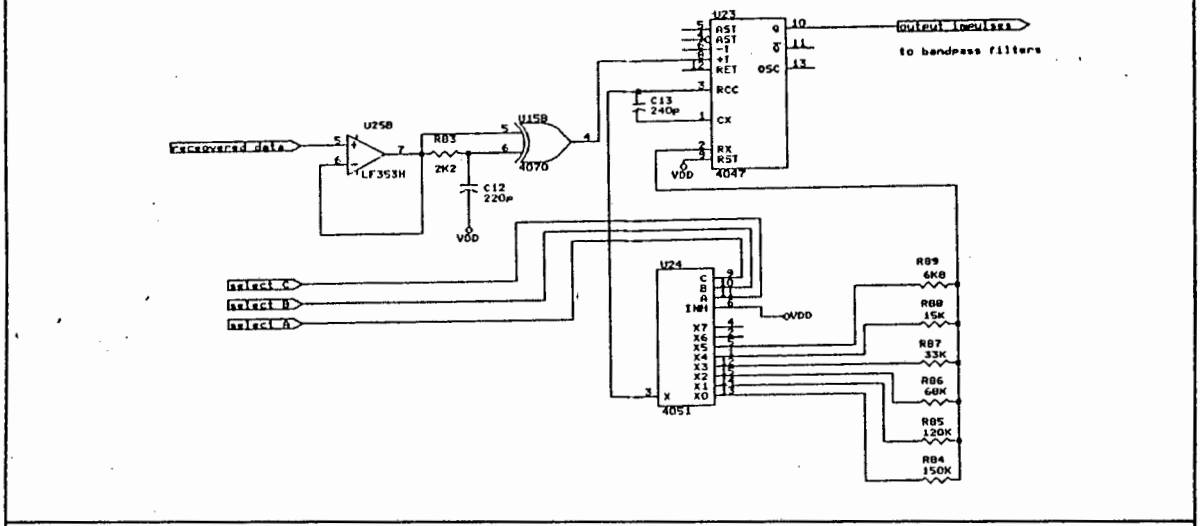

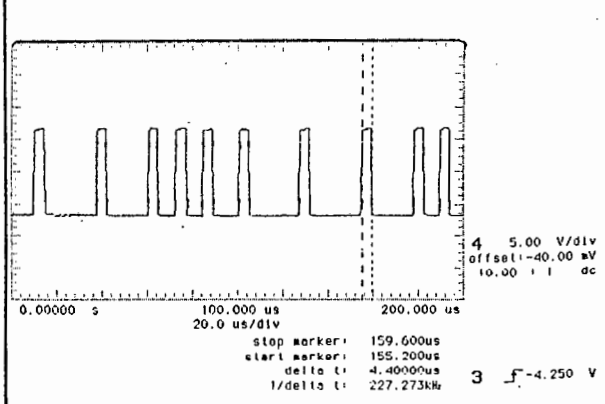

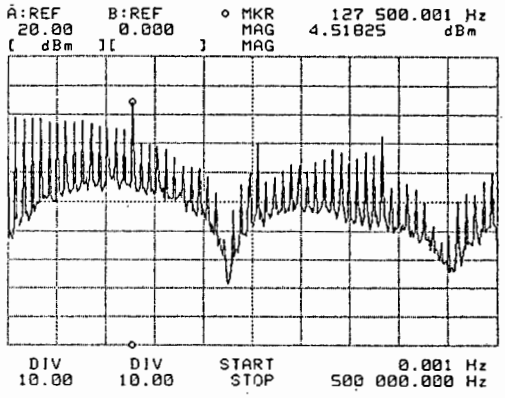

FIGURE 4.23 : *(a) Delay circuit for timing recovery (b) output pulses at 128kbps and (c) spectrum of pulses.*

4.3.2.1 BANDPASS FILTERS

Passive band pass filters have been used to provide the output sinusoid required. The input to the bandpass filters are the pulses of Fig. 4.23 (b). The filter circuit is shown in Fig. 4.24 (a). The output signal and spectrum are shown in (b) and (c) respectively, when operating at 128 KHz. The sinusoidal output provides the timing signal for the phase lock loop.

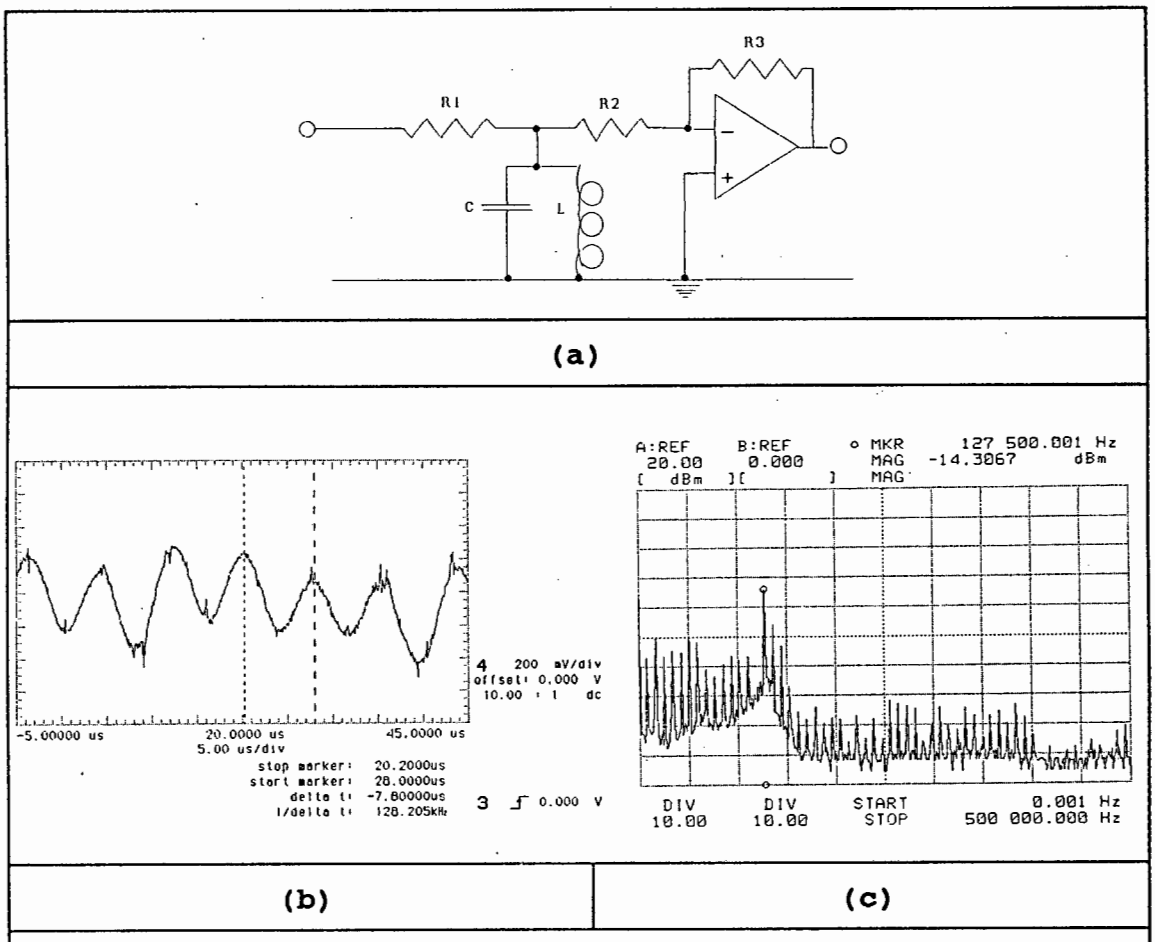

FIGURE 4.24 : *(a) Passive band pass filter output (b) signal and (c) spectrum.*

Six such circuits have been designed at the six resonant frequencies of interest (4 kHz, 8 kHz, 16 kHz, 32 kHz, 64 kHz and 128 kHz. The filters are set in parallel and each filter section is separated electrically by the output of the buffer operational amplifier which acts as a perfect voltage source. A multiplexer switches in the appropriate filter. Each passive filter is a tuned circuit consisting of an inductor and a capacitor tuned to the required frequency. The Q of these filters can be set to a wide range of values by adjusting resistor R_1 and R_2. However, the Q of the filter is limited by the Q of the inductor at the particular frequency of interest. The center frequency of each filter is:

$$f_r = \frac{1}{2\pi}\sqrt{\left[\frac{1}{L\cdot C} - \frac{r^2}{L^2}\right]} \quad Hz \qquad (4.19)$$

The gain at resonance is given by :

$$|H(2\pi f_r)| = -\left[\frac{R_3}{R_1 + R_2}\right]\left(\frac{1}{1 + R_1 // R_2 / |Z|}\right)$$

$$|Z| = \frac{L}{C} + \frac{L^2}{r^2 \cdot C^2} \qquad \Omega$$

At resonance $|Z| \gg R_1 // R_2$ and the gain can be approximated by

$$|H(2\pi f_r)| \approx -\left[\frac{R_3}{R_1 + R_2}\right]$$

The quality factor can be expressed as:

$$Q = \frac{R}{\omega_r L}\left(\frac{\omega_r^2 L^2 + r^2}{rR + \omega_r^2 L^2 + r^2}\right) \qquad (4.20)$$

where
$\omega_r = 2\pi f_r$ is the resonant frequency in rad/sec, **r**, is the internal resistance of the inductor in Ω , **R** is the parallel resistance of $\mathbf{R_1}$ and $\mathbf{R_2}$ in Ω, **L** is the inductance (H), **C** is the capacitance (F).

The measured output of the bandpass filter at f = 128 kHz is shown in fig. 4.24 (b). The input is a stream of 12 $V_{peak\text{-}peak}$ pulses, indicated in fig. 4.23 (b), the output is a 424 mV (rms) sinusoid. The output spectrum of Fig. 4.24 (c), contains a harmonic at f = 128 KHz, that is 15 dB above the next highest harmonic. This proved to be a suitable signal for the phase lock loop. The complete circuit diagram of all six filters is shown in appendix E. Some of the components were adjusted after measurement. Measurements of the six passive bandpass filters phase and amplitude response are also given in the appendix.

4.3.2.2 PHASE-LOCK-LOOP

The phase-lock-loop (PLL) is a closed loop tracking device that is capable of tracking the phase of a received signal that has a residual carrier component. The model of the phase locked loop is reviewed in appendix B, however the PLL device used had slightly different design equations which are given in the data sheets. An XR-215 device has been used consisting of a phase detector and a voltage controlled oscillator (VCO) on one monolithic i.c. The phase locked loop is completed by adding the loop filter externally as well as the components which set the VCO center frequency, and the loop filter. The complete circuit is shown in Fig. 4.25 (a).

The phase-lock loop is designed to lock onto six different frequencies. This is achieved by including a frequency divider in the loop. The dividers are four bit shift registers, 4520 devices (U22A,B). The VCO is set to run at 1.024 Mhz and divided down to the six bit rates (4 Khz to 128 KHz) using a divider. The correct divider output is selected using three control lines and a multiplexer (U23). A second multiplexer is used (U21) which taps the dividers at double the current operating frequency. This is used to provide a 90^{o} phase shifted replica of the recovered clock. Two d-latches (U24A,U18B) clocked at double the frequency, are used to provide the phase-shifted clock. The explanation for this is given here. Let the input to the PLL be written as

$$V_i = A\sin\left(\omega_i t + \theta_i\right)$$

and the local oscillator

$$V_o = B\cos\left(\omega_o t + \theta_o\right)$$

When the loop is in lock the local oscillator is in phase quadrature with the input signal, and the phase detector

output voltage is

$$V_d(t) = V_i \times V_o$$
$$= AB\sin(\omega_i t + \theta_i) \times \cos(\omega_o t + \theta_o)$$

$$= \frac{AB}{2}\{\sin(\Delta\omega + \Delta\theta) + \sin(\hat{\omega} + \hat{\theta})\}$$

Where :

$\hat{\omega} = \omega_i + \omega_o$

$\hat{\theta} = \theta_i + \theta_o$

The loop filter eliminates this higher frequency term and when the loop is in lock

$\Delta\omega = \omega_i - \omega_o = 0$

$\Delta\theta = \theta_i - \theta_o = 0$

The result is that $v_d(t) = 0$, which holds the loop in lock. For the loop in lock, the input and output signals of the PLL are shown in Fig. 4.25 (b) and (c) for f_b = 4 kbps and f_b = 128 kbps operation, respectively. The 90° phase relationship is clearly noticed in (a). Thus to derive a local clock that is in phase with the input data, the VCO output must be shifted by 90°. The recovered in-phase clock is used at the tone recovery multiplier, while the quadrature phase clock is used for the data recovery. The use of the clocks is further explained in sub sections 4.3.3 and 4.3.4 which follow.

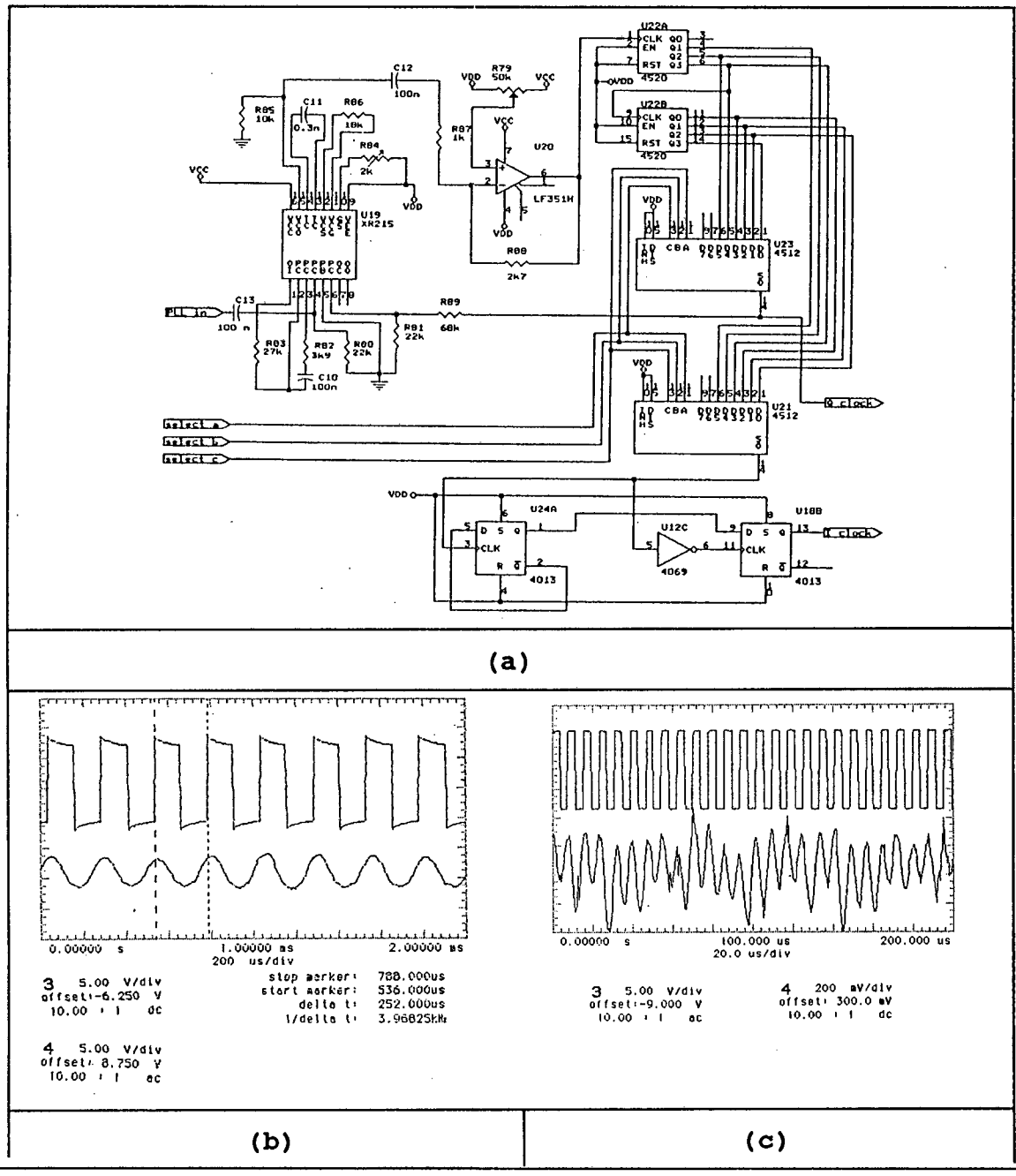

FIGURE 4.25 : *(a) Multi-tone Phase locked loop and input and output signals for (a) 4 kbps and (b) 128 kbps operation.*

The VCO center frequency, f_o , is set with a capacitor, C_o, chosen from curves given in the data book. The exact frequency has been set by variable resistor R84 which fine tunes the VCO.

VCO gain : $k_o = 0.7/C_o R_o \quad rad/sec/V$

Lock range : $\Delta\omega_L = K_o K_d$

Capture range : $\Delta\omega_c = \Delta\omega_L |F(j\Delta\omega_c)|$

The loop filter used is a passive lead-lag filter described by the following equation:

$$F(s) = \frac{1 + R_2 C_1 s}{1 + sC_1(R_2 + 2R_1)}$$

This has a -3dB frequency given by

$$f_{-3dB} = \frac{1}{2\pi C_1 \sqrt{4R_1^2 - R_2^2 + 4R_1 R_2}} \quad Hz$$

The natural frequency is given by

$$\omega_n = \sqrt{\frac{k_{ol}}{C_1(R_2 + 2R_1)}} \quad rad/sec$$

The damping ratio is

$$\zeta = \frac{1}{2}\sqrt{\frac{k_{ol}}{C_1(R_2 + 2R_1)}}\left(\frac{1}{k_{ol}} + R_2 C_1\right)$$

The same analysis used for the Costas loop applies here. The loop filter has a different equation to the previous loop filter transfer function. The component summary is given in table 4.3. Resistor, R_1 is an internal resistor provided on the XR-215 with a value $R_1 = 6k\Omega$. The phase detector gain is set at k_d = 2 V/rad. The open loop gain is given by $k_{ol} = k_o k_d$.

R_o	C_o	R_2	C_1	f_{-3dB}	k_o	k_{ol}
Ω	(F)	Ω	F	Hz	kHz/V	sec^{-1}
18 000	300 p	3 900	100 n	106	21	264000

TABLE 4.3 : *PLL component summary.*

Natural frequency : $\omega_n = 12886\ rad/sec = 2\ kHz$

Damping ratio : $\zeta = 2.5$

Hold-in range : $\omega_l = 264\ krad/sec = 42\ kHz$

Lock-in range : $\omega_c = 1.6\ krad/sec = 2.5\ kHz$

Bandwidth of loop filter : **f_{-3dB} = 106 Hz.** This provides the dc control signal. The bandwidth of the loop determines the immunity against phase noise as well as the transient response. From equation B-16 in appendix B, for a high open loop gain as in this case, the closed loop noise bandwidth is $B_N = 16.75$ kHz

4.3.3 (C) RATE CHANGING CIRCUIT

Without the rate changing circuit, the demodulator would be a straight forward DEBPSK modulator with a fixed Costas loop and fixed bit rate timing recovery. However, the demodulator is designed to demodulate six different bit rates and with this flexibility, a control system is necessary to communicate the occurrence of such changes from the modulator to the demodulator.

The system of controlling the bit rate at the demodulator as given by Fig. 3.18 is further discussed. Adding a tone to the null in the spectrum of a BPSK waveform to convey the occurrence of a new bit rate, has been explained. The only method that has been found of extracting the tone from the data+tone combination at the demodulator is by a bandpass filter, tuned to the tone frequency. Six such bandpass filters are required for each tone frequency.

4.3.3.1 BANDPASS FILTERS

To extract the tone from the base band spectrum, it is necessary to use six bandpass filters arranged in parallel. Each bandpass filter is set at one of the center frequencies, namely : 4 Khz, 8Khz, 16 Khz, 32 Khz, 64 Khz and 128Khz. The bandpass filters act as windows in the spectrum which must be set to a particular frequency. When

energy at the selected frequency is detected, the output of the filter is the required tone that indicates the new bit rate.

The input is the demodulated baseband (data+tone) spectrum. The output is the tone. Originally it was thought that all the filters could be left *open* at all times, and that when a tone arrived, it would be detected by the appropriate filter. However, this can not work because the input to the filters includes data energy. Thus, when receiving the high frequency data rates, the lower frequency bandpass filters will pass energy from the data spectrum. This will cause erroneous energy at the output.

In this case active band pass filters were used as a comparison with the passive filters (sub-section 4.3.2.1). The active circuit used, is a *Friend* circuit [4.6] shown in Fig. 4.26 (a). Six such filters were constructed, the complete circuit with multiplexer is shown in appendix F. The data at the input to these filters causes a step response at the output, which interferes with the filtering of the tone. The higher the Q of the filter, the slower the transient response causing more interference, thus the Q can not be set too high. A value of Q = 10 has been selected as a compromise.

Measurements of the six active filter phase and amplitude response are given in appendix F. The measured Q values had a range of, $5 < Q < 8$. Fig. 4.27 (b) and (c) shows the filtered tone and its spectrum, respectively at f_r = 128 kHz. The sum of the data and the tone appear at the filter input. The transient response caused by the data can be noticed. The filtered tone has a maximum, peak-peak voltage of 450 mV and an average, rms voltage of 160 mV. The spectrum shows the tone harmonic having equal energy to adjacent harmonics (resulting from the short data PN sequence of 15 bits), however, the energy at 128 KHz is sufficient.

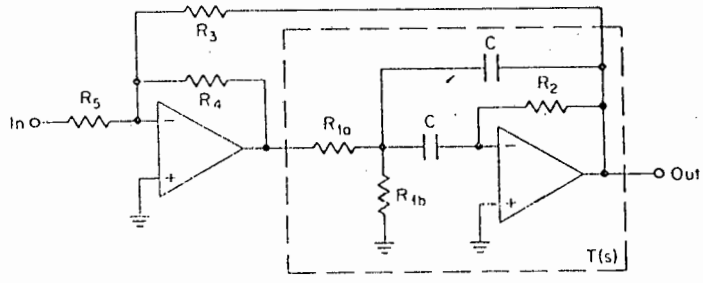

(a)

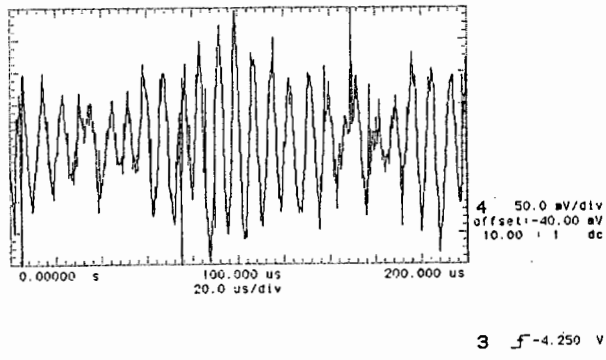

(b)

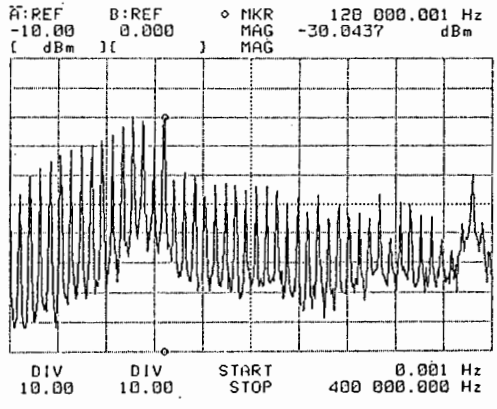

(c)

FIGURE 4.26 : *(a) Friend bandpass filter, (b) output signal and (c) output spectrum.*

The design equations for the Friend circuit are given below. The filter offers a Q enhancement depending on the op. amps.'s used. The first stage Q is selected as Q_r and the overall Q, is Q_{eff}. The first step is to calculate

$$\beta = 1 - \frac{Q_r}{Q_{eff}}$$

The component values are determined from

$$R_3 = \frac{R}{\beta}$$

$$R_4 = R$$

$$R_5 = \frac{R}{(1-\beta)A_r}$$

where R can be chosen and A_r is the required gain at resonance. The value of C can be chosen. The design equations for the Q-enhancement section are given for unity gain:

$$R_2 = \frac{Q_r}{\pi f_r C}$$

$$R_{1a} = \frac{R_2}{2}$$

$$R_{1b} = \frac{R_{1a}}{2Q_r^2 - 1}$$

4.3.3.2 COHERENT DETECTOR

Once extracted, two methods of demodulating information from the tone were investigated. The first method is an envelope detector, the second method is a coherent detector. The second method is preferred and has been implemented with one multiplier and one low-pass filter after the bank of band pass filters.

The **first method** was implemented and tested, however, the results have not been recorded here. The operation of the circuit was based on the envelope detector, which follows the recovered tone envelope. When the tone is present the rising energy level triggers a Schmitt trigger. When the tone is absent the Schmitt trigger remains at zero volts. This circuit is also sensitive to 180° phase shifts in the tone. When a 180° phase step is present at the input to the band pass filter which precedes the envelope detector, the output transient is a decay to zero V and then a recharging

slope to the steady state voltage. This envelope is followed and the phase shift is thus detected. The band pass filter is a second order system and the output transient depends on the damping and the natural frequency of the filter. Thus the speed of response to an input step can be set. The circuit became too cumbersome since the envelope detectors, half-wave rectifiers and the Schmitt triggers that are required were duplicated six times.

The **second method** is by coherent detection of the tone. The coherent detector as shown in Fig. 3.18, and the implementation is shown in Fig. 4.27 (a). The circuit consists of an XR2208 multiplier followed by an RC low pass filter. The filter has R70 = 100 k Ω and C7 = 10nF giving f_{-3dB} = 160 Hz. This is wide enough to pass data at low bit rates of under 200 bit/sec.

The inputs to the multiplier are the filtered tone and a recovered, in-phase clock from the bit timing circuit. The filtered tone is in-phase with the data, and as explained in the previous sub-section, an in-phase clock output from the bit timing recovery can be generated. This is used in a synchronous detector, to synchronously demodulate the received tone. Fig 4.27 (b) shows the filtered tone and the in-phase, local clock. This process is a correlator receiver as used in the Costas loop and can be described by equations 3.8 to 3.10.

Fig 4.27 (c) shows the spectrum of the filtered tone. the component at 4 KHz is 10 dB above the adjacent side-bands. The effect of the data channel causing transients at the output of the bandpass filter, can be seen from the output signals obtained in two cases:

1) When data is transmitted with the tone with the data channel ON , Fig. 4.27 (d) shows the filtered tone (lower trace) and the demodulated data from the tone (upper trace). Modulation is by ON-OFF keying at 6 bit/sec. The recovered maximum measured tone amplitude is 88 mV_{rms}.

2) Fig. 4.27 (e) shows the output of the same filter with the data channel OFF. In this case the tone has been modulated by ON-OFF keying at 7 bit/sec. Notice how the tone is demodulated without interference to an amplitude of 155 mV_{rms}. Thus in the Fig. 4.27 (d), the adjacent data transients interfere with the tone recovery process resulting in an attenuation of 56 %. This is adjacent channel interference.

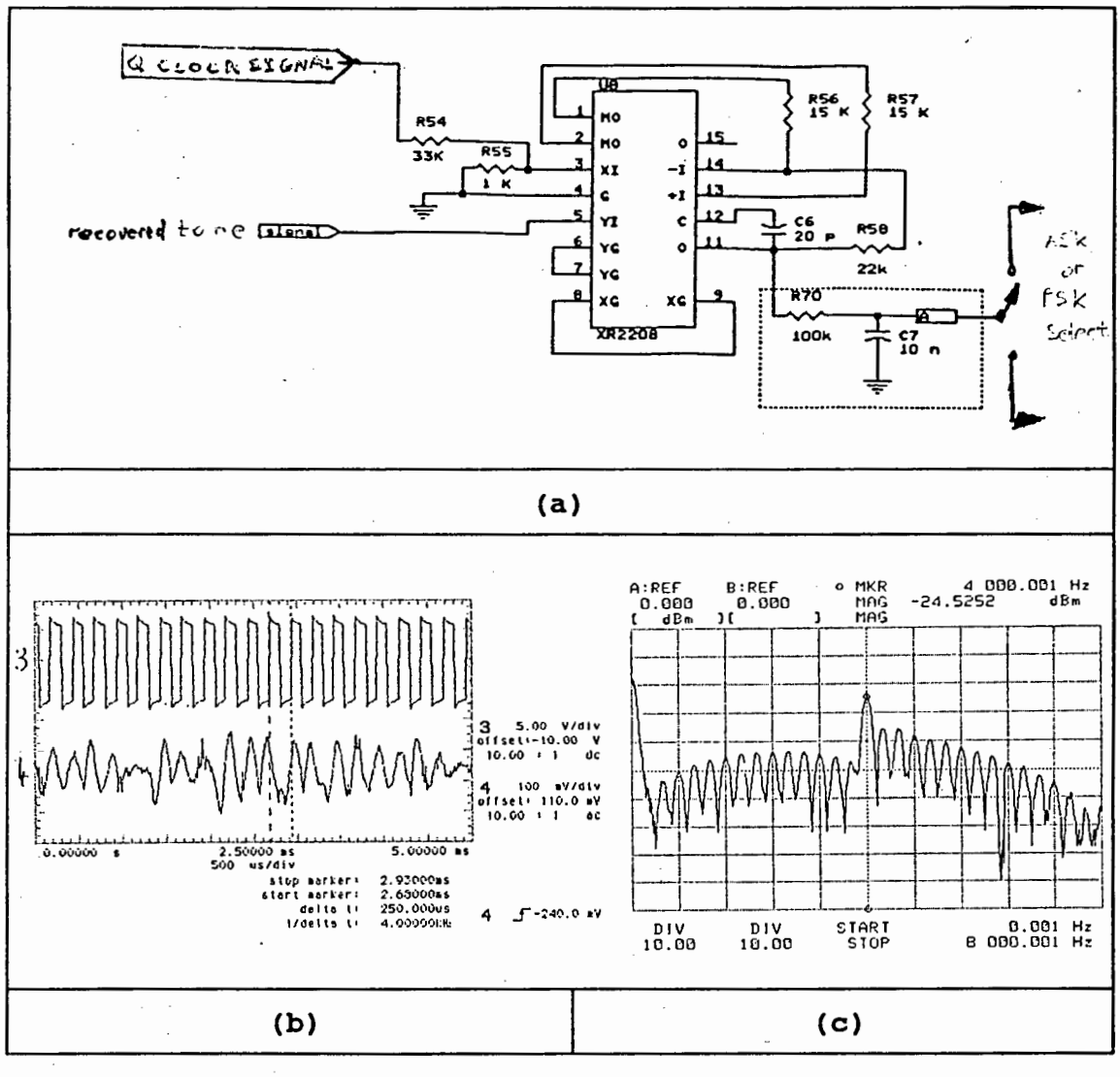

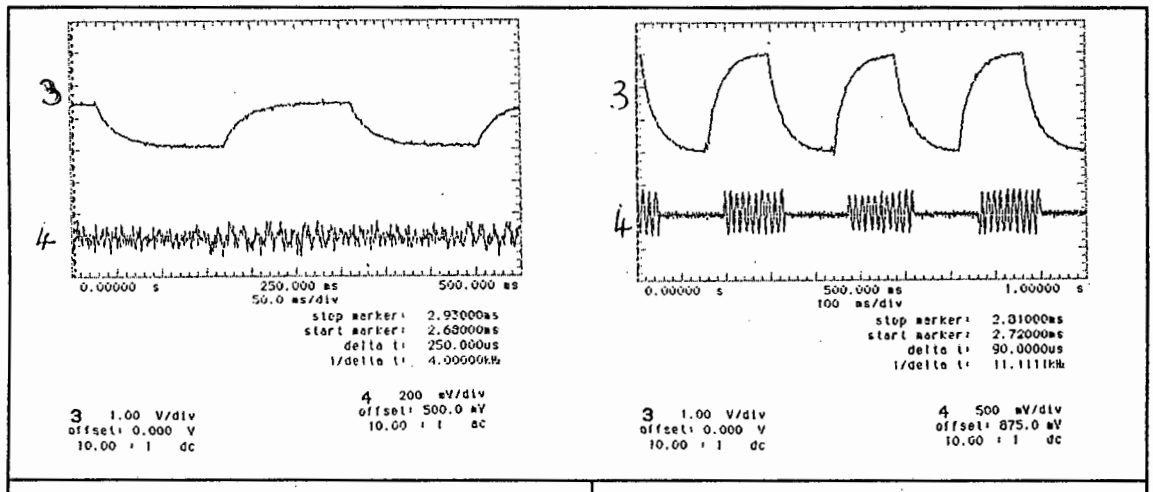

(d)	(e)

FIGURE 4.27 : *(a) Tone detector circuit with (b) input signals and (c) input spectrum with (d) data channel ON and (e) data channel OFF.*

4.3.4 (D) DATA RECOVERY AND DECODING

The demodulated data+tone that appears in the in-phase arm of the Costas loop is shown in Fig. 4.28 (a) the original data+tone signal at the modulator is shown in Fig. 4.28 (b) with t/d = 60 %. The data is recovered using a comparator which has a set threshold. This makes a decision on each bit whether a one or a zero has been received. The threshold is set with a potentiometer and the optimum threshold is found by minimising the bit error count in the presence of noise (see next chapter). The measured output appears different from the predicted output of Fig 3.20 because the figure does not show the effect of the next bit that occurs. In practice, the bit period is defined by the zero crossings, thus the end of the bit period will not be at a maximum as is the case of Fig. 3.20. The measured tone has been attenuated by the arm filters to about 14 % of the data amplitude. The predicted filter transfer function differed from the one that was implemented. The switched capacitor filters in the Costas loop arms, have the same amplitide response as the Butterworth filter, and a linear phase in the passband.

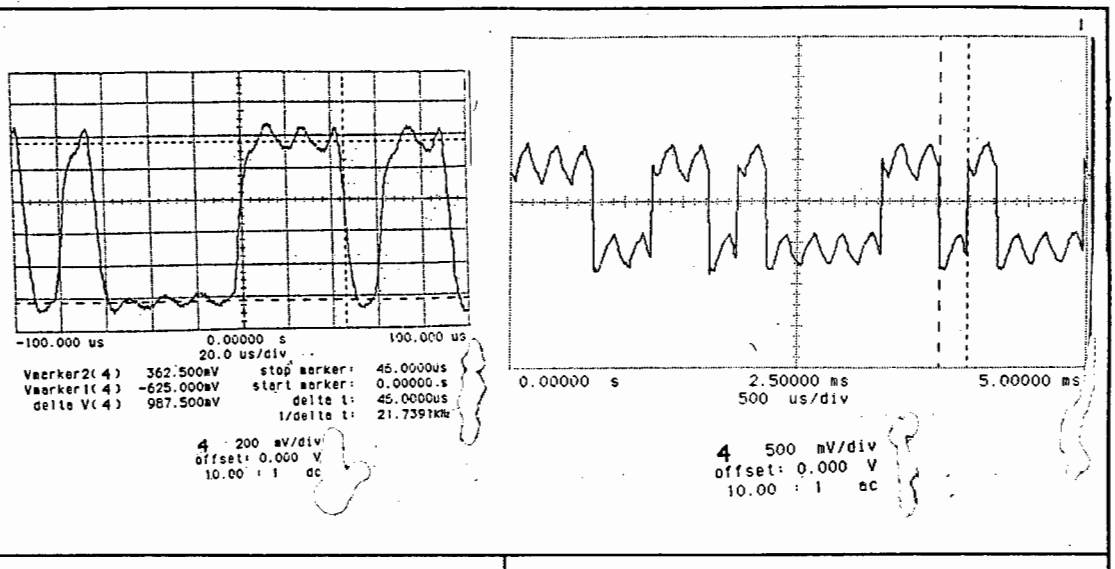

(a)	(b)

FIGURE 4.28 : *Measurement of data recovery process.*

After the hard-decision, data is then sent in two streams, one to the differential decoder, the other to the bit timing recovery circuit. The output of the latter is the data clock. At the decoder the data is first synchronised with the recovered clock from the PLL by a data-latch. This is necessary because there is a small delay of 500 nsec. introduced by the timing recovery circuit which puts the two streams out-of-phase. The data is then decoded in the differential decoder which has been implemented as shown in Fig. 4.29.

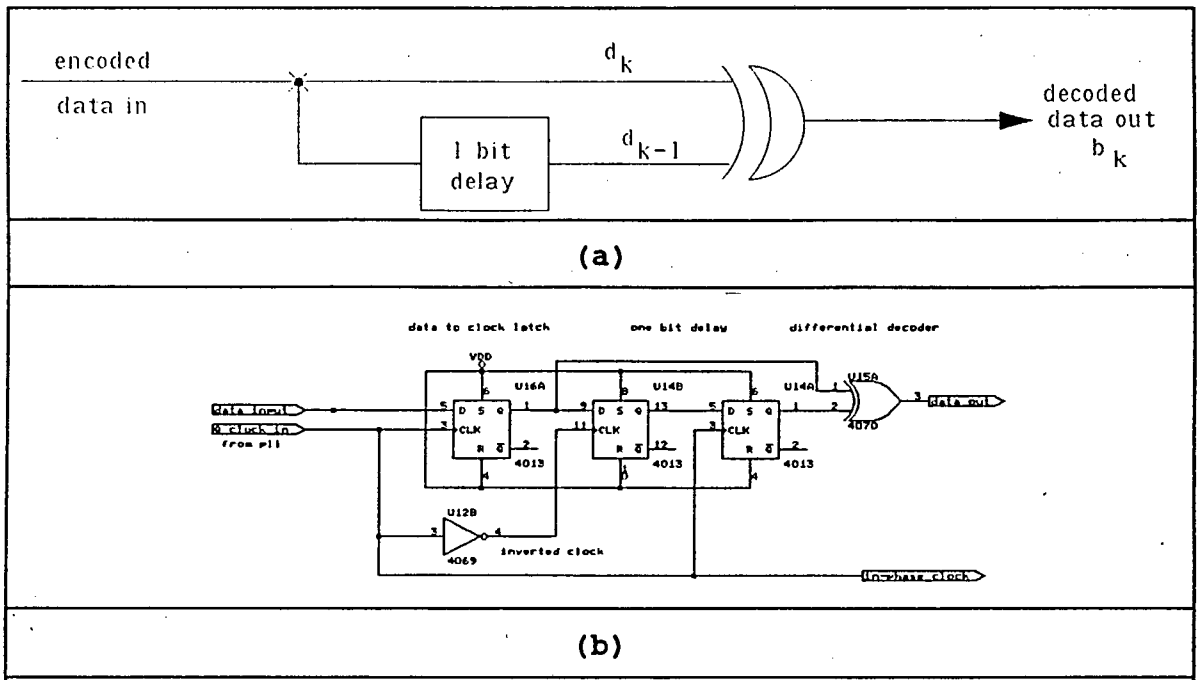

FIGURE 4.29 : *The differential decoder (a) theory and (b) implementation.*

Using a short PN sequence of L = 15 bits, Fig 4.30 (a) shows the recovered data (lower trace) and the original data stream (upper trace) at f_b = 4 kbps and (b) at f_b = 128 kbps.

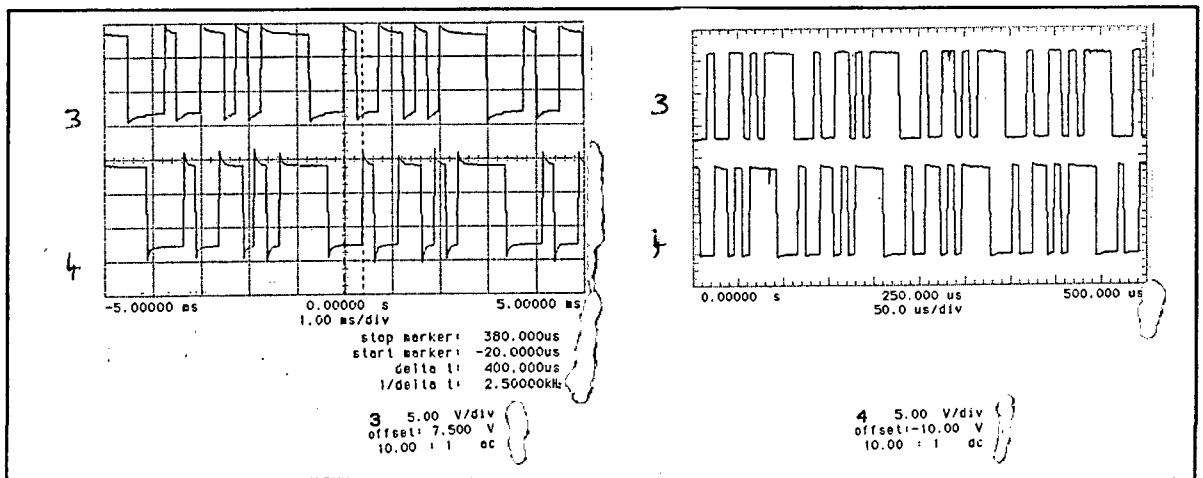

FIGURE 4.30 : *Original and recovered data stream.*

4.3.5 DEMODULATOR SUMMARY

A photograph of the demodulator is shown in Fig. 4.31 (a). The picture is not to scale and the real dimensions are given in Fig. 4.31 (b). The picture actually shows the complete system, since all the circuits were assembled together. The aluminium ground plane is visible. A key to boxes denoted with letters is given :

A: Modulator.
K: Pn-data generator.

Demodulator

B: Costas loop carrier recovery.
C: Passive band-pass filter bank.
D: Phase-lock-loop bit timing recovery.
E: Tone coherent demodulator and Data decoding.
F: Pre-PLL delay & multiply and white noise generator.
G: Active band-pass filter bank.
H: Data synchronisation for testing and counters for data rate control.

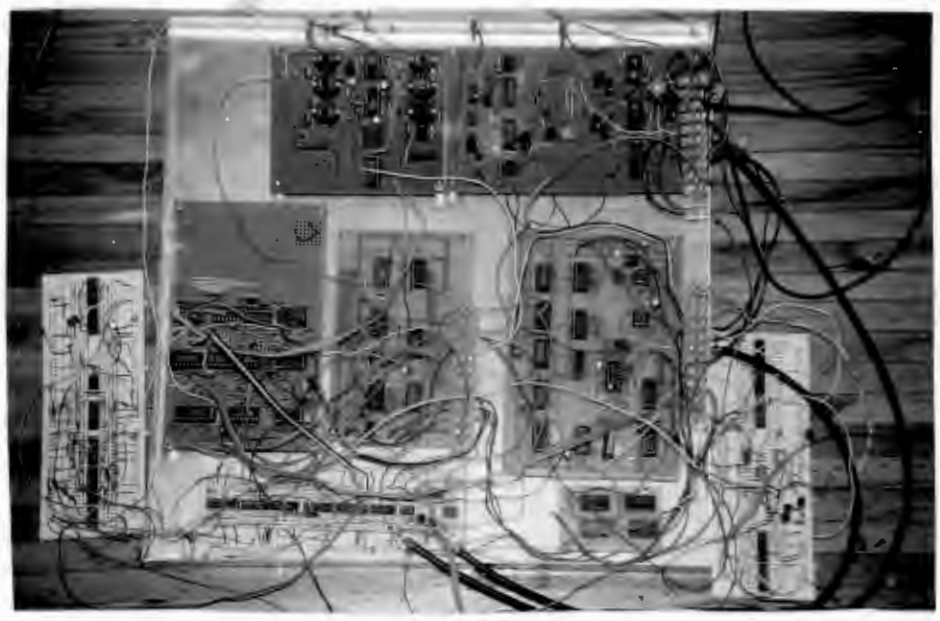

(a)

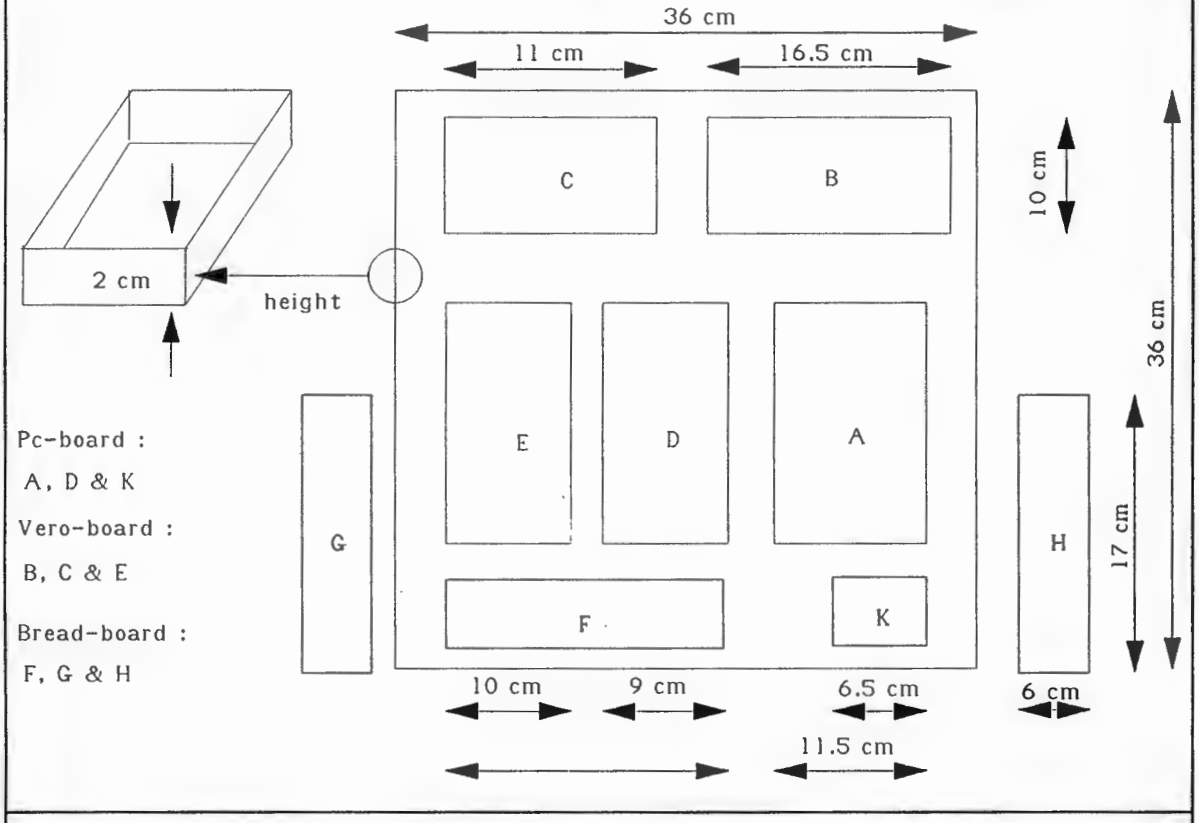

(b)

FIGURE 4.31 : *Photograph of the demodulator (including the modulator).*

4.4 INTERFACE WITH HOST COMPUTER

Although the modem has not been connected to a host computer, the interface requirements between the modem and a host computer is illustrated in Fig.4.32. The complete modem is has the following inputs and outputs.

From computer to modem:

1) Data to be transmitted.
2) Three control lines selecting the bit rate.
3) Enabling strobe to indicate a new bit rate.

From modem to computer:

4) Clock from modulator indicating the current bit rate.
5) Received data.
6) Received data clock.

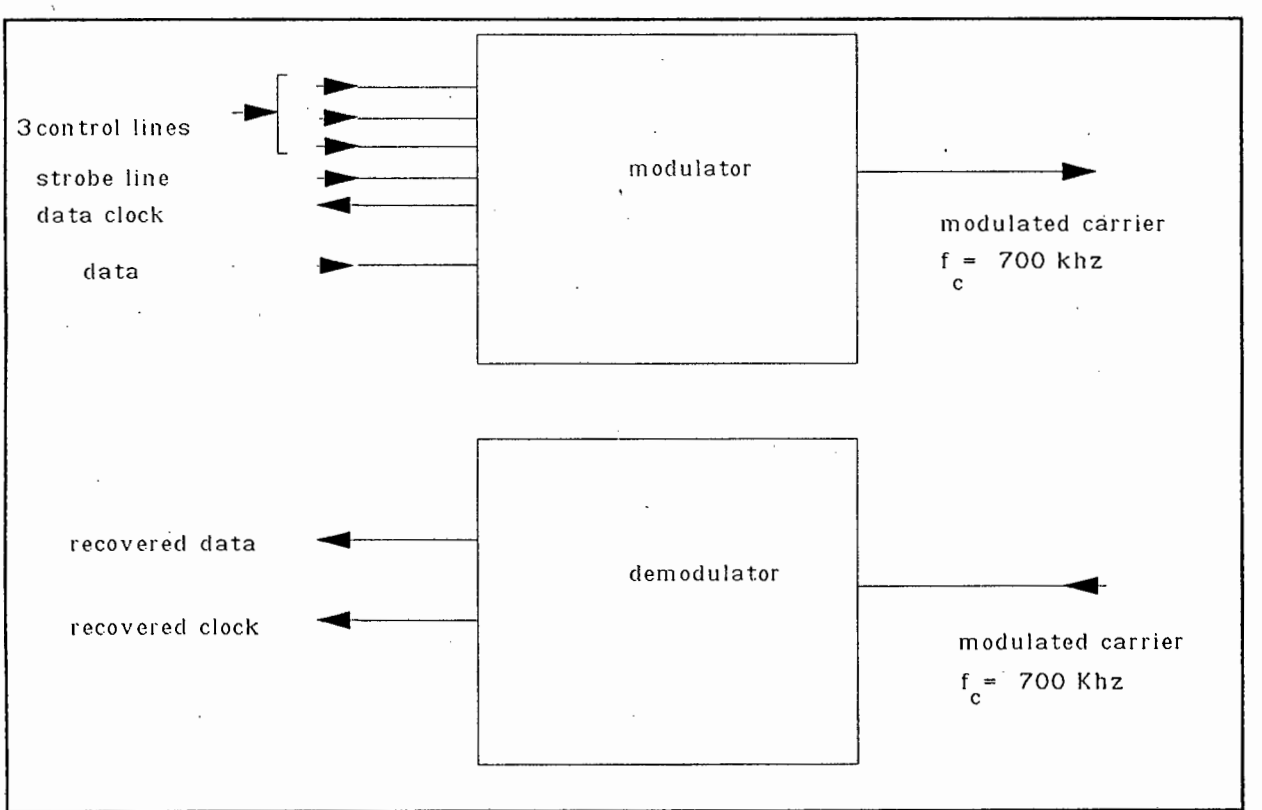

FIGURE 4.32 : *Modem showing inputs and outputs.*

When the host computer requires a bit rate change, a three bit word must be sent to the modem along with a strobe signal to indicate the occurrence of the new rate. The modulator then

modulates the tone which is sent with the data. The modulator then changes bit rate and data begins to be read into the modulator at the new data rate and is transmitted. The demodulator recovers the tone and the data. All bit rate detection is done within the demodulator and it is unnecessary for the host computer to be involved in any of the decision making about the current bit rate. In one modem unit there is no connection between the modulator and the demodulator sections.

4.5 CONCLUSION

The modem has been assembled and preliminary tests have been done. Such tests are qualitative and are carried out in a high S/N environment of at least 20 dB. The results show that:

1. The Costas loop carrier recovery locks onto the input signal at all of the six bit rates.

2. The bit timing recovery circuit, recovers the clock at all the six frequencies.

3. The data is successfully demodulated at the six bit rates.

4. The addition of the tone, with a tone-to-data ratio of 60 %, at the modulator does not cause the carrier recovery to fall out of lock. Neither does modulating the tone by either ASK or PSK at slow data rates of less than 500 bit/sec.

5. The tone can be successfully recovered at the demodulator. The tone can be demodulated using either ASK or PSK modulation schemes.

The results in the following chapter will quantify the above findings and reveal the extent of the usefulness of this modem.

4.6 REFERENCES

[4.1] Costas, J. P., **Synchronous Communications** , Proceedings of the IRE ,vol. 44, pp. 1713-1718, Dec. 1956.

[4.2] Lindsay, W. C. and Simon M. K., **Telecommunications Systems Engineering** ,Prentice-Hall INC. Englewood cliffs, New Jersey.

[4.3] Holmes, J. K., **Coherent Spread Spectrum Systems,** A Wiley-Science Publication, 1982.

[4.4] Gardner, L., **Phaselock Techniques**, John Wiley & Sons, Inc. 1966.

[4.5] Horowitz, P. and Hill, W., **The Art of Electronics**, Cambridge University Press, Cambridge, 1984.

[4.6] Van Valkenburg, M. E., **Analog Filter Design** , New York, Holt, Rinehart & Winston, Holt-Saunders, Japan, 1982.

C H A P T E R 5

TEST AND MEASUREMENT

5.1 INTRODUCTION

In this chapter, the performance of the modem is described quantitatively from measured experiments performed on the demodulator. The four parts of the demodulator have been tested, namely ; (A) the carrier recovery, (B) the bit synchronisation, (C) the rate changing circuit and (D) the data recovery. The constituents of the demodulator are tested as follows:

1. Data recovery in the presence of AWGN, by analysing the eye diagram obtained at the Costas loop arm.

2. The recovered carrier jitter is tested in the presence of AWGN.

3. The recovered bit timing jitter is tested in the presence of AWGN.

4. Demodulation of the tone indicating bit rate changes (with the data present) is analysed by a bit error test on a modulated tone and by measurement from an oscilloscope.

5. Demodulation of the data with the modulated tone present and with the tone absent. This is performed by a bit error test on the data.

6. The ability of the demodulator to switch bit rate is measured with a bit error count.

The modem does operate at six different bit rates, however, not all the bit rates were tested thoroughly. It is assumed that the results obtained in this chapter at one bit rate apply for the other bit rates. Standard laboratory equipment has been used and all tests were carried out in a laboratory. The digital oscilloscope used for many of the figures shown in this and in

previous chapters, is the Hewlett Packard 54501A Digitising Oscilloscope (50 Mhz), coupled with the Hewlett-Packard Thinkjet printer. The Hewlett-Packard 4195A Network/Spectrum analyser (10 Hz - 500 Mhz) has been used to view the spectra of systems and waveforms.

5.2 ADDED WHITE GAUSSIAN NOISE

In the final communication system, the modem will receive signals at a finite signal to noise ratio (S/N). The modem must therefore be tested under similar conditions in a known S/N environment. One method of generating a known S/N is to generate Gaussian noise that has a much greater power than the noise threshold of the receiver. The generated noise must be *white* within the receive bandwidth and must have a variable root-mean-square (rms) voltage. The input carrier is set to a fixed rms voltage. The two signals are added together at the input to the receiver. By varying the rms noise voltage, different S/N ratios can be achieved.

The S/N can be measured at the output of the demodulator. The point of measurement is immediately outside of the receive low pass arm filter, in the Costas loop. In this way, only the noise within the receive bandwidth is included in the measurement. That is, the received data in the absence of noise is measured as the rms signal voltage (V_S) and the received noise in the absence of data is measured as the rms noise voltage (σ). S/N is then given by :

$$S/N = 20\log\left(\frac{V_s}{\sigma}\right) \quad dB$$

Using the Hewlett Packard Digital oscilloscope, an rms reading can be obtained. However, it is impractical to continually measure the noise voltage at the filter output, since the data would have to be turned on and off during an experiment. Therefore the wideband noise is measured at the noise source

output and an attenuation factor is found between the noise at the receiver input and the noise at the receiver output. This noise attenuation factor is different at different bit rates.

The measured rms data signal voltage at the receiver filter output, for all experiments is V_S = 233 mV. The data shown in Fig. 5.1 is at a data rate of 64 kb/s. The Figure shows two traces, the top trace is the received data with added noise and the lower trace is the wideband noise. The noise attenuation factor through the demodulator at a bit rate of f_b = 64 kbps, is approximately, K_N = 0.2 . The signal to noise at the receiver output is :

$$S/N = 20\log\left(\frac{233}{(576 \cdot 0.2)}\right) = 6 \quad dB$$

Note that the readings given by the scope, *current, min, max,* and *average*. The *average rms voltage* reading has been used.

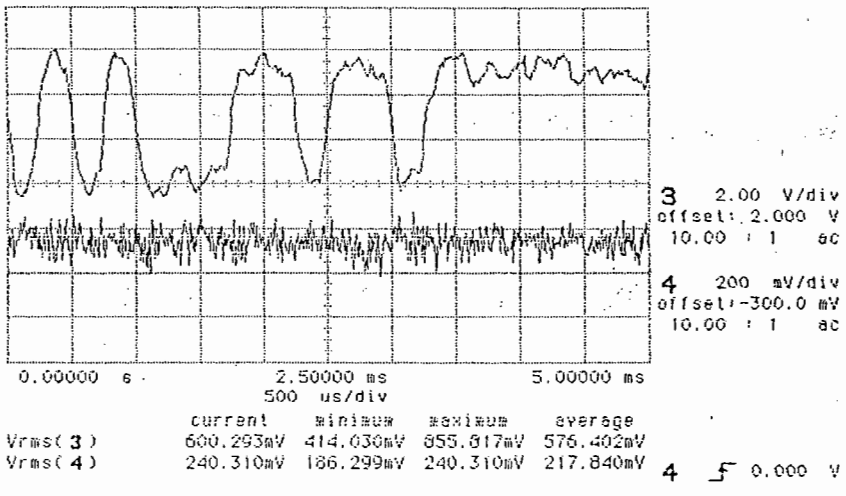

FIGURE 5.1 : *Noise measurements.*

5.2.1 NOISE SOURCE

A noise generator has been constructed and appears in Fig. 5.2. The noise is white over a wide bandwidth of at least 2 Mhz which is sufficient for this purpose. The noise is generated by reverse-biasing the emitter-base junction of a transistor. The first amplifier is a PN918 RF transistor and

the second is a LM6361 wideband op. amp. setup with a variable gain. The feedback resistor, R176, sets the final output voltage. In this way different rms noise voltage levels can be added to the signal. The rms noise voltage range extends from 4 mV to 750 mV.

Any required S/N environment can be created by adding white noise to the signal at the input of the receiver. The noise source voltage can be set to 700 mV rms which is much greater than the noise floor of the receiver (less than 1 mV rms), thus the noise source dominates and is significant.

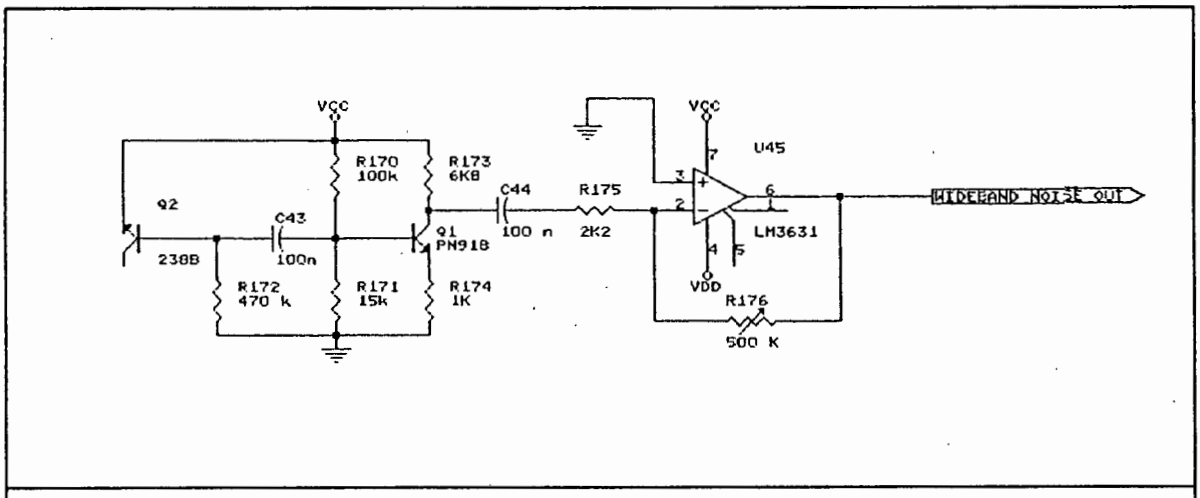

FIGURE 5.2 : *Noise generator.*

5.2.2 FINITE CREST FACTOR NOISE

Theoretically, an ideal, Gaussian noise source has infinitely high peaks; in other words there is a finite chance that a peak as high as 7σ (or even higher) will occur, even though this probability is only 10^{-12} [5.1].

The *crest factor*, **c**, of a waveform is the ratio of the peak voltage to the rms voltage. For example, the crest factor of a sine wave is $\sqrt{2}$, or 3 dB. The crest factor of the noise source that has been assembled, is at its minimum when the noise output voltage is at a maximum of $\sigma = 750\,mV_{rms}$. The maximum peak voltage output of the noise source is equal to

the power supply, Vcc = + 6 V. The minimum crest factor is calculated as being $c = 20\log(6/0.75) = 18 dB$. This represents 8 times the rms value or 8σ.

The chance that a peak of this amplitude will occur and be clipped by the power supply is $< 10^{-12}$. This noise source has a very large crest factor and the noise produced will be approximately Gaussian even when the noise voltage is at a maximum.

5.3 BIT ERROR COUNT

Overall data recovery is tested with an error count on the received bits. The original bit stream is delayed to match the delay of the modem and compared with the output bit stream using an X-OR logic gate. The output is clocked with the demodulator recovered clock through an AND gate. This clocking is necessary to change an output error bit to two edges (one high and one low). This is required because the counter device will count edges, not levels, and if a string of adjacent errors occurs, the X-OR gate output remains high during that time, and the counter records only one error.

The circuit is shown in Fig. 5.3, the original bit stream is delayed by three bit periods. Shift register U45A is used for this which is clocked by the demodulator recovered clock. The recovered clock has been inverted by an AND gate U46B, so that the clocking edge falls in the center of both the recovered data stream and the original data stream. The recovered data stream is also clocked through a single-bit shift register with this inverted clock so that the two stream are identically synchronised. The propagation delay of system has found to be two bit periods at all of the bit rates. X-OR gate U15D compares the two streams and the AND gate U46A clocks the result. The bit error output is read by a digital counter.

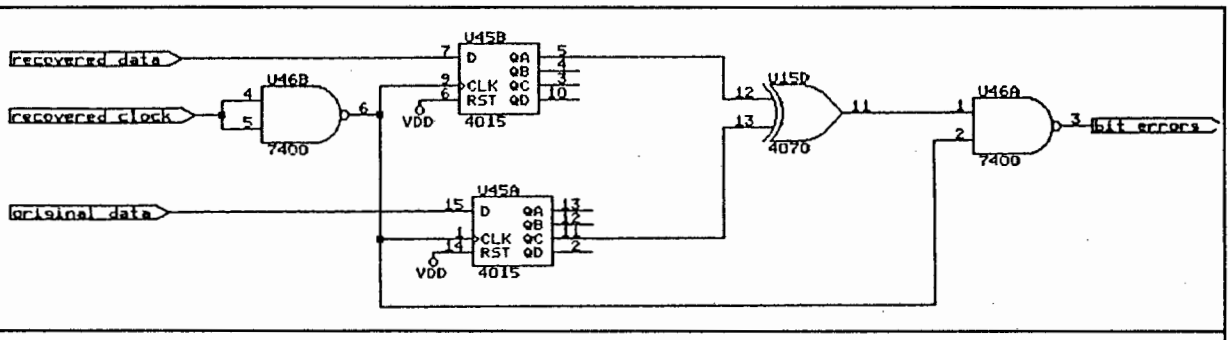

FIGURE 5.3 : *Bit error counter.*

5.4 EYE DIAGRAMS [5.1]

The quality of digital transmission links is frequently evaluated by means of **eye diagrams**, or **eye patterns.** Eye diagrams provide a qualitative means of displaying system imperfections and to provide a first-order approximation of system performance. A two-level eye-diagram measurement is setup by connecting the bit rate clock, f_b, to the external trigger of the oscilloscope and the recovered bit stream to another of the oscilloscope inputs. Eye diagrams were obtained on the digital oscilloscope by setting the display persistence to infinity. The measured eye diagrams are given in figures 5.4 (a) to (d). The long PN sequence of L = 65 363 bits was used for these results. The modem was operating at the lowest bit rate of 4 kbit/sec.

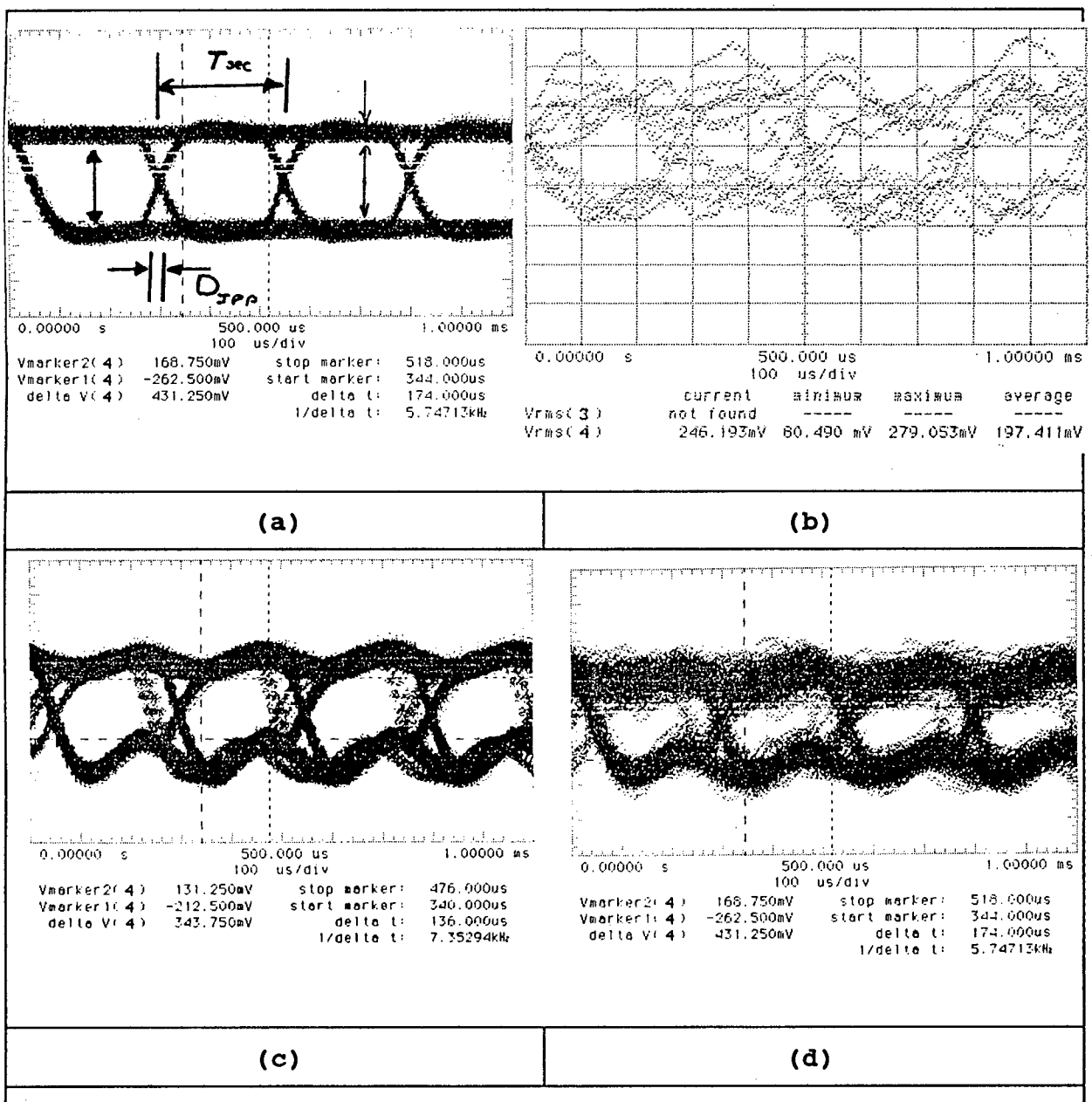

FIGURE 5.4 : *Eye diagrams of a received bit stream (a) data, no tone, high S/N (b) data, no tone, low S/N (c) data with tone, high S/N (d) data with tone, low S/N. The vertical scale is 200 mV/DIV for all four figures.*

Fig 5.4 (a) is the demodulated output when only the data is transmitted (no tone), with a S/N = 35 dB, (b) the same transmitted signal and S/N = 4 dB. Fig. 5.4 (c) is the demodulated output when the data + the tone is transmitted and S/N = 35 dB (the ghosted trace was caused by the oscilloscope not tracking), and (d) the same transmitted signal with S/N = 7 dB.

Examination of Fig. 5.4 (a) indicates that in the sampling instants (center of bit), all traces cross the normalised +1 or -1 levels. The level has smeared out to 25 % of the vertical eye opening. This indicates the intersymbol interference (ISI) caused by the transient response of the Butterworth filter. The second order Butterworth filters have a linear phase response which minimises spreading (ISI) of the received filtered pulses.

Furthermore, note that the threshold-level crossings have smeared out, indicating that the zero crossings are pattern dependent. The peak-to-peak time difference of the zero crossings is known as peak-to-peak data-transmission jitter, D_{jpp}. Data-transition jitter can be specified in seconds or as a ratio D_{jpp}/T_b %, where T_b is the bit duration. The peak-to-peak jitter of each diagram is given in table 5.1 in both measures.

Figure 5.4	Data S/N (dB)	D_{jpp} (msec)	D_{jpp} (%)
(a)	20	0.02	8
(b)	4	0.125	24
(c)	20	0.03	12
(d)	7	0.10	13

Table 5.1 : *Eye diagram measure-ments.*

Data-transition jitter by itself does not necessarily lead to performance degradation. However, data-transition jitter combined with clock jitter may lead to significant performance degradation. In the absence of AWGN, fig. 5.1 (c) shows that the effect of the added tone does cause vertical eye closure, not however, at the centre and at the ends of each bit. At these points the tone contribution is less pronounced, effectively zero. The horizontal eye closure is hardly noticed and there is a 4 % difference to the case without the tone.

The effect of AWGN causes more vertical eye closure than horizontal eye closure. In Fig. 5.1 (b), the vertical smearing has risen to 60 % of the eye opening while the data jitter caused by the horizontal eye closure is only D_{jpp} = 12 %.

In order to convert the analog signals of Fig. 5.4 to digital data, a comparator is used that makes a decision whether a one or a zero has been received. Since no timing is available, a sample and hold can not be used. The comparator level is set to the horizontal center of the eye by measurement of the voltage. This setting is crucial and causes bit errors if incorrectly set. The comparator output provides a digital signal that can be used to recover timing. When the added is present, the comparators' decision is made at the ends of each bit where the tone contribution is almost zero.

5.5 CARRIER RECOVERY

The primary role of the Costas loop is to lock onto a suppressed carrier and regenerate an in-phase replica of this carrier signal. Two variable resistors allow the loop to be set in different configurations. Using the method of section 4.3.1.3 the loop has been set up as shown in table 5.2.

R_{VCO}	R_3	R_2	R_1	C	f_{-3dB}	K_{VCO}	F(0)	ζ	ω_n	K_{ol}
(Ω)	(Ω)	(Ω)	(Ω)	(nF)	Hz	V/rad	V/V		rad/sec	sec^{-1}
2700	694	6800	180	1	227	228	3.85	0.3	2692	5078
Tracking range $\Delta\omega_t \approx +/- 808$ Hz **Lock-in range** $\Delta\omega_t \approx 231$ Hz										

TABLE 5.2 : *Costas loop parameter settings.*

In acquisition mode the lock up time of the loop was measured by applying the modulated carrier and switching it ON and OFF. This input step causes a dc step response at the output of the loop filter. The time constant of the step is the acquisition time which was found to be $\tau_{CT} = 5msec$.

When in lock, the in-phase and quadrature-phase local oscillators are both at exactly 700 Khz, which can be checked with a frequency counter. Also, the voltage on the in-phase arm of the loop should be the demodulated data and the quadrature arm shows zero volts. Connecting the input modulated carrier to the Costas loop and switching through the bit rates, the six diagrams of Fig. 5.5 were obtained on the oscilloscope. Each diagram shows the in-phase channel and quadrature-phase channel voltages. The in-phase arm contains the demodulated data and the quadrature-phase arm contains the control voltage.

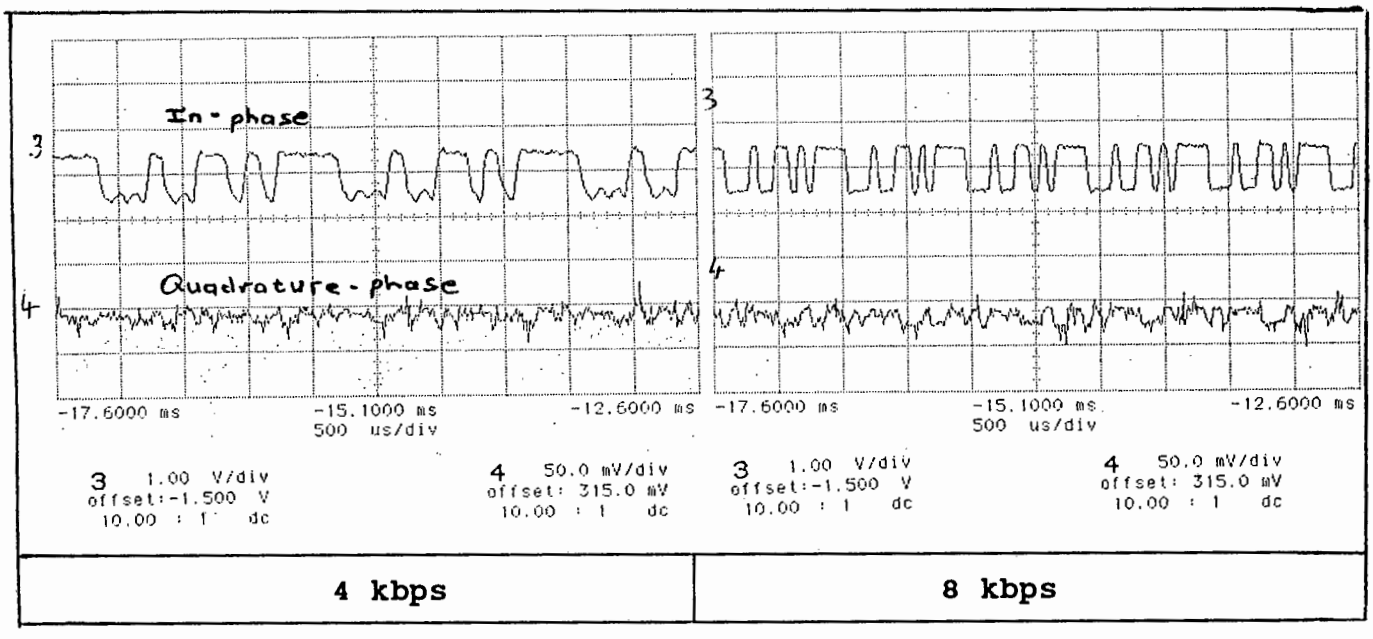

4 kbps	8 kbps

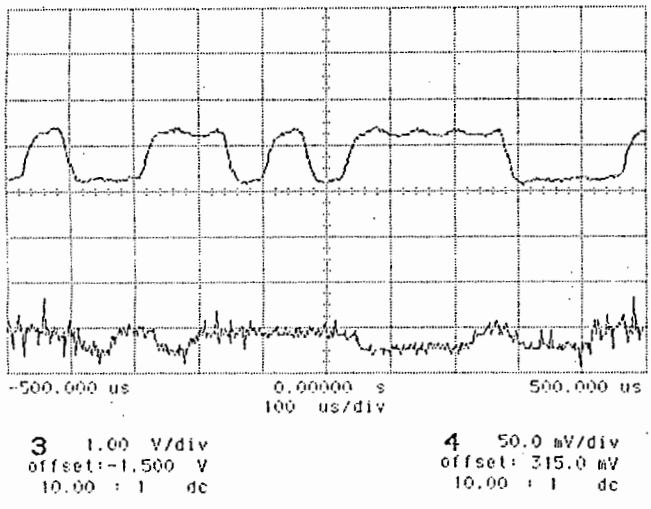

16 kbps

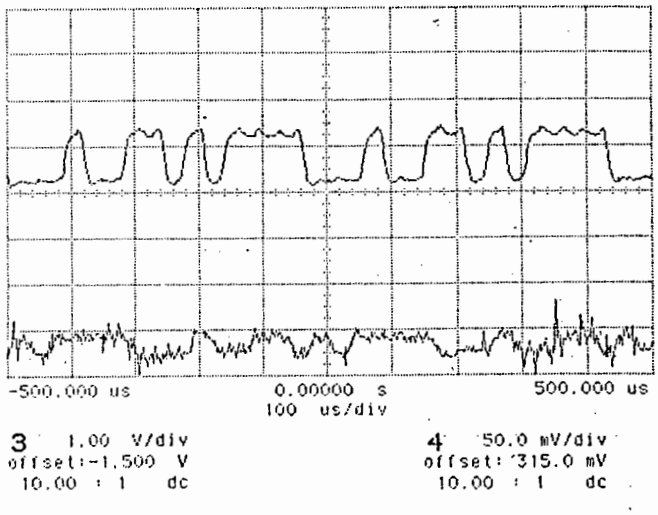

32 kbps

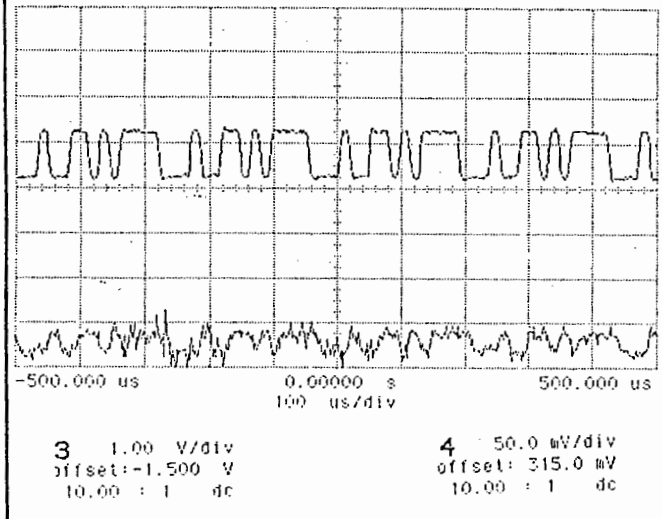

64 kbps

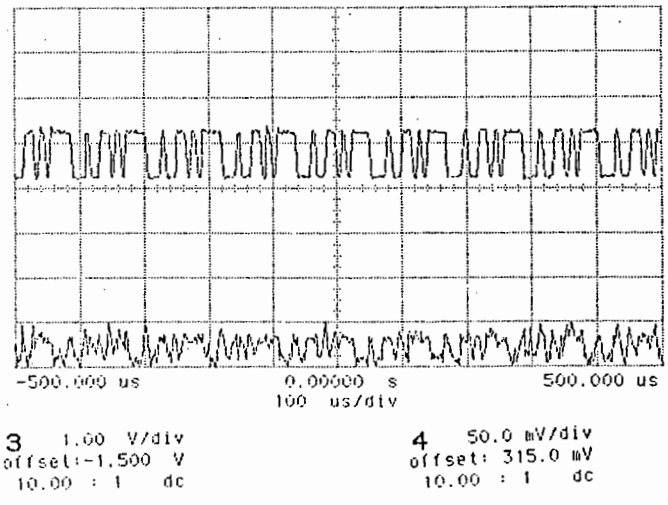

128 kbps

FIGURE 5.5 : *In-phase and quadrature-phase arm voltage of a locked loop.*

The in-phase (top trace) and quadrature-phase local oscillators (the bottom trace) are displayed on the oscilloscope and appear as in Fig.**4.2**/. These two waveforms have a -90^{o} phase relationship.

5.5.1 LOCAL OSCILLATOR JITTER

The local oscillator frequency is controlled by the dc control voltage at the input to the VCO. Adding white noise at the receiver input, causes variance in this voltage. The frequency of the variance is limited by the loop filter bandwidth. In this case the loop filter bandwidth is, f_{-3dB} = 227 Hz. The closed loop noise bandwidth is B_N = 511 Hz. The dc control voltage variance results in local oscillator jitter, as the VCO output frequency *jitters* about the set point. In the Costas loop, imperfect squaring of the data at the loop filter also contributes to this clock jitter. The clock jitter is measured as the peak-to-peak variation of the clock edge. This can be viewed on an oscilloscope by triggering the X-channel of the scope onto a fixed clock at the modulator and observing the recovered clock on the Y-channel. This is illustrated in Fig.5.7. CC_{JPP} is the jitter, written as a percentage of the bit period. The jitter is measured at CC_{JPP} = 7.56 % in a S/N environment of E_b/N_o = 8 dB.

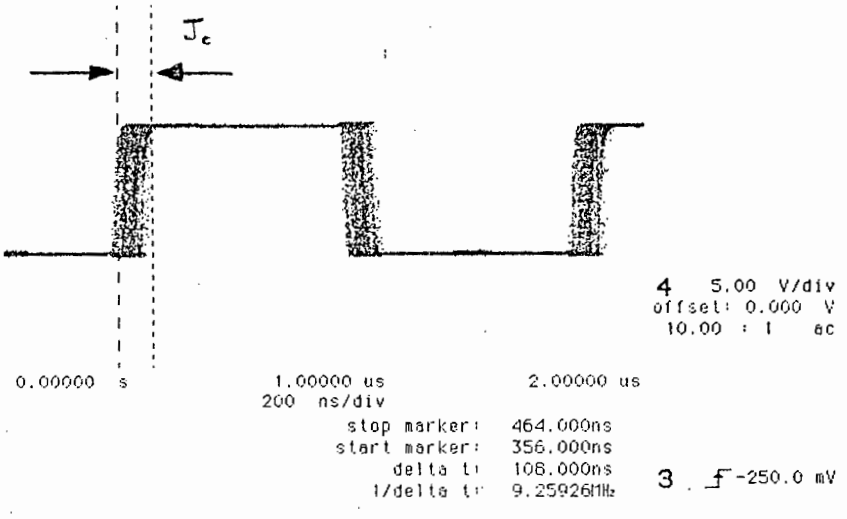

FIGURE 5.7 : *Carrier recovery clock jitter.*

5.6 BIT TIMING RECOVERY

The heart of the bit timing recovery circuit is the PLL. The operation of the loop is determined by its acquisition and tracking ability. The PLL has been set up as described in chapter 4, sub-section 4.3.2.2. The acquisition time of the phase lock loop was measured by applying an external clock to the input of the loop. The clock was switched ON and OFF and the transient at the output of the loop filter was measured to be $\tau_{BT} = 8msec$. The phase jitter of the local oscillator of the PLL has been tested in the presence of noise.

5.6.1 LOCAL OSCILLATOR JITTER

Bit timing recovery clock jitter is measured as done in the carrier loop. The peak-to-peak clock jitter of the PLL is shown in fig.5.8.

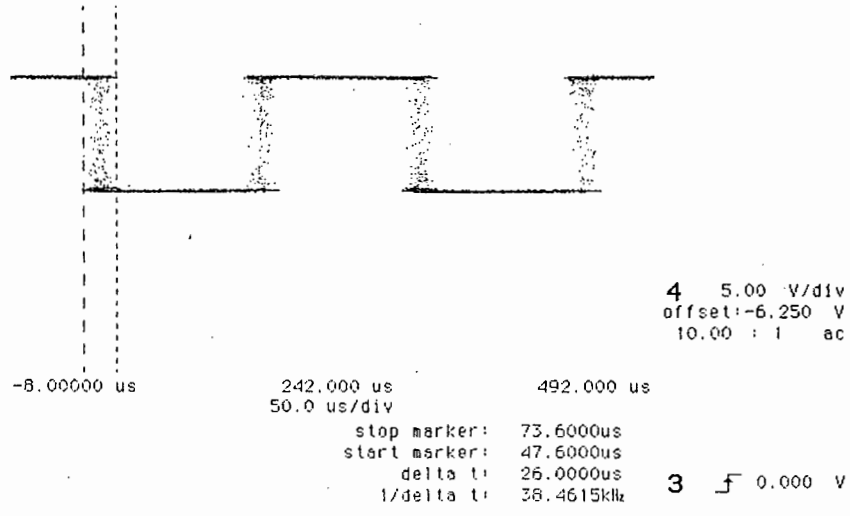

FIGURE 5.8 : *Phase locked loop clock jitter.*

By varying the S/N different values of clock jitter have been obtained. The closed loop noise bandwidth is B_N = 2.7 Khz. By varying the S/N at the input to the carrier recovery, data jitter results out of the Costas loop and this effect propagates to the PLL. The measurements made are shown in table 5.3.

BC_{JPP} (μsec)	BC_{JPP} (%) of bit	V_N (mV)	E_b/N_o (dB)
26	10.4	117	6
16	6.4	66	11
11	4.4	4	35

TABLE 5.3 : *Phase lock loop jitter.*

5.7 ERROR COUNT (Pe) VS S/N

Bit error rate tests are performed in the presence of AWGN. In order to compare the results with and without the added tone, two tests have been done : (1) transmitting data only, and (2) transmitting the data and the tone simultaneously. During the second test, the tone is amplitude shift key modulated at 6 bps.

These tests have not been done at all six bit rates, but only at one bit rate. It is assumed that the results are identical at the other bit rates.

METHOD

1. Set the PN sequence bit length L = 65636 bit.
2. Set the modulator and demodulator bit rate.
3. Add White Gaussian Noise at the input to the demodulator, by summing with the modulated carrier.
4. Set the data decision level. This is set by reducing the S/N to 4 dB and then adjusting the op. amp comparator threshold to minimise the error count.
5. Reset the noise to the minimum setting to begin the test.
6. Measure the noise source rms voltage.
7. Run the P_e counter over a set interval of T_e^* seconds.
8. At the end of the interval read the error count and record the noise reading on the oscilloscope.
9. Increment the noise source voltage by 50 mV and repeat step 7 until the noise source is at a maximum.

T_e^* depends on the bit rate used. High bit rates require a shorter interval than do low bit rates to count the same number of errors. When operating at 4 kbit/sec, it takes 4.2 minutes to count 10^6 bits. Therefore T_e = 250 seconds gives a minimum error count of 10^{-6}.

The probability of error is:

$$P_e = \frac{error\ \ count}{T_e \times bit\ \ rate} \quad bit/\sec$$

The counter is reset after each timing interval. The results that were obtained are shown in Fig. 5.9. The practical and the theoretical relationship between P_e and E_b/N_o are compared.

In case (a), the practical system is 3 dB worse than theory, at a low S/N. This compares well with the predicted practical result of table 3.1, reference [3.1]. The two curves merge at higher S/N to within 2 dB.

Comparing case (a) with case (b) at low S/N, the data channel is a maximum of 0.4 dB worse when the tone is on than when the tone is off. This difference reduces at high S/N ratios. Different amounts of tone was added and it was noticed that the carrier recovery would fall out of lock if the tone/data ratio exceeded 100 %.

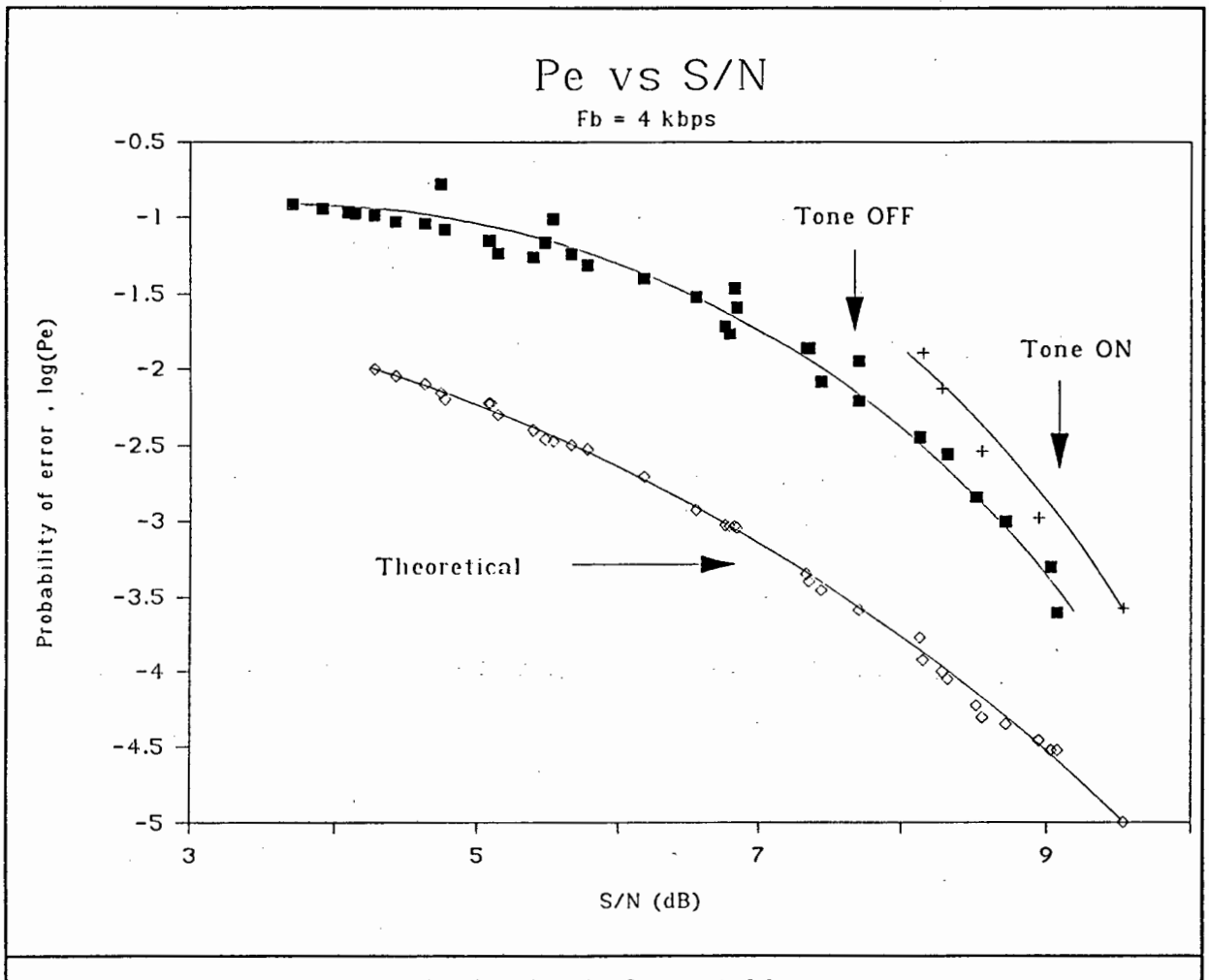

FIGURE 5.9 : *P_e vs. S/N test at f_b = 4 kbps.*

5.8 THE ABILITY OF THE DEMODULATOR TO SWITCH BIT RATE

This test, determines how well the modem can switch data rate and how much data is lost during a transition. One method of performing this test is to use the P_e counter of Fig. 5.3, that counts the bit errors during a rate change. The delay through the demodulator is the same integral number of bit periods, for all the bit rates, allowing this experiment to be performed. The result tests both (a) the ability of the carrier recovery loop to switch data rate; and (b) the ability of the bit timing recovery loop to switch data rate.

A short PN sequence of L = 15 bits was used. The bit rate selector on the modulator and the demodulator were hard-wired for these experiments. The bit rate was then controlled by a counter which switched through the three bit rates (4 kbps to 8 kbps to 16 kbps to 4 kbps etc.) at a regular speed determined by the applied clock. The clock is derived from an external oscillator and is not synchronised with the modems' data rate. The rate change control technique via the added tone was not used here. The following results were obtained. The bit rate transitions were set to occur at a frequency of 0.2 Hz. A slow switch speed was chosen so that the errors could be counted at each rate transition.

V_N (mV)	V_S (mV)	E_b/N_o (dB)	Time (min)
23	233	20	16

Bit rate change sequence :	4 kbps to 8 kbps	8kbps to 16 kbps	16 kbps to 4 kbps
Total error count after 16 min :	23	452	80
Average error count after 16 min :	0.4423	6.7	1.5
Total BER =	6×10^{-5}		

TABLE 5.4 : *Bit rate change test.*

The total number of bit errors counted divided by the total number of bits that occurred at the three different bit rates, indicates the total probability of error. The signal to noise environment was set at 20 dB. The test was not repeated at different signal to noise levels and it is assumed that an increase in the P_e will occur with decreasing S/N, as is the case when operating at a fixed bit rate.

The bit errors occurring during the first and third transitions (4 kbps to 8 kbps and 16 kbps to 4 kbps) are negligible. Most bit errors occurred during the 8 kbps and the 16 kbps rate change. Here, errors occurred over an average interval of $3.5bits * 8kbit/\sec + 3.5bits * 16kbit/\sec = 656.25\mu\sec$. This is far shorter than the lock up times of either the carrier loop (5 msec) or the bit timing loop (8 msec). This rules out the possibility that these loops fell out of lock. The cause of these errors is either :

1) The external clock which is used the switch the bit rate. This clock is not synchronised with the data rate and interrupts the data clock. This may results in an initial phase offset.

2) The phase synchronisation of the phase locked loop. The input to the phase locked loop is a sinusoid (output of band pass filter) with a growing transient. During the transient the

phase lock loop may not be exactly locked onto the input phase. This may cause the loop to slip cycles, until the input has reached steady state.

3) The costas loop may also have caused these bit errors by slipping cycles.

5.9 TRANSMITTING A MESSAGE TO INDICATE THE RATE CHANGE

Two different techniques have been used. The first is to phase shift key data into the tone (sub-section 3.10.2.2.1), and the second is to amplitude shift key modulate the tone (sub-section 3.10.2.2.2). Modulating the tone spreads the tone spectrum from a discrete line to a suppressed spectral line with side-bands (DSB-SC). If this spreading is too great it interferes with the adjacent baseband data and the tone can no longer be recovered. PSK was initially chosen to modulate the tone because it has a 6 dB theoretical improvement over ASK [3.1]

5.9.1 PSK TONE MODULATION

The tone is modulated by multiplication with a binary stream bit rates under 500 bit/sec. The output of the tone recovery low pass filter after PSK demodulation is an analogue polar bit stream. To convert this analog data, shown in Fig. 5.10 (a) to digital bits, a comparator is used with a threshold at zero volts. The circuit for this is given in Fig.5.10 (b)

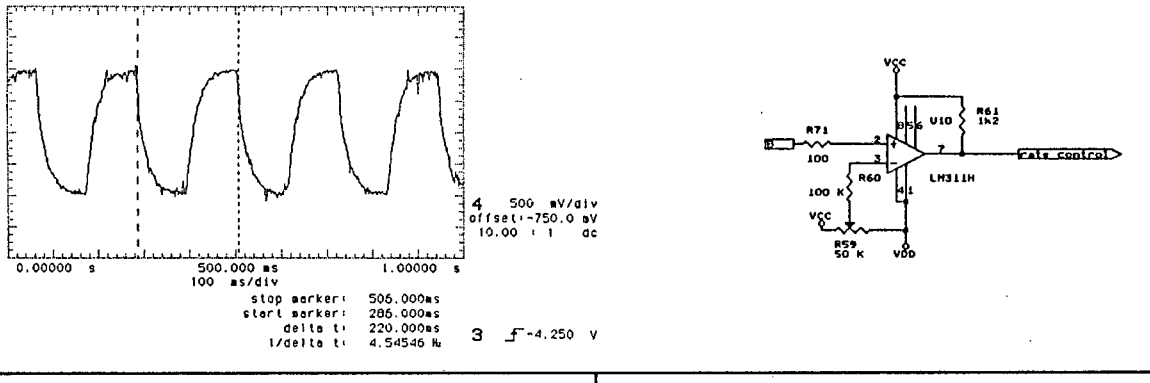

(a)	(b)

FIGURE 5.10 : *PSK tone recovery (a) recovered data and (b) D/A convertor.*

To test the ability of the modulator to communicate rate changes via this technique in the presence of noise, a bit error test was performed on the tone channel using the same method as done on the data channel, as follows:

The modem has been set up to operate a data channel at 4 kbps. The tone is added and modulated with a short PN sequence of L = 15 bits at a slow rate of 500 bps. Using the differential encoder and the decoder on this bit stream, the output bit stream is compared with input bit stream using the circuit of Fig.5.3. The nine steps of sub-section 5.7 are then performed. The results are shown below in Fig. 5.11.

The BER of the tone channel showed the same downward trend as the theoretical curve, although it is more linear. At low S/N there is a 2 dB difference between the curves, which becomes 2.5 dB at higher S/N. The tone is effected by the adjacent channel interference from the data.

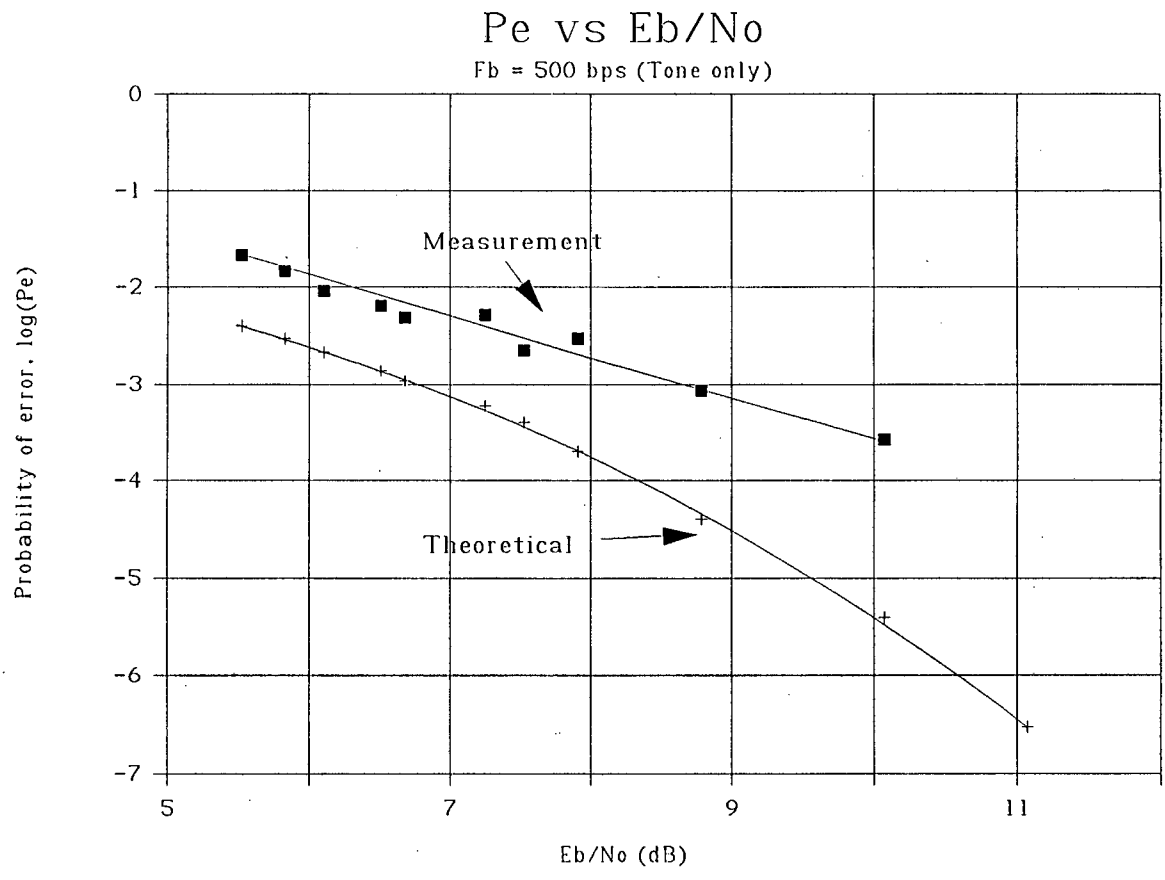

FIGURE 5.11 : *Bit error rate test on the modulated tone.*

The next step is to use this technique to control the bit rate of the demodulator. However, when implementing the technique, a problem arose that prevented any further use of this idea. The exact phase of the transmitted tone was difficult to predict as there existed a possible 180° ambiguity at the receiver. This is caused by a possible 180° phase ambiguity which can result by the Costas loop demodulation. The only method of eliminating this ambiguity is to employ differential encoding and decoding of the tone. However, contrary to the system used for the above BER experiment, this is impossible since only one bit will be transmitted which is demodulated without any timing information that is necessary to clock a differential decoder.

The problem manifests itself at the transition from one bit rate to another. It was noticed on the oscilloscope, that when the bit rate switched, the demodulated tone phase would sometimes switch by 180^{o} and sometimes not. This caused an occasional erroneous bit to be decoded. This indicated the likelihood of the Costas loop slipping half cycles during a bit rate change.

5.9.2 ASK TONE MODULATION

The alternative method of transmitting data via the tone is to turn the tone ON and OFF (amplitude shift keying). This method proved to be more successful and provided an unambiguous method of relaying one bit to signal a new bit rate. The 180^{o} tone ambiguity still occurred but could be eliminated with the circuit shown in Fig. 5.12 (a), explained as follows:

There are three possible states for the decoder output, + A Volt, -A Volt or 0 Volt. Zero is an absolute reference that is used to indicate the presence or absence of the tone. Two comparators are required, each set to trigger on the +A V or the -A V state. An X-OR gate then indicates the presence of the bit, when either one of the comparators is triggered. Hysteresis can be added to the comparators to improve the response to noisy inputs.

The input to the comparator is shown in Fig. 5.12 (b). The modem was switched between the two lowest bit rates of 4 kbps and 8 kbps. The bit rate change control was hard-wired from the modulator to the demodulator. The tone was PSK modulated by 6 bit/sec binary data. The three possible output voltages are shown. The diagram illustrates that the modem switches between the bit rates smoothly and that the tone is continuously recovered during the rate change.

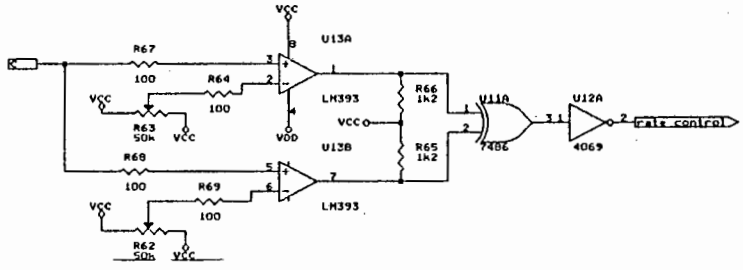

(a)

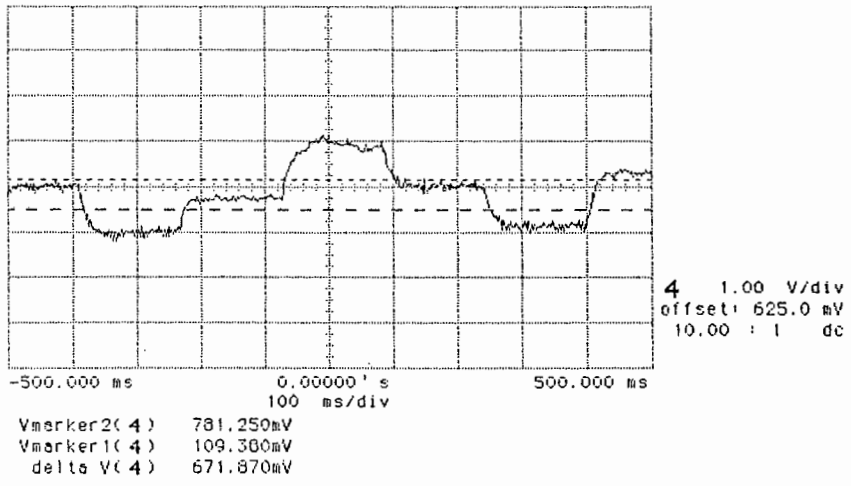

(b)

FIGURE 5.12 : *ASK tone demodulation.*

The next step is to use this output bit stream to control the bit rate of the demodulator. This has not been done here due to time limits. However, during the bit error rate test of sub-section, the recovered data stream was also monitored by inspection on an oscilloscope. It was noticed that even in the low S/N environment of E_b/N_o = 5dB, a 2 V bit could be clearly noticed on the oscilloscope.

5.10 CONCLUSION

The complete operation of the modem has been specified by measurement of the demodulator sub-circuits, namely: (i) The carrier recovery loop, (ii) The bit timing recovery loop, (iii) The data recovery process and (iv) The tone recovery process. All four sub-circuits operated satisfactorily.

The combined operation of (i), (ii) and (iii) are reflected in the bit error rate count in the presence of AWGN. Also note that second order Butterworth filtering has been used on the data, which is non-ideal. The measured practical performance was very close with the predicted practical performance and therefore, the modem can operate as a regular DEBPSK system.
The deviation of 0.4 dB, caused when the tone is added, is insignificant. In this case the tone was ASK modulated at 6 bps. The added tone does not degrade the performance of the data channel at this low data rate.

The tone can be used to signal a bit rate change and the probability of an error follows the same trend as the data channel. The auxiliary channel proved to be an effective method of transmitting information at rates up to 12.5 % of the data bit rate.

The carrier recovery loop has been described by the local clock jitter test and the eye diagram test. The noise equivalent bandwidth of the closed loop of 1.53kHz reduces the clock jitter caused by noise external to the loop. The narrow loop bandwidth is at the expense of longer acquisition time. The imperfect data recovery results in a self-noise at the loop filter output contributing towards clock jitter. This effect is limited by the narrow loop filter of 77 Hz.

The recovered data in the I-channel of the Costas loop is shown by the eye diagrams. Negligible ISI was measured even when the tone was ON. The horizontal eye opening only increased marginally when the tone was present and this does not increase the error rate significantly. The reason for the higher error rate caused with the tone ON, was that the decision level changed with the tone present and no adjustment was made to correct this. This imbalance in the recovery of the tone is caused by multiplier imbalances in the loop.

The bit timing recovery loop has been described by the local clock jitter test. The results show a trend of increasing jitter with decreasing S/N.

The ability of the demodulator to adjust to a rate change without incurring errors has not been verified. A finite error rate does occur during a bit rate change. However negligible errors occurred during rate changes from the lowest bit rate to the next higher bit rate. This result is promising and suggests that error free rate changing is possible. The higher error rate counted at the higher bit rate transition is caused by a bit timing phase error. This is either due to the external clock selecting new bit rates asynchronously or the phase locked slipping cycles before the input sinusoid reaches a steady state value.

To complete the modem it would have been necessary to connect the output of the rate switching circuit to the various multiplexers on the demodulator and control the demodulator from the modulator. This has not been done due to time limits.

5.11 REFERENCES

[5.1] Feher, Dr. K. , Engineers of Hewlett Packard ,**Telecommunications Measurements Analysis, and Instrumentation,** chap 7,11 .

C H A P T E R 6

CONCLUSION

6.1 CHAPTER SUMMARY

6.1.1 CHAPTER 1

Meteor Scatter Communications (MSC) is introduced as a reliable means of transmitting intermittent data over long distances of 2000 km. An adaptive bit rate modem is required to increase throughput by offering a variety of higher bit rates which can be selected automatically. The physical phenomena of MSC is well known and has been explained. An historical sketch shows the interest that has been given to this mode especially during the second half of the century. Hampered by technology, such a modem had not been realized until the 1980's. The opportunity has arrived to develop such a modem further. The specifications are given for an adaptive bit rate modem that will replace a constant bit rate running at 4 kbps in a currently operating system.

6.1.2 CHAPTER 2

The channel is the prime indicator when designing a modem. The channel defines the bit rate limits and throughput limits that are to be expected. The groundwork for the adaptive bit rate modem has been done and the allowable bit rates have been established.

The MSC channel is power limited and optimising data throughput hinges on the ability of the modulation technique to receive data in the lowest possible signal-to-noise environment.

The phase coherence of the channel is linear within the bandwidth of interest. The multipath effects do place an upper bound on the bit rate, but the effect of the signal fading dominates.

By considering a statistical model for both the occurrence and the duration of meteors, it is shown that an adaptive bit rate modem will theoretically increase throughput. The limits to this analysis are that only a single trail shape is considered and that practical system delays are ignored. The practical operational overheads delay the process of changing bit rates and result in a minimum time that can be spent at any one bit rate.

6.1.3 CHAPTER 3

The chosen modulation technique is DEBPSK. This is the simplest of the power efficient schemes available, in terms of low circuit complexity and the low power required to transmit.

Other schemes such as QPSK and MSK are useful at an added cost. DEQPSK doubles the spectral efficiency of DEBPSK however, doubling the transmit power required and the circuit complexity. MSK offers improved spectral efficiency with increased circuit complexity. Since no bandwidth restrictions have been placed in the specifications, this complexity is unnecessary.

The method of transmitting a tone has been proposed. A tone can be added to the baseband data warning the demodulator of an impending rate change. The effect of this modification to DEBPSK, can be eliminated with a matched filter at the receiver. Using sub-optimal filtering like second order Butterworth, the tone is not totally eliminated.

The tone can be recovered using band-pass filtering. Methods of indicating a rate change have been discussed and coherent detection of the tone demodulates any data carried on it.

This technique uses a frequency division multiplexed, auxiliary channel, compared with the time division multiplexed system that has already been implemented.

6.1.4 CHAPTER 4

The design and implementation of the modem has been completed. The system can be used to test the rate change mechanism that has been proposed. Attention has been given to Earthing and de-coupling power supplies. Both the modulator the demodulator operate at all the bit rates and can switch between the six bit rates.

The Costas loop operation is adequate at all bit rates. The costas loop managed to stay in lock at the low S/N levels of the tests and provided a basis for testing the rest of the demodulator. The switched capacitor arm filters operate as expected and offer great flexibility in determining an exact filter bandwidth. Flexibility in choosing the filter configuration is also given. Receiving the tone plus the data has no visible effect (viewed by oscilloscope) on the carrier recovery loop.

The bank of six, *passive*, band-pass filters is a cumbersome circuit but offers the designer exact Q setting. The gain is increased using an amplifier. The quality of inductor used determines the maximum filter Q. The inductors were hand wound. Variable inductor cores can be used to set the resonant frequency, but these were unavailable at the time.

The bank of six, active, Friend band-pass filters are neat and compact. The resonant frequency is set with a potentiometer and the Q can be enhancement if necessary. A setting of Q = 8 was found to be the best for filtering the tone from the data. This reduced the sidebands and provided a transient lasting 8 cycles.

The phase-lock-loop has been implemented with a frequency divider that operates at all the bit rates. A single closed loop response is used for all of the frequencies of interest.

The tone recovery circuit operates and demodulates data from the tone using both ASK and PSK modulation. A circuit for controlling the bit rate of the demodulator has not been completed due to time constraints.

6.1.5 CHAPTER 5

The experiments that have been done on the demodulator are summarised here:

1. Data recovery in the presence of AWGN.

Using second order Butterworth filtering, the results compare with those of predicted practical systems mentioned in table 3.1.

2. Carrier recovery in the presence of AWGN.

The Costas carrier recovery loop tracked the input even at low S/N levels and was reliable enough to be used for further measurements of recovered data at low S/N levels. The local oscillator phase jitter increases with decreasing S/N resulting in data pattern jitter.

3. Clock recovery in the presence of AWGN.

The phase-lock-loop tracks the recovered data even at low S/N levels.

4. Tone recovery in the presence of data and AWGN.

Using PSK modulation, the tone can be used to transmit data even at low S/N levels. However, no error code correcting can be used on this channel as will be used on the data channel. Thus, the specifications on this channel will be more stringent compared with those on the data channel. For this reason, PSK modulation with matched filtering should be used, if possible for best results.

Demodulation of the tone is effected by the presence of the data which resulted in a 56 % attenuation of the tone. This effect is mainly due to the data causing transients at the band pass filter outputs. These transients can be reduced by reducing the Q of the band pass filters below Q = 8.

5. Data recovery in the presence of the tone and AWGN.

The Pe vs S/N of the data showed similar results to those predicted. Using sub-optimum filtering, the data recovery was not significantly effected by the addition of the tone.

6. Bit rate switching ability.

The bit rate switching of the modem showed signs of effectively zero errors at one bit rate transition and then a finite (but small) error rate at higher bit rate transitions. This indicates that the zero error rate transitions are possible at least at some bit rates and should be possible at others as well.

6.2 DISCUSSION OF RESULTS

The required specifications outlined in chapter one, have been partially met. The data rates that have been achieved are: 4 kbps , 8 kbps , 16 kbps, 32 kbps, 64 kbps and 128 kbps.

The carrier synchronisation time is within the specification given. The bit clock synchronisation time is just out of the specification but this can be re-adjusted. Since conventional timing loops have been used, the acquisition times of both the Costas loop and the bit phase-lock-loop can be improved by switching in a wide loop bandwidth during acquisition and a narrow loop bandwidth during tracking. Table 6.1 summarises the results of the tests.

Power supply	V : I : P :	+/- 6 V 0.6 A each 7.2 Watts total
Carrier recovery	Lock up time : Track range : Acquisition range: Clock jitter :	5 msec 808 Hz 231 Hz 7.56 % (8 dB)
Bit Timing Recovery	Lock up time : Track range : Acquisition range: Clock jitter :	8 msec 42 KHz 2.5 KHz 6.4 % (11dB)
Data Recovery	Eye diagram D_{jpp} : Pe vs S/N (Tone OFF) : Pe vs S/N (6 kbps ASK Modulated tone ON) :	 24 % (4 dB) 10^{-2} @ 7.6 (dB) 10^{-3} @ 9.2 (dB) 10^{-2} @ 8 (dB) 10^{-3} @ 9.5 (dB)
Tone Recovery	Tone/data = 60 %. PSK modulated: Max. bit rate tested : Pe vs $(S/N)_{data}$: ASK modulated: Max. bit rate tested:	 500 bps 10^{-2} (6dB) 10^{-4} (11dB) No quantitative result. 100 bps
Bit rate switching	S/N @ 20 dB Average Error count: 4 bps - 8 bps : 8 bps - 16 bps : 16 bps - 4 bps :	 0.4 bits 6.7 bits 1.5 bits

Table 6.1 : Summary of results.

No complete test for a seamless bit transitions has been done. That is, the demodulator was never controlled by the modulator as originally planned. The tests were halted at the point where an output control signal was achieved in parallel with the bit rate change. However, it was shown that the demodulator could switch bit rates when the bit rate control is hard-wired from the modulator to the demodulator. During the bit rate change, a small but finite error count occurred. It is still necessary to *close the loop* and control the bit rate with the received control signal.

The results on the demodulator proved that switching bit rates with minimal bit errors is possible. This design offers a basis for further work. The design is flexible and can be interfaced with a host computer.

6.3 RECOMMENDATIONS

The small but finite errors incurred during this switching can be eliminated by improving the bit timing recovery circuit to eliminate initial transients at the input to the phase locked loop.

It is still necessary to *close the loop* and control the bit rate with the received control signal. This can be done synchronously with the rate change, as long as:

1. The bit rate change is initiated by a clock which is synchronised to the data clock.

2. The time constant of the control bit from the tone recovery, low pass filter is at least ten times longer than the bit period. Thus, to synchronise this bit with the rate change, it is necessary to delay the bit rate change with respect to the data bit by the amount of the time constant.

Matched filtering of the **data** outside of the carrier loop must be added in a final system. Matched filtering of the **tone** channel can also be done. However, the tone channel is too intermittent to recover timing and the matched filter would have to be asynchronous. This suggests using pulse shaping at the modulator and matched filtering of this waveform at the demodulator.

6.4 CONCLUDING REMARKS

The adaptive bit rate modem does require far more circuitry than a constant bit rate system. By making more use of the ever improving solid state technology, such as switched capacitor filters to replace the banks of band pass filters, a more compact design can be achieved.

The ability of the modem to switch bit rate has been demonstrated. Demodulating the data channel and the tone channel are not mutually exclusive. Demodulation of the data is marginally effected by the presence of a slowly (< 10 % of data rate) modulated tone. Demodulation of the tone is effected by the presence of the data which resulted in a 56 % attenuation of the tone.

The auxiliary channel has proved to be useful for indicating rate changes at low bit rates. Any method of controlling and communicating the bit rate change can be used with this adaptive bit rate modem, whether it be via an auxiliary channel or a message frame embedded in the data channel itself. This thesis has given a basis for the design of such a modem and shows that an adaptive bit rate modem can be realised.

APPENDIX A

NOISE EQUIVALENT BANDWIDTH

The noise equivalent bandwidth is a method of defining a filter bandwidth by normalising the passband to an ideal rectangular passband shape. Added White Gaussian noise is assummed to be present at the input to a filter. The equivalent noise bandwidth, B_N, is that ideal filter bandwidth which gives the same noise power as the actual filter. The noise equivalent bandwidth is found as follows:

AWGN has a constant power spectral density for all frequencies. Let the spectral density of white-noise be

$$S_W(f) = \frac{N_o}{2} \qquad -\infty < f < \infty$$

Where N_O is the single sided (positive frequencies only) spectral density. Now consider a filter with transfer function H(f) with white noise at its input. The bandwidth of an equivalent ideal filter with the same maximum gain, say H_O, that passes the same power. The power out of the original filter is

$$\sigma_Y^2 = N_o \int_0^\infty |H(f)|^2 df$$

and from the equivalent filter, it is

$$\sigma_Y = N_o H_o^2 B_N$$

Where B_N is its bandwidth (to be found). Setting these two equal to each other

$$B_N = \frac{1}{H_o^2} \int_0^\infty |H(f)|^2 df$$

This is referred to as the noise equivalent bandwidth of the filter. Fig. A.1 illustrates this concept.

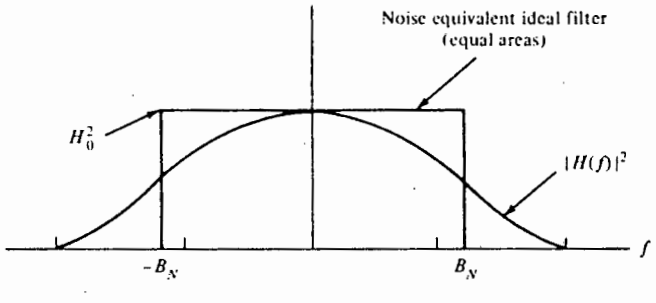

FIGURE A.1 : *Illustration of concept of noise equivalent bandwidth.*

The ratios of noise eqivalent bandwidths to a -3dB cutoff frequency of several filters are given in table A.1.

Filter Type	Order	B_N/B_3
Butterworth exact $B_N/B_3=\left[\frac{\pi/2n}{\sin(\pi/2n)}\right]$	**1**	$\pi/2$
	2	**1.11**
	3	**1.04**
	4	**1.03**

TABLE A.1 : *Noise equivalent bandwidth of various filters.*

Frequency of the voltage contolled oscillator (VCO) is controlled by the filtered error voltage v_2. Deviation of the VCO from its center frequency is $\Delta\omega = K_o v_2 rad/sec$, where K_O is the VCO gain constant in rad/sec/V. Since frequency is the derivitave of phase , the VCO operation may be described as

$$\frac{d\theta}{dt} = K_o v_2$$

By taking Laplace Transforms we obtain

$$L\left(\frac{d\theta_o(t)}{dt}\right) = s\theta_o(s) = K_o V_2(s) \qquad (B-2)$$

therefore

$$\theta_o(s) = \frac{K_o V_2(s)}{s} \qquad (B-3)$$

In other words, the phase of the VCO output will be proportional to the integral of the input control voltage .
By using Laplace notation the following equations are applicable:

$$V_d(s) = K_d\left(\theta_o(s) - \theta_i(s)\right) \qquad (B-4)$$
$$V_2(s) = F(s)V_d(s) \qquad (B-5)$$
$$\theta_o(s) = \frac{K_o V_2(s)}{s} \qquad (B-6)$$

A combination of these equations results in the basic loop equations

$$\frac{\theta_o(s)}{\theta_i(s)} = H(s) = \frac{K_o K_d F(s)}{s + K_o K_d F(s)} \qquad (B-7)$$

Error transmittance is given by

$$\frac{\theta_i(s) - \theta_o(s)}{\theta_o(s)} = \frac{s}{s + K_{od} \quad F(s)} \qquad (B-8)$$

Before proceeding it is necessary to discuss the loop filter F(s). A first order filter is used which results in a second-order, closed-loop transfer function.

1.1 SECOND-ORDER LOOP

The loop filter chosen is an active filter with Transfer Function:

$$F(s) = A\left(\frac{\tau_2 s + 1}{(\tau_1 + \tau_2)s + 1}\right) \qquad (B-9)$$

This is implemented using an op amp and circuit shown in Fig. B2.

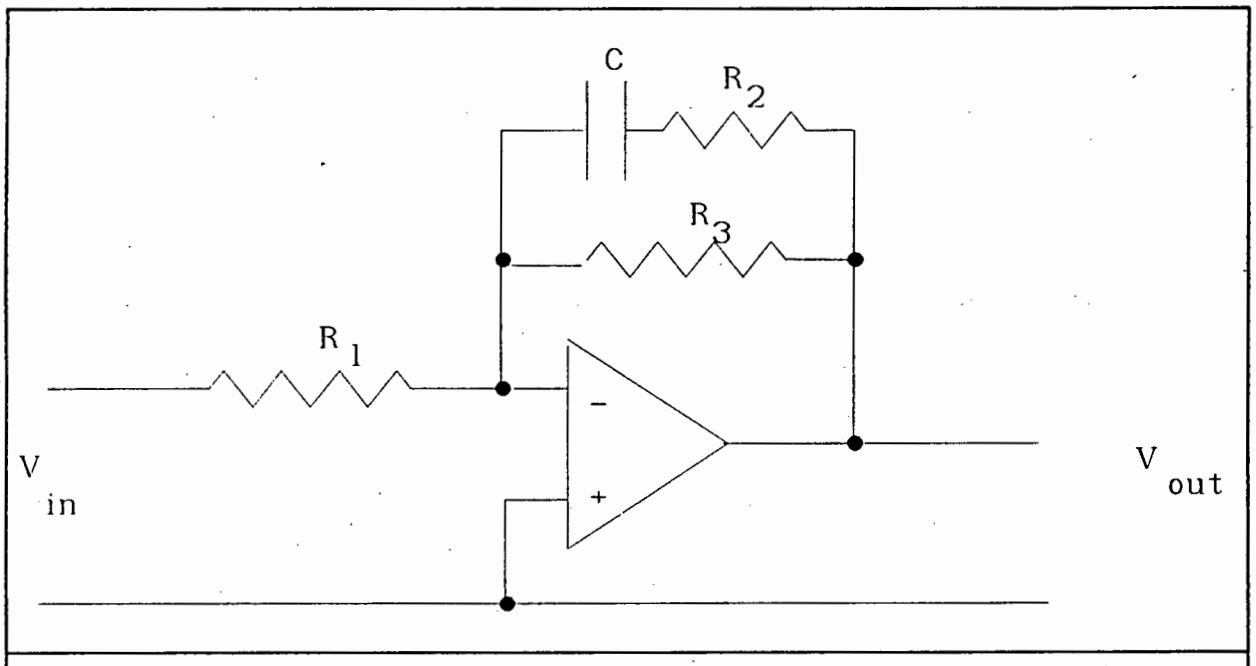

FIGURE B2 : *Active filter.*

The filter transfer function is :

$$F(s) = -A\frac{R_3}{}\left(\frac{R_2 C s + 1}{(R_1(1+A))\left((R_2 + R_3)Cs + 1\right) + R_3\left(1 + sCR_2\right)}\right)$$

Where A is the op. amp. open loop gain. A = 10^6 and F(s) becomes:

$$F(s) = -\frac{R_3}{R_1}\left(\frac{R_2 C s + 1}{(R_2 + R_3)Cs + 1}\right) \qquad (B-10)$$

Where $\tau_1 = R_3C$ and $\tau_2 = R_2C$. The dc gain of the filter has been limited to F(0) = - R_3/R_1, to prevent the output of the op. amp. from saturating.

The filter transfer, F(s) function has been plotted using Microcap software and is shown in Fig. B3. The component values for this plot are the values used in the design; viz; $R_1 = 180k\Omega$, $R_2 = 6k8\Omega$, $R_3 = 1M(var)$, $C = 33nF$. The dc gain is therefore a maximum at K_f = 5.56 . The filter -3dB bandwidth will also vary with R_3, and is given by

$$f_{-3dB} = \frac{1}{\left[2\pi C\sqrt{\left[R_3^2 - R_2^2 + 2R_3R_2\right]}\right]}$$

The argument under square root must always positive, therefore the limits on R_3 are

$2817\Omega \leq R_3 < 1M\Omega$

The maximum and minimum settings are $f_{-3dB\ min}$ = 4.79 Hz and $f_{-3dB\ max}$ = 58 969.0 Hz .

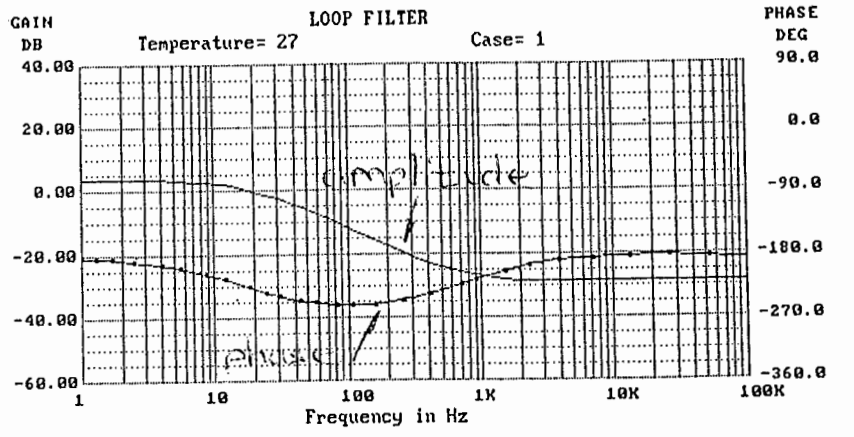

Frequency = 100.00000E+03 Hz. Gain = -28.672 Db
Phase angle= -186.413 Degrees Group delay= 0.00000E+00
Gain slope = -162.14310E-05 Db/Oct Peak gain = 3.507Db/F= 100.00000E-02

FIGURE B3 : *Transfer function of loop filter.*

The active filter of Fig. B2 inverts the signal denoted by the negative sign of equation B-10. This must be eliminated either by adding another invertor to the output of the filter or using a VCO that has a negative Hertz per volt gain (such as the XR2207). Intuitively, the open loop gain must be positive, since a positive frequency difference at the output of the phase detector results in a positive dc control voltage which increases the local oscillator frequency, reducing the phase difference. The negative sign is ignored from here onwards. The closed loop transfer function is given as:

$$T(s) = \frac{AK'F(s)}{s + AK'F(s)}$$

$$= \left(\frac{AK'(\tau_2 s + 1)}{s((\tau_2 + \tau_1)s + 1) + AK'(\tau_2 s + 1)} \right) \qquad (B-11)$$

Where $K' = K_o K_d$.

This transfer function may be written:

$$T(s) = \frac{s\omega_n\left(2\zeta - \frac{\omega_n}{K}\right) + \omega_n^2}{s^2 + 2\zeta\omega_n s + \omega_n^2} \qquad (B-12)$$

in which, drawing on servo terminology, ω_n is the "natural frequency" of the loop and ζ is the "damping ratio."

$$\omega_n = \sqrt{\frac{K_o K_d}{\tau_1 + \tau_2}} \quad rad/\sec \qquad (B-13)$$

$$\zeta = \frac{1}{2}\sqrt{\left(\frac{K_o K_d}{\tau_1 + \tau_2}\right)}\left(\tau_2 + \frac{1}{K_o K_d}\right) \qquad (B-14)$$

The factor $K_o K_d$ is known as the loop gain and has dimensions of sec^{-1} (Hz). Because the highest power of s in the denominator of the transfer function is two, the loop is known as a second order loop. The magnitude of the frequency response of a closed-loop for several values of damping factor is plotted in Fig. B4.

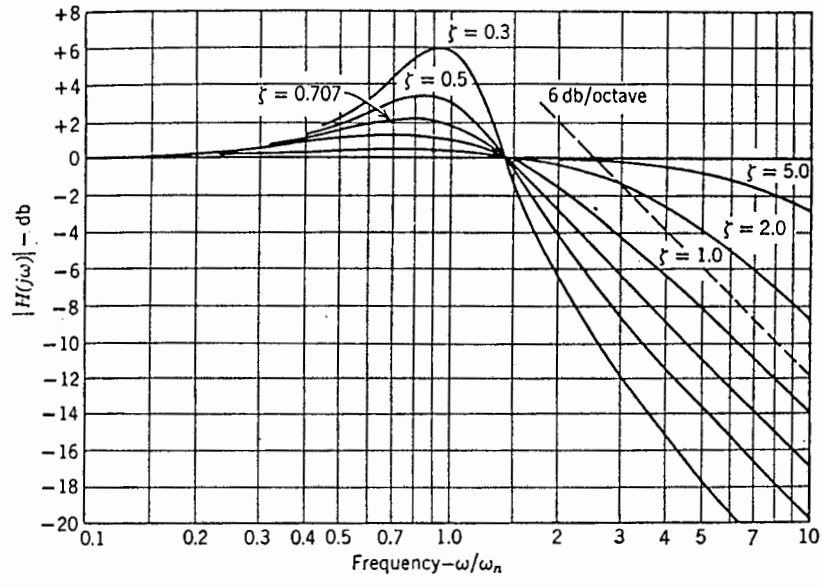

FIGURE B4 : *Frequency response of second order loop.*

It can seen that the loop performs a low-pass filtering operation on phase inputs.

The transfer function, H(s) has a well defined 3-db bandwidth which is labelled ω_{3db}. Its relation to ω_n is presented here to provide a comparison with a familiar concept of bandwidth. By setting

$|H(j\omega)|^2 = 1/2$

and solving for ω a relationship between ω_n and ω_{3db} is obtained. For different damping ratios ζ, the bandwidth varies over a range. Typical values are given in table B1 for various values of gain and damping.

ζ	ω_{3dB}/ω_n
0.500	1.82
0.707	2.06
1.00	2.48

TABLE B1 : *Values for a high gain loop.*

The error response of the loop asgiven before in (B-8) is plotted in Fig. B5 for $\zeta = 0.707$.

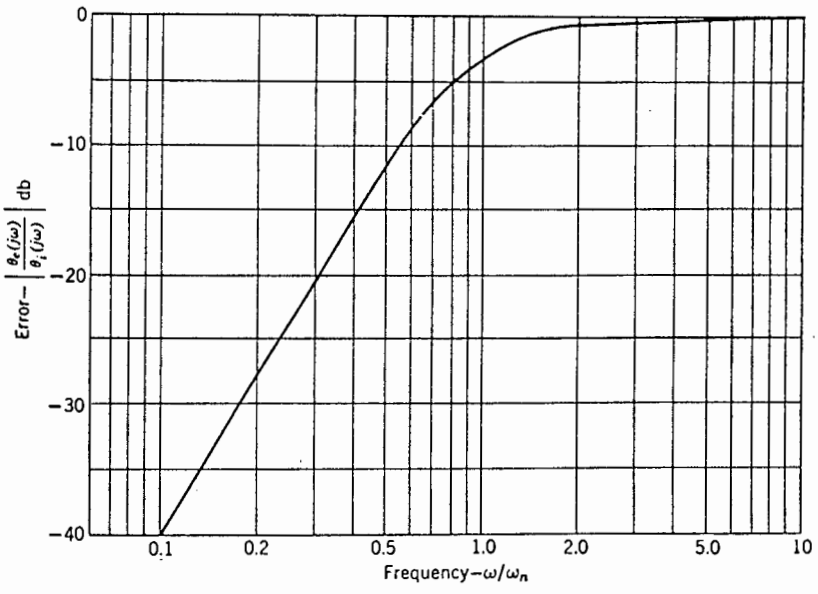

FIGURE B5 : *Error response of a high gain loop.*

A high-pass characteristic is obtained; that is the loop tracks low-frequency changes but cannot track high frequencies above ω_n .

1.2 LOOP STABILITY

A considerable degree of insight into PLL behaviour can be obtained by determining the locations of the poles of the closed-loop response. The open loop transfer function of the loop is

$$H(s) = K_{ol}\left(\frac{F(s)}{s}\right)$$

For the active lead-lag loop filter

$$H(s) = K_{ol}\left(\frac{\tau_2 s + 1}{s\left((\tau_1 + \tau_2)s + 1\right)}\right)$$

Where $K_{ol} = A K'$. The open loop transfer function of the second order loop contains two poles and one zero; namely:

Zero at $\sigma = -\frac{1}{\tau_2}$

Pole at $\sigma = -\frac{1}{\tau_1 * \tau_2}$

Pole at $\sigma = 0$

The root locus plot appears in Fig. B6.

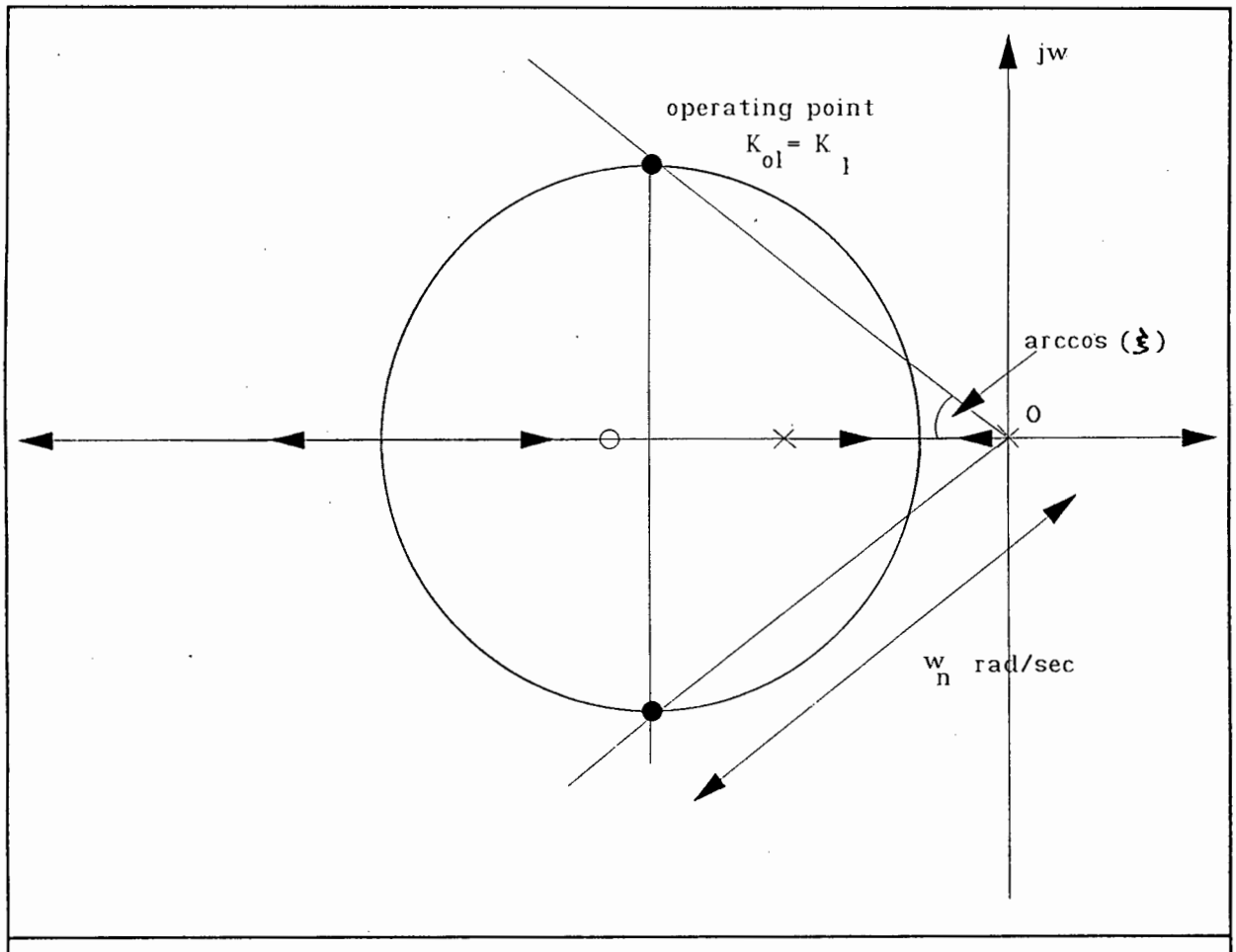

FIGURE B6 : *Root locus plot of system.*

With increasing gain , the two poles migrate along the σ axis towards each other until they meet and become complex conjugate pairs whose path is a circle centered at the zero. The poles meet on the real axis once again, where one ends at the zero and the other continues to infinity.

1.3 SUMMARY

From the root-locus plot it can be concluded that the system is unconditionally stable for all values of K_{ol}, the open loop gain. The operating condition can be chosen by selecting any one of the three parameters (ω_n, ζ, K_{ol}) and calculating the other two.

The natural frequency ($\omega_n rad/sec$) determines the bandwidth of the closed loop, a narrow bandwidth will provide good noise immunity but will reduce the lock-in range of the loop. The lock in range is the input range of frequencies, about the VCO center frequency, that will cause the loop to lock up. If the input frequency falls outside of this range, the loop will not lock up.

The damping ratio (ζ, dimensionless) determines the settling time of the loop transient when the loop is excited by a change in input. The damping ratio can be chosen independently of the natural frequency.

Open Loop Gain (K_{ol} Hz) is the product of the gains of all the constitiuent components of the loop. The open loop gain determines the tracking range of the loop. This is the range of frequencies , about the VCO center frequency, for which the loop will remain in lock, once it is in lock. In this way the loop can follow the input if minor doppler shifts occur in the frequency of the input carrier. The open loop gain determines the position of the closed loop poles on the root locus diagram.

a summary of the design equations for a high gain second order loop obtained from [4.4] are stated below:

The input noise threshold of the system.

$$P = FkT(2B_N) \quad Watt \quad (B-15)$$

F : noise figure of the loop.
B : equivalent noise bandwidth of the closed loop, **Hz.**

k : Boltzmann's constant , $1.381 \times 10_{-23}$ JK^{-1}.

T : noise temperature, 298 ^{o}K.

Equivalent Noise Bandwidth

For a second order loop with gain, $K_{ol} >> 1$.

$$B_N = \frac{\omega_n}{2}\left(\zeta + \frac{1}{4\zeta}\right) \quad Hz \qquad (B-16)$$

Hold-in range

The frequency range, about the center frequency of the VCO through which the loop will remain locked onto that input frequency, given by:

$$\Delta\omega_H = \pm K_{ol} \quad rad/\sec \qquad (B-17)$$

Lock-In range.

The maximum frequency range about the center frequency of the VCO over which the loop will acquire lock.

$$\Delta\omega_L \approx 2\zeta\omega_n \quad rad/\sec \qquad (B-18)$$

The time constants are obtained by combining equations B-13 and B-14:

$$\tau_1 + \tau_2 = \frac{K_{ol}}{\omega_n^2} \quad \sec \qquad (B-19)$$

$$\tau_2 = \left[\frac{2\zeta}{\omega_n} - \frac{1}{K_{ol}}\right] \quad \sec \qquad (B-20)$$

APPENDIX C

COSTAS LOOP

1.1 PHASE VARIANCE

In this section, the linearised phase error variance of the Costas loop is obtained which is stationery. The actual phase error variance is unbounded, so that it is not a useful measure of tracking performance. The complete derivation appears in reference [4.3] and steps have been skipped over here. Consider the Costas loop model of Fig. C-1.

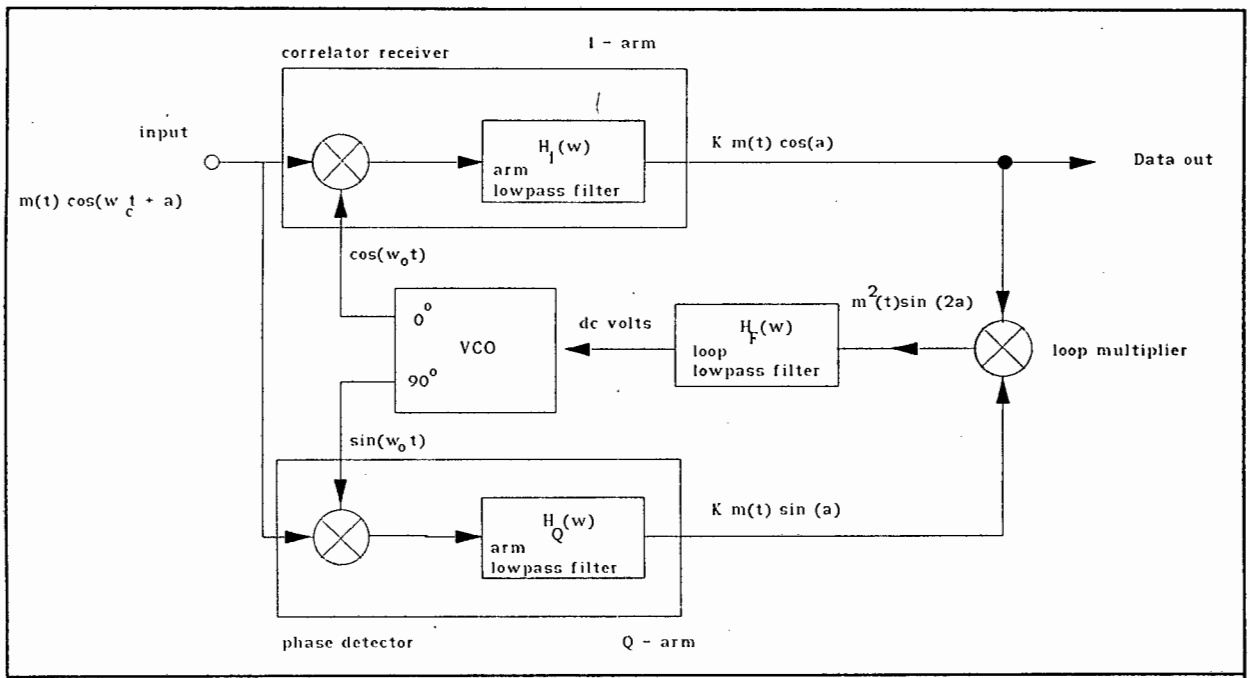

FIGURE C-1 : *Costas loop model.*

Consider the suppressed carrier modulation given by equation C-1 :

$$y(t) = \sqrt{2}\,A m(t)\sin\left(\omega_1 t + \theta_o\right) + n(t) \qquad (C-1)$$

Where $m(t) = \pm 1$ during the symbol period of **T** seconds. **A** is the rms amplitude, ω_1 is the carrier frequency (rad/sec) and θ_o is the unknown phase.

The wideband WGN is modelled as:

$$n(t) = \sqrt{2}\,n_c(t)\cos\left(\omega_1 t + \theta_o\right) + \sqrt{2}\,n_s(t)\sin\left(\omega_1 t + \theta_o\right) \qquad (C-2)$$

Where the spectral density of $\mathbf{n_C(t)}$ and $\mathbf{n_S(t)}$ is equal to $\mathbf{N_O/2}$. The local oscillators are denoted

$$V_I = \sin(\omega_i t + \hat{\theta})$$

$$V_Q = \cos(\omega_i t + \hat{\theta})$$

for the in-phase and quadrature-arm, respectively. At the filtered phase detector output (quadrature-phase arm) after the low pass filter, the filtered product of the local oscillator and the input carrier is

$$y_c(t) = A\tilde{m}(t)\sin\phi + \tilde{n}_c\cos\phi + \tilde{n}_s(t)\sin\phi \qquad (C-3)$$

where

$$\phi = \hat{\theta} - \theta o + (\omega_i - \omega_o)t \qquad (C-3a)$$

and $\tilde{m}(t)$ the filtered version of the data sequence. We have assumed that the lowpass filter removes the double-frequency terms and both $\tilde{n}_c(t)$ and $\tilde{n}_s(t)$ are band-limited sample functions of low-pass Gaussian processes with a one-sided noise bandwidth of B_{LP} Hz. Out of the correlator receiver (In-phase arm), after filtering by the low pass filter, we have

$$y_s(t) = A\tilde{m}(t)\cos\phi - \tilde{n}_c\sin\phi + \tilde{n}_s(t)\cos\phi \qquad (C-4)$$

where all variables are as defined before. After the loop multiplier, the error signal z(t) is given by

$$z(t) = \frac{A^2}{2}(\tilde{m})^2\sin(2\phi) + A\tilde{m}\tilde{n}_s\sin(2\phi)$$

$$+\left(\frac{\tilde{n}_s^2}{2} + \frac{\tilde{n}_c^2}{2}\right)\sin(2\phi) + (A\tilde{m} + \tilde{n}_s)\tilde{n}_c\cos(2\phi) \quad (C-6)$$

where the t dependence has been dropped for convenience. The output of the VCO is given as

$$\hat{\theta} = \frac{K_{VCO}F(s)}{s}z(t) \qquad (C-7)$$

Substituting (C-6) into (C-7) and (C-3a):

$$\dot{\phi} + \frac{A^2KF(s)}{2}(\tilde{m})^2\sin(2\phi) =$$

$$KF(s)\left\{\frac{\tilde{n}_c^2}{2} - \frac{\tilde{n}_s^2}{2} - A\tilde{m}\tilde{n}_s\sin(2\phi) - (A\tilde{m}\tilde{n}_c + \tilde{n}_s\tilde{n}_c)\cos(2\phi)\right\}$$

$$+(\omega_1 - \omega_o) \quad (C-8)$$

where K = K_{VCO} times any multiplier or filter gains in the loop and $\omega_1 - \omega_o$ is the initial frequency difference between the incoming signal and the VCO frequency.

Let $2\phi = \Phi_o$ and $\mathbf{P} = \mathbf{A^2}$, so that Equ. C-8 can be re-written

$$\dot{\Phi}_o + KPF(s)(\tilde{m})^2 \sin(\Phi_o) = -KF(s)(-\tilde{n}_c^2 + \tilde{n}_s^2 + 2A\tilde{m}\tilde{n}_s)\sin(\Phi_o) + 2(A\tilde{m}\tilde{n}_c + \tilde{n}_s\tilde{n}_c)\cos(\Phi_o) + 2(\omega_1 - \omega_o) \qquad (C-9)$$

This is the stochastic differential equation (SDE) for the Costas loop. From this, the phase error variance $\sigma_{\phi_o}^2$ of the loop is calculated as [4.3]. This expression contains two sources of noise: The first is caused by the added white Gaussian noise at the loop input. This noise is filtered, and causes phase variance at the output of the loop filter. The second is caused by the filtered data in the arms of the loop. When the loop is just out of lock, The product of the filtered data at of the output of the loop filter is, $(\tilde{m})^2$. This is termed *self-noise* and should ideally by unity but usually is not. This is because sub-optimal filtering in the arms does not recover rectangular data can not be multiplied to exactly unity.

The result is an expression of phase variance given by:

$$\sigma_{\phi_o}^2 = \frac{4N_oB_L}{\alpha P} \frac{\left(\frac{\alpha'}{\alpha} + \frac{N_oB'_{LP}}{\alpha P}\right)}{1 - \left(\frac{8TB_L}{(\alpha P)^2}\sum_{l=1}^{\infty} R_d^2(lT)\right)} \quad rad^2 \qquad (C-10)$$

where :

T is the the bit period, sec.
$N_o/2$ is the two-sided white noise spectral density, W/Hz.

B_{LP} is the arm filter bandwidth, Hz, given by

$$B_{LP} = \frac{1}{2}\int_{-\infty}^{\infty} |H(f)|^2 df$$

B_{LP}' Hz, is defined by :

$$B'_{LP} = \frac{1}{2}\int_{-\infty}^{\infty} |H(f)|^4 df$$

B_L is the one-sided closed loop noise bandwidth, Hz, such that **B_L** << **B_{LP}**.

$$\alpha = \int_{-\infty}^{\infty} S_m(\omega) \left| H_{LP}(\omega) \right|^2 \frac{d\omega}{2\pi}$$

$$\alpha' = \int_{-\infty}^{\infty} S_m(\omega) \left| H_{LP}(\omega) \right|^4 \frac{d\omega}{2\pi}$$

The auto-correlation of the arm filtered data is given by

$$R_d(\tau) = \int_{-\infty}^{\infty} S_m(\omega) \left| H_{LP}(\omega) \right|^2 e^{j\omega\tau} \frac{d\omega}{2\pi}$$

The use of these equations is described in the text of chapter 4.

1.2 DYNAMIC AND TRANSIENT RESPONSE

The following is a derivation of the dynamic response of the Costas loop. The loop behaviour is considered to be linear and the effects of noise have not been included.

Consider the loop with transmittances written in the Laplace variable, **s** , as shown in Fig. C-2. The two arm filters are represented as pure gains, K_{f1} and K_{f2}, since the poles of these filters do not effect the transient response of the closed loop, this is further explained.

The arm multipliers are linear and have gains of k_{m1} V^{-1} , k_{m2} V^{-1}. The loop multiplier is linear and has a gain of k_{m3} V^{-1} . The loop filter has a pass-band gain written as F(0) or K_f , the complete transfer function will be further explained. The voltage controlled oscillator performs an integration and is modelled as a transmittance ; H(s) = K_{VCO} / s . The gain has units of V/rad.

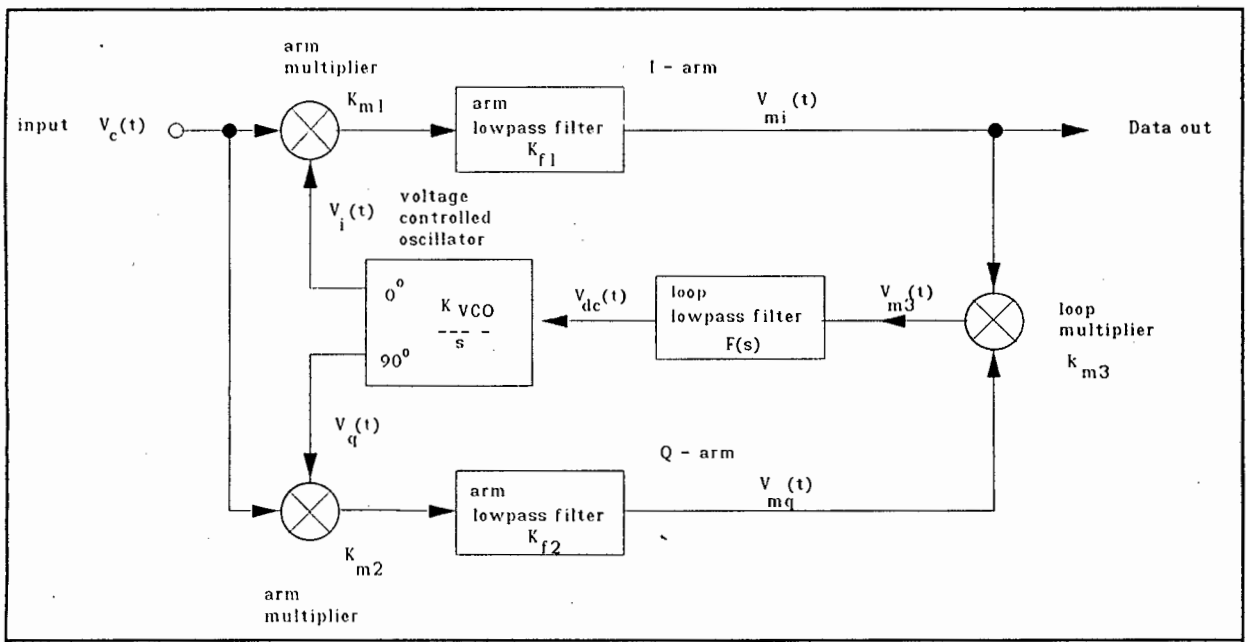

FIGURE C-2 : *Transient Response of Costas Loop.*

The input to the loop is given by

$$V_c(t) = \sqrt{2}\,Am(t)\sin(\omega_c t + \theta_c) \quad V \qquad (C-11)$$

The VCO has two output voltages, an in-phase value and a quadrature-phase value. The two outputs are given as:

In-phase:

$$V_i(t) = V_i \sin(\omega_o t + \theta_o) \quad V$$

Quadrature-phase:

$$V_q(t) = V_q \cos(\omega_o t + \theta_o) \quad V$$

After the multiplier in the **In-phase Arm**

$$V_{mi}(t) = K_{m1} V_c(t) V_i(t) \quad V$$

$$V_{mi}(t) = K_{m1}\sqrt{2}\,Am(t)V_i\left(\sin(\omega_c t + \theta_c) * (\sin(\omega_o t + \theta_o))\right) \quad V \qquad (C-12)$$

Using a trigonometric identity

$$V_{mi}(t) = \frac{\sqrt{2}}{2}(AV_i)(K_{m1})(m(t))(\sin(\Delta\omega t + \Delta\theta) + \sin(\hat{\omega} t + \hat{\theta})) \quad V \qquad (C-13)$$

where :

$$\Delta\omega = \omega_c - \omega_o \quad rad/\sec$$

$$\hat{\omega} = \omega_c + \omega_o \quad rad/\sec$$

$$\Delta\theta = \theta_c - \theta_o \qquad rad$$

$$\hat{\theta} = \theta_c + \theta_o \qquad rad$$

After the multiplier in the **Quadrature-phase Arm**

$$V_{mq}(t) = K_{m2} V_c(t) V_q(t) \qquad V$$

$$V_{mq}(t) = K_{m2}\sqrt{2}\, A\, m(t) V_q\left(\sin(\omega_c t + \theta_c) * (\cos(\omega_o t + \theta_o))\right) \qquad V \qquad (C-14)$$

Similarly as above:

$$V_{mq}(t) = \frac{\sqrt{2}}{2}(AV_q)(K_{m2})(\sin(\Delta\omega t + \Delta\theta) + \sin(\hat{\omega} t + \hat{\theta})) \qquad V \qquad (C-15)$$

The low pass filters eliminate the double frequency terms in (C-13) and (C-15) above, the result is :

$$V_{mi}(t) = \frac{\sqrt{2}}{2}(\hat{V})(\hat{m}(t))(K_{m1} K_{f1})(\cos(\Delta\omega t + \Delta\theta)) \qquad V \qquad (C-16)$$

Similarly in the other arm:

$$V_{mq}(t) = \frac{\sqrt{2}}{2}(\hat{V})(\hat{m}(t))(K_{m2} K_{f2})(\sin(\Delta\omega t + \Delta\theta)) \qquad V \qquad (C-17)$$

$\hat{m}(t)$ is the data at the output of the low pass filter. The term $\hat{V} = AV_q = AV_i$. The transfer function of these arm filters are of no concern to the dynamics of the loop as the poles of the cut off frequency of the filters are at much higher frequency than that of the loop filter which will dominate.

The first assumption is that the loop is almost in lock such that the frequency difference is zero, that is, $\Delta\omega = 0$.

The second assumption is that for small phase differences, the loop behaviour is *linear*, since $\Delta\theta < 0.1\, rad \Rightarrow \sin(\Delta\theta) \approx \Delta\theta$ and $\cos(\Delta\theta) \approx 1$. A linear approximation of Fig. C-2 can be drawn and is given in Fig C-3.

The in-phase arm reveals the demodulated data and can be described as a correlator receiver with voltage:

$$V_{mi}(t) = \frac{\sqrt{2}}{2}(\hat{V})(K_{m1} K_{f1})(\hat{m}(t)) \qquad V \qquad (C-16)$$

Which is the demodulated data multiplied by a gain. If the loop moves out-of-lock but remains within the linear operating region, the data is attenuated proportionally to the phase error, but does not contribute to the loop tracking.

The quadrature-phase arm behaves as a phase detector with voltage:

$$V_{mq}(t) = K_{PD1}(\hat{m}(t))(\Delta\theta) \qquad V \qquad (C-17)$$

The quadrature arm is identical to a phase locked loop and performs the loop tracking control. The multiplier-arm filter is the phase detector with units V/rad. The input carrier amplitude, local oscillator amplitude, multiplier gain and low pass filter gain are combined into a phase detector gain having units of V/rad. $\mathbf{K_{PD1}}$ rad/V is thus a function of the voltage levels of the local oscillator as well as the input signal. To eliminate this dependency, the input voltage and local oscillator voltage are set as constants.

This is written as

$$K_{PD1} = \frac{\sqrt{2}}{2}(\hat{V})(K_{m2}K_{f2}) \qquad V/rad$$

Equations (C-17) and (C-16) are multiplied at the linear loop multiplier to give the following result:

$$V_{m3}(t) = V_{mi}V_{mq}(t)K_{m3} \qquad V$$

$$= \frac{\sqrt{2}}{2}(\hat{V})\left[K_{PD1}K_{m1}K_{f1}K_{m3}(\hat{m}(t))^2(\Delta\theta)\right] \qquad V \qquad (C-18)$$

$\mathbf{K_{m3}}$ is the linear multiplier gain with units of V^{-1}. It assumed that the data is perfectly recovered by the arm filters such that $(\hat{m}(t))^2 = 1$

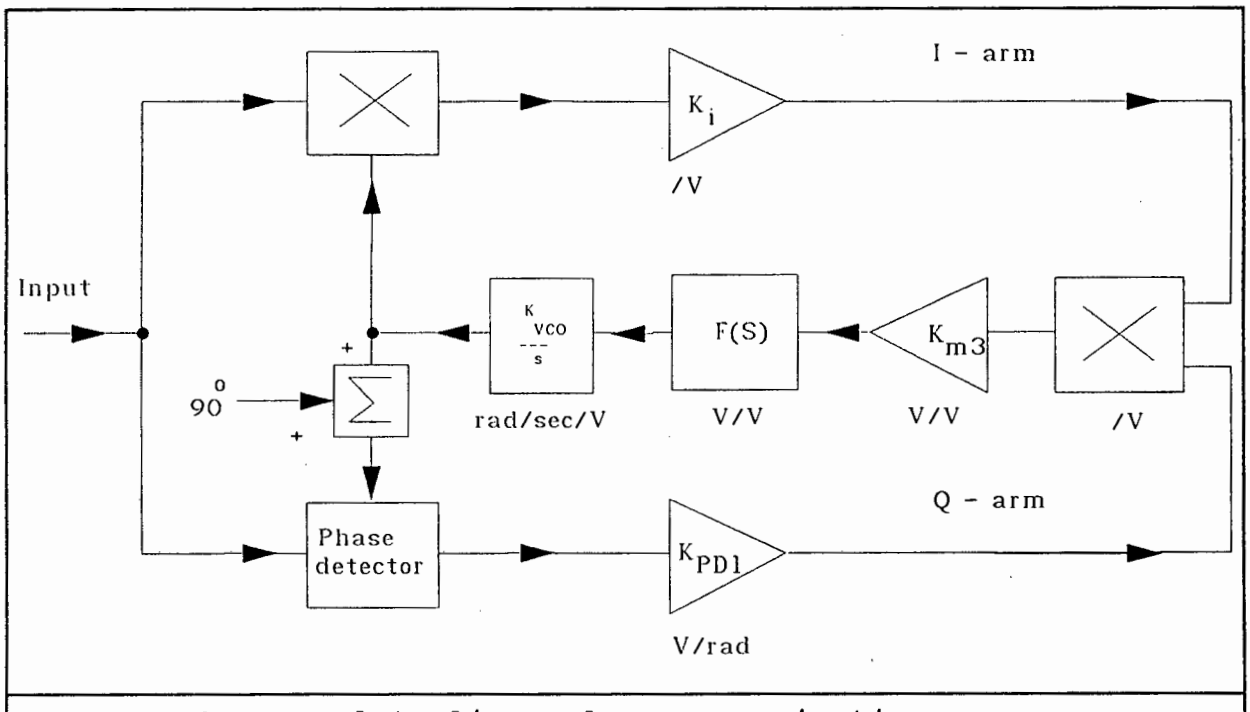

FIGURE C-3 : *Complete linear loop approximation.*

The in-phase arm remains essentially unity, and the quadrature-phase arm performs the tracking, the gain of the in-phase multiplier-low pass filter is not V/rad but V^{-1}. The loop multiplier is a linear multiplier and is not further simplified.

Equation (C-18) becomes:

$$V_{m3}(t) = (\hat{K})(\Delta\theta) \quad (V) \quad (C-19)$$

Where

$$\hat{k} = \frac{\sqrt{2}}{2}(\hat{V})\left[K_{PD1} K_{m1} K_{f1} K_{m3}\right] \quad (C-20)$$

Applying this to the loop filter, the output dc control voltage is:

$$V_{dc}(s) = V_{m3}(s) * F(s) \quad V \quad (C-21)$$

This is applied to the VCO, the result is :

$$V_{VCO}(s) = V_{m3}(s) F(s)\left(\frac{K_{VCO}}{s}\right) \quad (C-23)$$

$$V_{VCO}(s) = (\hat{K})(\Delta\theta) F(s)\left(\frac{K_{VCO}}{s}\right) \quad (C-24)$$

The VCO integrates the dc voltage and the output is the local oscillator phase, therefore :

$$\theta_o(s) = V_{VCO}(s)$$

and from (C-15) above :

$$\Delta\theta = \theta_c - \theta_o$$

Giving :

$$\theta_o(s) = (\hat{K}) F(s)\left(\frac{K_{VCO}}{s}\right)\left(\Delta\theta_o(s) - \Delta\theta_c(s)\right) \quad (C-25)$$

The open loop transfer function is given as:

$$H_o(s) = (\hat{K}) F(s)\left(\frac{K_{VCO}}{s}\right) \quad (C-26)$$

The open loop gain is completely given as

$$k_{ol} = \frac{\sqrt{2}}{2}(\hat{V}) K_{m3} \cdot K_{PD1} \cdot F(0) \cdot K_{m1} : K_{f1} \quad K_{VCO} \qquad (C-27)$$

which has units of sec^{-1}. The loop filter dc gain, $k_{f1} = F(0)$. The open loop transfer function of the Costas loop resembles that of the simple phase-locked Loop. The units around the loop are given. The linear approximation of the loop has been redrawn as shown in Fig. C-4.

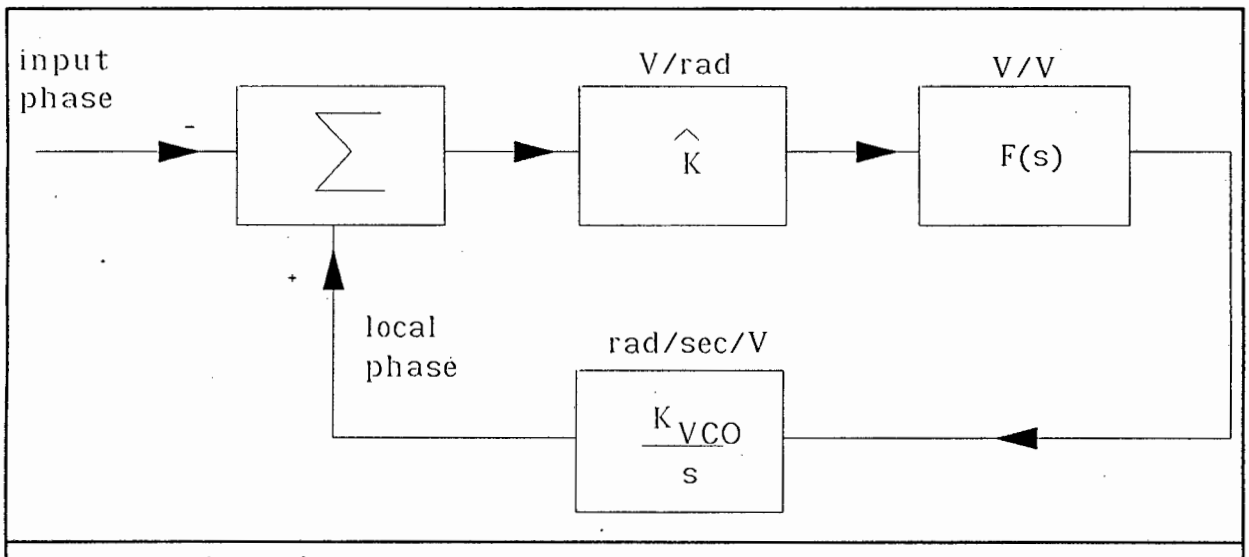

FIGURE C-4 : *Linear Costas Loop model.*

The closed loop transfer function can then be written as:

$$T(s) = \frac{\theta_o(s)}{\theta_c(s)} = \frac{\hat{K} K_{VCO} F(s)}{s + \hat{K} K_{VCO} F(s)} \qquad (C-28)$$

This is the complete closed loop transfer function and the Costas loop may now be analysed using Phase-locked loop theory. The phase locked loop theory is given in appendix B.

APPENDIX D

SWITCHED CAPACITOR FILTER DESIGN

DESIGN EQUATIONS

Cut off frequency, f_o :

$$f_o = \frac{f_{CLK}}{50} \times \left(\sqrt{\left(\frac{R_2}{R_4} + 1 \right)} \right)$$

Q = Quality factor:

$$Q = \sqrt{\frac{r_2}{R_4}} \times \left(\frac{R_3}{R_2} \right)$$

Highpass Gain as $f \rightarrow f_{CLK}/2$:

$$H_{OHP} = -\frac{R_2}{R_1}$$

Bandpass Gain at **f = f_o** :

$$H_{OBP} = -\frac{R_3}{R_1}$$

Lowpass gain as $f \rightarrow 0$:

$$H_{OLP} = -\frac{R_4}{R_1}$$

An important characteristic of sampled-data systems is their effect on signals at frequencies greater than the sampling or clock frequency applied to it. The sampling frequency must be atleast twice the highest spectral component in the input spectrum to the filter otherwise aliasing will occur. To avoid aliasing, an anti-aliasing low pass filter can be included just before the filter to eliminate the very high frequency components like the double frequency term which result at the output of a double balanced multiplier . This will occur at 1.4 Mhz in this case. Passive RC filters have been used with $R = 6k\Omega$ and **C = 100 pF.** This gives a -3dB frequency of f_{-3dB} **= 265 Khz** which is found to be adequate.

The function of the switched capacitor filter is to further limit the spectrum to the bit rate frequency , which eliminates noise.

The four resistors have values given in table D-1. The designed parameters are given in table D-2. The switched capacitor circuit is shown in Fig D1.

R_1 $k\Omega$	**R_2** $k\Omega$	**R_3** $k\Omega$	**R_4** $k\Omega$
10	**27**	**10**	**10**

TABLE D-1 : *Resistor values of switched capacitor filt er.*

f_{CLK}	f_o	Q	H_{OHP}	H_{OBP}	H_{OLP}
3500 Khz	135 Khz	0.608	- 2.7	-1	- 1
1750 Khz	68 Khz	0.608	- 2.7	-1	- 1
875 Khz	34 Khz	0.608	- 2.7	-1	- 1
437.5 Khz	17 Khz	0.608	- 2.7	-1	- 1
218.75 Khz	8.4 Khz	0.608	- 2.7	-1	- 1
109.375 Khz	4.18 Khz	0.608	- 2.7	-1	- 1

TABLE D-2 : *Table of the six switched capacitor filter parameters.*

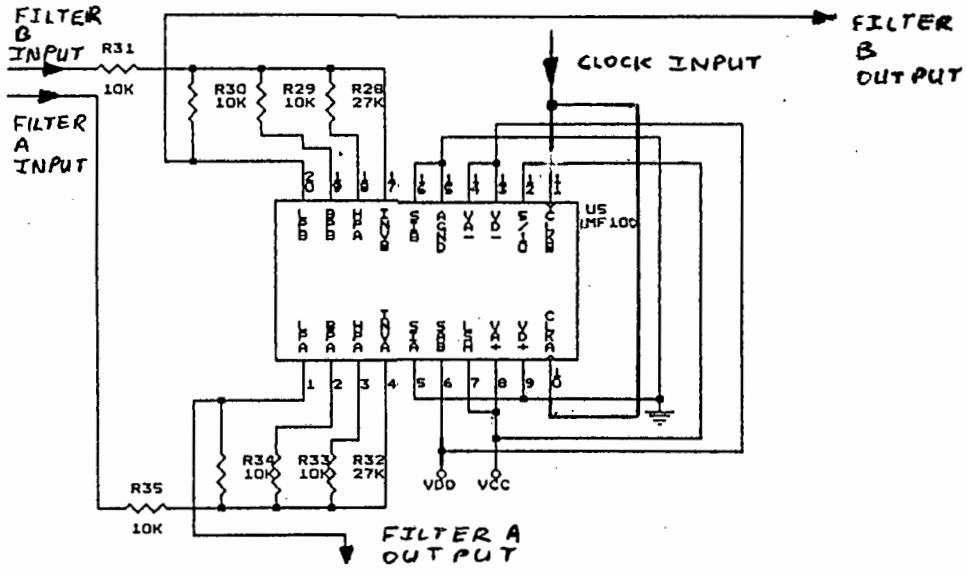

FIGURE D1 : *Switched capacitor circuit consisting of the LMF100 device.*

The following six pages illustrate the phase and amplitude response of each of the arm filters, as selected by applying the appropriate clock frequency. The amplitude response has been obtained on the 4195A Hewlewtt Packard Network/Spectrum analyser and using the 4741 plotter. The amplitude response is given in two views, a close up of the passband in one view and the stop band in the other. This is to show the sampling frequency of the applied clock of each filter. This is noticed as the discrete component.

F = 4 khz , Amplitude Response

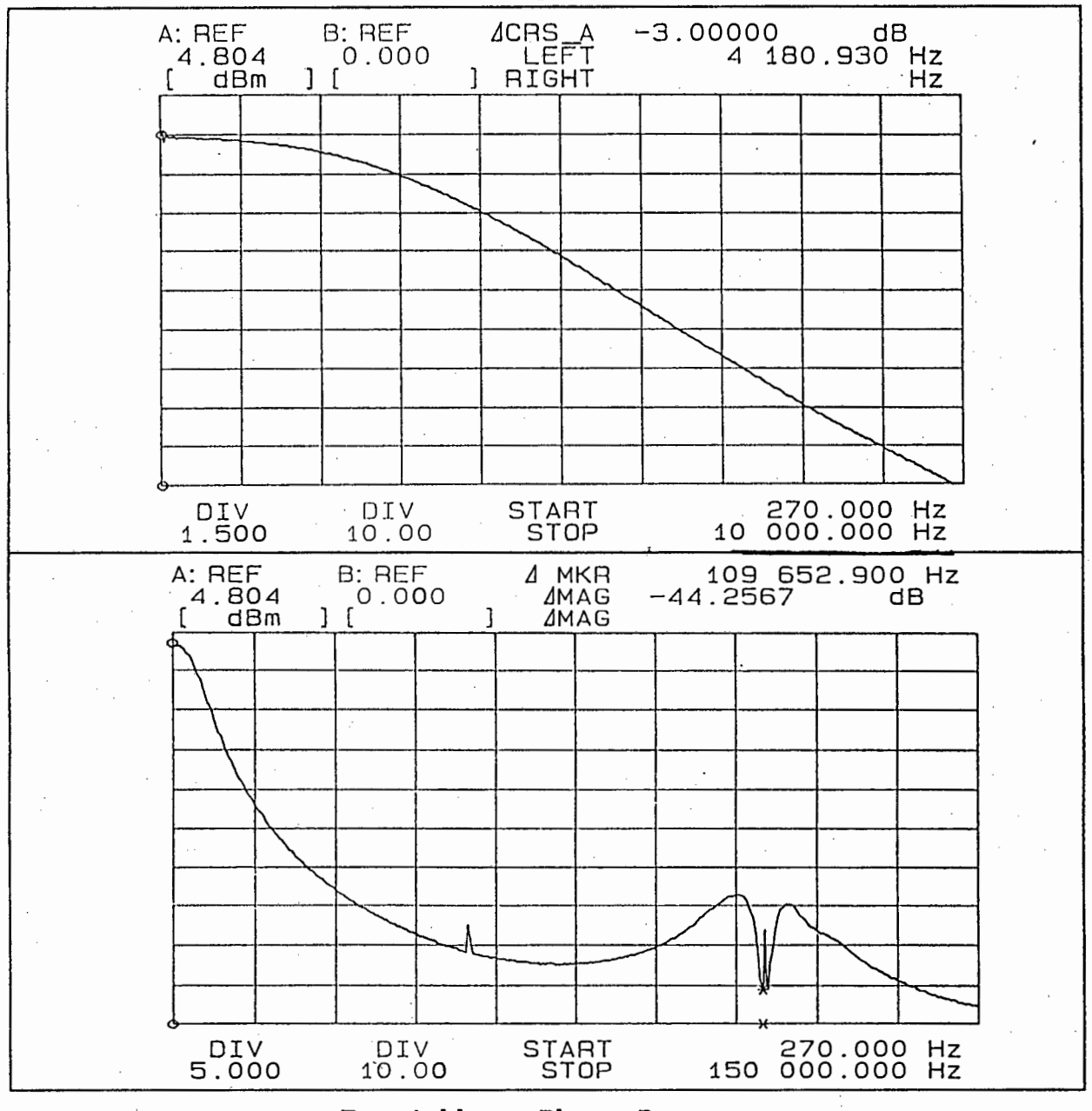

F = 4 khz , Phase Response

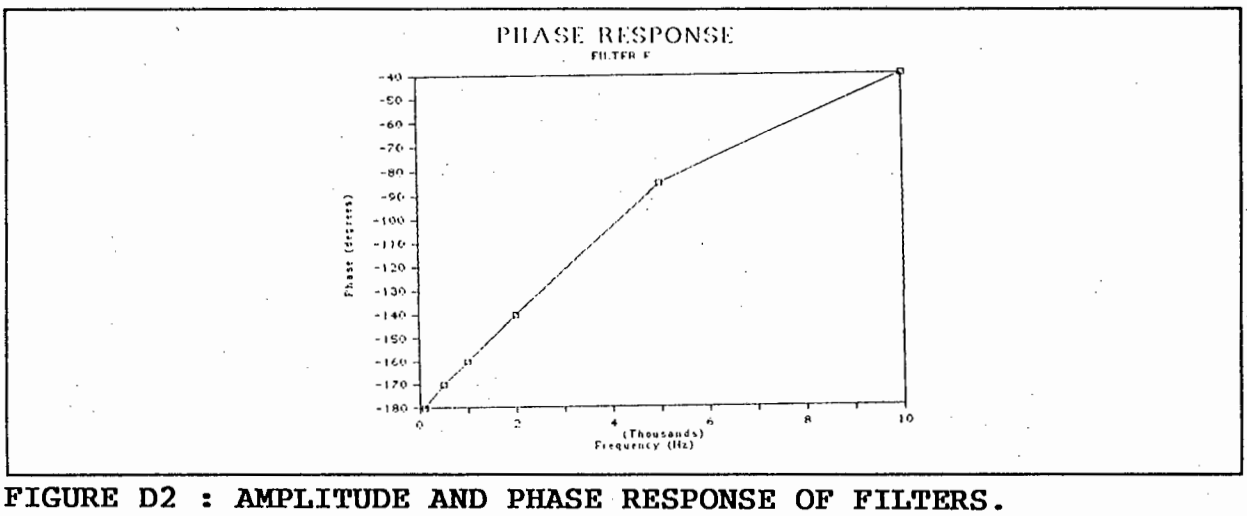

FIGURE D2 : AMPLITUDE AND PHASE RESPONSE OF FILTERS.

F = 8 khz , Amplitude Response

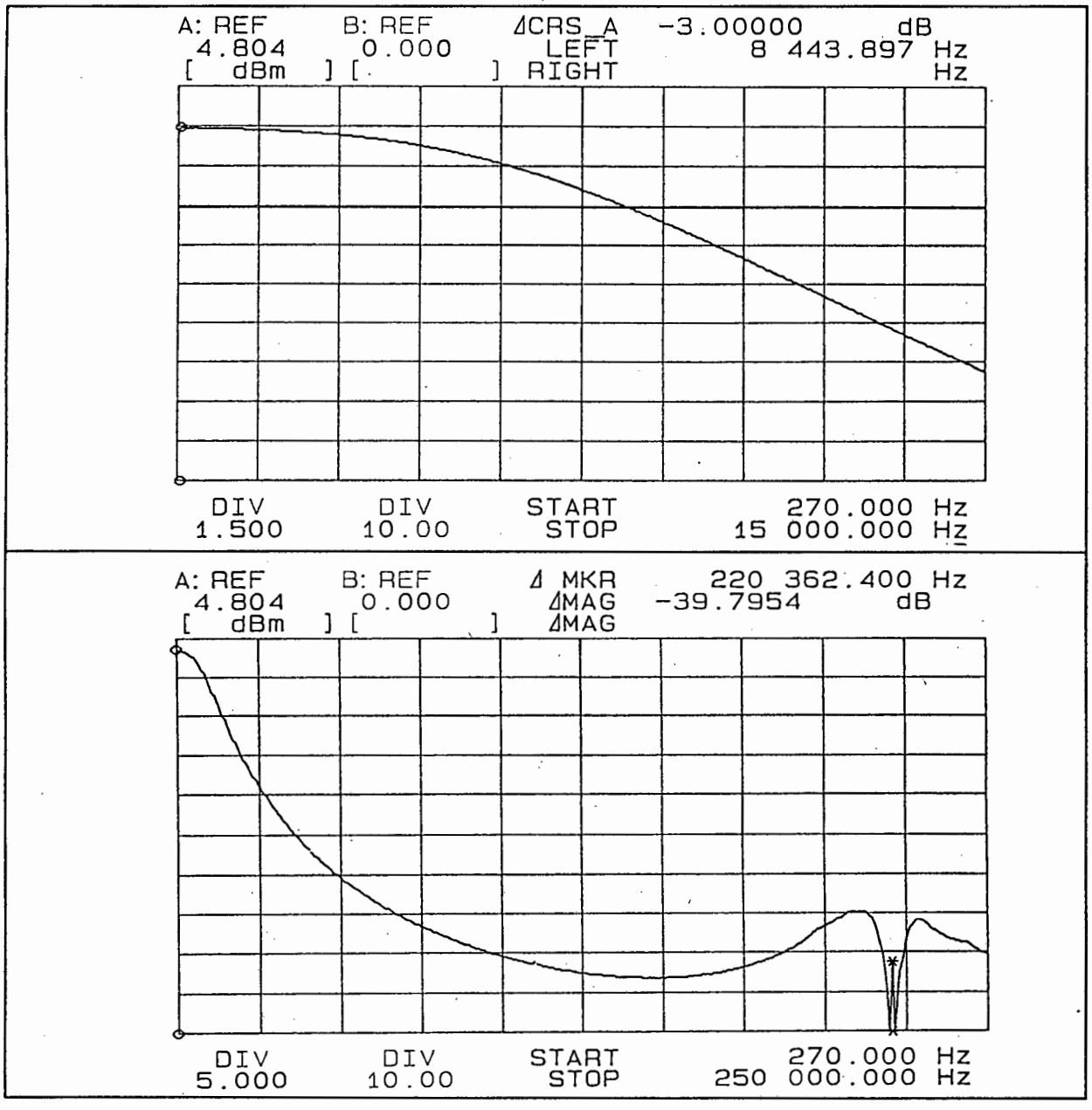

F = 8 khz , Phase Response

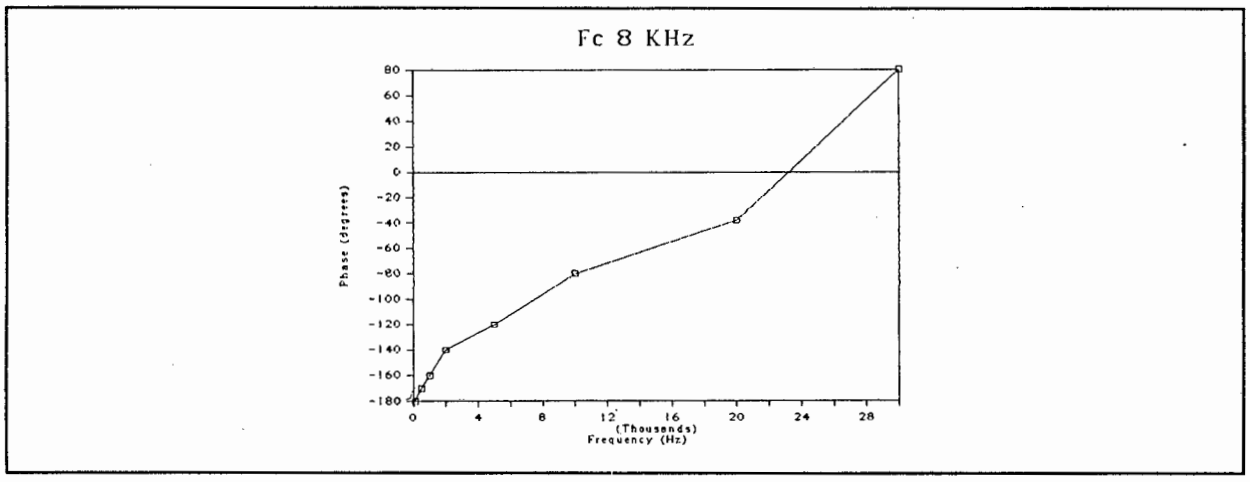

F = 16 khz , Amplitude Response

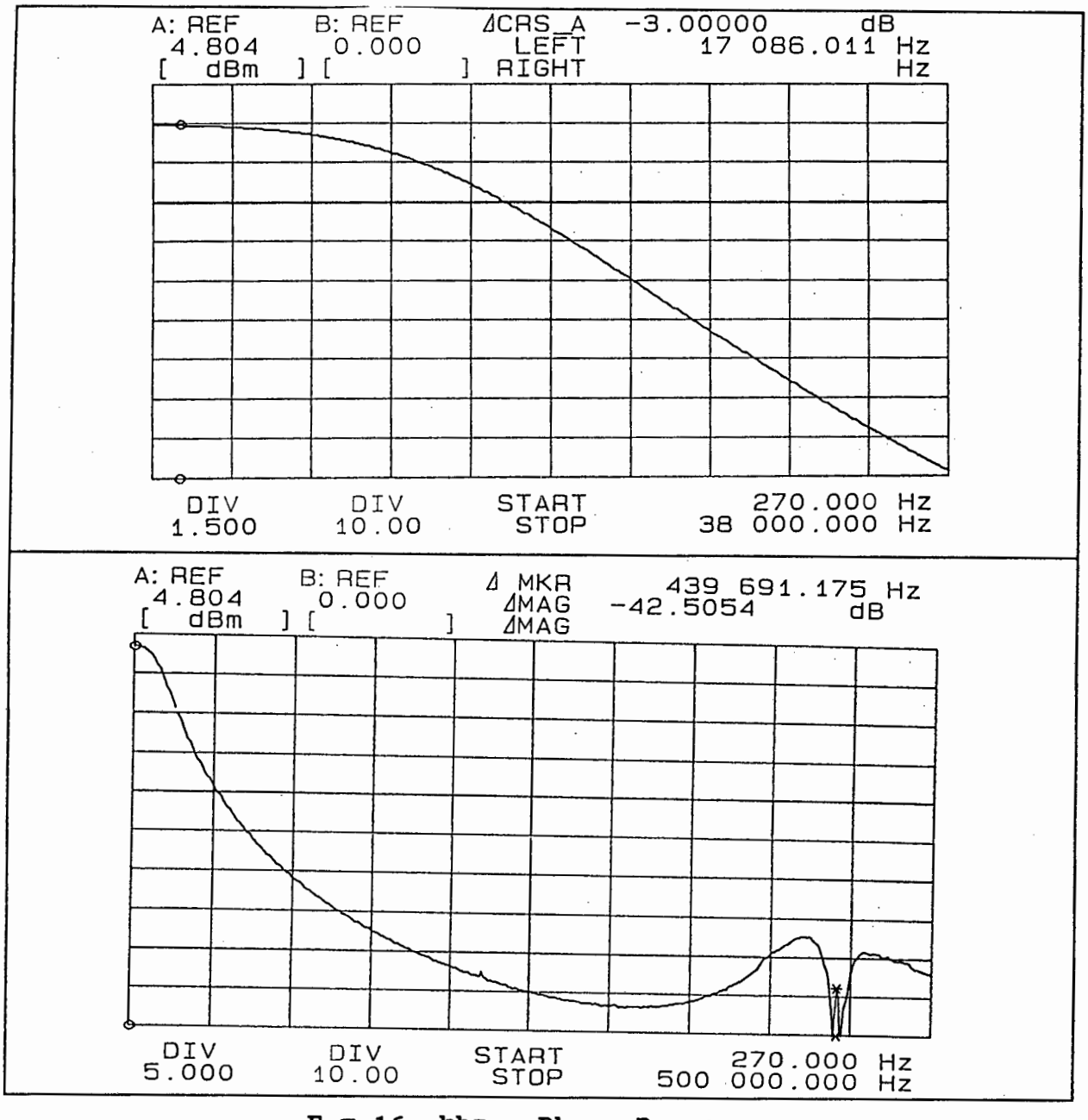

F = 16 khz , Phase Response

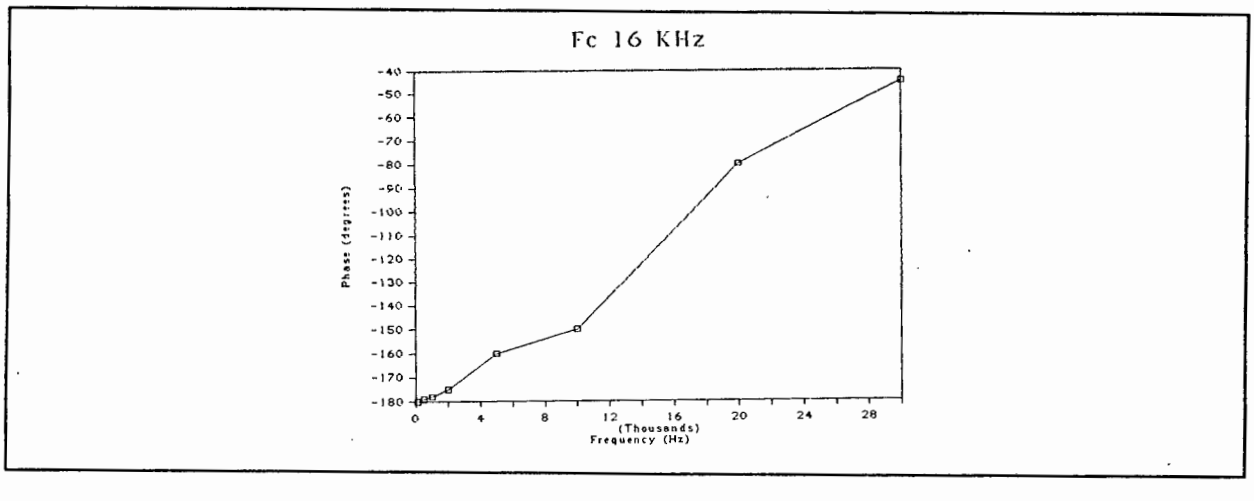

F = 32 khz , Amplitude Response

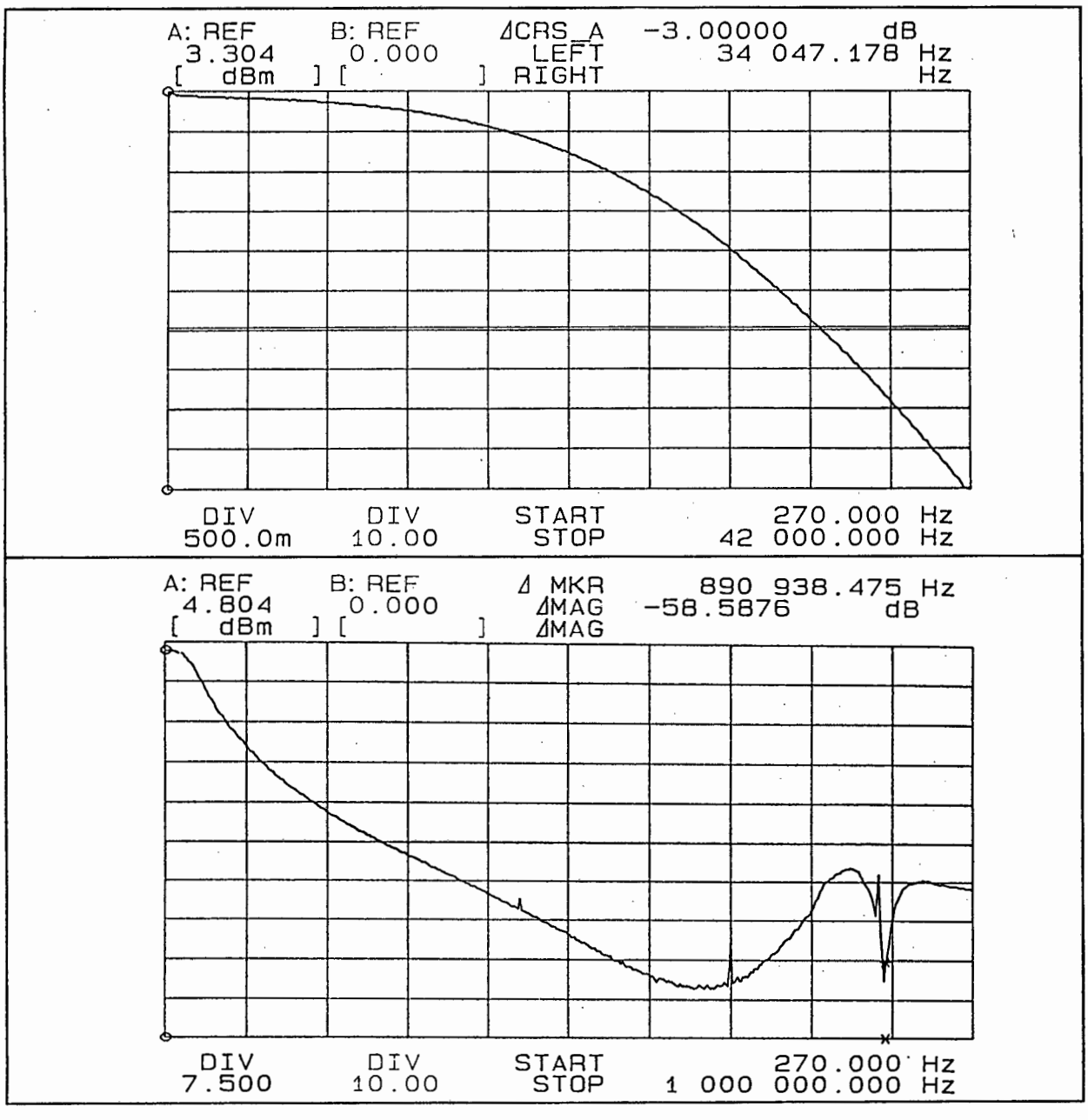

F = 32 khz , Phase Response

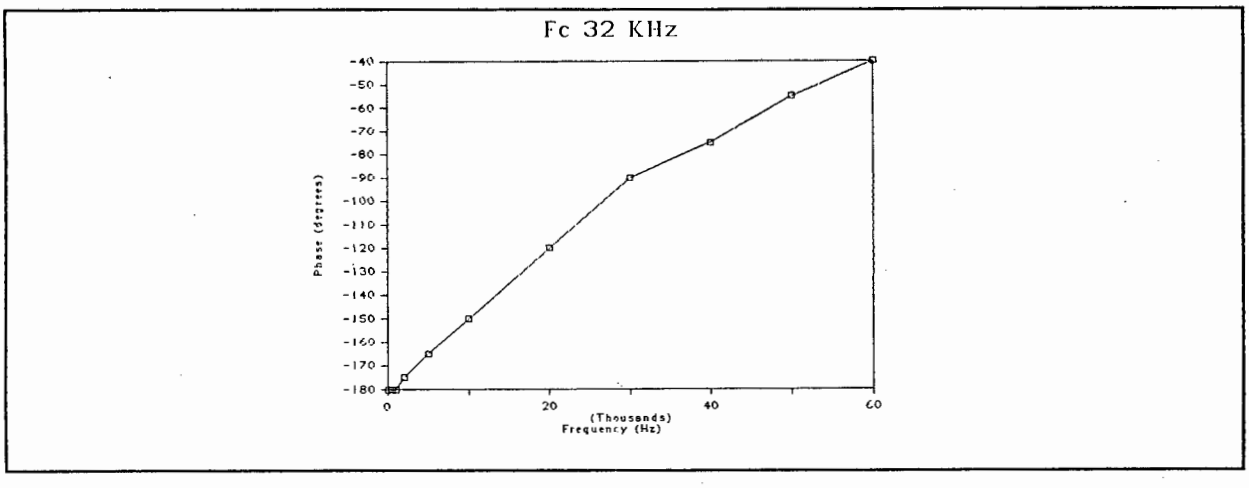

F = 64 khz , Amplitude Response

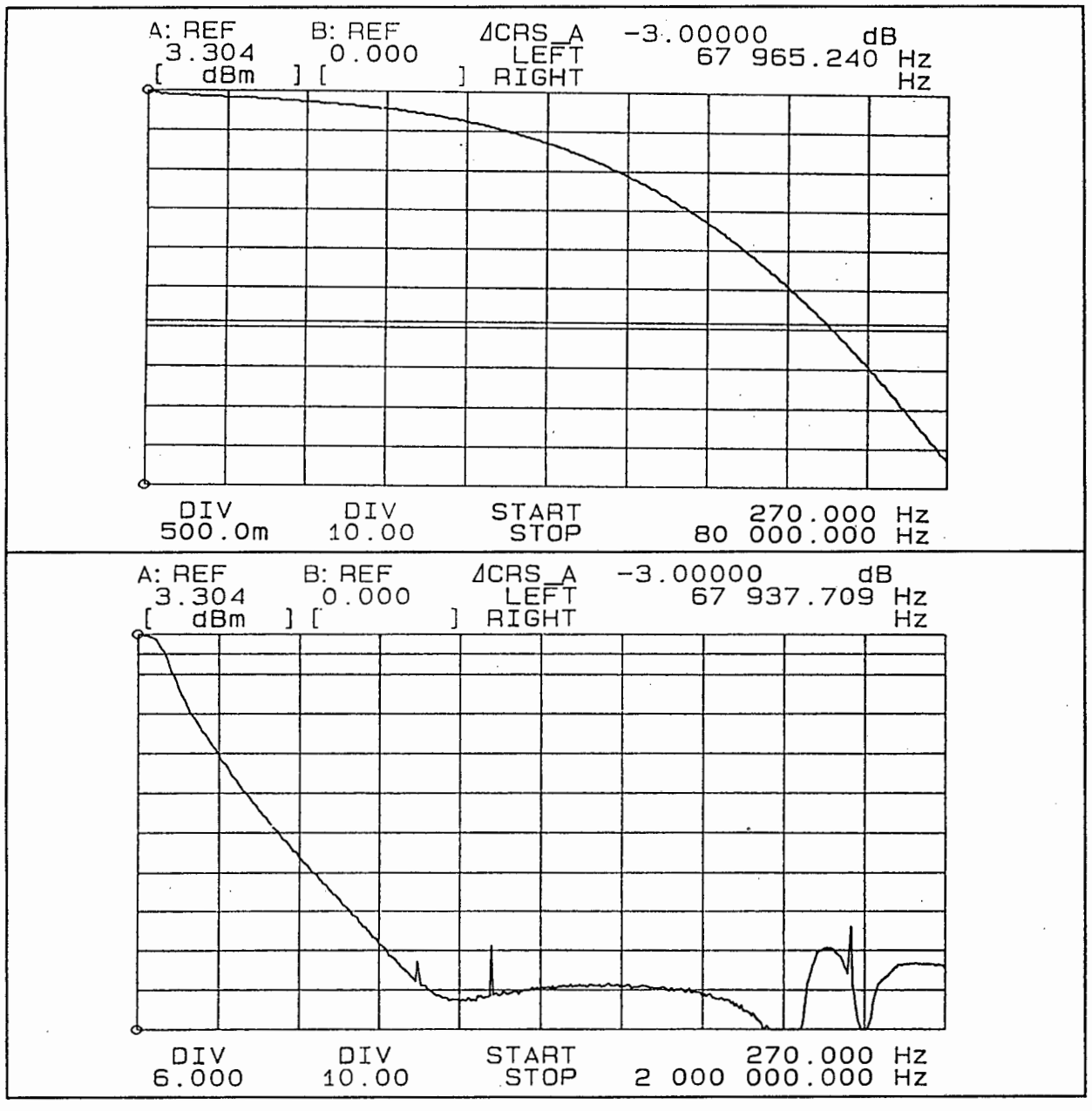

F = 64 khz , Phase Response

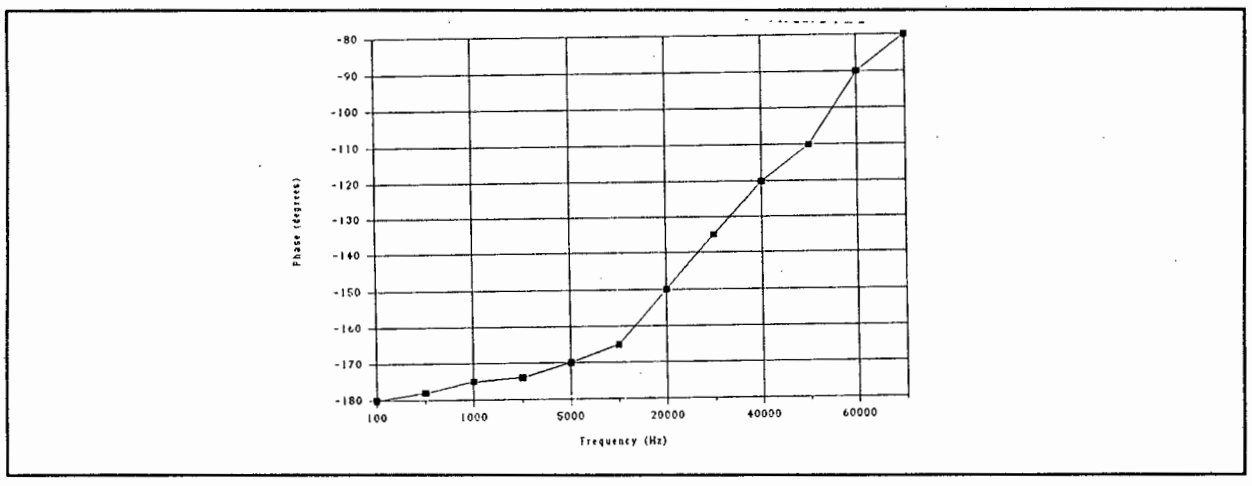

F = 128 khz , Amplitude Response

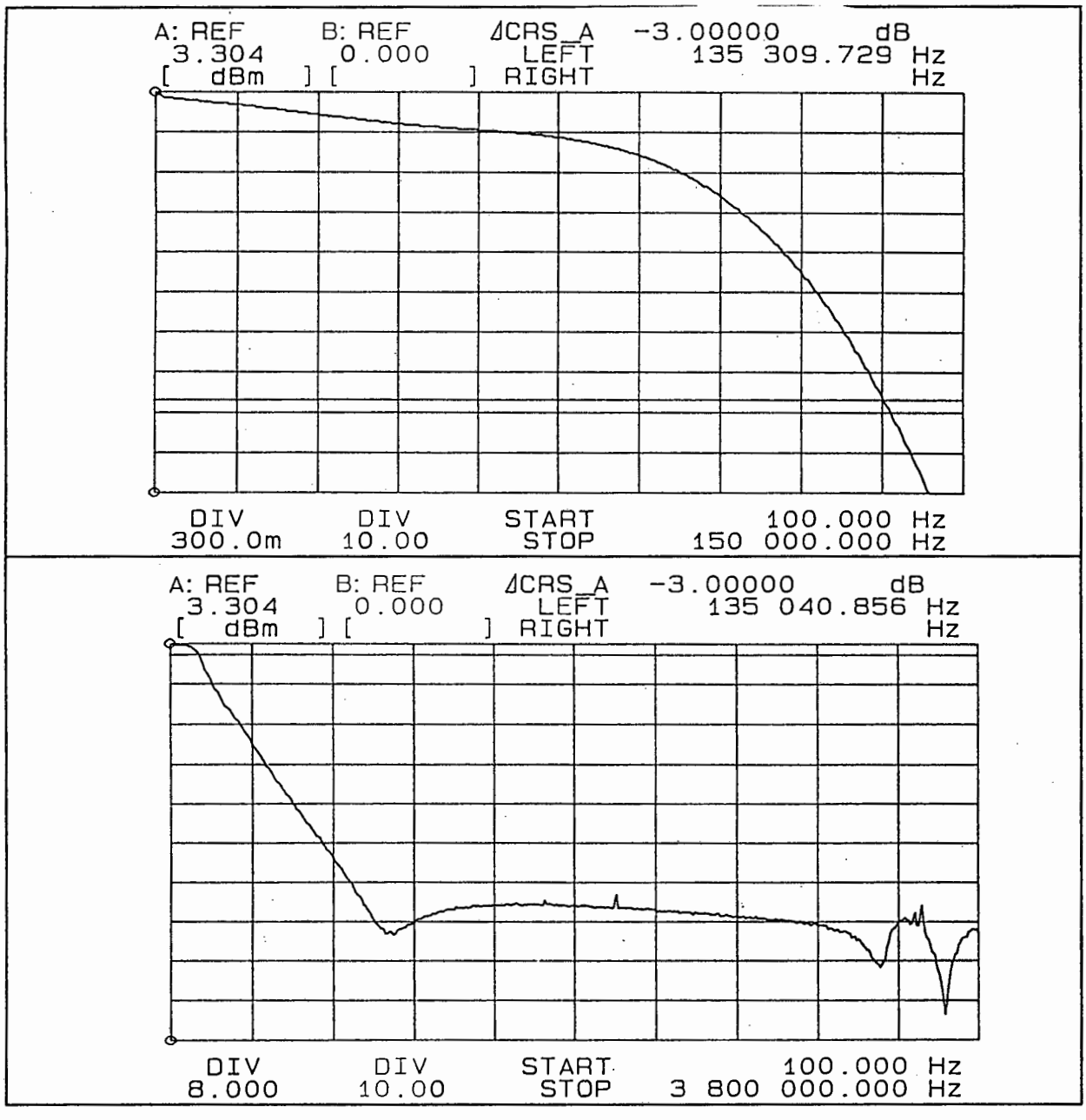

F = 128 khz , Phase Response

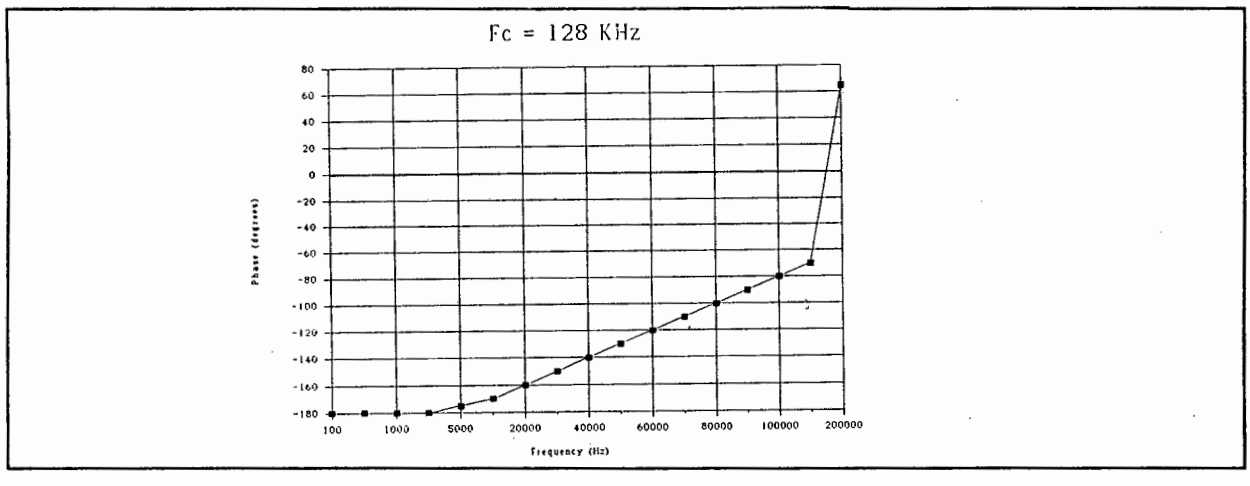

APPENDIX E

PASSIVE BAND PASS FILTERS

1.1 CIRCUIT DIAGRAM OF SIX PARALLEL FILTERS with MULTIPLEXER

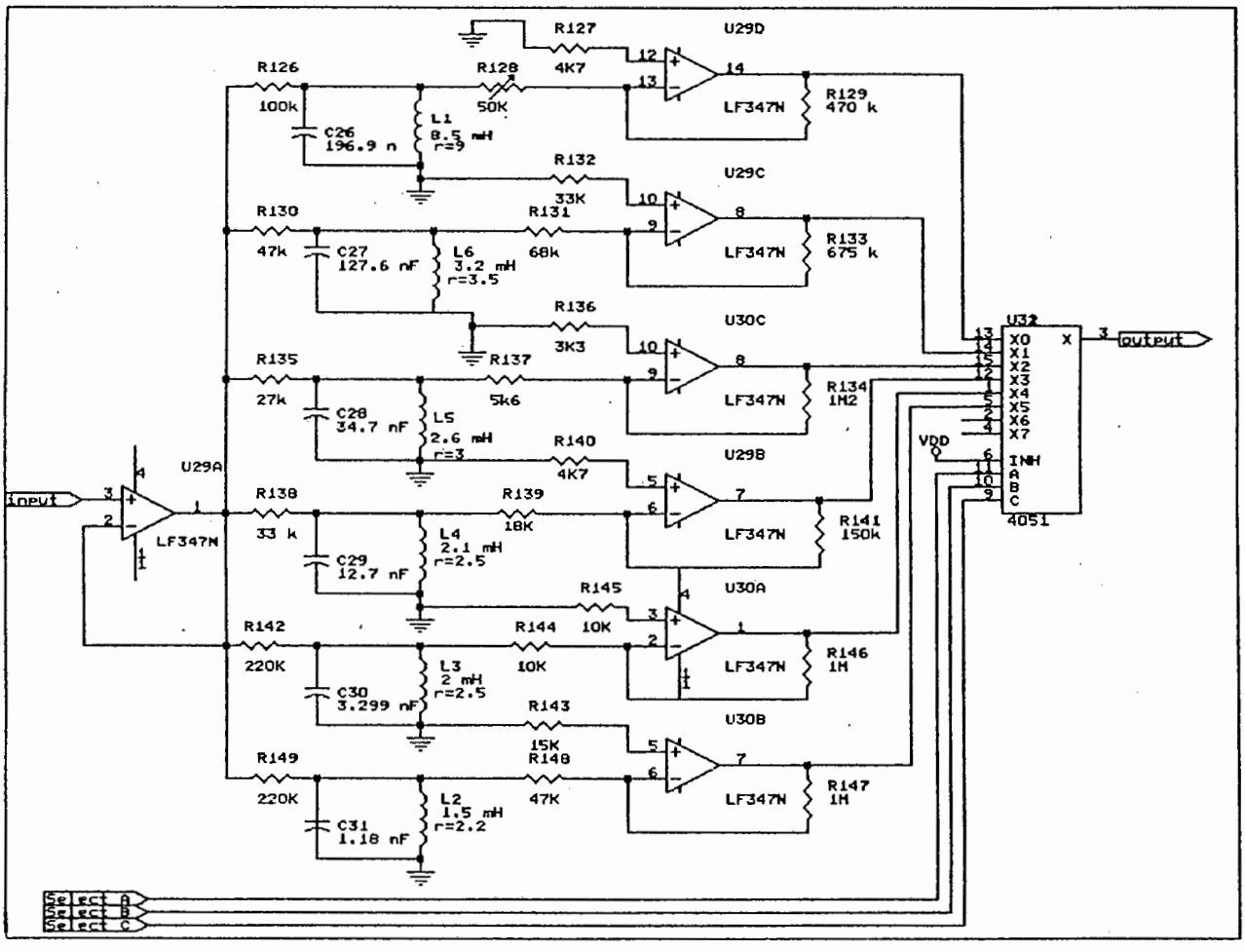

FIGURE E1 : CIRCUIT DIAGRAM OF PASSIVE BAND PASS FILTERS.

1.2 AMPLITUDE AND PHASE RESPONSE

AMPLITUDE @ f = 4 kHz

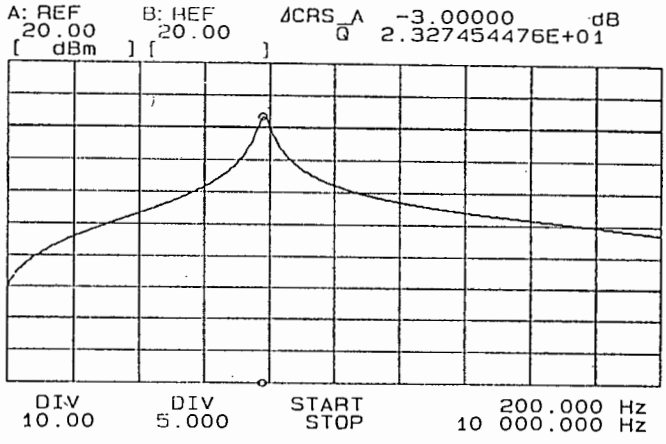

PHASE RESPONSE

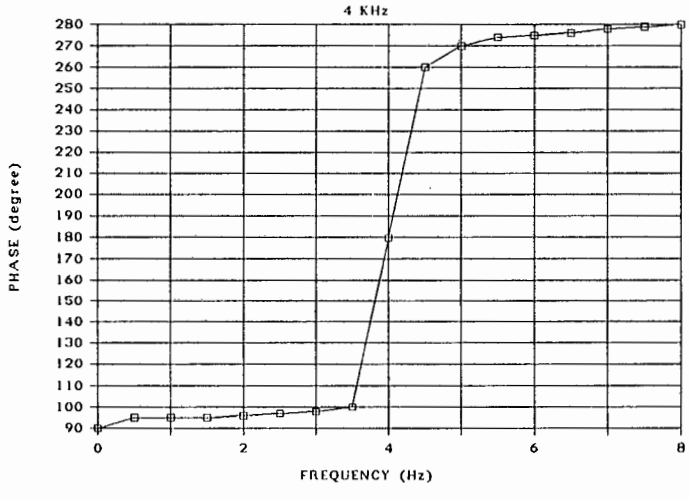

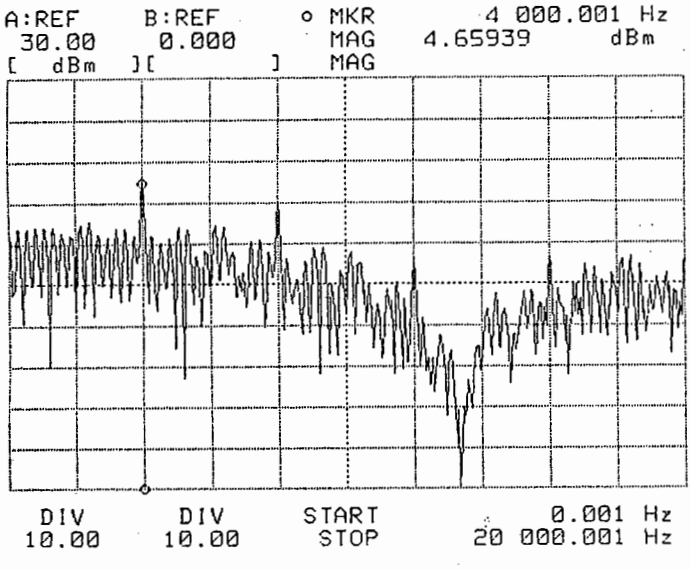

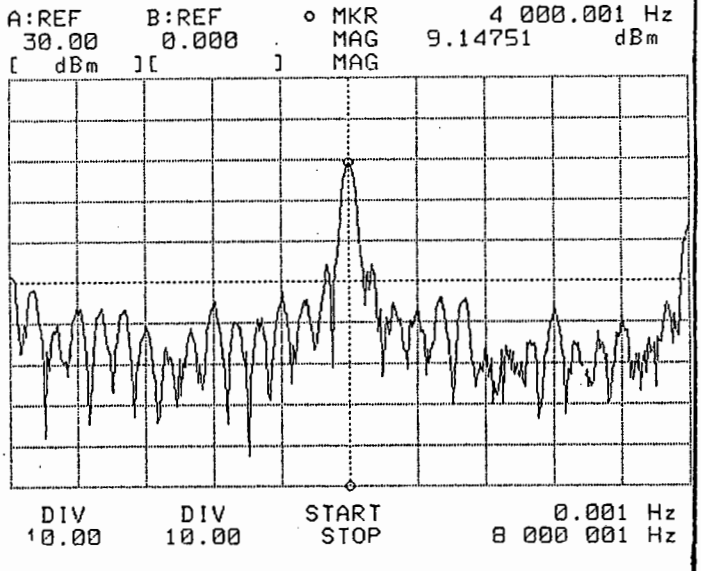

Input and output spectrum

FIGURE E2 : AMPLITUDE AND PHASE RESPONSE OF FILTERS WITH INPUT AND OUTPUT SPECTRA.

AMPLITUDE @ f = 8 kHz

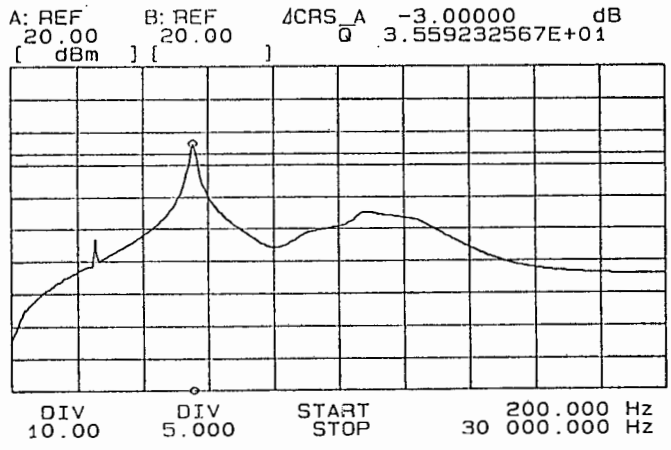

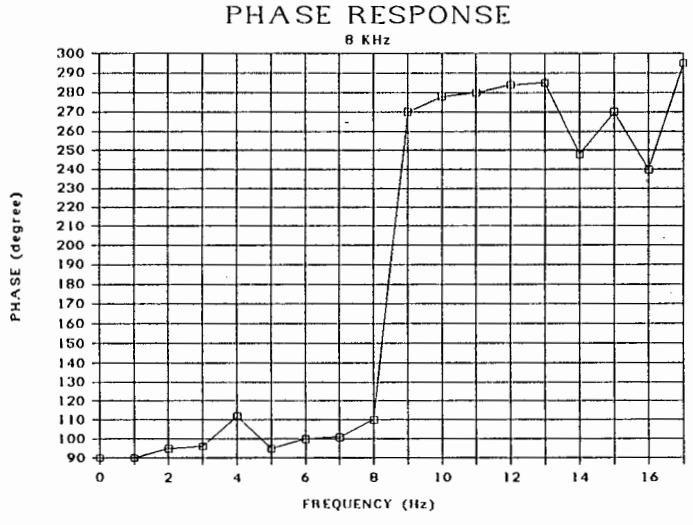

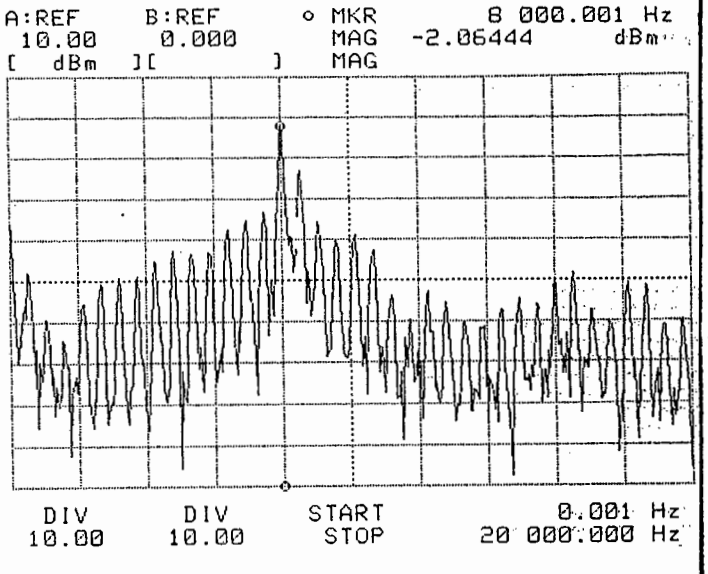

Input and output spectrum

AMPLITUDE @ f = 16 kHz

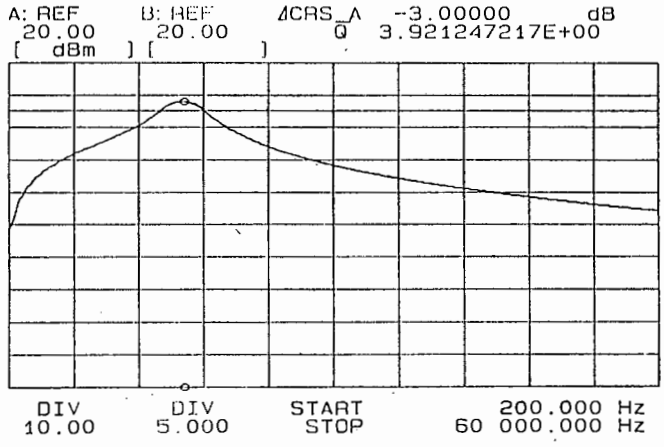

PHASE RESPONSE

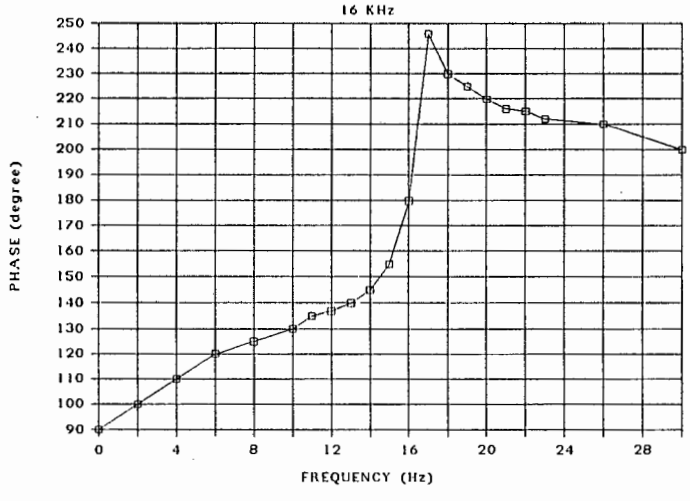

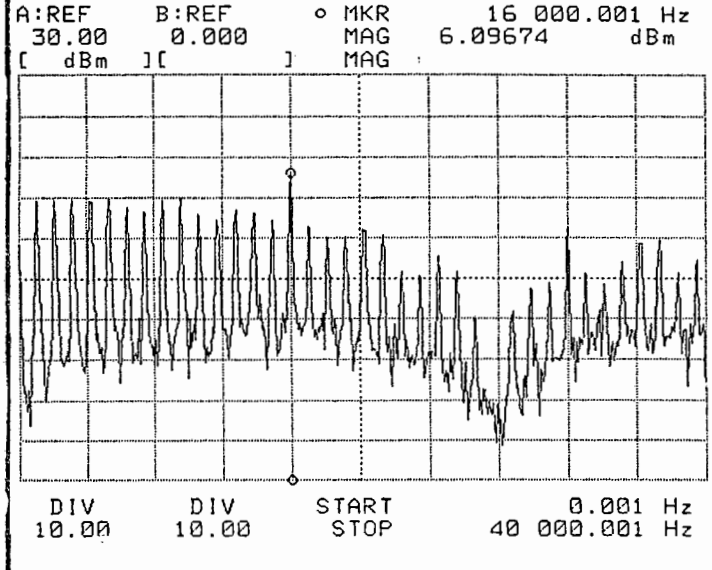

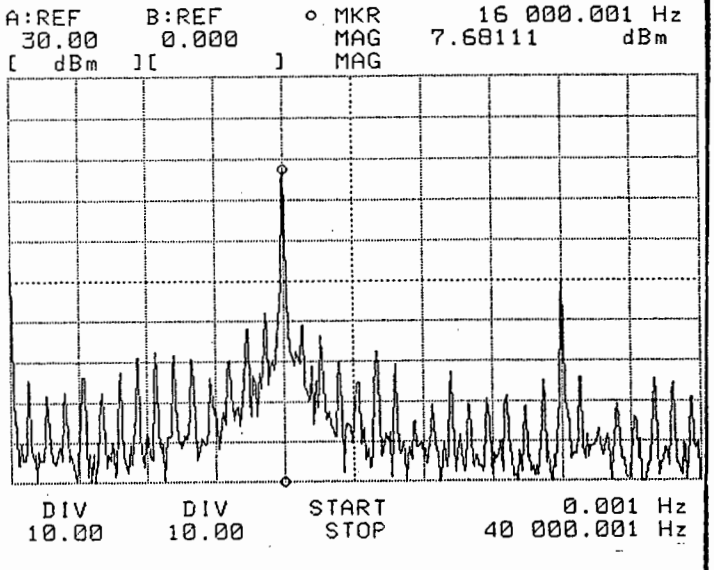

Input and output spectrum

AMPLITUDE @ f = 32 kHz

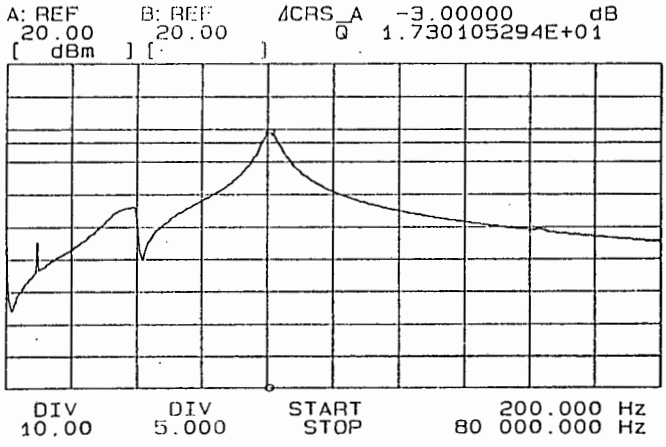

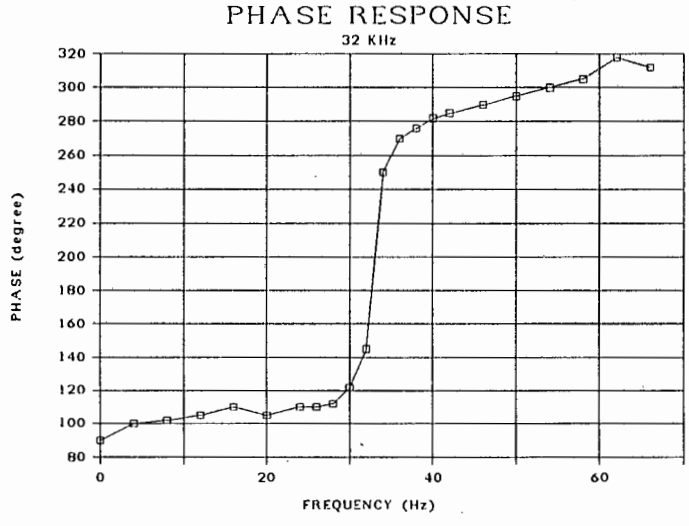

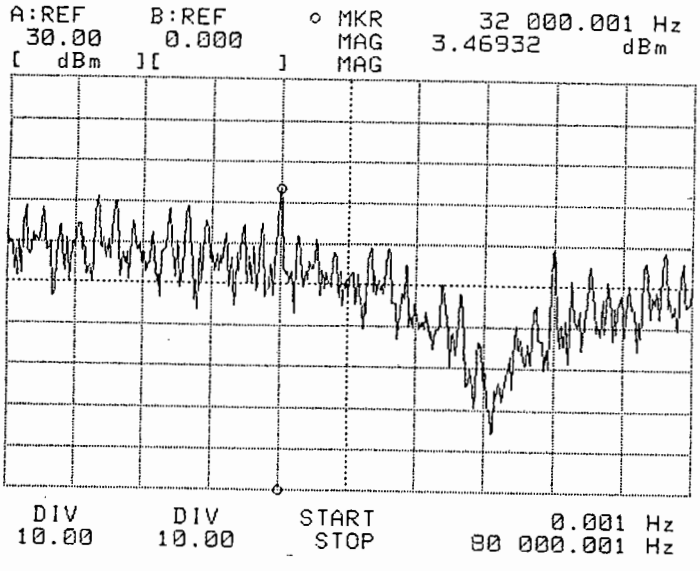

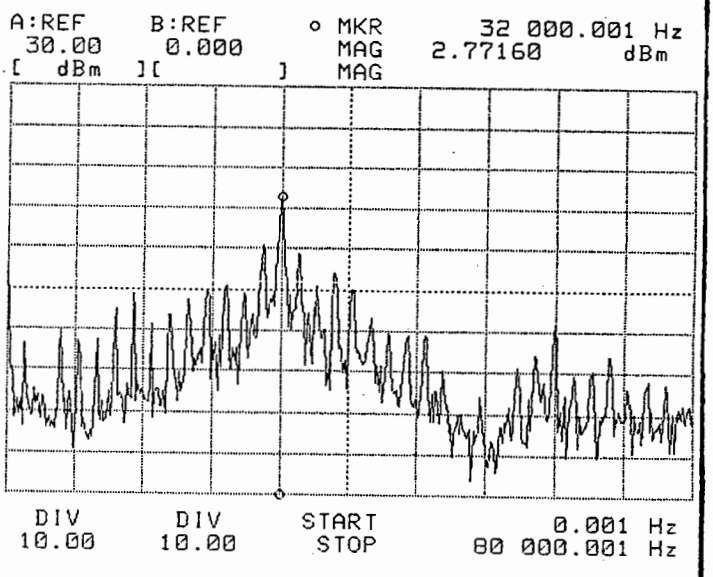

Input and output spectrum

AMPLITUDE @ f = 64 kHz

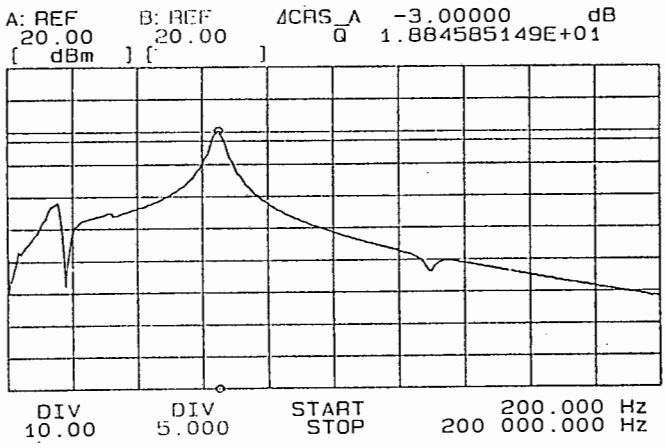

PHASE RESPONSE

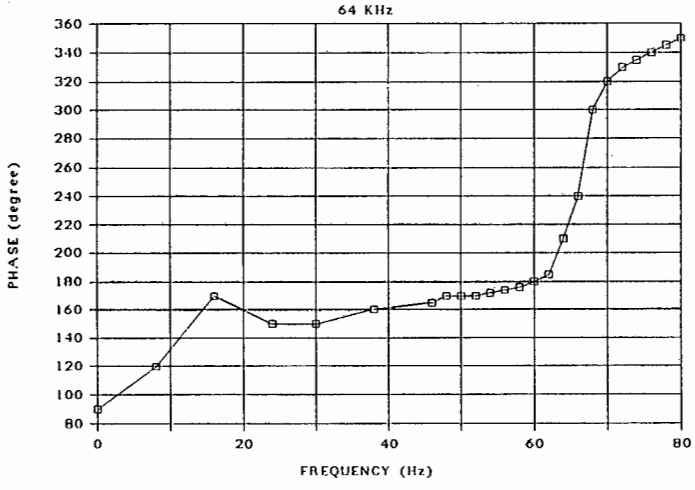

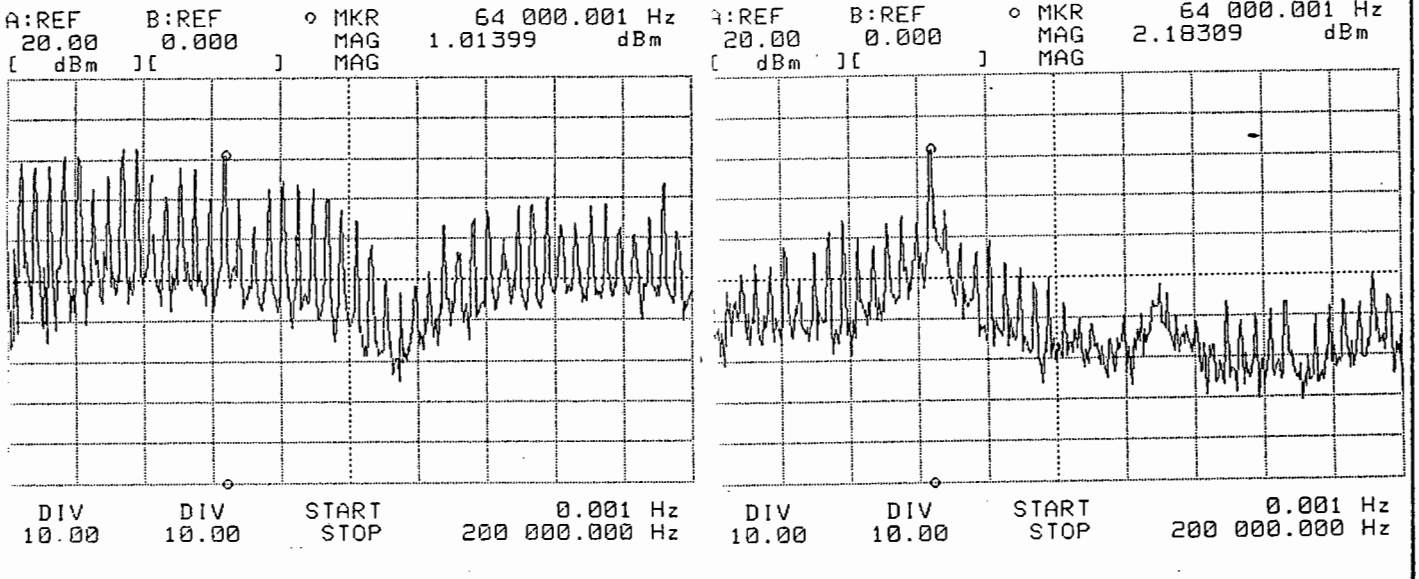

Input and output spectrum

AMPLITUDE @ f = 128 kHz

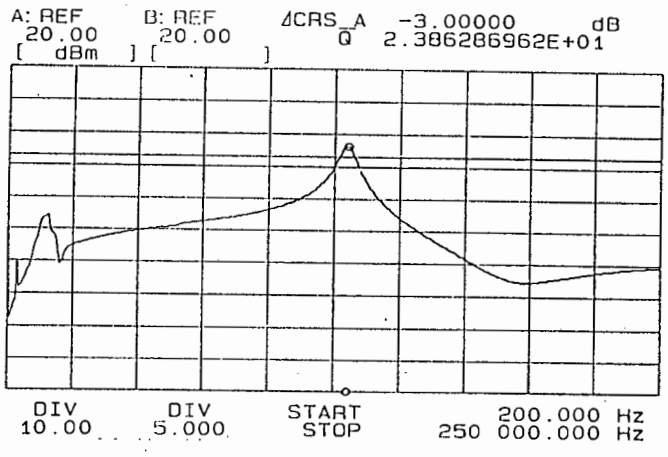

PHASE RESPONSE

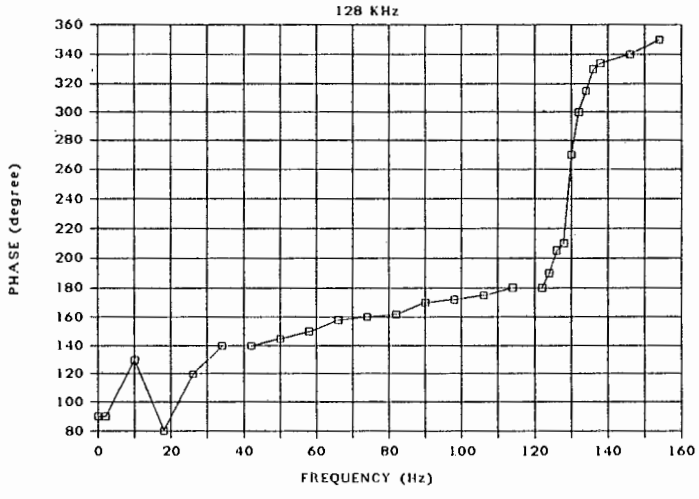

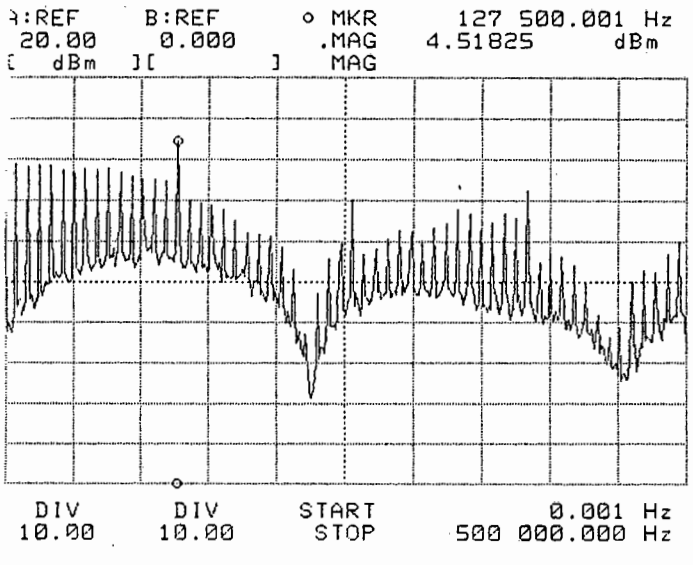

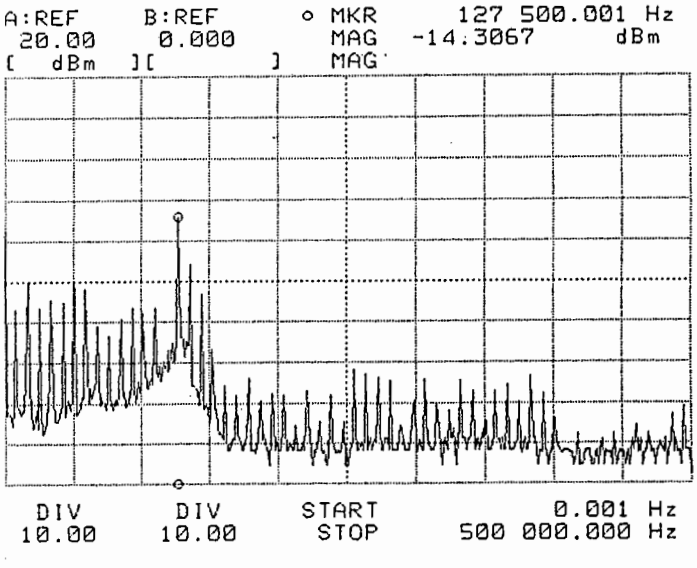

Input and output spectrum

APPENDIX F

ACTIVE BAND PASS FILTERS

1.1 CIRCUIT DIAGRAM OF SIX PARALELL BAND PASS FILTERS

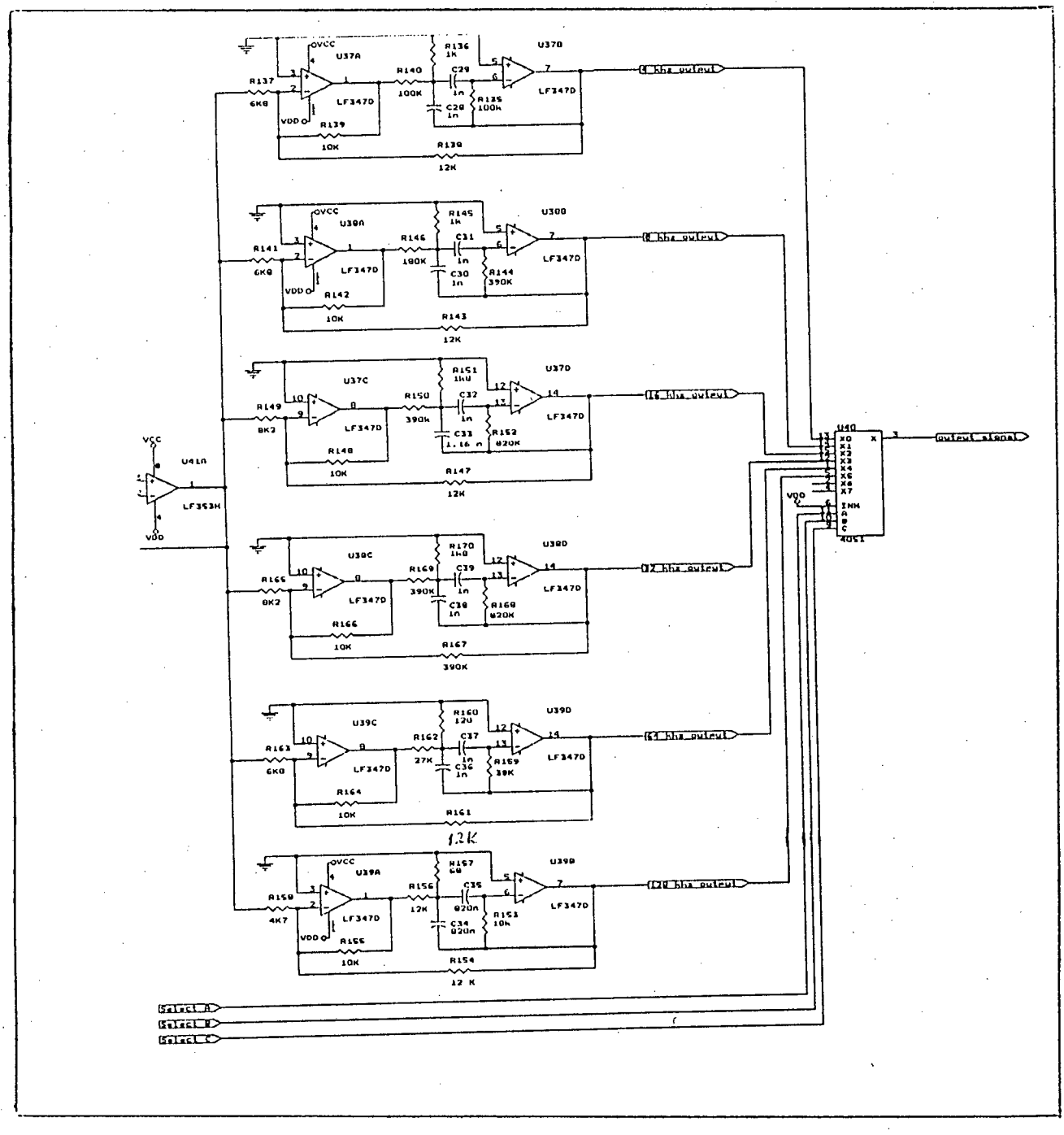

FIGURE F1 : CIRCUIT DIAGRAM OF ACTIVE BAND PASS FILTERS.

1.2 AMPLITUDE AND PHASE RESPONSE

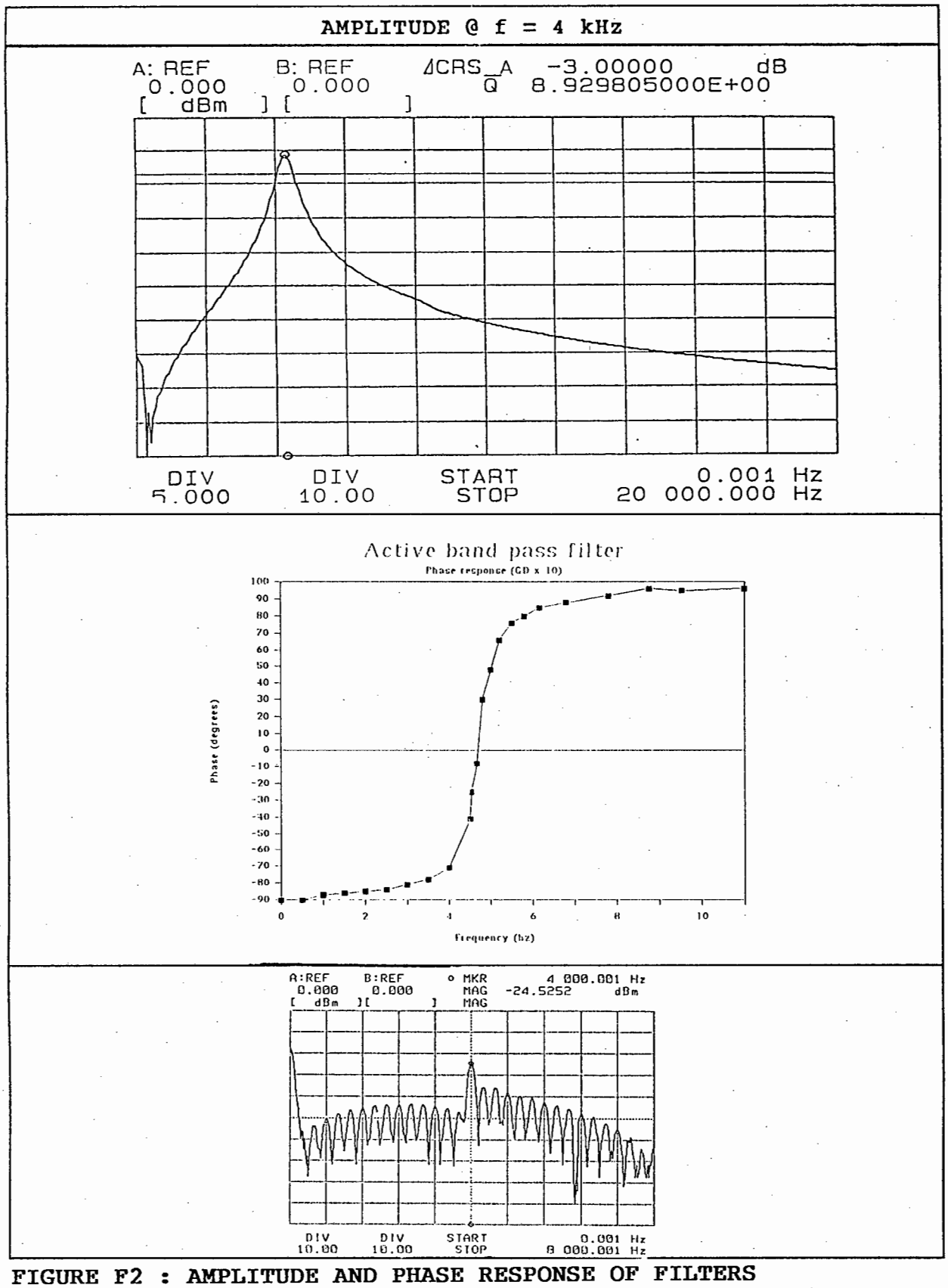

FIGURE F2 : AMPLITUDE AND PHASE RESPONSE OF FILTERS WITH OUTPUT SPECTRA.

AMPLITUDE @ f = 8 kHz

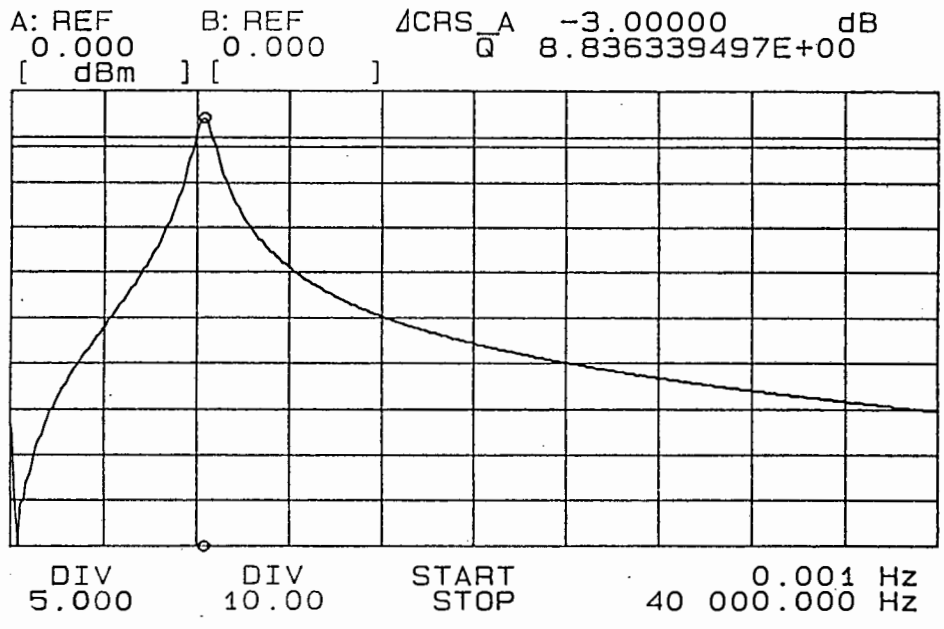

Active band-pass Phase response

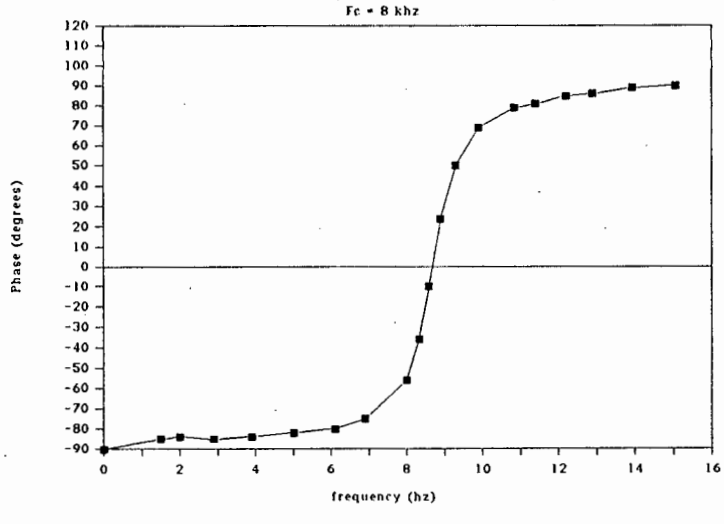

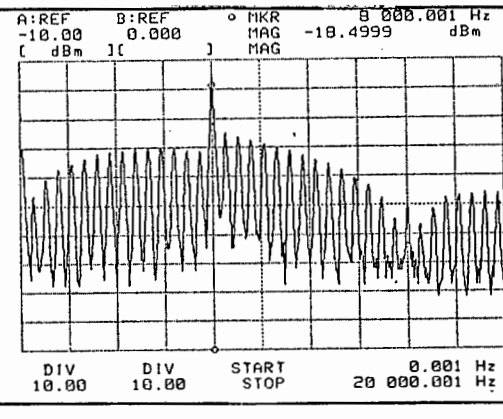

AMPLITUDE @ f = 16 kHz

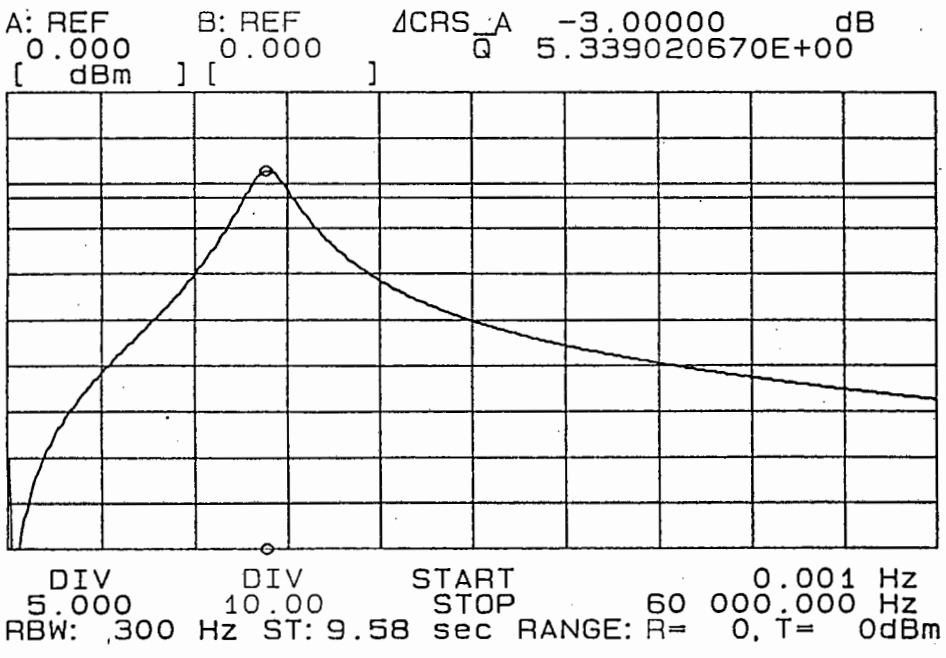

Active band pass filter Phase response

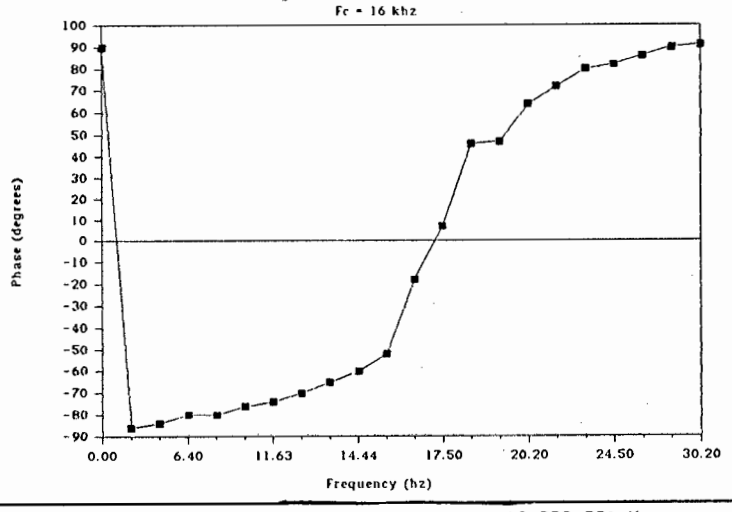

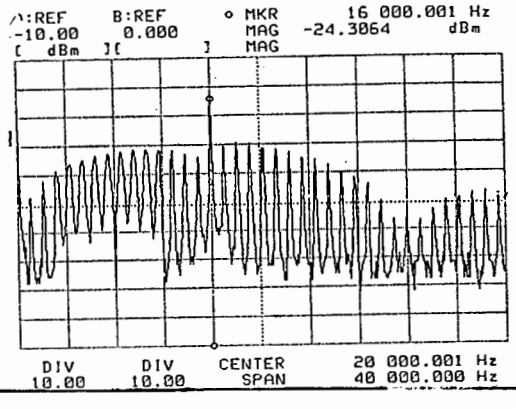

AMPLITUDE @ f = 32 kHz

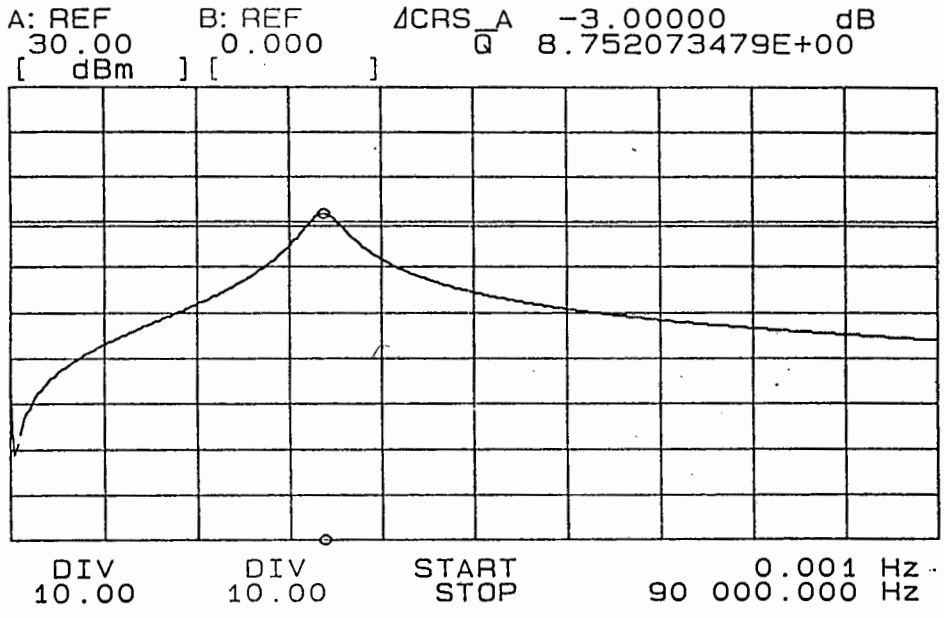

Active band pass filter Phase response

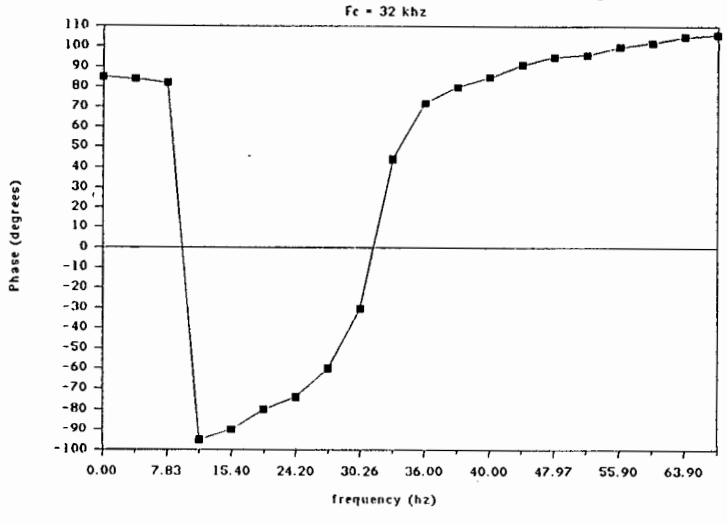

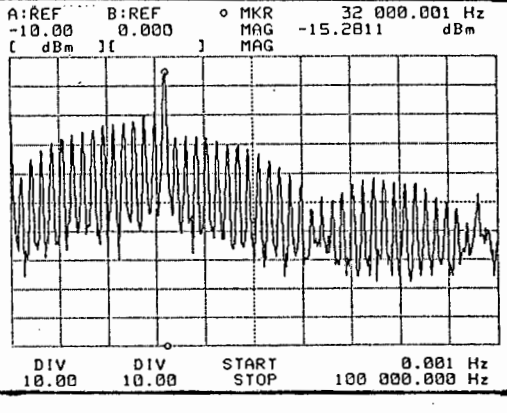

AMPLITUDE @ f = 64 kHz

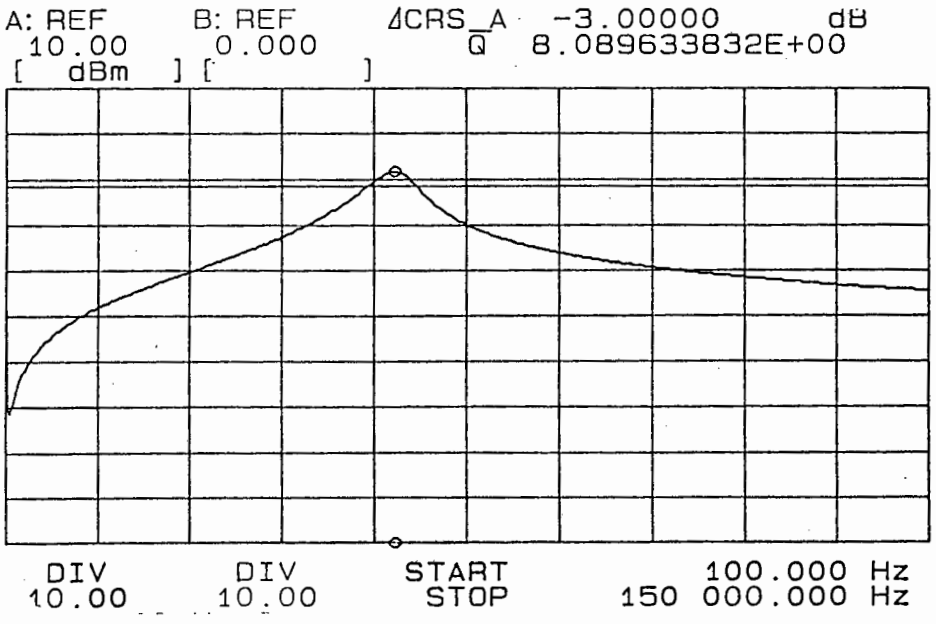

Active BPF Phase response

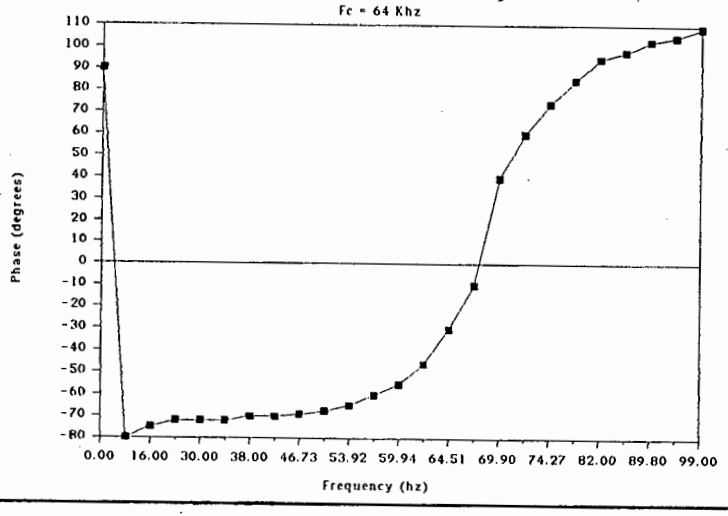

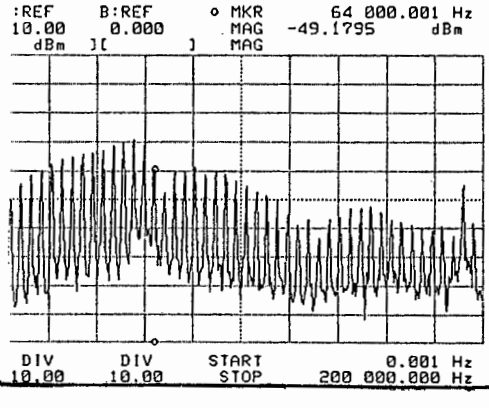

AMPLITUDE @ f = 128 kHz

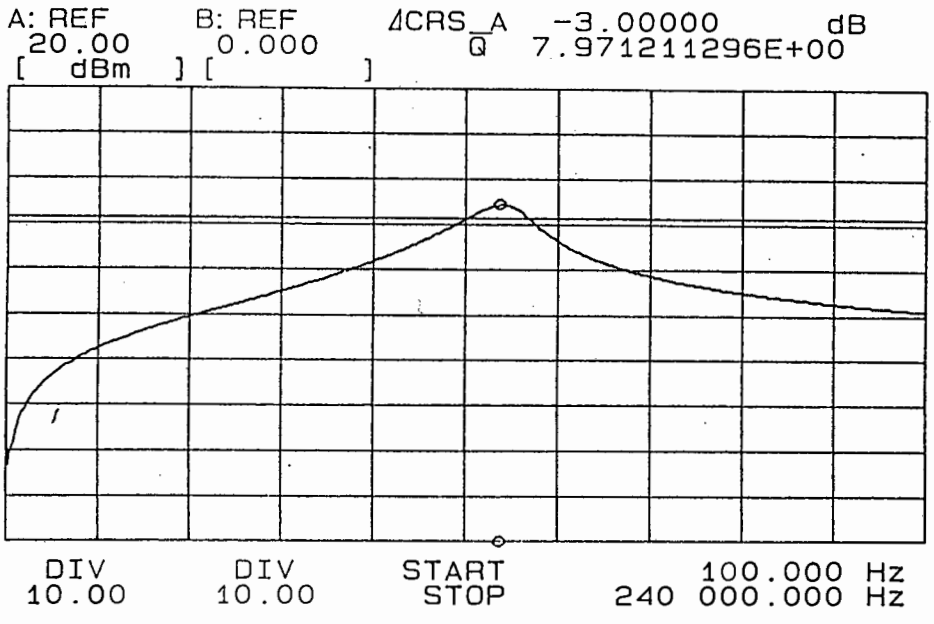

Active band pass filter Phase response

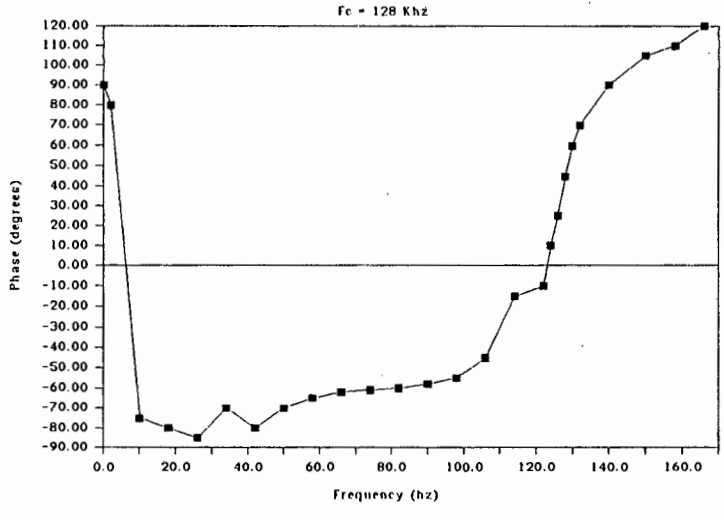

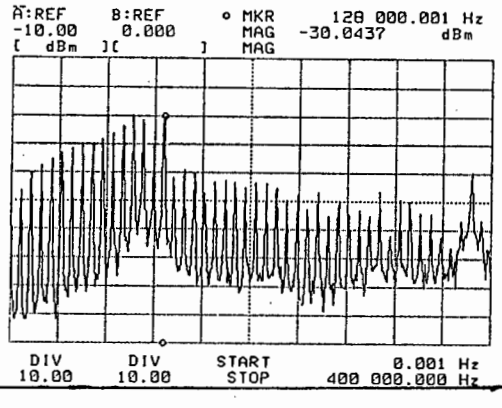

APPENDIX G

1.1 PROBABILITY OF ERROR, $P_e = f(E_b/N_o)$

The probability of error is derived for a general receiver filter structure. The P_e vs E_b/N_o for particular receive filters can then be derived. Two low pass receiver filters that are of interest are the ideal matched filter and the second order Butterworth filter.

The modulator performs the following mapping:

$$m(t) = \begin{cases} s_1 \quad (t) & if \quad b_k = 0 \\ s_2 \quad t & if \quad b_k = 1 \end{cases}$$

Where $s_1(t)$ and $s_2(t)$ are two elementary waveforms having a duration of T_b seconds, and having finite energy, that is,

$$E_{1b} = \int_0^{T_b} s_1^2(t)dt \quad < \quad infinty$$

$$E_{2b} = \int_0^{T_b} s_2^2(t)dt \quad < \quad infinty$$

A modulator and a possible binary demodulator are shown in Fig. G-1.

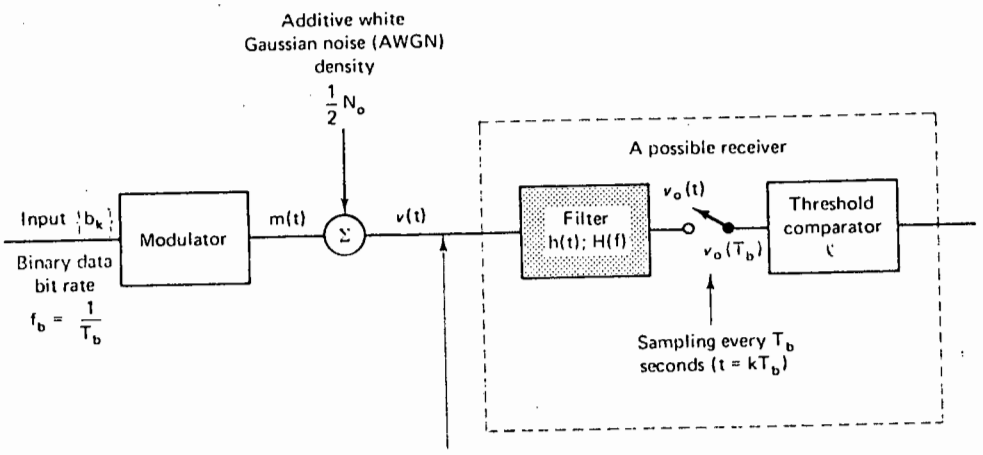

FIGURE G-1 : *Modulator, with additive white Gaussian noise (AWGN) and demodulator.*

In this case, the system contains no transmit filter and only a receive filter. Therefore, 100% of the binary spectrum is transmitted.

The transfer function of the optimum receive filter, H(f), its impulse response h(t), and the probability of error peformance of the optimum system are all obtained as a result of the following derivation.

The received carrier plus noise prior to the receive filter is

$$v(t) = \begin{Bmatrix} s_1 & (t) & + & n & (t) \\ s_2 & (t) & + & n & (t) \end{Bmatrix}$$

($0 < t < T_b$), depending on whether the $s_1(t)$ or $s_2(t)$ signal was transmitted. The system propagation delay is assumed to be zero. Now, let $s_1(t)$ and $s_2(t)$ be selected such that

$$s_{o1}(T_b) < s_{o2}(T_b)$$

The decision rule is based on the criteria

$s_2(t)$ was sent if $v_o(T_b) > l$

$s_1(t)$ was sent if $v_o(T_b) < l$

Where l is the threshold level of $v_o(T_b)$, the sampled output, and $s_1(t)$ and $s_2(t)$ are the signal components of the receive filter output in the sampling $t = T_b$. These filtered signals are due to the $s_1(t)$ and $s_2(t)$ transmitted signals, respectively. In the sampling instant ($t=T_b$) the signal plus noise voltage at the threshold comparator input is given by

$$v_o(T_b) = s_{o1}(T_b) + n_{o1}(T_b)$$

or

$$v_o(T_b) = s_{o2}(T_b) + n_{o2}(T_b)$$

where $n_{o1}(t)$ and $n_{o2}(t)$ represent the filtered noise components. Let the AWGN have a double-sided spectral density of

$$G_n(f) = \frac{1}{2} N_o$$

Thus the filtered noise has a power spectral density $S_{no}(f)$, given by

$$S_{no}(f) = |H(f)|^2 G_n(f)$$

$$= |H(f)|^2 \frac{1}{2} N_o$$

The receiver filter is a linear network; hence the additive Gaussian channel noise remains Gaussian after the receiver filter. The probability density function of Gaussian noise remains Gaussian even if it is filtered by a time invariant linear filter.

The noise is stationary; thus at the sampling instant, N = $n_o(T_b)$, it is a random variable with a probability density given by

$$f_N(\eta) = \frac{e^{\frac{-\eta^2}{2\sigma_o^2}}}{\sqrt{2\pi\sigma_o^2}}$$

Where the total noise power N_T (variance σ_o^2) at the receiver filter output is given by

$$N_T = \sigma_o^2 = \int_{-\infty}^{\infty} |H(f)|^2 G_n(f) df$$

The mean value of the noise is zero, by symmetry. The sampler output has two possible states:

$$V_1 = v_1(T_b) = s_{o1}(T_b) + N \qquad if\ s_1(t)\ is\ transmitted.$$

or

$$V_2 = v_2(T_b) = s_{o2}(T_b) + N \qquad if\ s_2(t)\ is\ transmitted.$$

The conditional probability density functions (pdf) of the receive filter output in the sampling instants t=k.T_b are illustrated in Fig. G-2.

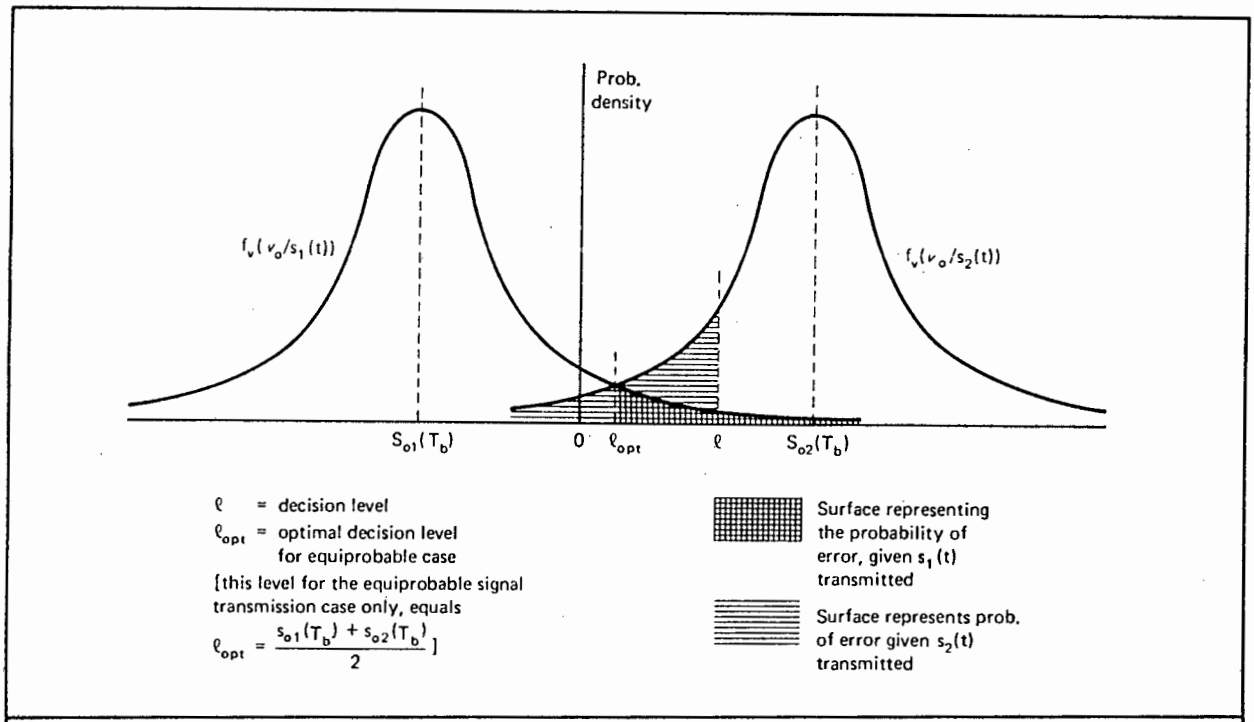

FIGURE G-2 : *Conditional probability density functions of the receiver filter output in the sampling instant ($t = T_b$).*

The probability of error derivation.

For the general case:
Probability of transmission of an s1(t) signal is p_1.
Probability of transmission of an s2(t) signal is p_2.

the average probability of error is

$$P_e = p_1 \cdot P\left[e \backslash s_1(t)\right] + p_2 \cdot P\left[e \backslash s_2(t)\right]$$

It will be assumed that the transmitted signals have equal probabilities, $p_1 = p_2 = 0.5$ and

$$P_e = 0.5P\left(e \backslash s_1(t)\right) + 0.5P\left(e \backslash s_2(t)\right) \qquad (G.1)$$

The probability of error, assuming that s1(t) is transmitted, is given by

$$P\left[e \backslash s_1(t)\right] = \int_{\ell}^{\infty} f_{v_o}\left[v_o \backslash s_1(t)\right] dv$$

$$= \int_{l}^{\infty} \frac{e^{\frac{-\left[v_o - s_{o1}(T)\right]^2}{2\sigma_o^2}}}{\sqrt{2\pi\sigma_o^2}} dv_o \qquad (G.2)$$

Similarly for $s_2(t)$.

These probabilities are shown as shaded surfaces in Fig. G-2. Combining equations (G.1) and (G.2),

$$P_e = \frac{1}{2}\int_{l}^{\infty} \frac{1}{\sqrt{2\pi N_T}} e^{\frac{-\left[v_o - s_{o1}\right]^2}{2N_T}} dv_o$$

$$+ \frac{1}{2}\int_{-\infty}^{l} \frac{1}{\sqrt{2\pi N_T}} e^{\frac{-\left[v_o - s_{o2}\right]^2}{2N_T}} dv_o \qquad (G.3)$$

The optimum threshold level l_{opt} can be derived by finding the first differential with respect to l in expression (G.3). If the first differential is set to zero, the optimum setting of the threshold level l is obtained:

$$l_{opt} = 0.5\left[s_{o1}(T_b) + s_{o2}(t_b)\right]$$

This level is at the intersection of the two conditional pdf's illustrated in Fig. G-2.

Insertion of the best choice of the threshold level l_{opt} into equation (G.3) gives:

$$P_e = 0.5\,erfc\left[\frac{s_{o2}(T_b) - s_{o1}(T_b)}{2\sqrt{2}\sigma_o}\right] \qquad (G.4)$$

Where erfc(y) is defined by

$$erfc(y) \Leftrightarrow \frac{2}{\sqrt{\pi}}\int_{y}^{\infty} e^{-z^2} dz \qquad y > 0$$

This integral is given by tables [3.1].

1.2 TRANSFER FUNCTION OF THE OPTIMAL RECEIVER

From equation (G.4) it can be concluded that the probability of error is a function of the difference (distance) between the two output signals in the samlping instant, t = T, and of the rms noise voltage σ_o. The optimum filter transfer function H(f), that leads to the smallest P_e, and therefore best performance, is obtained by maximisation of the ratio

$$\gamma = \frac{s_{o2}(T_b) - s_{o1}(T_b)}{\sigma_o} \qquad (G.5)$$

The derivation is simplified by maximising γ^2, eliminating the requirement $s_{o1}(T_b) < s_{o2}(T_b)$

Let the difference in the filtered outputs be

$$S_{od}(t) = S_{o2}(t) - S_{o1}(t)$$

and the difference in the sampling instants by

$$S_{od}(t) = S_{o2}(T_b) - S_{o1}(T_b)$$

Thus

$$\gamma^2 = \frac{s_{od}^2(T_b)}{\sigma_o^2} = \frac{s_{od}^2(T_b)}{E\{n_o^2(T_b)\}} \qquad (G.6)$$

The difference of the filtered outputs may be obtained by inverse Fourier transform,

$$s_{od}(t) = F^{-1}[S_{od}(f)H(f)] = \int_{-\infty}^{\infty} H(f)S_{od}(f)e^{j2\pi ft}df \qquad (G.7)$$

The noise power (variance) of the stationery noise process at the filter output is given by

$$\sigma_o^2 = E\{n_o^2(T_b)\}$$

$$= \int_{-\infty}^{\infty} G_n(f)|H(f)|^2 df$$

$$= \frac{1}{2}N_o \int_{-\infty}^{\infty} |H(f)|^2 df \qquad (G.8)$$

Combining equations (G.7) and (G.8) and substituting into (G.6), we obtain

$$\gamma^2 = \frac{\left| \int_{-\infty}^{\infty} H(f)S_{od}(f)e^{j2\pi fT_b}df \right|^2}{\frac{1}{2}N_o \int_{-\infty}^{\infty} |H(f)|^2 df}$$

To maximise γ^2 we employ *Schwartz's inequality*. This inequality states

$$\left| \int_{-\infty}^{\infty} X(f)Y(f)^* df \right|^2 \leq \int_{-\infty}^{\infty} |X(f)|^2 df \int_{-\infty}^{\infty} |Y(f)|^2 df$$

where X(f) and Y(f) are arbitrary complex functions of a common variable f. Equality holds if

$$X(f) = kY^*(f)$$

where k is an arbitrary constant and $Y^*(f)$ [illegible] is the complex conjugate of Y(f). The following substitution can be done to The Schwartz inequality, put

X(f) = H(f)

$$Y^*(f) = S_{od}(f)e^{j2\pi f T_b}$$

This results in

$$\gamma^2 = \frac{1}{G_n(f)} \frac{\left| \int_{-\infty}^{\infty} X(f)Y^*(f)df \right|^2}{\int_{-\infty}^{\infty} |H(f)|^2 df}$$

Applying Schwartz's inequality

$$\leq \frac{2}{N_o} \int_{-\infty}^{\infty} |H(f)|^2 df \frac{\int_{-\infty}^{\infty} |S_{od}(f)|^2 df}{\int_{-\infty}^{\infty} |H(f)|^2 df}$$

$$\Rightarrow \gamma^2 \leq \frac{2}{N_o} \int_{-\infty}^{\infty} |S_{od}(f)|^2 df \qquad (G.9)$$

Based on Schwartz's inequality and the additive white Gaussian noise assumption, $G_n(f) = N_o/2$, it can be concluded that the equality holds, i.e. the signal-to noise ratio is maximised if

$$H(f) = m S_{od}^*(f) e^{-j2\pi T_b f} df$$

where *m* is a constant that represents the receiver filter gain. The gain constant of linear filters has evidently no influence on the output signal-to-noise ratio. Thus, without loss of generality, set *m* = 1. The optimum receiver transfer function $H_o(f)$ is thus given by

$$H_o(f) = S_{od}^*(f) e^{-j2\pi T_b f} \qquad (G.10)$$

APPENDIX H

THE COMPLETE CIRCUIT DIAGRAM

of the

MODULATOR AND DEMODULATOR

MODULATOR

DEMODULATOR

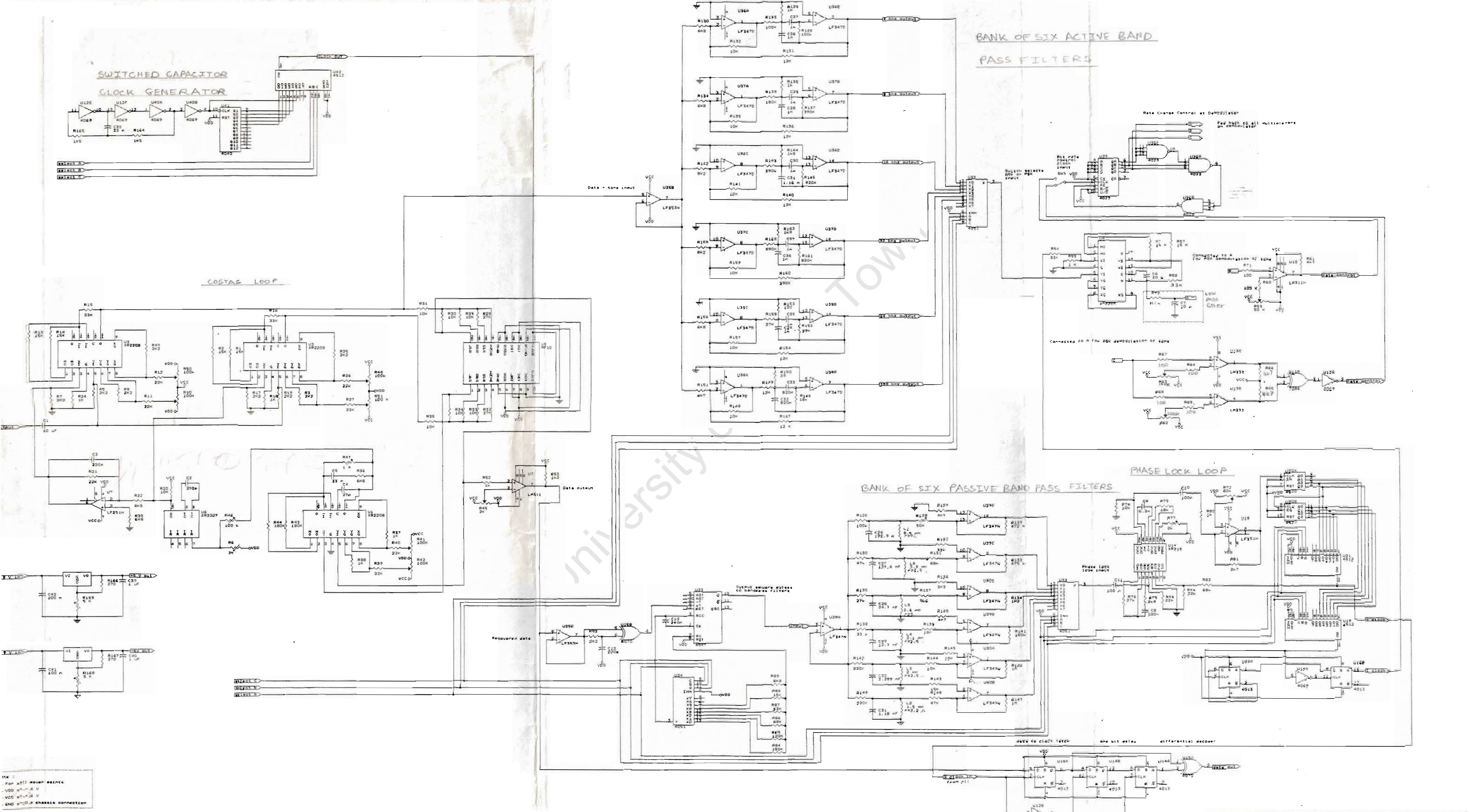

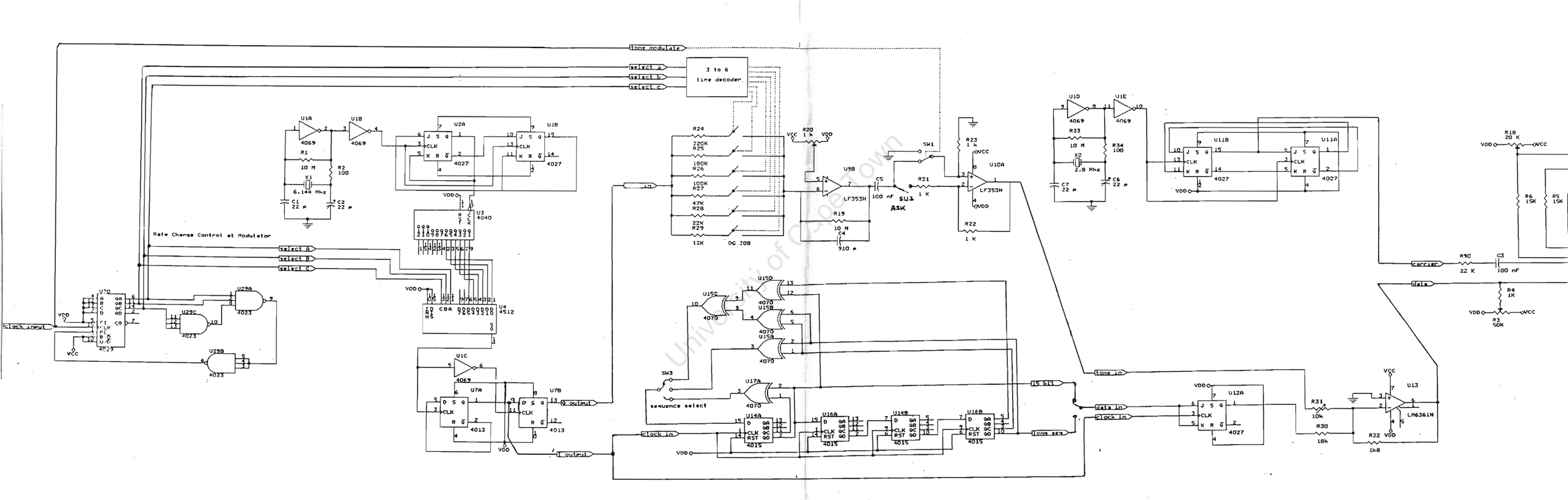
tone modulate
select a
select b
select c
3 to 6
line decoder
U1A
4069
U1B
4069
R1
10 M
R2
100
X1
6.144 Mhz
C1
22 p
C2
22 p
U2A
U2B
4027
U3
4040
Rate Change Control at Modulator
select A
select B
select C
U4
4512
clock input
U7C
4029
U29A
U29C
U29B
4023
U1C
4069
U7A
U7B
4013
Q output
T output
in
R24
220K
R25
180K
R26
100K
R27
47K
R28
22K
R29
12K
DG 308
VCC
R20
1 k
VDD
U9B
LF353H
C5
100 nF
SW1
ASK
R21
1 K
R19
10 M
C4
910 p
R23
1 k
U10A
R22
1 K
U1D
4069
U1E
4069
R33
10 M
R34
100
X2
2.8 Mhz
C7
22 p
C6
22 p
U11B
U11A
R10
20 K
R6
15K
R5
15K
carrier
R10
22 K
C3
100 nF
data
R4
1K
R3
50K
U15D
U15C
U15B
U15A
4070
SW3
sequence select
U17A
U14A
U14B
U16A
U16B
4015
clock in
15 bit
tone seq
tone in
data in
clock in
U12A
U13
LM6361M
R31
10k
R30
18k
R32
1k8